Jacob et al., J Remote Sensing & GIS 2016, 5:1
DOI: 10.4172/2469-4134.1000152

Journal of Remote Sensing & GIS

Research Article Open Access

Ecogeographically and Non-Ecogeographically Forecasting Discontinuous Canopied *Simulium damnosum* s.l. Habitats by Interpolating Metrizable Sub-Mixel Mean Solar Exoatmospheric Quantum Scalar Irradiance where θ_i is a Zenith Angle and Diatomically Etiolated Xanthophylls with Azimutually Isotropic Sources of Chloroplastic Carotenoid Zeaxanthins Spectrally Extracted from a Decomposed RapidEye™ Red Edge Normalized Difference Vegetation Index Reference Targeted Biosignature: A Case Study in Burkina Faso and Uganda

Benjamin G. Jacob[1]*, Robert J.Novak [2], Laurent D. Toe[2], Moussa S. Sanfo[2], Koala Lassane[2], Daniel A. Griffith[3], Thomson L. Lakwo[4], Peace Habomugisha[5], Moses N. Katabarwa[6] and Thomas R. Unnasch[1]

[1]*Global Health Infectious Disease Research Program, Department of Global Health, University of South Florida, Tampa, Florida, United States of America*
[2]*African Programme for Onchocerciasis Control, World Health Organization, Ouagadougou, Burkina Faso*
[3]*School of Economic, Political and Policy Sciences, University of Texas at Dallas, Richardson, Texas, United States of America*
[4]*Vector Control Division, Ministry of Health, Kampala, Uganda*
[5]*The Carter Center, Kampala, Uganda*
[6]*Emory University and The Carter Center, Atlanta, Georgia, United States of America*

Abstract

We interpolated a geospectrally decomposed 5 meter (m) RapidEye™,Red Edge, Normalized Difference Vegetation Index (NDVI), unmixed, endmember, biosignature of a georeferenced, larval habitat of *Similium damnosum* s.l.,a black fly vector of onchocerciasis. We did so to identify unknown, unsampled, prolific, habitats in African riverine environments. The *S. damnosum* s.l.larval habitat was initially geosampled in a riverine village in Burkina Faso and overlaid onto the 5m resolution data. The Band Mathfunction of ENVI 4.8™ was employed to calculate the RedEdge NDVI. Before applying the spectral index to the imagery raw mixel ("mixed pixel") values, digital numbers(DN)] were converted into physically meaningful units to differentiate absorption reflectance spectra and immature *Similium* productivity based on habitat size.Linear regression was used to equate and quantitate band data to DN and the reflectance values which in the geospectral,sub-mixel, risk analysis was equivalent to removing the solar irradiance and the atmospheric path radiance in the object-based classifier. A radiometric calibration tool then calibrated the spaceborne sensor data to radiance and top-of-atmosphere (ToA) reflectance.Additionally,Fast Line-of-sight Atmospheric Analysis of Spectral Hypercubes (FLAASH®)removed the effects of multiscattering in the scene.We calculated the internal relative reflectance which normalized the image to a scene average spectrum. ENVI's Log Residuals Correction Tool removed the instrument gain, topographic effects, and albedo effects from the reflectance, transmittance, wavelenght emissitivities. The instantaneous fraction of direct beam radiation intercepted by the habitat canopy was calculated and described as fPAR = 1 - exp (-k (leaf area index)/$\cos\theta_s$) where the extinction coefficient k was a function of leaf angle distribution.We employed a successive progressive algorithm, a two stream radiative atmospheric transfer analyses, a geometric-optical model and a bidirectional reflectance distribution function to unmix the *S. damnosum s.l.,* larval habitat,canopied endmembers.The non-parametric, residual, explanatorial, decomposed, sub-mixel estimators derived from the RapidEye™data were then used to construct a Boolean model.Therefater,the imaged larval habitat and its geospatially, ecohydrological, within-canopy pigments (e.g., chorophyll, zeathinins) were defined and a Red Edge,NDVI, endmember biosignature was decomposed in ENVI. An autocorrelation uncertainty matrix was deconvolved into combinations of the unmixed canopied endmembers.Subsequently, the NDVI, endmember biosignature, decomposed, canopied endmembers with its multiple ToA noise-adjusted coefficients were kriged in Geospatial Analyst of ArcGIS 10.3®to identify unknown, unsampled, prolific, *S. damnosum s.l.,* georeferencable, larval habitats along a northern Ugandan riverine ecosystem. Of the forecasted prolific, shaded, larval habitats by the canopy model, 72% were found to contain *S. damnosum s.l.* larvae when field verified. The sensitivity of the test was 78.26 while the specifity was 100.

Keywords: Rapid Eye; *Similium-damnosum s.l;* Red EdgeNDVI; ENVI 4.8; ArcGIS 10.3; Interpolation; Burkina Faso; Uganda

Introduction

Geospectrally decomposable, QuickBird, visible and near infrared(NIR) (www.digitalglobe.com), sub-meter (m) resolution (i.e., 0.61m), sub-mixel (i.e., mixed pixel), endmember (i.e., reference biosignature) fractions of incident radiation reflected, transmitted and absorbed by prolific, georeferenced, canopied, larval habitats of *Similium damnosum* s.l., a black fly vector of onchocerciasis, is crucial in implementing control strategies in African riverine environments [1]. Onchocerciasis is a parasitic disease caused by the filarial worm *Onchocerca volvulus* which is transmitted through the bites of infected blackflies of *Simulium* species (http://www.who.int/topics/onchocerciasis). For any given remotely sensed, georeferncable, logical

***Corresponding author:** Benjamin G. Jacob, 1Global Health Infectious Disease Research Program, Department of Global Health, University of South Florida, Tampa, Florida, USA, Tel: 813-974-9784; E-mail: bjacob1@health.usf.edu

Received June 04, 2015; **Accepted** December 26, 2015; **Published** December 28, 2015

Citation: Jacob BG, Novak RJ, Toe LD, Sanfo MS, Lassane K, et al. (2016) Ecogeographically and Non-Ecogeographically Forecasting Discontinuous Canopied *Simulium damnosum* s.l. Habitats by Interpolating Metrizable Sub-Mixel Mean Solar Exoatmospheric Quantum Scalar Irradiance where θ_i is a Zenith Angle and Diatomically Etiolated Xanthophylls with Azimutually Isotropic Sources of Chloroplastic Carotenoid Zeaxanthins Spectrally Extracted from a Decomposed RapidEye™ Red Edge Normalized Difference Vegetation Index Reference Biosignature: A Case Study in Burkina Faso and Uganda. J Remote Sensing & GIS 5: 152. doi:10.4172/2469-4134.1000152

material, the optical spectrum is a plot of fractionalized reflectance, emissivity transmittance, log-transformed as a function of the incident wavelength which makes it possible to identify different canopied, land use land cover (LULC geo-classified), classes and separate them by their endmember, spectral curves (http://fas.org/irp/imint/docs/rst/). Disturbances in empirically, decomposable, ecogeographical, processes or, time series dependent, vegetated canopied, LULC-oriented, biophysical attributes, for example of imaged, sub-meter resolution, shaded and sparsely-shaded regressively quantitatively, delineated, georeferncable, seasonally geosampled, *S. damnosum* s.l., riverine, larval habitat, covariate, parameter estimators (e.g., refractive fraction of leaf weight, leaf- and plant constituent spectra) can alter radiative interactions with the surface and, thus the amount of radiation-related, wavelenght, emissivities and transmittance received by a remote sensing detector [1,2].

The ability to unambiguously interpret time series, probabilistically regressed, geoclassified, vegetation-related, LULC, canopied, endmember, emissivity wavelenght derivative spectra and unmixed, decomposable, biogeochemical, photosynthetic, radiance estimates (e.g., foliar lignin) for a geosampled, georeferencable, shaded or sparsely-shaded, prolific, *S. damnosum* s.l., larval habitat may hinge directly on the ability to resolve the multitude of remotely sensed, riverine, ecohydrological, erroneous, wavelenght, transmittance co-factors (e.g atmospheric correction of at-sensor radiances and the consequent, uncertainties in a retrieved turbidity-related, reflectance, emissivity, parameterized estimator) in an ArcGIS cyberenvironment, *simulids* constitute important components of riverine ecosystems and breed in fast flowing highly oxygenated water [1]. Based on empirical work, a number of possible innovative algorithms in ArcGIS (e.g., Geospatial Analyst) may be employed for exploiting sub-mixel, canopy scale, photosynthetic responses for a geo-spatiotemporally, geosampled, seasonal, georeferencable, canopied, productive, *S. damnosum* s.l., riverine, larval habitat. The interpolatable decomposable data may be optimally determined by plotting isoclines yield in eco-geographical space of regressed canopy densities and light environment explanators. An isocline is a curve through points at which the simplest parent function's slope will always be the same, regardless of initial conditions [2,3]. Histograms in ArcGIS can be used to interpret the significance of an operationizable, unmixed dataset of prolific, riverine, larval habitat, seasonal, geo-spatiotemporally regressed, LULC, endmember changes induced as a response to an empiricial dataset of independent categorical variables representing decreases in the benthic light environment, for example, which may reveal Poissonized probabilities, for precisely quantitating seasonal ecogeographic, riverine predictors (productivity, disturbance rate, plant functional composition and species richness gradients) and non-ecogeographic (control of sub-mixel transitions in the composition of high-latitude, riverine, canopied vegetation endmembers during droughts, etc) against seasonal, geosampled, immature count. Quantitating the complex interplay between immature *Similium* productivity, physical and biotic disturbances, seasonal canopy plant functional composition and richness in an ArcGIS cyberenvironment may be vital for developing optimal control strategies. Regression information about spatial and temporal heterogeneities in seasonal productivity is key for designing effective vector entomological management programs [4].

Rational decision-making processes for the employment of resources currently for vector control of immature *Similium* include improving the efficacy, cost-effectiveness and bioecological soundness for sustainability (http://www.who.int/). Pursuing multivariate, regressive, probabilistic, quantitative, estimation algorithms in ArcGIS and object-based technology (e.g., ENVI technology) may aid in implementing control strategies for robustly, targeting, seasonally productive, *S. damnosum* s.l., larval habitats. Object based methods, aim to delineate readily usable objects from imagery while at the same time combining image processing and GIS functionalities in order to utilize spectral and contextual information in an integrative fashion (www.esri.com). Geospectrally unmixing, optimal, photosynthetic and non-photosynthetic (NPV), time series dependent, canopied explanators (e.g., trailing vegetation LULC-oriented, seasonal catchment variables such as slope coefficients) and quantizing the non-linearizable, canopied, covariate, parameter estimator, reflectance, wavelenght emissivities may reveal shaded and sparsely shaded, *S. damnosum* s.l.,larval habitat canopy Euclineanized distances between unmixed transmission spectrum of leaves and their light absorbing compounds (e.g chlorophylls, carotenoids, water, cellulose, lignin, starch, proteins, etc.). Autopredicted probabilities may reveal eco-epidemiological, regressed variables may then be quantitatively geospatially associated with imaged, seasonal, immature, blackfly, productivity. Geo-spatiotemporal, forecastable, Arc-GIS- derived, object-based classifiers may generate, risk maps capturing spatial foraging oviposition behavior for understanding canopy emissivities and seasonal shifts in terms of immature *Similium* productivity for implementing control strategies [e.g., Intergrated Vector Management (IVM)]. Rather than relying on a single method of vector control (e.g chemical spraying), IVM stresses the importance of first understanding the local vector ecology and local patterns of disease transmission, and then choosing the appropriate vector control tools from the range of options available (http://www.who.int/). It is remotely conceivable that environmental management interventions generated employing ArcGIS cyberenvironments and object-based technology [e.g., Spectral Angle Mapper (SAM) and Spectral Information Divergence (SID) classification algorithms] significantly lower immature seasonal *Similium* productivity and act as an incentive to enhance community participation and sustainability.

Optimally geospectrally decomposed, *S. damnsoum* s.l., riverine, larval habitat, sub-resolution, sub-mixel, canopy vegetation, LULC reflectance derivative, endmember, forecast spectra rendered in object-based technology may reveal a function of tissue (i.e. foliage clumping leaf, orientation) for controlling explanatorily interpolatable, geomorphologically disturbed landscape reflectance biosignatures. Viewing geometrically synthesized variables in ArcGIS cyberenvironments may be found to be seasonally, geospatially associated with hyper/hypo, immature, habitat productivity. Object-based technologies are technologies in which objects have encapsulation [2]. Object-based image analysis (OBIA), a technique employed to analyze digital imagery, was developed relatively recently compared to traditional, mixel-based, image analysis (http://wiki.landscapetoolbox.org/doku). Optical remote sensing has expanded from the use of panchromatic and multispectral sensors to off-nadir instruments and object-based classifers in ArcGIS [4]. While sub-mixel-based, endmember, image analysis is based on the reflectance emissivity and transmisstance information, OBIA is based on information from a set of similar image objects [2]. More specifically, in OBIA geospatial processing, optical solutions, image objects are groups of mixels that are similar to one another based on a measure of spectral properties (i.e., color, size, shape, and texture) as well as context from a ecogeographically parameterized neighborhood surrounding the mixels. Remote sensing LULC imagery for vector entomological investigations (e.g., vulnearbility, mapping hyperendemic and mesoendemic transmission zones) necessitates the captured wavelenght, emissivity data to be converted into tangible georeferncable field explanatorial information in ArcGIS. By so doing,the data may be utilized in conjunction with other seasonally, probabilistically, regressable, eco-epidemiological data (e.g., unmixed, shaded endmember, *S. damnosum* s.l., riverine, larval habitat, canopy, foliar nitrogen, reflectance emissity, transmittance) within a gridded autoregressive, weighted, matrix. As long as mixel sizes remain typically coarser than, or at the best, similar in size to the entomological objects (e.g.,imaged prolific, canopied, *S. damnosum* s.l., riverine habitat) of interest, emphasis may be placed on per-mixel analysis, or even sub-mixel analysis in OBIA for this conversion, but with increasing spatial resolutions alternative paths may require deriving disturbed objects that are made up of several mixels. In contrast to typical Landsat resolutions, moderate and high resolution images in ArcGIS cyberenvironments support several scales within their images (www.esri.com).

Through a comprehensive literature review several thousand abstracts have been screened, and more than 820 OBIA-related articles comprising 145 journal papers, 84 book chapters and nearly 600 conference papers, have been scrutinized in detail [4]. It becomes evident that the first years of the OBIA/geospatial object based image analysis (GEOBIA) developments were characterized by the dominance of 'grey' literature, but that the number of peer-reviewed journal articles has increased sharply over the last four to five years (e.g 1). The mixel paradigm is beginning to dissolve and the OBIA methods are making considerable progress towards a spatially explicit information extraction workflow, such as is required for optimal spatial planning as well as for many environmental monitoring programs (e.g.,IVM) for vector entomology. OBIA builds on older segmentation, edge-detection, feature extraction and classification concepts employed in remote sensing. Image segmentation in OBIA, from an algorithmic perspective is generally divided into four categories: (a) point-based, (b) edge-based, (c) region-based and (d) combined (www.esri.com). Segments have additional geospectral information compared to single mixels (e.g. mean values per band, and also median values, minimum and maximum values, mean ratios, variance etc.) (http://www.exelisvis.com/docs). The primary advantage of OBIA offers other than the diversification of explanatorial, time series, geospectral value descriptions of geosampled, geospatial objects in Cloud technology, is the additional band information for precise, georeferencable, forecast, eco-epidemiological, eco-innovational, seasonal vulnerability, risk mapping of decomposable objects of interest (e.g georeferncable, seasonally flooded, *S. damnosum* s.l. riverine larval habitats).

By sequentially, algorithmically, unmixing, productive, georeferencable, geosampled, *S. damnosum* s.l., larval habitat, canopy, photosynthesizing organs with their seasonal illumination conditions in riverine, LULC, ecogeograhically and non-ecogeographically classified scenes, in, an OBIA, [e.g., ENVI Feature Extraction Module (ENVI FX] may be optimally iteratively quantitated with the habitat's respective wavelength reflection proportions which may then be subsequently regressed in an ArcGIS cyberenvironment against seasonal habitat productivity count values. By so doing, robust, forecasting, vulnerability eco-epidmiological, risk maps may be generated. Photosynthesizing organs significantly affect important planetary biogeochemical cycles [2]. Cartographically quantizing, time series dependent, ecogeographiclly and non-ecogeographically, explanatorial, time series dependent, probabilistic relationships between canopy shaded riverine, larval habitat, immature, seasonal productivity with leaf optical characteristics and plant biochemical properties may establish seasonal changes in oviposition behavior response to leaf aging or environmental stresses (e.g., droughts). Mature canopy leaves of a seasonally imaged georefernced, productive canopied, *S. damnosum* s.l., riverine, immature habitat may tend to have reduced chlorophyll content during specific sample frames (e.g., dry season), which in turn, may increase both the reflectance and transmittance in the visible spectrum when geospatially, correlating, immature, seasonal productivity with decomposed, endmember, wavelength spectrum. Since leaf intrinsic scattering properties reveal very little explanatorial, geospectral variation, leaf optical properties of a geo-spatiotemporally, geosampled, shaded and non-shaded, prolific, decomposed, *S. damnosum* s.l., riverine, larval habitat in an ENVI model may be seasonally related to their canopy absorption properties based on larval productivity. As such, vulnerability time series, forecastable, vulnerability, transmission-oriented, endemic, risk maps may be parsimoniously generated in ArcGIS for implementing targeted environmental management (IVM) based on a sound understanding of the seasonal heterogeneity in immature, riverine, *Similium* productivity.

Imaging spectrometry is a unique type of optical remote sensing as the surface, canopy, LULC radiance transmittance is geosampled incontiguous, narrow spectral bands. Narrow spectral bands can measure many individual emissitivty absorption features of interest to entomologists or experimenters such as pigment composition and content, canopy water content, canopy dry plant litter (i.e., senesced leaves and stems), or wood and other aspects of foliar chemistry. This unmixed OBIA data may then be subsequently geospatially attached to georefernced, shade canopied, *Similium* habitat, eco-epidemiological data in ArcGIS to determine hyper/hypo seasonal, productive habitat geolocations. Many contributions in GIS literature have applied similar tactics in other disciplines. For example, in Suplick-Ploense et al. [3] narrow-band canopy spectral reflectance within 400 to 1100 nm was employed for imaging different canopied LULC, turf grass species and cultivars under drought stress. Sods of four Bermuda grasses (*Cynodon dactylon* L. × *C. transvaalensis)*, three seashore paspalums (*Paspalum vaginatum* Swartz), Zoysiagrass (*Zoysia japonica*), and St. Augustine grass (*Stenotaphrum secundatum*), and three seeded tall fescues (*Festuca arundinacea LULCs*) were geospectrally evaluated. Turf quality decreased 12% to 27% and leaf firing increased 12% to 55% in 12 canopied grasses in response to drought stress imposed over three dry-down cycles. The peak correlations occurred at 673 to 693 nm and 667 to 687 nm for quantitatively regressing, geospectrally decomposing quality and leaf firing in Bermuda grasse-related, canopied, LULC variables, respectively.

All three tall fescues had the strongest correlation at 671 nm for both canopy turf quality and leaf firing. The highest correlations in the NIR at 750, 775, or 870 nm were found in three seashore paspalums, while at 687 to 693 nm, the transmittance emmisivities were reflected by Zoysiagrass and St. Augustine grass LULC. Although all the canopied grass LULCs exhibited some correlations between the geosampled, regressed, covariate, parameter estimators and turf quality or leaf firing, significant correlation coefficients were only observed in five grasses. Multivariate regression models based on selected canopy wavelengths for turf quality and leaf firing were observed for 7 turf quality and 9 leaf firing grasses in ENVI. Wavelengths in the photosynthetic region at 658 to 700 nm and NIR from 700 to 800nm predominated in the canopy LULC models of most grasses. This experiment proved that turf quality and leaf firing may be well forecasted in tall fescue by employing remotely sensed, time series dependent, explanatorial, forecastable, canopy optical, eco-epidemiological, risk models, evidenced by a coefficient of determination (R^2) above 0.50. The results indicated that correlations of canopy leaf reflectance versus turf quality and leaf firing varied with turf grass species and cultivars, and photosynthetic regions specifically from 664 to 687nm which were relatively important in robustly optically regressively quantitating turf quality and leaf firing in selected canopied Bermuda grass, tall fescue, Zoysiagrass and St. Augustine grass LULCs under drought stress.

Regressed, experimental, remotely sensed measurements of canopied, LULC, explanatorial, leaf optical properties in ArcGIS has progressed in GIS literature. Multiple, deterministic approaches based on diverse representations of light interactions with canopy plant leaves have been developed in ArcGIS [2]. These models are distinguished by the underlying physics and by their ability to map geometerical complexities of the leaf. In these optical models, individually decomposed cells may be described in detail by their shape, size, position, and biochemical content. The simplest, unmixing, ArcGIS, sequential algorithms can even consider the blade as a single scattering and absorbing layer. At a minimum, these physically realistic models can render precise information about the refractive index and the specific geo-spatiotemporal, eco-hydrological, absorption coefficients of the decomposed, canopied, leaf constituents. Canopy height, topography and the vertical distribution of canopy elements may be optimally derived. Generalized linear and additive models, as well as binary hierarchical regression trees may be constructed in ArcGIS which may reveal that the absorption spectrum of geospectrally, unmixed, geosampled, remotely quantized canopy chlorophyll can expand over the entire visible region from 400 nm to 750 nm, with a minimum at 550 nm, for example. The absorption spectrum of canopy water starts at wavelengths longer than 950 nm, with three main absorption peaks [4]. The absorption spectrum of a geospectrally derived, georeferencable, prolific, flooded, riverine, *S. damnosum* s.l. larval habitat canopy leaf dry matter may be minimal (~<0.1,) in the visible and NIR, and stronger at wavelengths longer than 1100 nm, for example. Spectral analogies may be however observed between sub-mixed, resolution wavelengths for which the optical properties (i.e., absorption, reflectance, or transmittance) of the canopied elements are similar. Green plants show the full range of variation of canopy leaf optical properties [2]. The relationship between canopy reflectance and leaf reflectance LULC measured in ArcGIS concurrently over a georeferencable, seasonally geosampled, riverine, productive, riverine, larval habitat could simulate canopy reflectance over the whole domain from leaf reflectance spectra measured over the whole spectral domain. These results may reveal that remotely quantized, seasonal, canopy, spectral analogies of immature *Similium* riverine habitat emissivity transmittance allows accurate reconstruction of the canopy reflectance endmember spectra in ENVI. Explicit assumptions about the very low spectral variation of leaf intrinsic scattering properties may be thus indirectly justifiable for a geo-spatiotemporal, geosampled, seasonally imaged, productive shade, canopied, georeferencable, *S. damnosum* s.l. riverine larval habitat interpolation-oriented , eco-epidemiological, forecasting,ArcGIS -derived risk model.

Jacob et al. [1] geospectrally regressively quantized the sensitivity of canopy reflectance (ρ_c) to QuickBird imaged leaf optical properties of a geosampled, shade, canopied, *S. damnosum s.l.* riverine, larval habitat in Togo. The authors investigated, concurrent, unmixed, regressively quantitated, leaf reflectance variations of the habitat canopy employing ($\partial\rho_c/\partial\lambda$) and ($\partial\rho l/\partial\lambda$): $\partial\rho c/\partial\rho l = (\partial\rho c/\partial\lambda)\ (\partial\rho l/\partial\lambda)^{-1}$ in ArcGIS. The canopied, image endmembers of the georeferenced, riverine habitat and its associated environmental attributes were extracted from ENVI®'s spectral library. Several spectra corresponding to the different backgrounds in the geosampled *S. damnosum s.l.* habitat (i.e., pre-Cambrian rock and spectral riffled water mixel components) had to be included since multiple diffuse scatterings between floating canopy leaves in the habitat, for example, and a bright soil background increased the NIR reflectance. Sub-meter resolution class representative mixels were then selected and compared to a reference training dataset. During the segmentation procedure, image objects were generated based on several adjustable criteria of homogeneity such as colour, shape, and texture.

Data pre-processing involved converting Digital Number (DN) values to radiance atmospheric correction employing fast-line-sight-atmospheric-analysis-spectral hypercubes (FLAASH™) and co-registration techniques. FLAASH™ is a first-principles atmospheric correction tool that corrects wavelengths in the visible through NIR and shortwave infrared regions, up to 3 µm (www.itvis.com). Image classification was conducted using the object-oriented approach. FLAASH™ generated a model (i.e., gmd file) that was subsequently converted to the image's DN to at-sensor radiance and computed at-sensor reflectance which was normalized thereafter employing

$$\rho BandN = \frac{\Pi(LbandN \rightarrow GainBandN + BiasBandN) \rightarrow D^2}{EBandN \rightarrow \left(Cos(90-\theta) \rightarrow \dfrac{\pi}{180} \right)}$$ where,

$_{\text{Band N}}$ was the reflectance for Band N, L_{bandN} was the DN for Band N, D was the normalized earth-sun distance and E_{bandN} was the solar elevation angle. The estimated accuracy for the explanatorily, geospectrally, extracted data was then optimally calculated:

$$P\left\{ -Z_{\frac{\alpha}{2}} < \frac{x-n\theta}{\sqrt{n\theta(1-\theta)}} < Z_{\frac{\alpha}{2}} \right\} = 1-\alpha$$ where, x=number of correct identified mixels, n=total number of mixels in the sample, θ=was the classifier identified *S. damnosum s.l.* habitat and the habitat's geospatially associated pre-Cambrian rock and riffle water which was remotely regressively quantized not larger than 0.4 ha. The model revealed satisfactory results (92.1%) with a lower detection limit of 0.1 ha. However, the authors found that this expression was strictly valid only when the habitat canopy optical properties of the soil background LULC endmember elements were either geospectrally flat or did not contribute significantly to reflectance.

Leaf structure and function are shown to result in distinctive variations in the absorption and reflection of solar radiation from plant canopies [4]. The leaf properties that determine the radiation-interception characteristics of geo-spatiotemporally imaged, shade, canopied, prolific, *S. damnosum* s.l. riverine geosampled, and larval habitat canopies may be directly linked to photosynthesis, stomatal resistance and evapotranspiration which may be inferred from measurements of reflected solar energy. The effects of off-nadir viewing and atmospheric constituents, coupled with the need to measure changing canopy vegetated, LULC-oriented, surface conditions may emphasize the need for multitemporal measurements of reflected radiation if seasonal immature *Similium* production is to be estimated. ArcGIS simulations employing time series dependent, canopy geo-spatiotemporal, endmember, risk-related, forecasting, eco-epidemiological models may demonstrate that the sensitivity of canopy reflectance to leaf reflectance is significant for large vegetation covered LULC, radiance fractions in geospectral domains where absorption is low in a canopied, seasonlly prolific, *S. damnosums*. l., larval habitat. In these conditions, multiple scattering may enhance the canopy leaf absorption features od the habitat in ArcGIS.

To override the limitations of propagational, reflectance emissitity, transmittance, probabilistic uncertainties in the descriptors canopy architecture, ArcGIS simulations may be conducted on the experimental data. Concurrent canopy and leaf reflectance spectra may be measured for a range of seasonally productive riverine canopies. The results may reveal good agreement with other ecohydrological-related, canopied species habitats and their theoretical findings. Conclusions may be drawn about the applicability of these findings, with particular attention to the potential detectability of leaf biochemical composition from unmixed, regressed canopy vegetative, LULC reflectance sensed from eco- geographic and non-ecographic space for targeting unsampled, unknown seasaonlly productive riverine habitats.

Seasonally shaded NPV such as standing litter may disproportionately affect qualitatively regressively quantitating, shaded, discontinuous, georeferenced, *S. damnosum* s.l.-related, riverine, hyperproductive, immature habitats. Mapping ecogeographical canopy radiation fields and their bidirectional radiance transmittance in ArcGIS may be an effective way to remotely, geo-spectrally, explanatorily quantize, canopy density by dividing the canopy LULCs into many small equal-sized units through rasterization, Therefater by comparing the number of aboveground returns to the total number of lidar returns, for example, unmixed, canopy vegetated, LULC reflectance may be seasaonlly quantiated with immature seasonal, Similium productivity. In ArcGIS multiple LULCs may be geo-classified. Examples include grasslands, shrublands, savannas, and open woodlands, LULCs which collectively cover over many African arid and semi-arid riverine environments. NPV may be then defined in ArcGIS cyberenvironments as dead or simply dormant, canopy vegetated LULC, geospatial, geospectral objects (e.g grasses between rainfalls surrounding a georefernced, productive, *S. damnosum* s.l., ecohydrological, riverine habitat), for example. Plant material lacking chlorophyll are also referred to as NPV which include materials such as dry leaf matter (e.g., dry grass and litter) [4]. Also included in the NPV category for categorizing the decomposed riverine habitat data in an OBIA may be woody structures including stems, and branches in the canopy.

The presence of NPV in an empirical datset of non-linear, explanatorily decomposable, canopy endmembers, NPV biosignatures can be geospatially optically quantized and geospectrally associated with NIR transmission and scattering of green, vegetation, LULC reflectance. If the canopied LULC radiance is unquantated in a forecasting, explanatory, regression-related, eco-epidemiological, risk model, the residual forecasts of important georeferncable, riverine, *S. damnosum* s.l., larval habitat, NPV covariate, time series, reflectance, emissivity transmitatnce, parameter estimators may be susceptible to large sources of error and probabilistic uncertainties especially over canopied explanators representing atmospheric conditions. Further, in many canopies, much of the NPV is obscured below a potentially closed leaf canopy; thus the wavelengths employed to measure NPV (e.g., shortwave infrared) may be unable to penetrate through the upper canopy to interact with this NPV.

When exposed, NPV scatters photons very efficiently in the shortwave infrared (IR) range, in direct contrast to green vegetation which absorbs strongly in the shortwave IR range [4]. As such, only exposed NPV on a geosampled, explanatorial, georeferenced, *S. damnosum* s.l., riverine, larval habitats will have a significant effect on geospectral, eco-epidemiological, ecohydrological reflectance as emitted from riverine, canopy, vegetated LULCs. In general, photons in the visible wavelength region are efficiently absorbed by live, green canopy vegetation LULCs. Likewise, photons in the SWIR-2 region of the spectrum are efficiently absorbed by water. In contrast to live vegetation, dead, dry, or senescent canopy vegetation scatters photons very efficiently throughout the spectrum, with most scattering occurring in the SWIR-1 and SWIR-2 ranges. Models of canopy gross photosynthesis generally incorporate a description of light interception and attenuation through the canopy and of single leaf gross photosynthesis in response to irradiance, or photon flux density. These illumination variables are then combined to give the rate of canopy gross photosynthesis [4].

The description of canopy photosynthesis and respiration lies at the core of most biophysical simulation models in ArcGIS. These models may be catalyzed by acclimatory responses of protein, including photosynthetic enzymes, to environmental conditions of light, temperature and CO_2 during growth, as this will affect the rate of photosynthesis demand in a geo-spatiotemporally, geosampled, *S. damnosum* s.l., riverine, larval habitat. Models may be presented that have been several developments since then with different degrees of complexity. ArcGIS models may consider homogeneous light distribution through a geo-spatiotemporally, geosampled, *S. damnosum* s.l. larval habitat canopy, while later developments may separate it into direct and diffuse beams, and include other factors such as the movement of the sun across the sky in a African riverine environment. For leaf photosynthesis, early models had a fixed light response curve for photosynthesis while later models include variation in leaf nitrogen through the canopy [2]. Most descriptions of leaf photosynthesis in canopy photosynthesis models are based on the non-rectangular hyperbola, which is a versatile semi-empirical approach for describing the light response for leaf photosynthesis [4]. Whereas the initial focus may be to explore the influence of light interception and attenuation on canopy leaf photosynthesis in ArcGIS as it influences canopy photosynthesis, later models may address issues such as the importance of diurnal variation in irradiance and temperature of the riveine habitat canopy.

It is well established that the photosynthetic potential of canopy leaves is influenced by the environment in which they are grown, including irradiance, temperature, nitrogen availability and CO_2 concentration. The inclusion of acclimation into canopy photosynthesis models has generally focused on the acclimation of photosynthetic potential to light and its subsequent variation through the depth of the canopy [4]. Charles-Edwards (1981) assumed that the light-saturated, leaf, photosynthetic potential for leaves within the canopy may be proportional to the attenuation of light at that position in the canopy. This has been applied widely in literature. A fixed quantity of canopy foilar for example, within a geo-spatiotemporally, geosampled, *S. damnosum* s.l., riverine habitat canopy may be optimally, cartographically delineated by seeking an optimum distribution such that canopy photosynthesis variables are maximized, employing a similar expression to Charles-Edwards' assumption theoretically. Canopy foliar biomass defined as the product of leaf dry matter content and leaf area index, is an important measurement for global biogeochemical cycles.

The change in geospectral explanatorial, unmixed LULC reflectance due to increasing amounts of NPV may be captured in OBIA. The absorbing and scattering properties of a geo-spatiotemporal, geosampled, *S. damnosum* s.l., seasonal, riverine, larval habitat, discontinous NPV covariate, parameter estimator reflectance, emitted transmittance may be then defined by their chemical bonds of NPVs and by their three- dimensional (3-D) structure in ArcGIS. In ArcMap, 3D Analyst new surfaces may be created from GIS data for analyzing canopy negative LULC surfaces by querying attribute values at a geolocation on the surface, for analyzing the visibility of parts of the surface from different landscape geolocations (www.esri.com). As such, an entomologist or experimenter could optimally determine total, shaded, and non-shaded, vegetated LULC, geometerical, explanatorial, surface area and the volume above *S. damnosum* s.l., seasonal, riverine, larval habitat-related or below the LULC surface, for example, while simultaneously generating profiles along a 3D line on the surface.

High spatial resolution, 3-D, measurements of canopy vegetation LULC by remote sensing are advancing ecological research and environmental management. However, substantial logistical costs limit this application, especially for observing phenological dynamics in riverine ecosystem structures and remotely diagnosing, time series, canopy, spectral traits of a decomposable, productive, shade canopied, riverine, productive, *S. damnosum* s.l., larval habitat. Recently a new aerial remote sensing system enabling routine and inexpensive aerial 3D measurements of canopy structure and geospectral attributes, with properties similar to those of lidar, but with red-green-blue (RGB) geospectral attributes for each canopied point, enabled high frequency observations within a single growing season. This "Ecosynth" methodology applied photogrammetric "Structure from Motion" computer vision algorithms to a large empirical dataset of highly overlapping low altitude (< 130 m) aerial photographs acquired employing off-the-shelf digital cameras mounted on an inexpensive, lightweight, hobbyist-grade, unmanned aerial system (UAS). Ecosynth 3D point clouds with densities of 30–67 points m^{-2} were rendered using commercial computer vision software from digital photographs acquired repeatedly by UAS over three 6.25 ha (250 m × 250 m) temperate, LULC, Deciduous forest, LULC sites in Maryland USA.

Ecosynth point clouds were georeferenced with a precision of 1.2–4.1 m horizontal, radial, root mean square error (RMSE) and 0.4–1.2 m vertical RMSE. Understory digital terrain models (DTMs) and canopy height models (CHMs) were generated from leaf-on and leaf-off point clouds in ArcGIS using procedures commonly applied to lidar point clouds. At two sites, Ecosynth CHMs were strong predictors of field-measured tree heights (R^2s of 0.63 to 0.84) and were highly correlated with a lidar CHM (R^2 of 0.87) acquired 4 days earlier, though Ecosynth-based estimates of aboveground biomass densities which included significant errors (31-36% of field-based estimates). Repeated scanning of a 50 m × 50 m forested area at six different times across a 16 month period revealed ecogeographically significant dynamics in canopy color at different heights and a structural shift upward in canopy density, as demonstrated by changes in vertical height profiles of point density and relative RGB brightness. Changes in canopy relative greenness were highly correlated (R^2=0.87) with the regressed, MODIS, time series data for the same area and vertical differences in canopy color revealed the early green up of the dominant canopy species, *Liriodendron tulipifera*, which subsequently revealed strong evidence that Ecosynth time series measurements can capture vegetation-oriented, LULC, structural and spectral, phenological dynamics at the spatial scale of individual trees. The ability to observe canopy phenology in 3D may represent a breakthrough in imaging seasonal riverine, canopy shaded *S. damnosum* s.l. larval habitat ecohydrological processes. Inexpensive user-deployed technologies for multispectral 3D scanning of vegetation at landscape scales (< 1 km^2) heralds a new era of participatory remote sensing by field ecologists, community foresters and the interested public [4].

Quantitative regressive estimation of fractional canopy cover of NPV and bare soil geoclassified, LULC in ArcGIS and an OBIA classifier may be critical for natural resource management and for seasonally modeling carbon dynamics in a geo-spatiotemporally, geosampled, decomposable, seasonally productive, georeferencable, *S. damnosum* s.l. riverine larval habitat endmember, and eco-epidemiological, forecasting risk model. Despite the widely recognized importance of accumulated carbon storage in-canopied ecosystems, (e.g geospatial cluster of highly productive, georefernced, shaded, *S. damnosum* s.l. larval habitats in an African meandering riverine pathway), geospectral explicit, real-time, mapping and monitoring of carbon stocks in these habitats have remained a challenge due to excessive heterogeneity of green canopy, vegetation-oriented LULC, unmixed endmembers, diffusion and ubiquitous patterns of LULC and inexact, geospectral unmixing technologies. Regional, high resolution, probabilistic, regression-related, eco-epidemiological, forecast, risk mapping of LULC canopied vegetation cover and biomass in ArcGIS and in OBIA may be central to qualitatively remotely regressively quantitating terrestrial carbon cycles in a flooded, georefernced, seasonally prolific, riverine, larval habitat, for example, especially in the context of canopy carbon management. In the context of terrestrial, seasonal, carbon sink mechanisms, the potential role played by decomposable, georeferencable, LULC, time series, regressable, parameter estimator reflectance, emissity transmissitance, covariate coefficient, wavelenght, empirical values may be stressed in an ArcGIS geodatabase to remotely, qualitatively, geospectrally quantitate, extractable photosynthetic and NPV variables for enhancing mapping processes driven by canopy cover [2]. A carbon sink is a natural or artificial reservoir that accumulates and stores some carbon-containing chemical compound for an indefinite period [4]. The process by which carbon sinks remove carbon dioxide (CO_2) from the atmosphere is known as carbon sequestration [2].

Carbon sequestration is the process of capturing long-term storage of atmospheric CO_2 and may refer specifically to the process of removing carbon from the atmosphere and depositing it in a reservoir (e.g., a discontinous canopy gap in a geosampled, seasonally productive, georeferenced, riverine, shaded, *S. damnosum* s.l larval habitat). When carried out deliberately in ArcGIS, this process may also be referred to as carbon dioxide removal, which is common in geoengineering disciplines. Carbon capture and storage occurs, where carbon dioxide is removed from flue gases (e.g discontinous riverine canopy vegetation LULC readings at power stations) before being stored in underground reservoirs. Natural biogeochemical cycling of carbon between the atmosphere and reservoirs, such as by chemical weathering of rocks may be remotely captured in time series LULC change analyses in ArcGIS (www.esri.ccom). Jacob et al. [1] decomposed a 0.61 m reflectance signal emitted from a weathered, pre-Cambrian rock, georeferenced, *S. damnosum s.l.* riverine, larval habitat, biosignature by establishing the sensitivity and dynamic ranges of a 3-D, canopy-oriented, radiative model, for field verifying a ArcGIS constructed stochastically forecasted, eco-epidemiological, vulnerability, risk map generated by unmixed canopied, endmember spectra.

Nitrogen fixing shrub *Dichrostachys cinerea* in a mesic savanna in Zambia was recently unmixed and was remotely qualitatively regressively quantitated for delineating pools in ArcGIS of soil nitrogen phosphrous and carbon availabilities [4]. The authors evaluated whether these effects induced feedbacks upon the growth of understory vegetation and encroaching shrubs. *Dichrostachys cinerea* shrubs increased total nitrogen and phosphrous pools, as well as resin-absorbed nitrogen and soil extractable phosphorous in the top 10-cm soil. Shrubs and understory grasses differed in their foliar nitrogen and phosphrous concentrations along gradients of increasing encroachment, suggesting that the eco-graphically imaged grassland LULCs obtained nutrients in different ways. Thus, the authors assumed that the grasses probably were obtained mainly from the surface upper soil layers, whereas the shrubs may have acquired nitrogen through symbiotic fixation to obtain phosprous from deeper soil layers. The storage of soil carbon increased significantly under *D. cinerea* in the ArcGIS model and was apparently not limited by shortages of either nitrogen or phosphorous. The authors concluded that the shrub *D. cinerea* did not create a negative feedback loop by inducing phosphorous-limiting conditions, probably because they obtained phosphrous from deeper soil layers. Further, carbon sequestration was found not to be limited by a shortage of nitrogen, so that mesic savanna encroached by the species could represent a carbon sink for several decades. As such, a geospectrally decomposed, derivative, spectroscopic, biosignature, endmember, woody encroachment, reflectance, covariate, time series dependent, geosampled, parameter estimator may be regressively, qualitatively quantitated in ArcGIS for representing nitrogen stocks and foliage in a geospatiotemporally, moderate to high resolution, imaged, seasonally productive, geosampled, *S. damnosum s.l.*, riverine habitat.

Canopy nitrogen provides a measure of nitrogen concentration of remotely sensed foliage [2]. Reflectance measurements in the shortwave infrared range measures relative amounts of nitrogen contained in vegetation canopies [4]. Reflectance at 1510 nm is largely determined by nitrogen concentration of leaves, as well as the overall foliage biomass of the canopy (www.esri.com). Together, leaf nitrogen concentration and canopy foliar biomass may be combined in the 1510 nm range to predict total canopy nitrogen content in a geo-spatiotemporally, geosampled, seasonally productive, *S. damnosum* s.l., riverine, larval habitat. The tabulated riverine habitat canopy nitrogen content may be compared to a reference reflectance at 1680 nm, which should optimally contain a similar signal due to foliar biomass, but without the influence of nitrogen absorption. Regressively quantitated eco-geographically, geo-spatiotemporally, cartographic relationships between delineated, geospatial canopy decomposed, endmember, nitrogen and other ecohydrological, time series dependent, photosynthetic and NPV explanatorial, time series dependent, empirically geosampled, eco-physiological, predictor variables (e.g., nuclearized distance between canopy twigs) may help forecast seasonally high immature *Similium* seasonal productivity.

The presence of NPV, and nonlinear geopectral unmixed regressors with NIR transmission and multiple canopy isotropic scattering by green vegetation LULC reflectance can complicate the seasonal interpretation of remotely sensed, geo-spatiotemporally, geosampled, *S. damnosum* s.l., riverine, larval habitat, empirical predictor variables as spectral mixtures. Spectral mixtures that include green, canopy, LULC vegetation has the potential of being non-linear due to transmissance and scattering of NIR light by canopy green leaves and the high spectral contrast between red and NIR of the leaves [4]. Transmission by canopy leaves of a geospatiotemporally, geosampled shaded, *S. damnosum* s.l., georeferncable, riverine, larval habitat can lead to multiple scattering and nonlinear mixing. As such, a linear ArcGIS model applied to spectral mixtures of canopy,vegetation-oriented, geoclassified LULC and soils of a prolific, flooded, riverine habitat and shaded empirical geosampled datasets of seasonally parameter estimator, reflectance, emissivity, transmittance wavelengtht covariates may overestimate the fraction of green vegetation in an endmember biosignature while underestimating the shade-related, LULC, explanatorial predictors. Further, the residualized error probabilities in the regression estimates of predictors ecogeographically georepresenting high reflection vegetated, LULC canopied surface, log-transformed, explanatorial, predictor variables (e.g., soil fraction radiance) may be mispecified (deflated pseudo R^2 values) depending on the spectral shape of the soil. While the horizontal extent of covers can be adequately quantized from a linear mixing perspective, the interaction of photons with vegetation LULC explanatorial components in vertical space is known to be highly nonlinear [4].

Among various linear approaches, only ray tracing techniques has to as be shown to account for the complexity of internal leaf structure as it appears in a photomicrograph. They require however a detailed description of individual cells and their unique arrangement inside tissues. The optical constants of canopied leaf materials (cell walls, cytoplasm, pigments, air cavities, etc.) may be then be defined in an unmixed, endmember, canopied, unmixed, interpolated biosignature of moderate to high resolution imaged, highly productive riverine, *S. damnosum* s.l habitat. Using the laws of reflection, refraction, and absorption, the model may be able to simulate the propagation of individual photons incident on the canopy leaf surface. Unfortunately if a non-sufficient number of rays are simulated, statistically valid linearizable, endmember estimates of the radiation transfer in a seasonally geosampled, *S. damnosum* s.l. canopy leaf may not be deduced.

The degree of nonlinearity in empirically geosampled, seasonally productive, georeferncable, canopy shaded, *S. damnosum* s.l., riverine, larval habitat varies depending on soil reflectance and leaf transmittance reflectance [1]. Nonlinearity in volumetric (e.g ArcGIS, sub-resolution, delineated canopies with increasing leaf area) makes it extremely difficult to study the role of tissue and structural attributes that determine canopy and landscape radiative characteristics using field measurements based on illumination conditions, and viewing geometry alone. Nonlinear imaging-spectrometeric data increases with an increase in leaf transmittance or an increase in background [4]. Thus, a geospectral, geospatial, time series dependent, forecast, eco-epidemiological, risk model, forecast analyses based solely on non-linear, explanatorial, estimation model outputs without direct connection to field-measurable, regressable seasonal, canopied quantities (i.e immature productivity) can lead to erroneous conclusions since the realistic wavelength range of the model time series dependent, covariate parameter estimator values would not be known.

Unmixed, fractionalized, canopy radiance wavelength spectra in ArcGIS can be parsimoniously geo-spatiotemporally, regressively, quantitated in geographic space (e.g autocorrelation) to determine clustering tendencies in non-linearly dependent, seasonal, transmission-oriented, hyperendemic, explanatorial, biophysical canopy-related, endmember, covariate, parameter estimator interactions (e.g trailing vegetation and immature *Similium* production) during specific sample frames (e.g flooding) in an African riverine ecosystem [1]. Spatial autocorrelation may arise from common geosampled variables (e.g., operationizable, datasets of georeferencable, empirically regressable, productive shaded and non-shaded, *S. damnosum* s.l. larval habitat populations) and their seasonal, measures of geospectrally extracted canopied endmember attributable variability associated with geolocations or from direct quantitated Eucleandized interaction between geolocations (Griffith 2003). Orthogonal eigenvectors can have an impact on significance levels on creating detectable differences in non-probabilistic, attribute measures [2]. These impacts motivated Clifford, Richardson, and Hémon (1989) to apply the phrase "effective degrees of freedom"—the equivalent number of degrees of freedom for geospatially unautocorrelated (i.e., independent) observations, for exploiting redundant or pseudo-duplicated information contained in georeferenced empirical covariate, parameter estimator datasets due to the relative aggregated geolocations of clustered observations [e.g., negative autocorrelation (i.e., dissimiliar attributes amassed in ecogeographic space)] representing mapped georefernced, *S. damnosum* s.l. riverine, larval habitat photosynthetic and NPV geospecified regressors]. The duplicate information in question in an empirical geosampled dataset of vector entomological, time series dependent, covariate, parameter estimators may arise from probabilistically regressively quantitated LULC trends induced by common variables or from information sharing resulting from spatial interaction (e.g., canopied, ecogeographic diffusion) [4].

As spatial autocorrelation latent in georeferenced data increases, the amount of duplicate information contained in geo-spatiotemporally regressively delineated, canopied, S. damnosum s.l habitat data also increases [2]. This property suggests invoking the research question asking what the optimal, number of independent, *S. damnosum* s.l. riverine, larval habitat, photosynthetic and NPV geo-specified, seasonal, georeferencable, explanatorial, field and remote-specified observations, (i.e. *n*) is, that is equivalent to the sample size, *n*. This is the notion of effective sample size. Intuitively speaking, when zero spatial autocorrelation prevails, n*=n; when perfect positive spatial autocorrelation prevails in a univariate regional mean problem, n*=1. Equations may be then ecogeographically cartographically presented in ArcGIS for estimating n* based on the sampling distribution of a sample mean or sample correlation coefficient with the goal of obtaining some predetermined level of precision, employing the following spatial statistical model specifications: (1) simultaneous autoregressive, (2) geostatistical semivariogram, and (3) spatial filter [4]. These equations may be then evaluated with endmember simulation experiments which may be illustrated with selected empirical examples found in GIS literature for remotely analyzing decomposable, seasonal, *S. damnosum* s.l. riverine, canopied, sub-mixel reflectance, emissivity, transmittance data, feature attributes. In contrast to multispectral sensors, imaging spectroscopy can render probabilistically uncertainty-oriented, regressively quantitated, estimates of canopy absorption [4] which may be employed to precisely, elucidate, non-linear, autocorrelations in regressively quantized, seasonal relationships of, immature, *S. damnosum* s.l., larval habitat, ArcGIS delineated, covariate, parameter estimators based on specific, geosampled, riverine, canopied vegetated, geoclassified, explanatorial, LULC surfaces [3].

The terrestrial component of unmixed, probabilistically regressed, geosampled, georeferncable, seasonally, cartographically delineated, *S. damnosum* s.l. riverine, larval habitat canopy response variables can addresses the physics of energy and riverine water exchanges at the land surface. In Jacob et al. [1] for example, initially, an unmixing successive progressive algorithm (SPA) in ArcGIS parsimoniously extracted a dataset of geospectrally, geo-spatiotemporal, sub-mixel, canopy shaded, non-shaded endmembers from a QuickBird imaged, rendered, georeferenced, *S. damnosum* s.l., riverine, larval habitat scene, based on field-geosampled, eco-epidemiological count data. SPA builds on the convex geometry endmember search algorithms by including a constraint on the spatial adjacency of endmember candidate mixels, whereby reduction of the susceptibility to outlier mixels occurs when generating realistic canopied endmembers [2]. The task of geolocating decomposable, canopied, larval habitat, geospectral, canopy endmembers was actually associated with the identification of the simplex vertices, in eco-geographic regression space was the foundation for the time series geometric interpretation of the sub-meter resolution, imaged, riverine, larval habitat, sub-mixel, geosampled, eco-epidemiological data in the extraction algebraic algorithm. These georeferencable, unmixed explanatorial, sub-mixel, data attributes was analyzed based on convex rectilinear or curvilinear covariate, parameter estimators optimally devised in an ENVI module.

Many geoprocessing workflows were then employed to run specific operations employing the decomposed, shade, canopied, *S. damnosum* s.l., riverine, larval habitat empirical biosignature coordinates and geometrical information in ArcGIS API Javascript. The process created new, temporary, canopy LULC, explanatorial, data feature classes (trailing vegetation, sedge etc.). Geometrical objects can be used in ArcGIS for both input and output residual forecasting to make geoprocessing simpler (www.esri.com). The geometerical, endmember, geospatial objects from the geosampled, georeferncable, riverine, larval habitat canopy was then created employing Geometry, Multipoint, PointGeometry, Polygon, andPolyline classes.

Thereafter, a spatial constraint was introduced employing the spatial-spectral endmember extraction algorithm (SSEE) in the SPA that subsequently made use of the riverine, larval habitat, image mixes during searchs for optimal, homogenous, canopied endmembers to regress. The SSEE operates differently from SPA using a roving endmember search window that covers the entire input image as it is designed to find similar but distinct endmembers [4]. A non-linear framework was constructed employing the unmixed, LULC, explanatorial, geospectrally geosampled, absorption-related, decomposed, photosynthetic and NPV, canopy-oriented, covariate, parameter estimator, coefficient values in ArcGIS. By so doing, immersed canopy hanging vegetation LULC was found to be an important operationizable predictor in a reflection response model.

Importantly, in Jacob et al. [1], the SPA employed the spectral angle and the spatial adjacency of the georefernced, sub-mixel, *S. damnosum* s.l., riverine larval habitat, sub-meter resolution, explanatorily decomposed, empirical, endmember, biosignature-oriented, unmixed, predictor variables which did not constrain the selection of candidate, geospectral absorption, canopied LULC endmembers for representing any extracted, photosynthetic or NPV explanatorial regressor. The authors designed the SPA employing empirically geosampled, time series dependent, larval habitat, unmixed, incident, shade, canopied, radiation observations based on the assumption that many canopy targets had spatial continuity (e.g. floating grass LULC). The authors assumed a spatial constraint would be beneficial in the canopy endmember search. The authors also assumed that the regressable, sub-mixel, explanatorial, time series dependent, georefernced, riverine, larval habitat, unmixed, photosynthetic and NPV, canopied, LULC reflectance –oriented, transmittance, wavelenght, parameter estimators, covariate coefficient values depicted in ENVI were spatially adjacent and thus were more likely to have similar absorption properties thereby, representing one optimal georeferncable, *S. damnosum* s.l., larval habitat, eco-geographical representative canopy endmember, optical, parameter estimator, covariate coefficient value. The fractionialized, explanatorial, canopy endmember, residualized, radiance forecasts rendered from the unmixed, sub-mixel, eco-epidemiological, risk model revealed the probability that two adjacent decomposed, larval habitat 0.61m spatial resolution, mixels both being spurious was low. Experiments on the geospectrally decomposed, entomological-related, georeferenced, larval habitat canopy, biophysical, absorption rates demonstrated that SPA can have high efficiency in pure canopy endmember extractability due to minimal user interaction. In particular, this component calculated the balance between net radiative, turbulent, riverine fluxes for probabilistically regressively, quantitating, non-homogeneously canopy distributed centers of isotropic multiple scattering. By so doing, realistic 3D effects of photosynthetically and NPV emitted transmittance canopy radiation wavelenghts was efficiently calculated which was useful for constructing a robust, larval habitat, forecasting, stochastic interpolator employing the unmixed radiatiative, remotely sensed, sub-meter, mixel resolution, directional information.

In ArcGIS, geometric operations, geospectral interpolation is conducted by dividing the image into blocks, for detecting traces of rescaling and rotation in each block. In the mathematical field of numerical analysis, interpolation is a method of constructing new data points within the range of a discrete set of known data points [1]. Interpolation algorithms in ArcGIS have been employed in multiple disciplines. For example, Gallagher [5], developed a unified way to determine realistic, probabilisitc, geo-spatiotemporally regressable explanators of rescaling and rotation by exploring geospectrally-induced, reference signatures, and applied it to image forensics. Motivated by the image rescaling estimation method proposed, he developed an image, rotation angle, residual, probabilistic, target estimator based on quantized relations between the rotation angle and the frequencies at which peaks occurred due to interpolation in the spectrum of theimage's edge map. He then employed rescaling/rotation detection to detect maliciously adjusted objects inserted into images.

Interestingly, Popescu and Farid [6] presented their early method to find rescaling traces hidden in any portion of an image without resorting to a reference image by employing expectation maximization (EM) iterations. An EMalgorithm is an method for finding maximum likelihood or maximum a posteriori (MAP) estimates from an operational, empirical, covariate, parameter estimator, unmixed dataset of time series dependent, georeferencable, ArcGIS-friendly explanators (e.g., empirically decomposable, seasonal, canopied, *S. damnosum* s.l., riverine, larval habitat, endmember, ecosystem functioning regressors), especially when the model depends on unobserved empirical datasets dataset of latent, eco-geographically, endmember, geosampled, predictor variables [2]. A MAP estimate is a mode of the posterior distribution which may be utilized to obtain a georeferncable, explanatorial, point estimate of an unobserved quantity on the basis of a empirically regressable, time series dependent, explanatorial, georeferencable, data feature attribute [4]. Mahdian and Saic [7] used periodicity due to interpolation to perform blind image authentication. They introduced Radon transform on the basis of second derivative to detect rotation without estimation of the rotation angle. In mathematics, the Radon transform is the integral transform consisting of the integral of a function over straight lines. The Radon transform is also an integral transform whose inverse is used to reconstruct images from medical computed topography (CT) scans [2].

In another work, Mahdian et al. [8] employed noise inconsistency to aid in the detection of image rescaling for image splicing detection in ArcGIS. Kirchner [9] constructed a rescaling detector based on periodic artifacts in the residue of a local, extrapolated, non-linearizable, geo-spatiotemporal, geo-spectral, explanatorial, covariate, time series, dependent, probabilistic, parameter estimator. He analytically derived the expected position of characteristic rescaling peaks and formed an optimizable, explanatorial, endmember, absorption detector. Prasad et al. [10] localized tampered areas employing OBIA by labeling a mixel as 1 where the second derivative changed sign, otherwise labeling it as 0. If multiple, geometrically dependent, binary operations are involved in an OBIA, different, geospectral, unmixing processing, absorption, algorithmic sequences may be useful for regressively quantitating different peaks in an ArcGIS interpolatable, qualitatively, empirically, geosampled, dataset of georeferencable, riverine, *S. damnosum* s.l., larval habitat, photosynthetic and NPV, time series dependent, emissivity reflectance, wavelenght, covariate, parameter estimator, estimator coefficient values.

A simulation study above sparse, partial and dense vegetation canopies of a geo-spatiotemporally, geosampled, *S. damnosum* s.l., riverine larval habitat may improve the knowledge of the behaviour of the composite radiative temperature and emissivity. Canopy structural parameters have been introduced in the analytical parameterization of the directional canopy emissivity and directional canopy radiance: namely directional gap fraction and angular cavity effect coefficient. The parameterization has been physically defined allowing its extension to a wide range of Leaf Inclination Distribution Functions (LIDF) in ArcGIS. When single values are used as leaves and soil temperatures, they prove to be retrieved with insignificant errors from two directional measurements of the canopy radiance (namely at 0 and 55 from nadir), provided that the canopy structure parameters are known (www.esri.com). A sensitivity study to the different parameters may reveal the great importance of the accuracy on leaf area estimation. It may be determined that an accuracy of 10 per cent is required to retrieve the canopy leaf temperature with an accuracy better than 0.5 degK, the same requirement being 5 per cent for the retrieval of soil temperature during African riverine flooding sampled time frames. The radiometric noise may be vital for accurate regressable temperature sensitive covariate, wavelenght, parameter, estimators. The linearized effects may be catalyzed in an autoregressive algorithm by encompassing v different angles for the measurements. The effect of a Gaussian noise may be quantized as lower than 0.5 degK on the retrieved soil and foliage temperatures for example. Uncertainties on the leaf and soil emissivities (e.g., Delta epsilon 0.01) can create minute errors in the retrieval of (lower than 0.5 degK). For example, if the inclination dependence of the leaves temperature is considered in the regression equation, a 1 degK error may be observed in the retrieved soil and foliage temperatures. This error may be due to the fact that the effective foliage temperature varies with the view angle (a few 10^{-1} deg K at 55) in a geo-spatiotemporally geosampled, *S. damnosum* s.l. riverine larval habitat which would imply errors in the inversion scheme. This effect may be corrected in ArcGIS by using an angular corrective term delta depending only on the off-nadir angle employed in the eco-epidemiological, forecasting, probabilsitic, risk model.

Regardless, extensively heterogeneous, geospatially horizontal, geospectrally extractable, explanatorily interpolatable, shaded and non-shaded, canopied, probabilistic, regression–oriented, terrestrial biome-related, explanatorial, predictor variables can obscure accurately regressively quantizing stochastic and/or deterministic or deterministic relationships between canopy endmember, response-related, photosynthetic and NPV covariate parameter estimator coefficient values due to multiple scattering. As such, explanatorial, geospectrally decomposable, unmixed, canopied, biosignature-related, biomass regression-oriented, probabilistic, uncertainties in incident mean solar radiation calculations at the leaf and canopy scale may be vigorously propagated in non-linearly, qualitatively, quantitative platforms. Thus, empirically probabilistic, estimates of regressed soil biochemistry, structural unmixed, canopy variable radiance values cartographically delineating of seasonally, geosampled, *S. damnosum* s.l., riverine, larval habitat, photosynthetic and NPV canopied LULCs may be misspecified, for example. Time series maps of explanatorily, geospectrally decomposable, canopy vegetation, LULC, reflectance models contain significant classification errors (e.g., heteroskedasticty multicollinearity), since current understanding of how to scale mixed, photosynthetic and NPV, canopied, LULC-oriented, empirically extracted explanatorily interpolatable, predictor variables such as stand age, and density classes from local regressed estimates [2].

A sensor with a cosine response [i.e., follows Lambert's cosinelaw] allows measurement of explanatorial, flux densities through a given plane, (i.e. flux densities per unit area) [2]. In optics, Lambert's cosine law states that the radiant intensity or luminous intensity observed from an ideal diffusely reflecting surface (e.g., an individual, georefernced, *S. damnosum* s.l., riverine, larval habitat, canopy plant leaf), or ideal diffuse radiator, may be directly proportional to the cosine of the angle (i.e., θ) remotely geo-spatiotemporally quantitated Euclideanized distances between the direction of the incident light and the surface normal. Surface incidence is governed by the Lambert cosine law which states that the relative intensity of radiation or light on a surface is equal to the cosine of the angle of incidence, and that the relative area over which it is distributed is the inverse of this value [4]. Thus, when a parallel beam of georeferncable, *S. damnosum* s.l., riverine, larval habitat, canopy radiation of given cross-sectional, geolocation spreads over a relatively flat surface, the area that it covers is inversely proportional to the cosine of the angle between the beam and a plane normal to the surface.

Thus, time series, explanatorily regressed, probabilistic uncertainties in canopy LULC irradiance emitted from a geo-spatiotemporally-imaged, prolific, georefernced, seasonally shaded, *S. damnosum* s.l., geosampled, riverine, larval habitat, may be qualitatively regressively quantitated using a dataset of time series dependent, photosynthetic and NPV unmixed, endmember, biosignature-oriented, covariate coefficients values associated to beam disproportionality based on the tabulated cosine of the endmember sub-mixel, angles. These time series, explanatorial, regressive, quantizable, non-linear, integer values may remotely describe fluctuating elevations of African flooded riverine landscapes in which clustered,(i.e., positively autocorrelated) geospatial aggregations of prolific, georefernced, canopied, immature habitats, (i.e., possible high density hyperendemic transmission foci). In radiometry, irradiance is the radiant fluxreceived by a surface per unit area, and spectral irradiance is the irradiance of a surface per unit frequency or wavelength, depending on whether the spectrum is taken as a function of frequency or of wavelength [2].

The SI unit of irradiance is the watt per square meter (W/m^2), while that of spectral irradiance is the watt per square metre per hertz ($W{\cdot}m^{-2}{\cdot}Hz^{-1}$) or the watt per square meter per meter ($W{\cdot}m^{-3}$)—commonly the watt per square meter per nanometer ($W{\cdot}m^{-2}{\cdot}nm^{-1}$) [4]. Differences of modeled surface upward and downward longwave and shortwave irradiances may be optimally calculated in ArcGIS for canopied, geo-spatiotemporally, geosampled, prolific, georefernced, shaded, *S. damnosum* s.l., riverine, larval habitat, images employing modeled irradiance computed with active sensor-derived and passive sensor-derived cloud and aerosol properties. The irradiance differences may be then optimally calculated for various temporal and spatial scales, monthly gridded, monthly zonal, monthly global, and annual, global, meterological, covariate, parameter estimators.

Parameterizations in a global canopy model (GCM) are designed to describe the 'collective effects' of processes that occur at scales smaller than GCM grid sizes [4]. Radiation exchange within the canopy plays a crucial role in the canopy microclimate [2]. Parameterizations of many processes such as radiation transfer and autoconversion employ the assumption of independent column approximation (ICA), [i.e., there is no interaction between sub-columns and the grid-averaged regression probability uncertainty effects] which subsequently depend only on the probability distribution function (PDF) of relevant canopied, endmember predictive, variables] [2]. Radiative transfer is the physical phenomenon of energy transfer in the form of electromagnetic radiation [4]. The propagation of radiation through a medium (i.e, riverine, larval habitat, *S. damnosum* s.l., vegetation canopy) in a GCM is affected by absorption, emission, and scattering processes [3], thus acurate simulation of canopy microclimate in ArcGIS is contingent on successful mixel decomposition and precise time series simulation of the surface radiation balance.

Independent column approximation approaches employ one-point statistical information (e.g., PDF), called sub-grid variability and structural information (e.g., spatial organization and arrangement) that can be remotely characterized by multi-point explanatorial, statistics in ArcGIS. However, coherent structures have been found at scales ranging from droplet clusters to organized cloud, and have complex interactions with canopied radiation, dynamical processes (e.g., bi-directional, reflectance of floating vegetation LULC around a georeferncable, geospectrally decomposable, prolific, flooded, *S. damnosum* s.l., larval habitat) in mesoscale riverine ecosystems. Failure to include sub-grid cloud and convection structures in a radiative transfer equation may thus lead to inadequate simulations of large-scale, georefernced, *S. damnosum* s.l., riverine, canopied, larval habitats, and their remotely sensed, shaded and non-shaded, photosynthetic and NPV –oriented, LULC-related probabilistically regressable, biophysical, seasonal constituents, for example. It has been found that ignoring cloud spatial organization tends to non-regressively underestimate or overestimate the domain-average radiation fluxes which may be dependent on many co-factors, (e.g., solar angle and cloud geometry) [4].

The terrestrial component of GCMs requires computationally efficient algorithms for qualitatively quantizing the multi-scattered canopy radiation contributions from heating and solar radiation [2]. Much of the seasonally geosampled, canopy vegetated, LULC geo-classifed, geosampled, productive, *S. damnosum* s.l., riverine, larval habitats have strong 3-D controls on its radiation [1]. The scattering from a 3-D object of isotropic scatters may be formulated abstractly and an approach to solution may be optimally described for robustly, parsimoniously, geospectrally, explanatorily interpolating, canopied, seasonally, prolific, *S. damnosum* s.l., riverine, larval habitats, biogeochemical, photosynthetic and NPV–oriented, regressed, decomposed, data products. A Laplace integral representation of the 3-D integral equation for radiative transfer may then be discretized.

The Laplace transform is related to the Fourier transform but whereas the Fourier transform expresses a function or signal as a superposition of sinusoids, the Laplace transform expresses a function, more generally, as a superposition of moments [2]. Fourier transform of a function of time itself is a complex-valued function of frequency, whose absolute value represents the amount of that frequency residually present in the original function, and whose complex argument is the phase offset of the basic sinusoid in that frequency [4]. Given a simple mathematical or functional description of an input or output to an explanatorial, geo-spatiotemporally, geosampled, canopied, *S. damnosums*.l., georeferencable, prolific, riverine, larval habitat, decomposable system in ArcGIS, the Laplace transform can provide an alternative functional description that may algebraically simplify the process of geospectrally analyzing the behavior of the system by synthesizing seasonal, unmixed, canopy, biosignature-oriented, explanatorial, architectural specifications. Laplace transformation from the time domain to the frequency domain transforms differential equations into algebraic equations and convolution into multiplication [2]. Such discretization can provide the solution in terms of solutions to 3-D Helmholtz equations. In mathematics, the Helmholtz equation is the partial differential equation $\Delta^2 A + K^2 A = 0$ where ∇^2 is the Laplacian, k is the wavenumber and A is the amplitude [4].

A Green's function approximate solution along the paths of entering and exiting, seasonally geosampled, prolific, *S. damnosum* s.l. riverine larval habitats canopy radiation may also be integrated over an empirically operationizable, geosampled dataset of geo-spatiotemporally decomposable, canopy, radiation absorption covariate, parameter estimator coefficient values for robustly, regressively, qualitatively quantizing the paths which may be assumed to coincide except for direction in a GCM. In mathematics, a Green's function is the impulse response of an inhomogenous difefrential equation defined on a domain, with specified initial conditions or boundary conditions [4]. Via the superposition principle, the convolution of a Green's function with an arbitrary function $f(x)$ on that domain is the solution to an inhomogeneous differential equation for $f(x)$ [2]. The resulting approximate description of an heuristically optimizable, empirical, explanatorial dataset of multi-scattered, riverine, larval, habitat, canopy radiation regressors may correspond to replacing the 3-D scattering paths with a 1-D path with attenuation in an empirical, geo-spatiotemporal, *S. damnosum* s.l., eco-epidemiological, risk, forecasting, GCM amplified by a diffusivity factor. This description can be combined with previously derived analytic solutions for remotely, qualitatively regressively, robustly, quantitating, single scattered, canopy radiation for parsimoniously providing an efficient seasonal eco-geographic representation of the bidirectional scattering from a geospectrally extracted,3-D –explanatorily interpolated, *S. damnosum* s.l., riverine, larval habitat, geo-spatial, georeferenceable, canopy object, intended for use in the GCM.

Given the detailed riverine, eco-graphically georeferncable, *S. damnosum* s.l., larval habitat cloud field, the canopy radiation field can be found by numerically solving the 3-D transport equation in ArcGIS. However, in many applications, the knowledge of 3-D cloud field is unavailable. Satellite observations provide the only practical means to obtain a synoptic view of Earth's ecosystems, including their geospatial distribution, extent, and temporal dynamics [4]. Thus, it is often difficult to draw any theoretical conclusion based on numerous configurations of a 3-D cloud field [2]. Further, numerically solving the 3-D problem may be too expensive for practical applications for precisely, seasonally, forecasting, hyperendemically-related, productive, geo-spectrally explanatorily, interpolatable, decomposable, shaded or non-shaded, *S. damnosum* s.l. riverine, larval habitat, canopied endmembers. Traditional field-based, geo-sampling, eco-epidemiological methods are prohibitively expensive and time-consuming at large geospatial scales, and as such these methods are inadequate for today's remote sensing needs [4]. In geo-spatiotemporal, geosampled, *S. damnosum* s.l.–related, canopy-related, forecasting larval habitat, eco-epidemiological, regression-related, risk models constructed in ArcGIS it is a standard practice to employ the ICA assumption, [i.e., divide the domain into two (clear and cloudy) or more subcolumns] and independently calculate the radiation flux within each sub-column [1,3].

Previous efforts on parameterization of 3-D, cloud-radiation, canopied interaction terms in large-scale canopy-related, *S. damsnosum* s.l. riverine, larval habitat GCMs generated in ArcGIS have focused on binary medium or oversimplified closure assumptions. Interestingly, a statistical physics-like simulation approach that makes a direct connection between the statistical eco-characterization of cloud structure and the geostatistical moments of the radiation field by properly averaging the 3-D regressive equation in ArcGIS may reduce probability uncertainties in a radiative transfer equation for precisely geospatially, remotely targeting, prolific, unknown, unsampled, georeferencable, riverine, immature habitats employing decomposed, geospectrally, explanatorily interpolated, bio-signature canopy endmember, photosynthetic and NPV, empirically geosampled, geopredictive variables. The unknowns of the resultant statistical radiative transport (SRT) equations may also be calculated in ArcGIS and, by so doing, the statistical moments of the radiation field, and the riverine larval habitat model inputs could be optimally rendered as some statistical moments of the 3-D, canopied, medium structure. It may be shown that a spatial correlation function can serve as the key to statistically eco-geographically describing time series, cloud–radiation, seasonal interactions in an empirically geo-spatio temporally, explanatorily interpolated dataset of clustered, unknown, unsampled, geosampled, productive, *S. damnosum* s.l., georefernced, riverine, shade, canopied, larval habitats.

Further, employing the 3-D, medium irradiance differences, the regression, probabilistic uncertainties of the radiative surface of prolific, shaded, geo-spatiotemporally, geosampled, *S. damnosum* s.l., riverine, larval habitat, decomposed canopy, irradiances may be optimally estimated in ArcGIS. The uncertainty (e.g., 1 r) of the annual global surface downward longwave and shortwave may be seasonally respectively, 5 W m^{-2} (out of 345 W m^{-2}) and 4 W m^{-2}(out of 200 W m^{-2}), for example, after known bias errors are removed. Similarly, the uncertainty of the annual global surface upward longwave and shortwave for regressed georeferenced, canopied, riverine, larval habitat photosynthetic and NPV, explanatorial, time series, predictor variables may be tabulated respectively as 3 W m^{-2}(out of 400 W m^{-2}) and 3 W m^{-2}(out of 25 W m^{-2}). Accurately quantitating, regression, probabilistic, geospectral uncertainties may model canopy irradiances employing cloud properties derived from imagers on a sun-synchronous orbit that covers the globe every day (e.g., moderate-resolution imaging spectrometer) or, modeled irradiances computed for nadir view on active sensors or, on a sun-synchronous orbit such as Cloud-Aerosol Lidar, Infrared Pathfinder Satellite Observation and CloudSat. If the assumption is that longwave and shortwave georeferenced, canopied, reflectance wavelength transmittance probabilities quantized *S. damnosum* s.l., habitat, eco-epidemiological, regression-related forecasting, risk model estimators are independent of each other, but up- and downward components are correlated with each other, the remotely tabulated erroneous variables in global annual mean net surface irradiance may be low for the georefernced habitat (e.g., 15 W m^{-2}). One-sigma uncertainty bounds of the satellite-based, net surface irradiance may also be approximated with low W m^{-2} measures for the georeferenced, riverine, larval habitat, canopied, leaf optical properties.

Leaf optical properties have been successfully included for homogeneous canopies (i.e., no higher level of organization) at the computational level in GCMs [4]. For this purpose, multi-scattered, isotropic, seasonal, *S. damnosum* s.l., larval habitat, canopy radiation maybe conceptualized as consisting of discrete streams of non-opaque exiting radiation. Canopy radiation interacting at multiple scales of the riverine habitat can then be addressed with an adding principle in ArcGIS. Each riverine, larval habitat, canopy level may be thereafter robustly summarized by its "input–output". That is, since the incident radiation is of external origin, it arrives at the outside of a georeferenced, geosampled, canopied, seasonally productive, riverine habitat, and then enters in and some fraction again exits in various directions. The description of this exiting radiation may be then remotely qualitatively defined as an unmixed, canopied, endmember biosignature, log-transformed, non-linear regressor in an autoregressive GCM. The optical properties of a plant cell (i.e., photosynthetic capability) can then be employed to construct the optical properties of a riverine, larval habitat, canopy leaf and the latter can be used to construct optical properties at higher levels of organization up to that of the canopy.

Alternatively, the geosampled, georeferncable, *S. damnosum* s.l., larval habitat, canopy radiation may be eco-geographically and/or non-ecoeographically represented by precisely tabulating polynomials in the cosine of their angle made by the direction of the radiative flux relative to the same reference direction, (e.g. the vertical) in ArcGIS. These approaches may qualitatively regressively quantitate low order numerical discretizations of the continuous directionality of the riverine, larval habitat, multi-scattered, isotropic canopy radiation. The photosynthetic and NPV geospectrally, explanatorily interpolated, decomposed, covariate, parameter estimator, emissivity transmittance coefficients may describe the canopy scattering from other terrestrial LULC, riverine, vegetation LULC surrounding the habitat. Further, employing robust, seasonal, and photosynthetic and NPV, remotely sensed, decomposable, probabilistic, geo-spatiotemporal,geosampled, explanators as independent variables in the regression equation may create computational simplicity when constructing an autoregressive GCM in ArcGIS with acceptable discretization error. Unfortunately, currently ecologists and other experimenters are not able to explicitly remotely address the additional autoregressive, uncertainty-oriented, probabilistic, complexities in any geometric analytical module in an ArcGIS cyberenvironment for parsimoniously regressively capturing ellipsoidal, within-canopy, georeferencable geospatial, objects (e.g., trailing vegetation) in a geo-spatiotemporally, geosampled, seasonally productive, ecogeographically or non-ecogeographically associated with, shade canopied, riverine, *S. damnosum* s.l. larval habitat.

Sensor data without an accurate cosine correction can also render a severe autoregressive propagational error in an ArcGIS validation algorithm under diffuse radiation conditions within a riverine, *S. damnosum* s.l., larval habitat, canopied geolocation at low solar elevation angles. The cosine error at angle 0 is the percent difference of the ratio of the measured output at angle 0 and normal incidence as compared to the cosine of angle0 [2], which may be repeatable for various azimuth angles in ArcGIS when accurately remotely, qualitatively, regressively quantizing seasonal, shaded, *S. damnosum* s.l., larval habitat, canopy-oriented, photosynthetic and NPV radiance transmittance emittance values. Totally diffuse radiation can introduce a cosine error of approximately 2.5%in a, geo-spatiotemporally-dependent, geosampled, *S. damnosum* s.l., canopied, riverine, larval habitat, sub-mixel, endmember, geospectral, stochastic interpolator [1].

Jacob et al. [1]employed a regression matrix, for qualitatively quantitating an operational dataset of seasonally geosampled, productive, *S. damnosum* s.l., vegetation canopied LULC, riverine, larval habitat, sub-meter resolution unmixed biosignature, forecasting, eco-epidemiological, explanatorily, risk model variables with autocorrelated disturbances as follows: $Y_t = X_t^i \beta + V_t$ $V_t = \varepsilon_t - \varphi_1 v_{t-1} - \ldots - \varphi_m V_{t-m} \varepsilon_t N\left(0, \sigma^2\right)$. In these equations, $Y_t$were log-transformed, dependent, decomposed, sub-meter (0.61 m) wave length values, $X_t$was a column vector of the decomposed, probabilistic, regressor variables, β was a column vector of structural parameters, whereϵ_t was normally and independently distributed with a mean of 0 and a variance of σ2. Note that in the parameterization, the signs of the autoregressive parameters were reversed from the parameterization documented in literature. ArcGIS probabilistic, uncertainty-oriented, photosynthetic, end member estimation methods for the optimizable, geo-spatiotemporal geosampled, canopied, *S. damnosum* s.l., georeferenced, riverine, larval habitat, time series, eco-geographical, explanatorial, error model initially employed a default method. Yule-Walker (YW) estimation was performed in ArcGIS. The Yule-Walker method (i.e., the two-step full transform method) computationally was designed in ArcGIS by letting φ represent the vector of the geo-spatiotemporally, geosampled, autoregressive *S. damnosum* s.l. parameters, $\varphi = \left(\varphi_1, \varphi_2, \ldots\ldots, \varphi_m\right)^1$ and by letting the variance matrix of the error vector be $V = \left(V_t, \ldots\ldots V_N\right)'$ be $\sum, E\left(VV'\right) = \sum = \sigma^2 V$. According to Jacob et al. (2013) ,in an empirical probabilistic, regressed datset of geosampled, immature, *S. damnosum* s.l., riverine, larval habitat-related, explanatorial, eco-epidemiological, time series dependent, uncertainty-oriented, non-linear, risk model forecasts, the vector of autoregressive parameters φ is known the matrix V can be computed from decomposed, probabilistic, non-optimizable spatially pseudo-replicated uncertainty probabilities. $\sum$ which may be then delineated by $\sigma^2 V$ [2]. Given $\sum$, the efficient emissivity transmisstance estimates of the autoregressive, explantorial, endmember, canopied, *S. damnosum* s.l.,, riverine, larval habitat, time series dependent, regression parameters β may be computed using generalized least squares (GLS). In Jacob et al. [1] the GLS estimates yielded the unbiased explanatorial time series estimate of the variance σ^2 in the riverine larval habitat model spatially structured random intercept which subsequently accounted for the effect of the missing predictors in the model derivatives.

Thereafter, the YW alternated estimation of β employing the GLS with iterative equations which rendered the sample autocorrelation function. The YW method formed the OLS estimate of β. Next, φ was estimated from the sample autocorrelation function of the empirically autoregressed. explanatorial, field and remote, unmixed, immature *S. damnosum* s.l. riverine, larval habitat, photosynthetic and NPV, time series dependent, geospatial probabilistic, uncertainty –oriented, optical properties and OLS residuals. Then V was tabulated from the estimate of φ and $\sum$ was estimated from Vand the OLS estimate of σ^2. The autocorrelation eigenfunction decomposition algorithm corrected estimates of the canopied, *S. damnosum* s.l., shaded, larval habitat, time series dependent, regression parameters β which were then computed by GLS, employing the estimated $\sum$ weighted matrix. These were the Yule-Walker estimates. Other methods were the niterated YW, unconditional least squares (ULS), and maximum likelihood (ML). The ULS method is also referred to as nonlinear least squares (NLS) or exact least squares (ELS [2]).

The authors then defined the transformed error, e, as $e = L^{-1} n$ where $n = y - X\beta$.in ArcGIS The unconditional sum of squares for the model, S, was $S = n' V^{-1} n = e'e$ The ULS estimates were computed by minimizing S with respect to the geosampled, decomposed, canopied, *S. damnosum* s.l., shaded, larval habitat regression parameters β and φ_i. The full log likelihood function for the autoregressive error model was $l = -\frac{N}{2}\ln(2\Pi) - \frac{N}{2}\ln\left(\sigma^2\right) - \frac{1}{2}\ln(/V/) - \frac{S}{2\sigma^2}$ where V denoted the determinant of V for the ML method, the likelihood function was maximized by

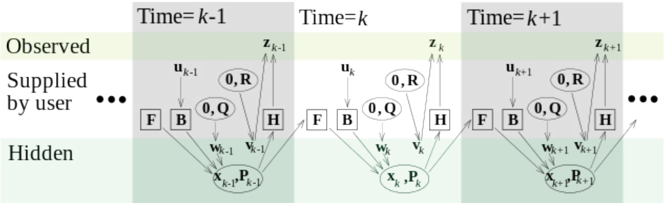

Figure 1: A Markov end member, probabilistic, canopied, prolific, *S. damnosum* s.l., larval habitat forecasting risk model underlying the Kalman filter representing the uncertainty auto regressive matrices.

minimizing an equivalent sum-of-squares function. Maximizing $\boldsymbol{l}$ with respect to σ^2 (and concentrating σ^2 out of the likelihood) and dropping the constant term $-\frac{N}{2}\ln(2\amalg)+1-\ln(N)$ then rendered the concentrated log likelihood function $l_C = -\frac{N}{2}\ln\left(S/v/^{1/N}\right)$. Rewriting the *S. damnosum* s.l.-related decomposed, endmember, regression variable term within the logarithm then rendered $S_{ml} = |L|^{1/N} e^{'}e|L|^{1/N}$

Thereafter, ArcGIS computed the ML estimates by minimizing the objective function which in Jacob et al. (2012) was expressed as $S_{ml} = |L|^{1/N} e^{'}e|L|^{1/N}$. The sample autocorrelation function was computed from the structural excessive, decomposed, canopied, *S. damnosum* s.l., shaded, larval habitat noise which was then subsequently qualitatively regressively quantitated employing $n_t = y_t - X_t^{'}b$, where b was an estimate of β. The sample autocorrelation function was the sum of all available lagged products of n_t of order $\boldsymbol{j}$ divided by l+j, where l was the number of such products. The calculation of **V** from φ for the generalized, canopy decomposition, endmember, $AR^{(m)}$ risk model was complicated, and the size of **V** was dependent on the number of photosynthetic and NPV canopied observations. Instead of actually calculating **V**and performing GLS in the usual way, a Kalman filter algorithm was instead used to transform the geosampled empirical data which was then employed to compute the GLS results through a recursive process.

The Kalman filters was based on linear dynamic systems discretized in the time domain. The filters were modeled on a Markov chain built on linear operators perturbed by the unmimxed, biosignature-related, geosampled, decomposed, canopied, *S. damnosum* s.l., shaded, larval habitat, regression errors including the Gaussian noise. Gaussian noise is statistical noise having a probability density function (PDF) equal to that of the normal distribution, which is also known as the Gaussian distribution [2]. In other words, the values that the noise can take on are Gaussian-distributed. The state of the system was then eco-geographically represented as a vector of the endmember, time series, photosynthetic and NPV, covariate parameter estimator, time series, reflectance emissivity coefficinet values. At each discrete time increment, a linear operator was applied to the state to generate the new state, with some noise mixed in, and optionally some information from the controls on the system. Then, another linear operator mixed with more noise rendered the observed outputs from the true ("hidden") state. The Kalman filter may be regarded as analogous to the hidden Markov model, with the key difference that the hidden state variables take values in a continuous space (as opposed to a discrete state space as in the hidden Markov model) [2]. There was a strong duality between the equations of the Kalman Filter and those of the hidden canopied, *S. damnosum* s.l., shaded, larval habitat, Markov model (Figure 1).

The algorithm estimated the internal state of the decomposed endmember riverine, canopy, larval habitat explanatorial regressors employing a sequence of noisy, decomposed, canopy endmember, autocorrelation observations in accordance with the framework of the Kalman filter in ArcGIS. This meant specifying the following matrices: $\mathbf{F}_k$, the state-transition model; $\mathbf{H}_k$, the observation model; $\mathbf{Q}_k$, the covariance of the process noise; $\mathbf{R}_k$, the covariance of the observation noise; and $\mathbf{B}_k$, the control-input model, for each time-step, *k*,

Ellipses representing the seasonally eco productive, canopied, *S. damnosum* s.l., shaded, larval habitat, multivariate, normal distributions with the mean and covariance matrix were enclosed in ArcGIS. Unenclosed values were then qualitatively regressively quantitated as vectors. In the simple case, the various matrices were constant with time, and thus the subscripts were dropped, but the Kalman filter allowed any of the decomposed, riverine, larval habitat, sub-meter resolution, canopied, endmember biosignature, optical properties to change at each time step. The Kalman filter model assumed the true state at time *k* which was evolved from the state at (*k* – 1) according to $X_K = F_K X_{K-1} + B_K u_k + W_K$ where$\mathbf{F}_k$ was the state transition model which was subsequently applied to the previous state $\mathbf{x}_{k-1}$, where $\mathbf{B}_k$ was the control-input model which was applied to the control vector $\mathbf{u}_k$. In the geo-spatiotemporally, geosampled, *S. damnosum* s.l., shaded, larval habitat, , spatially,probabilistically, regressed model $\mathbf{w}_k$ was the process noise which the authors assumed to be drawn from a zero mean, multivariate, normal distribution with covariance $\mathbf{Q}_k$. $W_K \sim N(0, Q_K)$. At time *k* then a decomposed, georefernced canopied, *S. damnosum* s.l., riverine larval habitat canopied endmember observation $\mathbf{z}_k$ of the true state $\mathbf{x}_k$was parameterized according to $Z_K = H_K X_K + V_K$ where $\mathbf{H}_k$ was the decomposed observation model which mapped the true state space into the observed space when $\mathbf{v}_k$ was the observation noise which Jacob et al. [1] assumed to be zero mean Gaussian white noise with covariance $\mathbf{R}_k$. $V_K \sim N(0, R_K)$. The initial state, and the noise vectors at each step $\{\mathbf{x}_0, \mathbf{w}_1, \ldots, \mathbf{w}_k, \mathbf{v}_1 \ldots \mathbf{v}_k\}$ were all then deemed to be mutually independent.

In all of the algorithmic estimation methods, the original decomposed, georefernced, canopied, *S. damnosum* s.l., shaded, larval habitat endmember data were transformed by the inverse of the Cholesky root of V in ArcGIS. Let L denote the Cholesky root of **V** then, $V = LL'$ with **L** lower triangular [2]. For the $AR^{(m)}$ eco-epidemiological, decomposed, forecasting, operationizable, emissivity transmisstance, reflectance, wavelenght, risk model, $\mathbf{L}^{-1}$ was a band diagonal matrix with $\boldsymbol{m}$ anomalous rows at the beginning and the autoregressive unmixed parameters along the remaining rows. Therefore, if there were no missing values, after the first m—1 canopy endmember observations the regressed data were transformed as $Z_t = x_t + \varphi_1 x_{t-1} + \ldots + \varphi_m x_{t-m}$. The transformation was carried out employing the Kalman filter, and the lower triangular matrix **L** which was never directly computed in ArcGIS. Although **L** was not computed explicitly, for ease of residual presentation the uncertainty probabilisticforecasts were spatially defined in termsof **L**.

If there are missing values, then the submatrix of **L** consisting of the rows and columns with nonmissing values are used to generate the transformations (www.esri.com).

The ULS and ML estimates employed a Gauss-Newton algorithm to minimize the sum of squares and maximize the log-likelihood, respectively. The relevant optimization wasperformed in ArcGIS simultaneously for both the regression and AR parameters. The OLS estimates of β and the Yule-Walker estimates of φ were employed as starting values for the uncertainty, first-order auto-evaluation. The Gauss-Newton algorithm requires the derivatives of **e** or $(L)^{1/N} e$ with respect to the decomposed, explanatorial, canopied parameters [2]. The derivatives with respect to the parameter vector β were then $\frac{\partial e}{\partial \beta'} = -L^{-1} X \frac{\partial |L|^{1/Ne}}{\partial \beta'} = |L|^{1/N} L^{-1} X$ The derivatives with respect to φ were then computed by differentiating the Kalman filter recurrences and the equations for the initial conditions. For the Yule-Walker method, the estimate of the error variance, S^2, was the error sum of squares from the application of GLS, divided by the error degrees of freedom (i.e, number of decomposed, canopied, *S. damnosum* s.l., shaded, larval habitat endmember observations ***N*** minus the number of free parameters). The variance-covariance matrix for the components of **b** was taken as $s^2 \left(X'V^{-1}X \right)^{-1}$ for the Yule-Walker method. For the ULS and ML methods, the variance-covariance matrix of the canopied, decomposed, larval habitat, parameter estimates was then computed as $s^2 \left(J'J \right)^{-1}$. For the ULS method, **J** was the matrix of the geospectral derivatives of **e** with respect to the unmixed, riverine, canopied, larval habitatdecomposable parameters. For the ML method, **J**wasthe matrix of derivatives of $|L|^{1/N} e$ divided by $|L|^{1/N}$. The estimate of the variance-covariance matrix of b assuming that φ was then $S^2 = \left(X'V^{-1}X \right)^{-1}$.

Spatially autocorrelated discontionus canopy species abundance or distribution datasets may generate spatially autocorrelated residuals in generalized linear models (GLMs) thus, a broader modelling framework may be required to remotely, qualitatively, regressively, quantitate geospectrally decomposed, *S. damnosum*.s.l., larval habitat, canopy bisignatures. Auto-logistic and related auto-models, implemented approximately as autocovariate regression, provide simple and direct modeling of endmember, spatialized, probabilistic *S. damnosum* s.l.-related population processes. However, Dormann questioned the validity of auto-logistic regression for fully observed decomposed endmember data, giving examples of apparent underestimation of covariate parameter estimators in residual analysis of simulated data. Dormann et al. extended this critique to auto-Poisson and certain auto-normal models, finding again that autocovariate-regressed endmember estimates for time series covariate parameter estimators bore little resemblance to values employed to generate 'snouter' data. Jacob et al. [1] acclaimed that compound probabilistic regression uncertainties associated may be associated other factors (e.g.,sampling error) such as algorithm selection, presence data, and variable collinearity. We note that all the above studies employed neighborhood weighting schemes inconsistent with auto-model definitions; in the auto-Poisson case, a further inconsistency was the failure to exclude cooperative interactions. Investigating the impact of implementation errors on auto-model probabilistic estimation employing both empirical, and simulated datasets of geospectrally decomposed, resampled, productive, shade canopied, *S. damnosum*sol s.l., riverine, larval habitats may show that when spatially "re-adjusted" endmember canopy data are re-analyzed employing valid weightings, very different residually forecasted, emissivity, transmisstance, reflectance wavelengtht, estimates are obtained for photosynthetic and NPV predictors. For auto-logistic and auto-normal *S. damnosum* s.l. riverine larval habitate co-epidemiological, forecasting canopy, risk models, the new estimates may agree closely with values used to generate the 'snouter' simulations. A substantial fraction of papers employing auto-logistic regression use these invalid neighborhood weightings, which have been embedded as default options in ArcGIS.

Commonly explanatorial, time series dependent, geospatial, probabilistic erroneous photosynthetic and NPV radiance covariate coefficients in autoregressed, canopy vegetation, LULC calculations in ArcGIS consists of the cosine error (or the angular error) and azimuth error. Angular error in a georeferencable, seasonally imaged, productive, riverine, *S. damnosum* s.l., shade, canopied, larval habitat may be measured by directing a collimated source at normal incidence androtating the sensor 360° about an axis directly through the center of the sphere at 90° from normal incidence. This may be repeatable for calculating various azimuth angles as necessary to characterize the sensor. The solar azimuth angle is the azimuth angle of the sun which may be determined by defining sun direction, whereas the solar zenith angle or its complementary angle solar elevationcan define how high the sun is [4]. There are conventions for the solar azimuth, however it is traditionally defined as the angle between a line due south and the shadow cast by a vertical rod on Earth. Angular error is due to variations in density in the diffusion sphere and the sphere area lost because ofthe sensor base [2]. Angular error is commonly less than 10% for an remotely sensible, georeferncable, seasonally productive, canopied, *S. damnosum* s.l., larval habitat based on geo-spatiotemporal, field geosampled, regressively aggregated, count data as the upwelling radiation is much smaller than the downwelling radiation in most African riverine environments [1].

The mathematical theories of regression for quantitating, canopy radiative, multi-scattering have already been extensively developed especially in literature in the context of astrophysics and neutron diffusion where the system-properties differ significantly from seasonally, geosampled, canopied, *S. damnosum* s.l., riverine, larval habitat, photosynthetic and NPV, explanatorial, time series, empirical emissivity transmisstance, reflectance wavelenght regressors. In particular, the astrophysical scattering systems in ArcGIS are commonly very deep and appropriately approximated as semi-infinite, whereas the study of neutron scattering has been focused on the issue of "criticality" where energy is scattered as is incident [4]. Geo-spatiotemporally-dependent, geosampled, *S. damnosum* s.l., canopied, riverine, larval habitat canopies, on the other hand, are often optically relatively thin and at most wavelengths their leaves absorb a substantial fraction of the radiation they attenuate [1]. Thus, a different analytic approach for spectral determination of explanatorily regressed, interpolatable, seasonally geosampled, riverine, larval habitats, canopy scattered radiation in an ArcGIS geo database may be required.

Interaction of solar radiation emitted from a prolific, geo-spatiotemporally, geosampled, shade, canopied, *S. damnosum* s.l., georeferencable, riverine, larval habitat can be described by the 3-D, radiative, transfer equation in ArcGIS [1]. Solar radiation scattered from a vegetation –related, sheded or non-shaded, canopy LULC and measured by satellite sensors results from interaction of photons traversing through the foliage medium, bounded at the bottom by a radiatively participating surface [4]. Solar radiation after passing through the atmosphere arrives either in the form of direct beam or diffuse, that is after molecular (Rayleigh) or particulate scattering from cloud or aerosol droplets. Rayleigh scatteringis the dominantly elastic scattering of light or other electromagnetic radiation by particles much smaller than the wavelength of the radiation [2]. The Rayleigh scattering does not change the state of material hence it is a parametric process. The particles may be individual atoms or molecules. It can occur when light travels through transparent solids and liquids, but is most prominently seen in gases. Rayleigh scattering results from the electric polarizability of the particles [2]. The oscillating electric field of a light wave acts on the charges within a particle, causing them to move at the same frequency. The particle therefore becomes a small radiating dipole whose radiation we see as scattered light. Rayleigh scattering of sunlight in the atmosphere causes diffuse sky radiation, which is the reason for the blue color of the sky and the yellow tone of the sun itself [4].

Rayleigh radiation can pass through geo-spatiotemporal, geosampled, *S. damnosum* s.l., riverine, larval habitat, vegetation -related, LULC-oriented, canopies in ArcGIS to reach the surface and is either absorbed by the canopy or surface or is reflected back to the atmosphere [3]. The treatment of the radiation passing through vegetation canopies is complicated by the presence of multiple levels of organization, from that of the chloroplast cells to that of the arrangement of individual plants within the landscape [2]. Thus, a comprehensive treatment of all the radiative details within a gridded, ArcGIS, -derived, eco-epidemiological, seasonal, weighted matrix matrix delineating 1 km^2 plot of riverine LULC where the centroid is the geosampled, riverine habitat, for example, could easily reduce the computation of terrestrial radiation while adequately generating realistic, regressively quantifiable, canopy-oriented, particulate, scattering measurements.

Radiation interacting at multiple scales of organization can be addressed with an adding principle in ArcGIS. The scattering objects that are then considered in treating radiation within the riverine larval habitat canopy would not generally be opaque. Radiation both reflects from a leaf surface and is transmitted diffusely through it [2]. However, this scattering at leaf level in a canopied *S. damnosum* s.l., riverine, larval habitat would be asymmetric, (i.e., the fraction of incident light reflected from the habitat canopy surface of a thick leaf differs from that transmitted). Scattering from leaves is further complicated by the geometry of leaf orientation which is commonly characterized by a statistical distribution.

The equation of radiative transfer in ArcGIS describes scattering interactions mathematically. Equations of radiative transfer have application in a wide variety of subjects including optics, astrophysics, atmospheric science, and remote sensing [2]. Analytic solutions to the radiative transfer equation (RTE) exist for simple cases but for more realistic media, with complex, multiple, canopy, emissivity transmittance, wavelenght, reflectance, scattering effects, such as those for determining radiance, fractional, geospectrally explanatorily, regressively interpolatable, estimates emitted from a geo-spatiotemporally, geosampled, *S. damnosum* s.l., riverine habitat, numerical methods in ArcGIS would be required. The interaction cross-section that appears in this equation may be treated as wavelength for independently considering the size of the scattering elements (e.g., canopy leaves, branches, twigs, etc.) relative to the wavelength of solar radiation of leaf structures in the geo refernced larval habitat canopy. Radiation incident on the top of the atmosphere is a monodirectional solar beam while the vegetation canopies are illuminated both by a monodirectional beam attenuated by atmospheric radiation [4].

Although spherical coordinates might appear to be the most obvious choice the path of entry of canopy radiation into a geo-spatiotemporally, geosampled *S. damnosum* s.l., georefernced, riverine, larval habitat, the photosynthetic and NPV explanatorial, regressive, covariate parameter estimator coefficients may be shown to be analytically integratable as a local system with a Cartesian metric. The dependence of these solutions may be addressed in ArcGIS by introducing a numerical integration. The integration can be written in terms of another transform variable,[e.g., q=1/(sp)] which may be log-transformed into a more familiar form for qualitatively quantizing a plane parallel system, with q interpreted as the cosine of the angle of the direction of the canopy radiation and the larval habitat canopy radiation as p. It has been established over the history of canopy radiative transfer research with such systems that a few integration points, even one (e.g. the classical 2-stream and Eddington approximations) provides useful accuracy for integration of remote expressions [2].

In the study of stellar atmospheres, it has been found that the plane - parallel approximation has led to many useful and simplifying expressions such as the Eddington approximation, in which the radiation field has two components: a component outward along the z axis that *I*out and a component inward that being *I*in. These approximations may be coupled with definitions of intensity flux and canopy radiation pressure in ArcGIS for robustly expressing the *I*out and *I*in for a prolific, geo-spatiotemporal, geosampled, productive, georeferenced, seasonally productive, *S. damnosum* s.l, shade canopied, riverine, larval habitat. An analytical approximation method may be presented to calculate the radiation flux in the riverine larval habitat employing the Eddington approximation when the upwelling quantized radiation from the habitat is negligibly small. Numerical experiments in ArcGIS may be carried out to investigate the feasibility of the method in an African riverine flooded or drought induced seasonal scenario. The results may reveal good consistency for remotely, regressively, targeting, canopy reflectivity of unsampled, unknown, riverine habitats at the top of atmosphere and transmissivity just above the canopy surface, in comparison with the exact values calculated by radiative transfer models in each case. Moreover, an obvious error might be introduced for the calculation of radiation flux at larger solar zenith angles when the roughness of the canopy LULC surface is neglected.

However, the governing radiative transfer equation for leaf canopies, in both 3-D and 1-D geometries in ArcGIS has certain unique features (e.g., the extinction coefficient is a function of the direction of photon travel). Also, the differential scattering cross-section in ArcGIS is not, as a rule, rotationally invariant in a canopied, productive, geosampled, georeferenced, *S. damnosum* s.l riverine larval habitat,(i.e., it generally depends on the absolute directions of photon travel and *0*, andnot just the scattering angle arccos^2 *0*.) as Jacob et al. [1] reports. Further, the single scattering albedo is also a function of spatial and directional variables. These properties may make solving the radiative transfer equation for a productive, shade canopied, geo-spatiotemporally, geosampled, prolific, *S. damnosum* s.l., georferenced, riverine, larval habitat, non-binomalized explanatorial model more complicated; for example, the expansion of the differential scattering cross-section in spherical harmonics cannot be used for generating a viable pseudo R^2.

In mathematics, spherical harmonics are a series of special functions defined on the surface of a sphere employed to solve some kinds of differential equations [4]. As Fourier series are a series of functions employed to regressively represent functions on a circle; spherical harmonics are a series of functions that are used to represent functions defined on the surface of a sphere [2]. Spherical harmonics are important in many theoretical and practical applications particularly in the computation of atomic orbital electron configurations, representation of gravitational fields, geoids, and the magnetic fields of planetary bodies and stars, and characterization of the cosmic microwave background radiation [4]. Spherical harmonics are functions definable in terms of spherical explanatorial coordinates which may be organized by angular frequencies, as seen in the rows of regression functions which may be employed for geo-spatiotemporally quantizing, canopy, multi-scattered radiance from 3-D computer graphics of a seasonally geosampled, productive, *S. damnosum* s.l., riverine, larval habitat. Spherical harmonics play a role in a wide variety of topics including indirect lighting (ambient occlusion, global illumination, pre-computed radiance transfer, etc.) and modelling of 3-D shapes [2]. Further, spherical harmonics of a differentially modelled georeferencable, explanatorial, interpolatable, riverine, larval habitat decomposed data may be geospectrally defined as the angular portion of a set of solutions to Laplace's equation in ArcGIS in three dimensions. Represented in a system of spherical coordinates, Laplace's spherical harmonics $Y\left(Y\quad\right)$ are a specific set of spherical harmonics that forms an orthogonal system.

In contrast to radiative transfer in clouds, the extinction coefficient in vegetation, LULC canopy models is wavelength independent especially when considering the size of scattering elements (leaves, branches, twigs, etc.) relative to the wavelength of solar radiation in ArcGIS. For radiative transfer-related algorithms, time series dependent, probabilistically regressable explanatorial, geospectral coefficients may correspond respectively to canopy micro-(e.g., distribution of canopy -type geometry) structures, leaf optical properties and boundary illumination conditions. Although the scattering and absorption processes are different, the optical distance between two arbitrary, canopied, eco-epidemiological capture, points within a georeferncable, riverine, *S. damnosum* s.l., larval habitat may depend on the wavelength. Spectral invariance results in the necessity to regressively quantitate various unique relationships when geo-spectrally explanatorily interpolating, decomposed, *S. damnosum* s.l., riverine, larval habitat, sub-mixel, biosignature related, canopy endmember, time series dependent, emissivity transmittance, wavelenght reflectance, predictor variables [3]. By so doing, compensation mechanisms may be revealed in ArcGIS for resolving difficulties in a radiative transfer equation due to the features of the extinction and the differential canopy multi-scattering cross-sections of these habitats.

Knyazikhin et al. [11] generated a synergistic algorithm in ArcGIS for remotely, qualitatively, regressively quantitating the fraction of absorbed photosynthetically radiation fields from canopy reflectance measured by moderate resolution imaging spectroradiometer (MODIS) and multi-angle imaging spectroradiometer (MISR) instruments aboard the EOS-AM 1 platform. The proposed algorithm was based on a 3-D formulation of the radiative transfer process in vegetation canopies. The model allowed usage of information provided by MODIS (single angle and up to 7 shortwave spectral bands) and MISR (nine angles and four short wave spectral bands) instruments within one algorithm. The algorithm optimally designed a retrieval mechanism for synergistically regressively, qualitatively, quantitating multiple biophysical, canopied, explanatorial variables from MODIS and MISR data. A 3-D formulation of the radiative transfer process was employed to derive simple but correct relationships between geospectral and angular biosignatures of vegetation, LULC, geo-classified, canopy geolocations based on structural and optical characteristics of the canopies. However, these relationships were not directly employed to obtain the best regression fit with measured geospectral and angular canopy reflectance. For accounting for explanatorial, emissivity transmittance, data, feature attributes, specific to the problem of radiative transfer in plant canopies, the authors adopted powerful techniques developed in nuclear reactor theory and atmospheric physics in the retrieval algorithm. This technique allowed the authors to explicitly separate the contribution of soil/understory reflectance from the exitant radiation field and to relate hemispherically integrated reflectance to optical remotely regressively quantifiable properties of canopied phytoelements. By so doing, the authors were able to split the complicated radiative transfer problem into several independent simpler sub-problems in ArcGIS. The solutions to these sub-problems were pre-computed and stored and then employed to retrieve various photosynthetic and NPV explanatorial, time series-related, canopy endmember covariate parameter estimator coefficient values. The authors noted that solutions of the sub-problems were components of various forms of energy conservation principle (e.g., canopy transmittance and absorbance of a vegetation canopy bounded by vacuum on all sides) which were optimally determined from general properties of the rendered radiative transfer, eco-epidemiological, risk, model, explanatorial, time series forecasts.

As such, by accounting for wavelenght emittance an empirical, explanatorial dataset of geo-spatiotemporal, geosampled, riverine-related, prolific, *S. damnosum s.l.,* riverine, larval habitat explanatorily interpolatable, operationizable, decomposable, geo referenceable, datafeature attributes specific to the problem of radiative transfer, powerful techniques may be developed. Further, employing reactor theory and atmospheric physics may split a complicated,3-D, radiative transfer, integration problem in ArcGIS by dividing multiple scattering canopied refluxs into two independent sub-problems and solutions. By so doing, the radiative transfer equations may be discretized separately for clear and cloudy regions within each georeferenced, *S. damnosum* s.l., riverine, larval habitat sub-location, for example which may help remotely represent the exchange of canopy radiation laterally between seasonally sub-modeled regions.

To qualitatively, regressively, remotely estimate canopy radiation regimes, in ArcGIS three important featuresmust be carefully formulatedand resolved which are

(1) the architecture of individual plant and the entire canopy

(2) optical properties of vegetation elements (e.g., leaves, stems) and soil; the former depends on ecophysiological conditions (water status, pigment concentration)

(3) atmospheric conditions which determine the incident radiation field [4].

By idealizing geosampled, georeferencable, *S. damnosum* s.l., riverine, larval habitat, vegetation canopy geo locationsin ArcGIS as a medium filled with small planar elements of negligible thickness and ignoring all other geospatial objects other than green leaves, the habitat, canopy, seasonal stress levels may be parsimoniously regressively quantized and remotely decomposed [1]. In addition, the finite size of vegetation-related, within-LULC canopy elements may be neglected in the 3-D radiative transfer equation. Instead the geosampled, riverine, larval habitat, explanatorial, vegetation LULC, geo-classified, canopy, covariate coefficients would be treated with non-dimensional planar scattering centers. Three variables, the leaf area density distribution function, the leaf normal distribution and the leaf scattering phase are used in the theory of radiative transfer in vegetation canopies to convey "information" about the total leaf area, leaf orientations andleaf optical properties [4]. Therefore, various geolocations of the riverine, larval habitat, vegetation canopy may be treated in ArcGIS as a non-dimensional planar scattering centers, (i.e., a turbid medium).

It should be emphasized that the turbid medium assumption is a mathematical idealization of canopied, explanatorial, LULC structure which ignores finite size of leaves. In reality, finite size scatters can cast shadows. This would cause a very sharp peak in reflected radiation about the retro-solar direction when qualitatively regressively quantitating important geolocations of a geo-spatiotemporally geosampled, shade canopied, *S. damnosum* s.l., productive, georeferenced, riverine, larval habitat (e.g., the "hot spot" effect) in ArcGIS. If the georeferenced, geosampled, riverine, larval, habitat canopy scatters cannot cast shadows, the turbid medium concept in its original formulation [Ross, 1981] would fail to predict or duplicate experimental observations of exiting canopy radiation about the retro-illumination direction of a cloud-covered, eco-epidemiological, capture point.

The 3-D variability of clouds has an important impact on the transfer of radiation in the Earth's atmosphere. The current practice in climate modeling in ArcGIS assumes clouds are horizontally homogeneous which entails significant errors (ww.esri.com). A new method, based on the backward Monte Carlo technique, has been developed in ArcGIS for computing the mean outgoing canopy radiation field from any type of stochastic ensemble of cloud structure. The most flexible and realistic treatment of canopy radiation for a particular empirical dataset of geo-spatiotemporally, geosampled, explanatorily decomposable, *S. damnosum* s.l.-related, photosynthetic and NPV, eco-graphical and non-ecogeographical, covariate, time series, empirically, probabilistically regressed, covariate, parameter estimators is that of "Monte-Carlo" since any and all geometrical configurations can be included in the context of statistical choices [4]. The accuracy of the technique has been verified by comparison with many realizations of deterministic radiative transfer in ArcGIS. The explanatorily method may illustrate how seasonal geospatial variability in an empirically regressed datasets of productive, *S. damnosum* s.l. georeferenced, canopied, riverine, larval habitat, remotely sensed, photosynthetic and NPV, geo-spatiotemporal, geosampled, explanatorial regressors can lead to improved representations of the radiative effects of clouds in a GCM. The rate of lateral exchange may be optimally determined by the area of cloud "edge." The validity of the method may be demonstrated by comparing the model residually forecasted, georefernced, canopied, productive, riverine habitats with rigorous 3-D radiative transfer calculations for varying cloud types in which the 3-D effect is strong, (e.g., cumulus). For example, the 3-D effect on shortwave cloud radiative forcing in ArcGIS may vary between around −25% and around +100%, depending on solar zenith angle for a flooded, seasonally prolific, shade, canopied, riverine, *S. damnosum* s.l., georefernced, habitat. Even with an otherwise very simplistic representation of a cloud over a African riverine environment, the new scheme may exhibit good agreement with the rigorous calculations in the shortwave, opening the way for efficient yet accurate eco-geographic representations of geospectrally, explanatorily interpolatable, unknown, unsampled, seasonally prolific, *S. damnosum* s.l. riverine larval, habitats in climate-oriented, canopy, endmember –related, forecasting, time series dependent, eco-epidemiological, risk models.

Although the multi-scattering and absorption processes are different at different wavelengths, the interaction probabilities for photons and vegetation-related, canopied LULC media may be probabilistically qualitatively, regressively quantized in ArcGIS by the structure of the canopy rather than photon frequency or the optics ofthe canopy. Photon transport theory aims at deriving the solar radiation regime [4]. Employing photon-related, explanatorial, uncertainty-related, regression -based method of statistical downscaling from global multimodel ensemble (MME) forecasts may result in capturing unique geospectrally invariant behavior for quantitating, seasonally, geosampled, georeferencable, riverine, *S. damnosum* s.l., larval habitat, vegetation LULCs, canopy bounded ecogeographic and non-ecogeographic geolocations from below by a non-reflecting surface. Indirect methods enable estimation of riverine, LULC, decomposed, canopied, time series, explanatorial properties by measurements of the radiation transmission through the canopy, making use of the radiative transfer theory [1]. By so doing, simple algebraic combinations in an ArcGIS-derived radiative transfer equation of the single-scattering albedo and canopy geospectral transmittances and reflectance of the regressed prolific, canopied, seasonal, riverine habitat covariate, parameter estimators habitat may eliminate dependencies on wavelength uncertainties through the specification of two canopy structure spectrally invariant variables– the recollision and escape probabilities.

The recollision probability is the probability that a photon scattered from a phytoelement will interact within the canopy and is related to the maximum eigenvalue of the radiative transfer equation [4]. The escape probability is the probability that a scattered photon will escape the vegetation in a given direction. These variables can specify an accurate relationship between the geospectral reflectance intensity response of an ArcGIS-related, eco-epidemiological, endemic, transmission-oriented, risk model platform delineating geo-spatiotemporally, geosampled, explanatorial, vegetated, prolific, georeferencable, shade, canopied, *S. damnosum* s.l. riverine, larval habitat to these model derivatives may be canopy scale, while allowing for accurate parameterization forprecise partitioning of the incoming radiation. This result may be essential toempirically regressing a geosampled, georeferencable, dataset of explanatorial, time series dependent, *S. damnosums*.l. riverine, larvalhabitat, canopy, endmember, risk-related, decomposable, biosignature oriented, forecasting, ecogeographic or non-ecogeographic, predictor variables as it would allow for parathions of the structural and radiometric components of the measured and/or modeled, canopy signals to be adequately qualitatively analyzed. The former would be a function of the larval habitat's canopy, age,density and arrangement whilethelatterwould be afunctionof the habitat'scanopy biochemical behavior. Consequently, thecanopyspectralinvariants as geo-spatiotemporally, remotely quantitated in a 3-D radiativetransfer equation in ArcGIS can offer a simple and accurate parameterization of the radiation block in a global, time series dependent, explanatorial, *S. damnosums*.l., georeferenced, prolific, riverine, larval habitat, canopied, endmember, geospectrally interpolatable, explanatorily forecasting, shaded or non-shaded, geospatial, eco-epidemiological, risk model based on climate, hydrology, biogeochemistry and/or ecology. Due to the highly non-linear response of photosynthesis to light, temperature and humidity, whole canopy photosynthesis cannot be derived from computed mean values of light and temperature. Complex models simulating both temporal and spatial geo-variability in environmental drivers and potentials is needed to accurately estimate variable geospatially associated with canopy photosynthesis and NPV covariate coefficients [4]. Overestimation of radiation coupling due to non-quantitation of seasonal geospatial clumping of species can generate mispecifications [2]. Recent advances in radiative transfer models in ArcGIS have led to complex 3-D models that are capable of simulating radiation interception in discontinuous canopies by considering complex phenomena such as penumbra and light scattering. The stochastic mixture radiative transfer (SMRT) model in ArcGIS has resolved some deficiencies in major existing mixture models (e.g., ignorance of species radiation coupling, unquantitated, scattering of photons).

A radiation treatment for an empirical, geo-spatiotemporally, geosampled dataset of *S. damnosum* s.l., georeferenced, empirically decomposed, prolific riverine, larval habitat, canopy endmember, geospectrally, explanatorily interpolatable, shaded and non-shaded, canopied, risk model, parameter estimators may be optimally regressed based upon various forecasting, ArcGIS, stochastic/deterministic, algorithms. In the radiative transfer equation the clouds and clear sky may be treated as a two-component mixture. These models, recently introduced in the kinetic theory literature, allow for non-Markovian statistics as well as both vertical and lateral variations in cloudiness states. Numerical results may be rendered given that different models of stochastic radiative transport point out varying levels of importance for treating the broken-cloud problem in an African riverine environment as a stochastic process, for example. It may be also shown that an integral Markovian model proposed within atmospheric radiation, explanatorial, *S. damnosum* s.l. riverine larval habitat eco-epidemiological, canopied, geospectral, explanatorily interpolatable, forecasting risk model is entirely equivalent to a special case of a simple low-order different model. The differential form may be easier than the integral form to implement in any general circulation model.

Soil Vegetation Atmosphere Transfer (SVAT) model, and Land Surface Process(LSP) models in ArcGIS may be coupled with a widely used crop-growth model, [e.g., Decision Support System for Agrotechnology Transfer (DSSAT)], to estimate energy and moisture fluxes canopied LULCs in African, riverine, canopied ecosystems for remotely estimating growing hanging vegetation endmembers geospatially associated to prolific, georeferenced, shaded and non-shaded, *S. damnosum* s.l. larval habitats. By so doing, detailed observations of soil and canopy emissivity transmittance, reflectance wavelenght characteristics, and various components of energy and water balance during a season-long field experiment of riverine, immature habitat, geosampled, canopied, covariate, parameter estimators may be parsimoniously analyzed. A georeferenced, geosampled,*S. damnosum* s.l., riverine, larval habitat, empirical, eco-epidemiological dataset of explanatorial, decomposed, photosynthetic or NPV covariate coefficients may be thereafter employed to calibrate the LSP with Latin HypercubeSampling and Pareto ranking. Latin hypercube sampling (LHS) is a statistical method for generating a sample of plausible collections of geospectrally dependent parameter estimator values from a multidimensional distribution [4].

For a given riverine ecosystem, the Pareto frontier or Pareto set is the set of parameterizations (allocations) that are all Pareto efficient [2]. Finding Pareto frontiers may be particularly useful when constructing optimally, geospectrally dependent, eco-epidemiological, risk-related, decomposable, geopredictive, time series models for identifying prolific, unknown, unsampled, georeferncable, shade, canopy vegetated, *S. damnosum* s.l.,riverine, larval habitats. By yielding all of the potential solutions, an ecologist or experimenter can make focused tradeoffs within a constrained set of explanatorily regressed,empirical geosampled dataset of time series dependent, field or remote, geo-specified,photosynthetic or NPV, geo-spatiotemporal, geosampled, larval habitat, emissivity transmittance, wavelenght, reflectance, covariate, parameter estimators, rather than needing to consider the absolute full regressive ranges of their co-variate coefficient values.

Further, comparisons may be conducted on the geosampled, riverine, larval habitat, canopied, vegetated, LULC shaded or non-shaded observations with regression-related,photosynthetic or NPV geo-spatiotemporal, forecasting, eco-epidemiological, risk model, emissivity transmittance, reflectance, wavelenght estimates of quantitated surface fluxes, soil moisture and temperature profiles in ArcGIS from both the stand-alone LSP and coupled LSP-DSSAT models. It may be found that the model derivativs of regressed radiation fluxes, soil moisture, and soil temperature, by both the LSP and LSP-DSSAT are very similar, indicating that a LSP-DSSAT georeferencable, eco-epidemiologcal,, time series dependent,*S. damnosum* s.l., larval habitat, geospectral explanatorial, probabilistic, risk model can be employed to simulate fluxes for dynamic canopied, shaded or non-shaded, vegetation-related LULCs without the need of in situ observations during riverine flooding. Moreover, because coupling may be achieved without structurally changing either of the riverine, larval habitat, emissivity transmittance, wavelenght, reflectance models, the methodology can be optimally extended to coupling other SVAT and vegetation, riverine-related, *S. damnosum* s.l., larval habitat, ArcGIS-derived, GCMs.

Alternatively, optimization emissivity, transmittance, wavelenght, reflectance models in ArcGIS may precisely regressively forecast total canopy leaf area and foliage photosynthetic and NPV potentials of a georeferncable, canopied, geospectrally dependent, prolific, *S. damnosum* s.l., riverine, larval habitat, eco-epidemiological, risk-related, model by incorporating available nitrogen or foliage biomass as regressors. Significantly smaller number of, time series dependent, endemic, quantitative regressive, eco-geographically and non-ecogeographically forecastable, parameter estimators may be required for these models as the spatial distributions of foliage and photosynthetic and NPV characteristics may be determined by assumptions about optimality. However, the simple optimization models considering only light as the key environmental co-factor may result in a significant bias between simulated and measured photosynthesis and NPV profiles within the canopy, limiting the use of such models in practical scaling applications.

Further, assuming that the georefernced, geosampled, prolific, riverine, larval, habitat canopy consists of identical, individual, non-competing plants can also lead to excess unquantited uncertainty in the probabilisitic, residual, model, explanatorial, time series dependent, wavelenght, transmittance, reflect anceforecasts. Leaf optical models models have been employed for remotely regressively quantizing competition between different individuals which may yield better correspondence between geosampled, riverine, larval habitat, probabiliistically, geo-spatiotemporally regressed, canopied data and predictions, suggesting that these optimization models have a large potential for forecasting prolific, georefernced, unknown, unsampled, seasonally, shaded or non-shaded *S. damnosum*s.l. habitats. More information of the functioning, *S. damnosum* s.l., riverine, larval habitat, plant canopies, in particular the response of the plant canopies to multiple, seasonal, environmental stresses as well as competitive interactions is still needed however to define alternative optimization functions in ArcGIS for correctly simulating and remotely qualitatively regressively quantitating photosynthetic and NPV productivity in these highly heterogeneous, canopied, geospatial objects.

In Jacob et al. [1] the canopy structure from a sub-meter resolution, imaged, georeferenced, shade canopied, *S. damnosum* s.l., riverine, larval habitat was parameterized in a geospectral, explanatorial, forecasting, eco-epidemiological, emissivity transmittance, reflectance, optical, risk model in terms of stochastic moments(i.e., the probability of finding a geosampled prolific, georeferenced, riverine, larval habitat imagedin a riverine basin in Togo) based on an empirical dataset of geo-spatiotemporally, kriged, field, decomposed, endmember, biosignature-related, photosynthetic and NPV, empirical, covariate, parameter estimator, coefficient regression values. The eco-geographical locations for multiple, riverine-based, *S. damnosum* s.l., larval ecosystem habitats geosampled from 2 pre-established eco-epidemiological study sites in Togo were identified and recorded from July 2009 to June 2010. Initially, the data was aggregated into PROC GEN MOD. An agglomerative, explanatorial, operationizable, time series, hierarchical, residual, cluster-based, eco-epidemiological, risk analysis was then performed. The geosampled clustered eco-epidemiological, study site data was then analyzed for statistical correlations using Monthly Biting Rates (MBR). Euclidean distance measurements and terrain-related, geomorphological statistics generated in ArcGIS. A digital time series overlay was then performed in ArcGIS employing the georeferenced ground coordinates of high and low density clusters stratified by Annual Biting Rates (ABR). This data was overlain onto multitemporal, sub-meter, sub-mixel resolution, satellite data (i.e., QuickBird 0.61m visible and NIR wavbands). Orthogonal spatial filter eigenvectors were then generated in SAS/GIS.

Univariate and non-lineardiagnostic, regression-based models (i.e., Logistic, Poisson Negative Binomial, Moran's *i*) were also employed to determine probability distributions and to identify statistically significant emissivity transmisstance, wavelenght, reflect anceparameter estimators from the sampled data. The Moran coefficient is a product moment correlated -related statistic which may be used to determine if like attributes aggregate in eco-geographical space [12]. Thereafter, Durbin-Watson test statistics were used to test the null hypothesis that the regression residuals were not autocorrelated against the alternative that the residuals followed an autoregressive process in AUTOREG. Durbin-Watson test statistics tests for first-order autocorrelation [www.sas.edu].

Bayesian uncertainty matrices were also constructed employing normal priors for each of the geosampled parameter estimators in PROC MCMC. The residuals revealed both geospatially structured and unstructured error effects in the high and low ABR-stratified clusters. The analyses also revealed that the estimators, Levels of turbidity and Presence of rocks were statistically significant for the high-ABR-stratified clusters, while the estimators Distance beween habitats and floating vegetation were important for the low-ABR-stratified cluster. Varying and constant coefficient regression models, ABR-stratified, ArcGIS-generated geospatial, sub-meter resolution, satellite imagery, a robust residual, intra-cluster, non-normality, diagnostic,validation test, MBR-based, eigendecomposition, spatial filter algorithms and Bayesian paradigm scan enable accurate autoregressive estimation of latent affects (i.e., heteroskedastic parameters) and other residual emissivity transmittance, wavelength, reflect anceerror probabilities for testing correlations between georeferencable, *S. damnosum* s.l., riverine, larval habitat, covariate, paramter estimators estimators. The asymptotic distribution of the resulting empirically residually adjusted, intra-cluster, probabilistic, predictor error, autocovariate coefficients can thereafter be established while explanatorial estimates of the asymptotic variance can lead to the construction of approximate confidence intervals for accurately, regressively targeting, productive *S. damnosum* s.l., habitats based on geo-spatiotemporal, field-geosampled, count data Further, a second moment was found to be responsible for robustly remotely describing the 3-D radiation effects, namely, radiation streaming through the canopy gaps without interaction with vegetation-related, explanatorial, geoclassified, LULC variables and geo-classified,emissivity transmittance, wavelenght reflectance variation. By so doing, the, radiation fluxes between differing seasonally productive, georeferenced, shaded, within-canopied, larval habitat, spectral components (e.g., turbid water, pre-Cambrian rock) were geo-spatiotemporally, probabilistically, regressively quantized.

In contrast to the empirical methods, geophysically-based approaches may operationally describe the processes of interaction of radiation within a geo-spatiotemporally-geosampled, prolific, *S. damnosum* s.l.georefernced, riverine, larval habitat, and discontinuous canopy employing an elementary volume of shaded, vegetation-related, LULC classes. Optical properties of a mixture in such volume may be represented in ArcGIS as weighted average of optical properties of pure species. The Radiative Transfer Equation (RTE) is used to model the radiation field with effective optical properties of mixed canopy [2]. The modeling principles of an RTE in ArcGIS may be implemented, for example, in a scaling scheme of the radiation block of a Common Land Model (CLM) for invasively remotely qualitatively examining explanatorial, LULC, time series, Thessian dependent, polygons associated to a georefernced, empirical datset of prolific, geosampled, *S. damsnoum*s.l., riverine, larval habitats.

The major limitation of the RTEs and CLM schemes in ArcGIS may be however that the linear, uncertainty-related, geo-spatiotemporally observational, explanatorial, *S. damnosum* s.l., riverine, larval habitat, predictor, error probabilities may be based on the turbid medium, mixture approximation, where canopy is ecogeographically and non-ecogeographically targeted as a mixture of vegetation species and gaps. Mixtures may exhibit various spatial heterogenic profiles of foliar distribution, leaf inclination and component species height [4]. Biased regressed estimations may however, be observed when qualitatively quantizing, explanatorily, interpolatable, decomposable, photosynthetic and NPV, covariate, parameter estimator, reflectance emissitivty, transmittance coefficients, representing immersed trailing vegetation in shaded and non-shaded, *S. damnosum s.l.,* riverine, larval habitat, canopy endmember grassland LULC species, for example. Most of the discrepancies may be due to unquantitated vertical heterogeneities which may be corrected by increasing the vertical description of the habitat canopies although, in practice, this would require procuring, time-consuming ArcGIS measurements. Regardless, the turbid medium analogy could be successfully employed in a wide range of riverine, *S. damnosum* s.l., georeferenced, canopied, remotely sensed, explanatorial measurements. However, a more detailed description of the canopy may be required for mixtures exhibiting vertical stratifications and inter/intra-species habitat canopy foliage overlapping.

Architectural models in ArcGIS remain a relevant tool for studying light partitioning in intercropping systems that exhibit strong vertical heterogeneities. Moreover, these models offer the possibility to integrate the effects of microclimate variations on canopy plant growth within a geo-spatiotemporally, prolific, georeferenced, *S. dasmnosum* s.l., larval habitat, eco-epidemiological, riverine, regression-related, forecast, risk models employing the turbid medium approach. With landscape scales, topography is a major factor that determines the geospatial variability of insolation. Variation in elevation, orientation (slope and aspect), and shadows cast by topographic features all affect the amount of insolation received at different locations. This variability also changes with time of day and time of year and in turn contributes to variability of microclimate including factors such as air and soil temperature regimes, evapotranspiration, snow melt patterns, soil moisture, and light available for canopy photosynthesis [4]. The solar radiation analysis tools in the ArcGIS Spatial Analyst extension enable mapping and analyze the effects of the sun over a geographic area for specific time periods (www.esri.com). These tools can account for atmospheric effects, site latitude and elevation, steepness (slope) and compass direction (aspect), daily and seasonal shifts of the sun angle, and effects of canopy shadows cast by surrounding riverine LULC topography of a geosampled, georeferenced, seasonally productive, *S. damnsoum* s.l., larval habitat. The resultant outputs can be easily integrated with other GIS data and can help model geophysical and ecobiological processes as they are affected by the sun. One major feature of the natural vegetation is missing geospatial structure of a mixture, which may substantially affect canopy radiation regime [4].

Three contrasted mixtures of wheat-pea, tall fescue-alfalfa and tall fescue-clover were sown according to various patterns and densities which were seasonallytime series regressively quantized in ArcGIS using the medium homogenous turbid assumption [6]. Three-dimensional plant mock-ups were derived from magnetic digitizations carried out at different stages of development. The benchmarks for light interception efficiency (LIE) estimates were provided by the combination of a light projective model and plant mock-ups, which also provided the inputs of a turbid medium model (SIRASCA) based on leaf geometries and inclination. SIRASCA was set to gradually account for vertical heterogeneity of the foliage, (i.e. the canopy was described as one, two or of leaves). Mixtures exhibited various and heterogeneous profiles of foliar distribution, leaf inclination and component species height. Nevertheless, most of the LIE was satisfactorily predicted by SIRASCA. Biased estimations were, however, observed for (1) grass species and (2) tall fescue-alfalfa mixtures grown at high density.

One of the major assumptions underlying the turbid medium approach is that the canopy can be considered as a homogeneous and continuous medium where leaves are small and randomly distributed. Such a hypothesis would be questionable in a geo-spatiotemporal, geosampled, ArcGIS-derived, *S. damnosum* s.l., productive, riverine, larval habitat, spectrally dependent, eco-epidemiological, forecasting, risk model which generally build up non-homogeneous canopies [1]. Indeed, these canopied habitats present several seasonal, vegetation–related, geoclassified, LULC patterns (e.g., hanging immersed, dead floating,) thus, leading to various geospatial heterogeneities. These canopies heterogeneities may be attributed to foliage overlapping or empty unstructured spaces between plant species. Canopy systems generally include various species with their own morphogenesis, phenology and radiation interception ability which subsequently are dependent on leaf geometrical features [4]. Remotely capturing these time series dependent, habitat–related, canopy contrasts in ArcGIS might lead to various inter and intra –species patterns of leaf dispersion, either random, regular or clumped. Although the turbid approach has been widely employed in the case of sole crop mapping and tree species identification, a major difficulty would arise for the validation of such an approach when regressively quantiating seasonal, *S. damnosum* s.l., larval habitat, canopy stands. Indeed, due to the impossibility of carrying out direct measurements of light partitioning in mixed canopies such as those of turbid medium based estimations, the field verifiable metrics would be miss pecified since the canopy end member stochastic/deterministic inter polatormay only be able to partially determine the total amount of transmitted radiation reaching the soil.

Surface-based approaches in ArcGIS may model the canopy structure of a geosampled, shade canopied, prolific, *S. damnosum* s.l. larval habitat employing realistic 3-D representations in which individual canopy plant architecture may be regressively explicitly described as a collection of interconnected phytoelements, including their geometry and optical properties. By so doing, canopy heterogeneities of the georeferenced riverine habitat may be explicitly taken into account when simulating radiative exchanges in these architectural models. Magnetic 3-D digitizing may be the most suitable technique for collecting information on plant architecture prior to *in silico* reconstruction [4]. Herbaceous canopy mixtures in the georefernced, *S. damnosum* s.l., riverine, larval habitat may also appear to be a relevant as they are easily accessible to these kinds of measurements; this is particularly so for grass –related, geocalssified, explanatorial, seasonal, LULC covariates which are widely employed in eco-epidemiological, entomological-related, forecast, risk paradigmss as categorical reflectance wavelenght, emissivity, transmittance variables.

In Jacob et al. [1], an extent of the canopied, radiance, fractional area within a geospectrally extracted, 0.61m, spatial resolution, mixel was solved in ArcGIS employing a georeferenced, geo-spatiotemporally dependent, explanatorily, geosampled, *S. damnosum* s.l., riverine, larval habitat-related, radiance, fractionalized, eco-epidemiological, canopy, endmember biosignature–related, risk model with a pre-determined class vector employing a geometric-optical model output. Most vegetation-based, time series-related, riverine LULC cover consisted of discrete plant crowns, of which the sub-mixel, biophysical, explanatorial observation departs from the underlying assumption of a homogenous and uniform medium [2]. The geometric-optical forest canopy reflectance, emissitivty, transmittance, risk model treated casted shadows on a contrasting background which explained the major portion of the variance in the sub-resolution, remotely sensed, image of a georeferenced, *S. damnosum* s.l., riverine, larval habitat-related, eco-epidemiological, sub-mixel, sub-meter resolution, decomposed canopy interpolatable, biosignature. The model was driven by inter-mixel variance generated from three sources: 1) the number of crowns in the larval habitat geospectrally extracted mixel; 2) the size of individual crowns; and 3) overlapping shadows [2]. The model employed parallel-ray geometry to describe the illumination of the 3-D geospatial object (i.e., georeferenced, geosampled, *S. damnosum* s.l., riverine, larval habitat-related, radiance, fractionalized, canopy endmember biosignature) and the shadow it casted. In geometry, parallel lines are lines in a plane which do not meet; that is, two lines in a plane that do not intersect or touch at any point are said to be parallel [2]. By extension, a line and a plane, or two planes, in 3-D Euclidean space in ArcGIS that do not share a sub-mixel, explanatorily interpolatable, decomposed point are said to be parallel(www.esri.com).

Remote images of canopy leaves of a georeferenced, geo-spatiotemporal, *S. damnosum* s.l., larval habitat-related, eco-epidemiological, decomposed, sub-mixel, biosignature would be assumed to be random and may seasonally overlap freely. Canopy leaf size (e.g., height) is distributed log-normally, and cone form described by the apex angle of the leaf [2], whichmay be affixed into a model regression as an independent variable. The model can also be inverted to render estimates of the size and shape and geo-spacing of the larval habitat canopy using satellite imagery and a minimum number of field-verifiable measurements. Field tests employing both 0.61m multispectral imagery of two canopy stands in Burkina Faso produced reasonable regression results for optimally forecasting an empirical dataset of prolific, georeferencable, pre-Cambrian–related, *S. damnosum* s.l., canopy-vegetated, riverine larval habitat, explanatorial, time series dependent, shaded or non-shaded, dependent variables (e.g., floating dead vegetation) [1].The model generated appeared to be sufficiently robust for remotely delineating geometric shapes (e.g., oval pre-Cambrian rocks) and mixtures of simple LULC shapes (e.g., canopy leaves). The overhead, reflectance emissivity, transmittance, time series explanators rendered from these models were then exported into an ArcGIS geodatabase for mapping, georefernced, prolific habitats at the eco-epidemiological study site.

An eco-epidemiological, geometric-optical, explanatorial, endemic, transmission-oriented, forecasting, denoising, diagnostic, ArcGIS eco-epidemiological, probabilistic, risk model would have wide potential use not only in regressing canopied, geo-spatiotemporal, probabilistic, prolific, georeferenced, shaded, *S. damnosum* s.l., riverine, larval habitat-related, geo-spectrally, decomposable canopied, vegetation-oriented, LULC, covariate, parameter estimator reflectance emissivity, wavelenght, transmittance coefficients, but also in other remote situations in which the unmixed, imaged endmember biosignature-related, canopy discrete objects resolution cannot be resolved individually. For example, the geometric-optical model in Jacob et. al. [1] separated the canopy radiation absorption into two components that were absorbed by sunlit and shaded leaves, and then the authors derived analytical solutions by integrating the residuals over the canopy layer at 0.61m, geospatial, geospectral, sub-mixel level. To model leaf-level and canopy-level empirical covariate time series, parameter estimators representing unmixed, photosynthetic and NPV rates in geo-spatiotemporally dependent, *S. damnosum* s.l., riverine, explanatorial, larval habitat, geometric-optical, ,risk model, leaf light absorption had to be linked to the biochemical process of gas diffusion through the leaf stomata. The canopy gap probability derived the operationalizable, eco-epidemiological, geometric-optical model, residual, non-normal, explanatorial, misspecified, residualized, regressed outputs.

Estimation of directional gap probability (P_{gap}) in ArcGIS from waveform, medium resolution, sensed, data may be both direct (i.e. physically-based) and minimize or remove requirements for field calibration which would be significant advance for seasonally mapping georefernced, canopied, *S. damnosum* s.l., larval habitat, risk geographic sample frames precisely. A new model for estimating P_{gap} from small footprint data may account for time series, regressed, residual differences in canopy volume (ρ_v) and ground reflectivity (ρ_g). These surveys may be acquired at multiple altitudes employing 5m waveform systems, for example, over an African riverine ecosystem. A derived waveform model for P_{gap} may be found to fit observed waveform data especially in cases where the assumption of constant ρ_v and ρ_g are satisfied. P_{gap} estimates rendered from the waveform model may be shown to be relatively insensitive to variation in sensor altitude. Comparison of P_{gap} with ground measurements may reveal a new waveform model which may render robust, geospectrally decomposable, explanatorily interpolatable, shaded and non-shaded, canopied, *S. damnosum* s.l., riverine, larval habitat, endmember, photosynthetic and NPV, probabilistically regressed, estimates corresponding to within 5% P_{gap}. The time series dependent, explanatorial forecasts may suggest that the waveform model can retrieve ρ_v/ρ_g and P_{gap} which may be a significant advance in remote retrieval of riverine, larval habitat-related, canopy structures, from a small footprint scene. By so doing, the need for local calibration, for providing direct estimates of P_{gap}in ArcGIS may be significantly reduced. If the assumptions of relatively stable ρ_v/ρ_g are shown to hold across a greater range of sensor surveys, and canopy structure configurations, this method may have wide practical application for retrieval of P_{gap} for identifying unknown, unsampled, productive,georeferenced, shaded or non-shaded, canopied, *S. damnosum* s.l., larval habitats geosampled inan African riverine environment.

However, explanatorial, georeferencable, canopied, endmember, decomposable, unmixed, biosignature-related, probabilistic, explanatorial, regressor properties and the equations obeyed by the ray density function in a *S. damnosum s.l* larval habitat sub-mixel, forecasting eco-epidemiological, canopy endmember, risk model in ArcGIS may have to be deduced prior to exporting the forecasts into an time series dependent, residualizable, geometric–optically, specified, forecastable, algorithmic, weighted framework. An ecologist or experimenter may need to generalize the radiative transfer theory for this purpose appropriately. For homogeneous statistical wave fields radiative transfer theory obtains polarization properties of light rays [4]. These concepts may have some relation with the phase-space picture of quantum mechanics when remotely, aggregating, an empirical dataset of decomposed sub-mixel, prolific, *S. damnosum* s.l., georefernced, geospectrally interpolatable, endmember-related, biosignature oriented riverine, larval habitat, explanatorial reflectance emissivity, wavelenght, transmittance regressors. Leaf clumping canopy characteristics such as density, crown shape, and length that commonly regulate radiation interception in a geosampled, shade, canopied, georeferenced, seasonally, prolific,*S. damnosum* s.l., riverine, larval habitat may be then undetectable from a remote perspective. These explanatorial, photosynthetic-related and NPV time series dependent, covariate, parameter estimator coefficients may remain remotely unquantitated in the radiative transfer model, thus generating mispecification in the forecasts.

Conversely, by employing, time series dependent, geometric-optical, radiance fractionalized, remotely sensed, proxy, biophysical, explanatorial, decomposable, endmember biosignature-oriented variables in ArcGIS robust, residualized, regressable, geospectrally, explanatorily, interpolatable, forecast estimates may be parsimoniously defined. Modeled gross primary production (GPP) for two deciduous forest stands explained more than 80% of the variance of flux tower measurements at both near hourly and daily time scales as measured in a geometric-optical model [10]. Ambient CO_2 concentration that influences daytime,canopy vegetation, optimum photosynthesis for a geosampled, georeferenced, prolific, riverine, *S. damnosum* s.l., larval habitat may be also considered in state-of-the-art, biogeochemical, time series dependent, geometric-optical, risk model constructed in ArcGIS. The proposed model may show promise in modeling radiative transfer processes for quantitating photosynthetic activities in vegetated LULC canopies, over discontinuous, productive, shade-oriented, riverine,*S. damnosum* s.l., larval habitat, however it may render regression-related, explanatorial, forecast-oriented, reflectance, wavelenght, emissivity, transmittance, probabilistic uncertainties due to shifting of erroneously log transformed meteorological variables.

One of the major uncertainties in predicting climate change comes from a full accounting of carbon-cycle feedbacks, which roughly double physical feedbacks [1, 2]. The geological component of the carbon cycle is where it interacts with the rock cycle in the processes of weathering and dissolution, precipitation of minerals, burial and subduction [4]. In the atmosphere, carbonic acid forms by a reaction with atmospheric carbon dioxide (CO_2) and water. As this weakly acidic water reaches the surface as rain, it reacts with minerals at Earth's surface, slowly dissolving them into their component ions through the process of chemical weathering. These component ions are carried in surface waters like streams and rivers eventually to the ocean, where they precipitate out as minerals like calcite ($CaCO_3$). Through

Citation: Jacob BG, Novak RJ, Toe LD, Sanfo MS, Lassane K, et al. (2016) Ecogeographically and Non-Ecogeographically Forecasting Discontinuous Canopied *Simulium damnosum* s.l. Habitats by Interpolating Metrizable Sub-Mixel Mean Solar Exoatmospheric Quantum Scalar Irradiance where θ_i is a Zenith Angle and Diatomically Etiolated Xanthophylls with Azimutally Isotropic Sources of Chloroplastic Carotenoid Zeaxanthins Spectrally Extracted from a Decomposed RapidEye™ Red Edge Normalized Difference Vegetation Index Reference Biosignature: A Case Study in Burkina Faso and Uganda. J Remote Sensing & GIS 5: 152. doi:10.4172/2469-4134.1000152

continued deposition and burial, this calcite sediment forms, may be a part of a geospatiotemporally, geosampled, prolific, georeferenced, *S. damnosum* s.l. riverine, larval habitat, forecasting, eco-epidemiological, probabilistic, explanatorial, risk model.

Most probabistically quantized, regression, reflectance emissivity, transmittance, wavelenght, uncertainties are a result of multiple pathways and time scales at within riverine ecosystems interact in space with a climate system. Most remote regressive uncertainties are a result of the many pathways and time scales at which ecosystems interact in linear space with the climate system and how these variables respond to change. Given understanding of explanatorial, time series dependent, ecophysiological, control-oriented regressors in photosynthesis and NPV response model outputs that can demonstrate the significance of carbon on controlling productivity, it is not surprising that a primary goal for employing imaging explanatorial, spectroscopic-oriented, independent variables for robustly remotely capturing prolific, georeferncable, *S. damnosum* s.l., larval habitats geosampled in an African riverine environment may be by quantifying canopy photosynthetic and NPV variable capacity in ArcGIS prior to performing the regression exercise for accurately forecasting, unknown, unsampled, productive, seasonal habitats. Because leaf reflectance could be affected by species structure, the indices to measure chlorophyll content may vary with plant species, space, and time series predictors [4].

Canopy reflectance is affected not only by leaf chlorophyll, but also by canopy scattering and soil reflectance [7]. Foliar chlorophyll content in riverine forested ecosystems plays a fundamental role in plant photosynthesis and can indicate vegetation stress and disturbance [8]. However, leaf chlorophyll retrieval is complicated as canopy reflectance in the visible and NIR wavelengths is affected by confounding effects not only from leaf pigment concentration but also leaf area index (LAI), canopy architecture, illumination and viewing geometry and understory vegetation. Leaf area indexis a dimensionless quantity that characterizes plant canopies [2] which may be defined in a geo-spatiotemporally, geosampled, *S. damnosum* s.l., riverine, larval habitat as the one-sided green leaf area per unit ground surface area (LAI = leaf area / ground area, m^2 / m^2) in broadleafcanopy [1]. Unlike empirical indices, which are often developed at leaf-level and can be species, site and time specific, a process LAI approach can account for the variation of other variables affecting canopy reflectance; therefore providing a more accurate estimate of chlorophyll content over multiple vegetation species, time-frames and across broader spatial extents.

Croft et al. [9]employed a linked canopy (4-Scale) and leaf (PROSPECT) to investigate the ability of radiative transfer models to estimate foliar chemistry for different canopy vegetation LULC types (e.g., broadleaf and needle leaf) from optical remote sensing data. Coniferous and deciduous sites were selected in Ontario, Canada, representing different dominant vegetation species, including black spruce (*Picea mariana*), sugar maple (*Acer saccharum)* and trembling aspen (*Populus tremuloides*), and a variety of canopy closures and structures. These sites were sampled over multiple time-frames to collect ground data including LAI, leaf reflectance spectra (400–2500 nm) and laboratory leaf chlorophyll content. Canopy reflectance data were acquired from the Compact Airborne Spectrographic Imager (CASI), Landsat 5 TM and Medium Resolution Imaging Spectrometer (MERIS). The model revealed that leaf chlorophyll content derived from satellite images had a good relationship with measured leaf chlorophyll content, {i.e., validation results of $R^2 = 0.62$; $p < 0.001$ (MERIS) and $R^2 = 0.65$; $p < 0.001$ (Landsat 5 TM)], and had a strong linearity with negligible systematic bias. CASI data gave a regression coefficient of $R^2 = 0.41$ ($p < 0.05$) on a reduced dataset. This research provided theoretical and operational bases for the retrieval of leaf chlorophyll content across different vegetation species, canopy structures and over broad spatial extents; crucial characteristics for inclusion in photosynthesis and carbon cycle geo-spatiotemporal, geosampled, explanatorily interpolatable, *S. damnosum* s.l., riverine, larval habitat, canopy forecasting, eco-epidemiological, risk model. The transformation from leaf to canopy geospectral response is complex, and cannot be done by simple extrapolation from leaf to canopy scale [2]. This change is especially true for complex heterogeneous canopies such as those associated with geo-spatiotemporally, geosampled, riverine, shaded, productive, *S. damnosum* s.l., larval habitat, canopy reflectance properties (e.g., leaf spatial distribution, and solar angle).

Interestingly, since canopy photosynthesis always begins when energy from light which is absorbed by proteins that contain chlorophyll, logic dictates this plant pigment may be vital for accurately, geospectrally, explanatorily, interpolating an NDVI, canopied, endmember, reference biosignature as extracted from a satellite imaged ,seasonally geosampled, shaded or non-shaded, georeferenced, prolific, *S. damnosum* s.l. riverine, canopy vegetated, larval habitat scene. C*hlorophyll* is a term used for several closely related green pigments found in cyanobacteria, algae and plants [2]. It may be found that foliar pigments such as chlorophyll play a crucial role in the riverine, larval habitat, canopy plant which may provide important information on gross primary productivity for a shaded and non-shaded, canopied, georeferenced, prolific, seasonally geosampled,riverine, *S. damnosum* s.l., larval habitat.Since the amount of solar radiation absorbed by a leaf may largely be a function of foliar concentrations of photosynthetic pigments, low concentrations of chlorophyll may directly limit photosynthetic potential and hence primary production of the geosampled riverine habitat canopy cover.

The relationship between leaf nitrogen and the carbon cycle in ArcGIS may be key to many climatically-oriented,riverine LULC,ecosystem processes as photosynthesis provides the energy and carbon-cycle molecules for growth and reproduction [4–7] and decomposition for nutrient cycling [7,8]. Ecologists and other experimenters have long recognized that nitrogen is the most limited nutrient for plant growth [9,10]. One effective and timely approach to precisely estimating canopy nitrogen content in ArcGIS is using calibrated relationships between crop, canopy, reflectance emissivity, wavelenght, transmittance parameters and lab-based wet chemical analysis data. As plant nitrogen concentration is linked to the amount of chlorophyll, many studies have focused on estimating crop leaf chlorophyll concentration, which can give an indirect assessment of canopy- or leaf-based nitrogen status of crops [13]. The most common method of deriving canopy nitrogen content using remote sensing data is to regressively quantitate emissivity related, geospectral indices by incorporating two or more characteristic wavebands into a simple ratio, or into a more complicated formula based on linear algorithms and nitrogen-related plant physiological significance[4].

The first National Aeronautics and Space Administration (NASA) Airborne Imaging Spectrometer (AIS-1), flown from 1983 to 1986, included only the 0.9- to 2.1-μm reflected infrared (IR) spectrum and the AIS-2 measured from 0.8 to 2.4 μm during which time frame the emphasis for detecting chemistry shifted from pigments to canopy water and nitrogen.Their absorption features occured in the reflected IR. The chlorophyll content is indirectly related to the nitrogen content [2]. The high correlation between (log 1/R)' and nitrogen and chlorophyll results from only subtle changes in the curvature of the reflectance spectrum[4,9].For example, lignin content was mapped from AIS-1 data over Blackhawk Island, WI, USA, in ArcGIS which allowed estimates of soil nitrogen availability by correlating nitrogen mineralization with foliage lignin content(www.nasa.gov). Lignin fills the spaces in the cell wall between cellulose, hemicellulose, and pectin components, especially in xylem tracheids, vessel elements and sclereid cells and is covalently linked to hemicellulose and, therefore, crosslinks different plant polysaccharides, conferring mechanical strength to the cell wall [4]. These features were corroborated although different studies identified different spectral bands as significant in multiple linear regression predictions.

Thereafter, NASA began to address the full costs of the Earth Observing System satellite program and the High Spectral Resolution Imaging Spectrometer (HIRIS), one of the original NASA facility instruments for the Terra platform, which was being considered for deselection because of its cost and uncertainty to the climate mission. Among the concerns were that high atmospheric CO_2 concentrations could lead to increased Carbon: Nitrogen (C: N) ratios and associated declining productivity because of higher lignin content in plant residues. This concern about future soil nitrogen availability provided a unique climate role that only HIRIS, with its contiguous narrow spectral bands across the visible and shortwave IR region, was capable of detecting. NASA then established the Accelerated Canopy Chemistry Program (ACCP) in 1991–1992 to determine whether there was a sound theoretical and empirical basis for estimating nitrogen and lignin concentrations in ecosystem canopies from remote sensing data (www.nasa.gov). NASA ultimately deselected HIRIS although this program led to numerous empirical studies to identify nitrogen and lignin from airborne Advanced Visible Infrared Imaging Spectrometer (AVIRIS) data. Despite the remote evidence, the significance of structural contributions to measurements of lignin and nitrogen, predictions have never explicitly been tested in ArcGIS before for identifying unknown, unsampled prolific, shade, canopied, geosampled, georefernced, riverine, *S. damnosum* s.l., larval habitats in African riverine environments.

However, unlike above-ground biomass production and canopy nitrogen uptake, canopy nitrogen content decreases with the progression of growth stages and may produce “dilution effects” in a prolific, georeferenced, shade canopied, *S. damnosum* s.l., riverine, larval habitat, eco-epidemiological, forecasting, geospectral, endmember, decomposed, biosignature-oriented, reflectance emissivity, wavelenght, transmittance-related, risk model.For example, the nitrogen content of a geospatial aggregation of seasonal, geosampled, *S. damnosum* s.l., riverine, larval habitat canopy plants may be probably highest at early growth stages and may thereafter decrease continually up to the stage of senescence as the nitrogen uptake per unit of above-ground biomass accumulation decreases and as the leaf area per unit crop mass decreases. In the vegetative growth period in particular, an increase in the rate of biomass production compared to that of the riverine, larval habitat, canopy nitrogen uptake may result in a rapid decrease in canopy nitrogen content. The variation in above-ground biomass and canopy structure dominates the canopy spectral reflectance [2]. Thus, the “dilution effect” and the variation in canopy structure probably will affect the selection of sensitive bands for spectral indices. These inconsistencies may result from an indirect estimation of plant nitrogen concentraton as nitrogen does not directly absorb radiation in the visible-NIR region [4]. Presently there is little knowledge available related to the derivation of canopy nitrogen content based on decomposed, geo-spectrally, explanatorily interpolatable, seasonal, geosampled, *S. damnosum* s.l., riverine, larval habitat, canopy plant-oriented, biosignature data.

Shortwave infrared bands in ArcGIS have been known to be powerful predictors for nitrogen while visible bands have best employed for detecting chlorophyll. In shortwave infrared regions, however, the absolute differences in reflectance at critical bands have been classified as extremely small while the bands of high correlation have been determined to be narrow. Geopectral, radiance-related, uncertainty-oriented, probability, wavelength-associated, quantification forecasting, risk models may be required to resolve these differences for accurately explanatorily interpolating an empiricial dataset of geosampled, *S. damnosum* s.l., riverine, larval habitat, sub-mixel, eco-epidemiological, dataset of shade canopied,decomposed,biosignature-related endmembers. However, the best IR bands from the leaf scale may not be good predictors of chemical content or concentration at that canopy scale; variability in canopy reflectance in the shortwave IR region which may have to be at least an order of magnitude beyond that necessary to detect signals from chemicals. The variability in first-difference log 1/*R*in ArcGIS may determine if canopy scale in a seasonally prolific, georeferenced, geosampled, *S. damnosum* s.l., riverine, larval habitat may be related to the arrangement of the moderate resolution imaged canopy leaves with respect to direct solar radiation, instrument noise, leaf fluttering, and small changes in atmospheric moisture.

Structural traits affecting light scattering over scales ranging from leaf cells to canopies in a geosampled,*S. damnosum* s.l., prolific, georefernced,riverine, larval habitat,explanatorily, shaded, canopy cover may be convergent with their biogeochemical traits. In some circumstances, assumptions of canopy structure may be ignored when qualitatively quantifying, biogeochemical, decompositions of a georeferenced dataset of empirically geosampled, riverine, larval habitat, unmixed, canopy cover, absorption-related covariate reflectance emissivity, wavlenght, transmittance, parameter estimator coefficients especially when dealing with the physical processes of photon scattering from leaves and plant canopies. Although there is recognition of the importance of multiple scattering particularly in the NIR, where plant compounds do not display strong absorption features [4], it has not been possible to quantify this phenomenon at the canopy scale in ArcGIS or any other cartographic geodatabase for robustly, geo-spectrally interpolating, ,immature, *S. damnosum* s.l. -related, immature habitat decomposed, habitat, endmember, biosignature spectra.

By means of geometrical optics in ArcGIS a canopy vegetated, prolific, riverine, shaded, *S. damnosum* s.l., georeferenced, geosampled, larval habitat, photosynthetic and NPV, decomposed, endmember, biosignature-oriented, geospectral,forecasting, eco-epidemiological, risk model may approximate the scattering intensity distribution employing a forward angular range (0–60°) for qualitatively, quantitating, gradient-index spheres which may be explanatorily illuminated by a plane wave.By so doing, the incident angle of reflected light in a prolific, riverine, larval habitat may be optimally quantized in ArcGIS by the scattering angle, thus improving the approximation accuracy. The scattering angle and the optical path length may also be numerically integratable by a general-purpose integrator in a canopy biosignature endmember, sub-mixel, forecasting, eco-epidemiological, risk model. With some special geometric-optical models, the scattering angle and the optical path length can be expressed by a unique function. The model however may fail to give good approximation results at scattering angles whose refractive rays are in the backward direction

[2]. For different index models, the geometrical-optics approximation is effective only for forward angles(typically those less than 60° or when the refractive-index difference of a particle is less than a certain expected value) [4].

Satellites observe radiation reflected in their direction whereas climate models need total solar energy reflected upward in all directions [2]. This distinction has led to the optical properties of vegetation canopies being represented somewhat differently in current climate models than they are in remote sensing. However, the current trend in forecast, risk-related, entomological, real-time, meteorological modeling is to generate the remotely sensed signal in the model and use the difference from that observed data to correct the model through data assimilation procedures.Because of the likely continuation of global terrestrial climate records through instruments onmeteorological satellites, data assimilation ofriverine terrestrial information should be further developed beyond its current framework in ArcGIS for remotely, geospectrally interpolating, shade, canopied, endmembers decomposed from a georeferenced productive,*S. damnosum* s.l., riverine, larval habitat for targeting unknown unsampled habitats. For this purpose, the computation of radiation in these models needs to be formulated to reproduce the directional information seen by a satellite of an African riverine environment.

In Jacob et al. [1] the final, sub meter resolution-derived (i.e., 0.61m)satellite forecasting, time series-dependent, *S. damnosum* s.l. predictive, ArcGIS, eco-epidemiological risk model included the unmixed, residualized explanatorial, canopy, endmember, forecasts as rendered from a geometric-optical analyses, a 3-D radiative transfer equation and an SPA. These geo-spatiotemporal, operationizable, eco-epidemiological, forecasts identified areas endemic for onchocerciasis in two African riverine communities employing a stochastically interpolated, endmember,reference, target signature devised from the unmixing, algorithmic outputs. The model ecogeographically and ecohydrologically predicted multiple sites where the black fly vector parasite breeds. Of 30 sites along the Sarakawa River in Northern Togo predicted to be prolific, shade canopied, riverine, larval habitats by the QuickBird model, all (100%) were found to contain *S. damnosum* s.l. larvae. In contrast, 52 sites not predicted by the model, but deemed to be potential habitats contained *S. damnosum* s.l. larvae. Together, these data suggest that the model exhibited a sensitivity and specificity approaching 100% for the prediction of *S. damnosum* s.l. riverine larval sites in Togo.

To test the generality of the QuickBird model it was applied to predict, georeferencable, prolific, shade canopied,*S. damnosum* s.l., riverine sites in northern Uganda. A total of 25 potential, *S. damnosum* s.l.,larval, habitat sites were predicted. Of the 25 sites forecasted to be suitable habitats by the model, 23 (92%; 95% CI 81–100%) were found to contain larvae. In contrast, just 2/10 (20%; 95% CI 0–45%) sites examined which were not predicted to represent larval habitats by the model were found to contain larvae. The model thus exhibited a sensitivity of 80% and a specificity of 92% when applied in the Ugandan riverine, eco-epidemiological,study site, a performance that was statistically significant ($p<0.0001$; Fisher's Exact test). The two sites that were not predicted by the model were nonetheless found to contain larvae consisting of low hanging streamside vegetation immersed in fast flowing water. Crosskey [11] revealed that shade canopied, *S. damnosum* s.l., larval habitats can be affected by ecogeographical, ecohydrological, non-temporally and temporally, explanatorily, dependent attributes (e.g., Precambrian rocks, floating vegetation, turbid waters). The mean number of larvae found at the sites predicted by the model (21.91) was significantly greater than the mean number of larvae at the sites consisting of immersed overhanging vegetation (4.0; $p<0.001$, Mann Whitney U test).

Unfortunately, the cost of QuickBird visible and NIR data may be too expensive [$17.00 U.S. dollars/ kilometre (km)] for African-based vector control programs to afford for implementing onchocerciasis control by habitat elimination in georeferenced riverine communities. Commonly for accurate, time series dependent, eco-epidemiological, forecast, ecogeographic, ecohydrological, risk mapping, of georeferenced, canopy, shade, vegetated, geosampled, prolific, *S. damnosum* s.l. riverine larval habitats , a minimum of 64 km^2 twice a year (e.g., rainy and dry riverine seasons) is required [1,3]. It may be more realistic to target immature, prolific, *Similium* habitats, in African riverine communities employing less expensive, medium resolution data.

Medium, resolution-derived, eco-epidemiological, datasets are characterized by a spatial resolution between 5m to 30m (www.esri.com). In African riverine environments, geo-spatiotemporally, geosampled, shade, canopy, vegetated, *S. damnosum* s.l. georeferenced, larval habitats differ in their capacity of immature production [1, 3] and, as a result, intervention efforts remotely, targeting, productive habitats may be more relevant. To date, entomological research has not focused on remote detection of seasonally prolific, shade, canopied,*S. damnosum* s.l.,geosampled,vegetated, unsampled, unknown, riverine, larval habitats in ArcGIS employing cost effective, medium resolution, data. Thus, optimal cost-effective geospatial/geospectral resolution has not been described either using varying proxy graphical indicators such as Normalized Difference Vegetation Indices (NDVI) for remotely targeting, seasonally productive, georeferenced, *S. damnosum s.l.* larval habitats in African riverine environments.

Normalized Difference Vegetation indices monitor terrestrial landscapes by satellite sensors [2] and have been highly successful in assessing vegetation condition, foliage, cover, phenology, and processes such as evapotranspiration (ET) and primary productivity related to the fraction of photosynthetically active radiation (fPAR) absorbed by a canopy [10,14]. Evaporation accounts for the movement of water to the air from sources such as the soil, canopy interception and waterbodies[13].fPAR generates ecobiophysical, explanatorial, illumination variables that can describe canopy structure irradiance and are related to functional process rates of energy and mass exchange[4]. In radiometry, irradiance is the radiant flux received by a surface per unit area, and spectral irradiance is the irradiance of asurface per unit frequency or wavelength, depending on whether the spectrum is taken as a function of frequency or of wavelength [13]. A new generation of NDVI data from the Moderate Resolution Imaging Spectrometer (MODIS) on the Terra satellite has been inter-calibrated with AVHRR NDVI, and provides near daily coverage of the earth. As ratios, NDVIs can be easily cross-calibrated across sensor systems, ensuring continuity of data sets for long-term monitoring of the land surface and climate-related processes [2]. A canopy radiative transfer model may show that an explanatorily interpolated, moderate resolution, geospectrally decomposed, NDVI biosignature is near-linearly related to area-averaged, net, carbon assimilation and plant transpiration, even at different values of f_c and LAI over a seasonal geosampled, shaded or non-shaded, canopied, productive, *S. damnosum* s.l., riverine, larval habitat.

There is a strong relationship between NDVI and agricultural yield and canopy vegetation LULC properties, such as length of growing season, onset date of greenness, and date of maximum photosynthetic activity. These reflectance emissivity, transmittance, phenological indicators emphasize different characteristics of terrestrial ecosystems to gain a better understanding of structure and function of canopy vegetated LULCs [2]. Phenology, (i.e., the timing of recurring life cycle events), may for example shift in response to natural or anthropogenic disturbances in agricultural ecosystems [4]. Environmental scientists have an increasing interest in spatially explicit phenological data to better understand agricultural change processes associated with LULC and climate change. In this context, remote sensing-based, time series explanatorial, NDVI may be used to obtain phenological data associated to productive, geosampled, geo-spatiotemporal, *S. damnosum* s.l., riverine, larval habitat at regional scales which may then be subsequently decomposed in an OBIA and then a endmember biosignature, of the unmixed canopy predictor variables may be explanatorily interpolated to identify unknown, unsampled, habitats in a riverine environment.

Alternative algorithms have been devised based on tree allometry and litterfall in order to measure forest canopy properties. Litter fall is the most important source of nutrient flux to the forest floor which has long been seen as a useful index of ecosystem productivity [4]. Litter production is an important component of the CO_2 cycle in seasonal tropical forests, strongly influencing C, nutrient, and energy fluxes [4,7], and is a reliable predictor of canopy processes [9]. However, quantifying litter production over long time scales and large spatial scales may be operationally challenging, using proxy, moderate resolution, graphical indicators, thus limiting the ability to develop links between litter production and canopy processes such as leaf area development and phenology in an imaged, georeferenced, geosampled, shaded and non-shaded, canopied, *S. damnosum* s.l. riverine larval habitats. Both the NDVI and Enhanced Vegetation Index (EVI) have been successfully applied to estimate forest tree productivity in tropical savannah and forests ecosystems [9] however, riverine ecosystem reflectance data obtained by a medium resolution imager may include various noise components such as varying sun-sensor-surface viewing geometries, cloud presence, aerosols and bidirectional reflectance distribution factors, thus limiting their efficacy for assessing geo-spatiotemporal dynamics in biophysical explanatorial, time series, processes in ArcGIS, for ecogeographically, ecohydrologically geospatially delineating, seasonal seasonally prolific, canopied, riverine habitats. As a result, signal extraction techniques in OBIA may be needed to improve the signal-noise ratio (SNR) in an eco-epidemiological, dataset of geospectrally decomposed, *S. damnosum* s.l., larval habitat, canopy endmembers may enhance the spectral response of biophysical vegetation-related LULC covariate reflectance emissivity, transmittance, wavelenght, parameter estimators eco-geographically, echohydrologically associated to the canopied , prolific, habitats prior to conducting interpolation exercises in ArcGIS.

Signal-to-noise ratio is a measure used in science and engineering that compares the level of a desired signal to the level of background noise [2]. It is defined as the ratio of signal power to the noise power, often expressed in decibels. Jacob et al. [1] found that the ratio higher than 1:1 (greater than 0 dB) indicated more SNR in an empirical regressed dataset of geo-spatiotemporally, sub-resolutionary, imaged, productive, shaded riverine *S. damsnoum* s.l., geo-spectrally, explanatorily decomposed, larval habitat, canopy, endmember predictors. While SNR is commonly quoted for electrical signals, it can be applied to any form of signal (such as isotope levels or biochemical signaling between cells) [4]. The SNR, the band width, and the channel capacity of a communication channel are connected by the Shannon–Hartley theorem.

In information theory, the Shannon–Hartley theorem tells the maximum rate at which information can be transmitted over a communications channel of a specified bandwidth in the presence of noise. It is an application of the noisy-channel coding theorem to the archetypal case of a continuous -time analog communications channel subject to Gaussian noise [2]. The theorem establishes Shannon's channel capacity for such a communication link, a bound on the maximum amount of error-free digital data (that is, information) that can be transmitted with a specified bandwidth in the presence of the noise interference, assuming that the signal power is bounded, and that the Gaussian noise (e.g., post-regressed, georeferenced, *S. damnosum* s.l., larval habitat, ArcGIS dataset of empirically decomposed medium resolution, NDVI biosignature –related data) is characterized by a moderate resolution spectral density, reflectance emissivity, transmittance, wavelenght, data feature attributes.

Needle/foliage biomass constitutes one of the most important pools of essential nutrients, which is vital for forest nutrient cycling including carbon cycling [2]. Litter fall can be seen as an indirect expression of forest canopy status, a consequence of the genetic make-up of the trees and the influence of environmental fluctuations, and thus, these litter fall –related, seasonal, remotely explanatorily, interpretable, geospatial objects can be employed as an indicator of a canopy health of a georeferenced, medium resolution –derived, NDVI, ecogeographically representing a canopy, shaded prolific, geosampled, *S. damnosum* s.l., riverine, larval habitat. Estimates of litter fallor leaf area, based on allometric functions remotely geosampled with medium resolution, time series images may accommodate a lot of seasonal,*S. damnosum* s.l., larval habitat changes due to inherent dynamics and interannual variability.

Further, an additional senescence factor that is a function, for example, of photosynthetic decomposed explanatorial, reflectance emissivity, wavelenght, transmittance variables that influence canopy such as self-shading and thinning activity may need to be incorporated into an efficient unmixing algorithm for remotely robustly, quantitating regressors representing field eco-geosampled, canopy pigments and stresses. Senescent leaves follow a typical trajectory, with decreases in chlorophyll followed by losses of other pigments and water [4]. Aging and stress increase reflectance over the visible and shortwave-infrared spectrum and decrease it in the NIR [4]. The difference in reflectance between the visible and NIR regions is the basis of vegetation indices (e.g., NDVI) [2]. Nevertheless, these methods are labor intensive, time-consuming and not error-free in ArcGIS or any other cartographic or object-based software because of their site and species-dependency. By contrast, remotely-sensed, decomposed medium resolution-derived, vegetation indices have novel potential but still need cross calibration by means of ground-based observations.

Indirect proxy measures of canopy properties employing ground-based instruments have been implemented, as documented by the rich literature. For example, Aman et al. [14] analyzed the correspondence between NDVI calculated from average reflectances and NDVI integrated from individual NDVIs by simulating Advanced Visible Infrared Imaging Spectrometer (AVHRR) data from high spatial resolution SPOT 1 HRV radiometer and medium resolution Landsat Thematic Mapper (TM) data. For the study sites located in tropical West Africa and temperate France, a strong correlation was found between the two types of NDVI computed. The authors concluded that NDVI derived from the medium, spatial resolution, sensor data can be used in lieu of NDVI integrated from fine spatial resolution data without introducing significant errors. On the other hand, a region consisting of a mixture of canopied, vegetated- and non-vegetated-related, LULC areas, revealed prominent discrepancies between NDVI derived from from low resolution measurements. The relative difference between the coarse sensor data was approaching 30%, for example when compared to medium resolution imagery. Successfully parameterizing scaled, heterogeneity effects on NDVI endmembers, employing simulated land and vegetation interpolation scenarios can aid in modeling the variances and covariance terms with medium resolution canopied sub-mixel scale values. These scales may qualitatively remotely and regressively quantitate indirect measures of canopied properties of a geosampled, *S. damnosum s.l.,* prolific, canopy, shaded or non-shaded, georeferncable, riverine, larval habitatemploying ground-based instruments.

As literature indicates, there exist many perspectives and discrepancies on the relationship between NDVI and endmember, fractional vegetation, LULC cover and the scale effect of medium resolution NDVI, graphical [2,4,15]. The principle behind derivation of fractional vegetation –related, time series dependent LULC cover from NDVI for optimally, remotely, explanatorily geospectrally targeting, prolific, canopied, georeferencable, *S. damnosum* s.l., riverine, larval habitats is to relate NDVI of mixels to reference NDVI values, such as the NDVIs of dense vegetation and bare soil LULC assuming the individual component NDVIs in the extracted habitat mixels can be represented by these reference NDVIs. However, even if component medium resolution-derived NDVIs can be estimated as the reference without error, there may be still sources of probabilistic, uncertainty caused by the scale effect of NDVI when retrieving vegetation-related, LULC endmember canopy fractions from the NDVI biosignature for accurately geo-spatiotemporally, regressively, targeting and interpolating productive, unknown, unsampled, *S. damnosum* s.l., riverine, larval habitats.

NDVI mixels may not be at the same spatial scale since it is a mixel scale [4]. It remains unclear the extent to which the mixel scale medium resolution NDVI corresponds to the sub-mixel scale, NDVI for optimally remotely and/or regressively targeting a prolific geosampled, georefernced, productive, *S. damnosum* s.l. shade, canopied, riverine, larval habitat for qualitatively quantitating what possible endmember relationships exist between them. The relationship between NDVI for targeting these habitats and fractional vegetation cover may be directly influenced by the scale effect of the medium resolution NDVI; thus, an understanding of this effect may be essential to understanding the relationship between NDVI and endmember fractional canopy vegetation-related, LULC cover, for example for accurate retrievals of radiance, fractions geospatially associated with productive, seasonal, *S. damnosum* s.l., riverine, larval habitat endmembers. There are only few studies that have examined the relationship between NDVI and fractional, vegetation-related, LULC, canopy cover taking into account of the scale effect of NDVI [2].

An ecologist or experimenter may present a method to correct the spatial scaling effect of regressed productive, georeferenced, seasonally-geosampled, *S. damnosum* s.l., riverine, larval habitat, endmember NDVIs by mathematic analysis in ArcGIS for determining the VI'sscale sensitivity with decomposed endmember, biosignature, reflectance emissitivty, transmittance, wavelenght data from a medium resolution, geospectral geodatabase. The result may show that the endmember NDVI dataset obtained by decomposing reflectance up-scaling covariate parameter estimators is larger than the up-scaled NDVI estimators. The NDVI sub-mixel scaling effect maybe more significant in a moderate resolution field when water (e.g., turbid, riverine, *S. damnosum* s.l. larval habitat endmembers,)exists in a scene, and may increase with the increase in the difference of the sum of visible reflectance and NIR reflectance between the canopy vegetation and soil-related LULCs, for example. A method may be proposed to estimate the FVC on the basis of a decomposed, medium resolution, NDVI-related, explanatorial, endmember biosignature-oriented, geospatial scaling, correctional, eco-epidemiological, predictive, risk model. The method may be accurate enough to assess the FVC taking into account the scaling effect in a medium resolution, NDVI, eco-geographically, ecohydrologically representing a geo-spatiotemporal, geospectrally, explanatorily interpolated, riverine-related, prolific, *S. damnosum* s.l., georferenced, shade, canopied, larval habitat.

When landscape components form large geospatially coherent NDVI patches and the vertical dimension of the vegetation is small in ArcGIS, geospectral interactions between decomposed canopy soil and vegetation LULC components in a geo-spatiotemporally, geosampled, imaged,*S. damnosum* s.l.,riverine, larval habitat may be negligible at moderate resolution. As such, the influence of the individual components on the observed riverine habitat, canopy, habitat, LULC reflectance may be described by their geospectral, ecohydrological, biophysical, time series, NDVI, ecogeographical, fractionalized properties using a linear,explanatorial, mixing model. Nonlinear algorithms may be then introduced when multiple scattering of radiation occurs amongst the different georefernced, larval habitat, endmember biosignature-related, target materials. Shadow components should not be assumed to be insignificant and negligible [4]. The medium resolution red and NIR reflectance of a extracted, unmixed, *S. damnosum* s.l., riverine, larval, habitat mixel may then allow averaging reflectance emissitivty, wavelenght, transmittance values of an empirical decomposed dataset of vegetation and soil-related empirically geosampled, geo-spectrally interpolatable, geo-spatiotemporal, eco-epidemiological, LULC-related, explanatorial, predictor variables employing vegetation endmember fractions, and vegetation reflectance in the red and NIR bands, respectively.

Bare soil LULC reflectance may also be robustly regressively quantitated using moderate resolution red and NIR bands in ArcGIS. The NDVI is a nonlinear function which varies between -1 and +1 but is undefined when red and NIR are zero[2].Caution must be taken however, in placing immediate confidence in negative values, generated by a higher reflectance in the visible region than in the IR region of a medium resolution-derived, NDVI biosignature, eco-geographically, ecohydrologically representing a geo-spatiotemporally geosampled, *S. damnosum* s.l., riverine, larval habitat, in ArcGIS as this effect may be due to the combination of clouds, bare soil and rock-related LULC in the scene. NDVI values vary with absorption of red light by plant chlorophyll and the reflection of IR radiation by water-filled leaf cells [4]. These geospectrally explanatorily interpolatable NDVI values in ArcGIS may be correlated with Intercepted Photosynthetically Active Radiation(IPAR) since in most geospatiotemporal, entomological-related, canopy endmember, eco-epidemiological, forecast, risk modelling cases (but not all), IPAR and hence NDVI is correlated with photosynthesis[1,3].

Intercepted photosynthetically active radiation (IPAR) is an important variable in vegetation processes such as water and energy exchange [4,13]. The instantaneous fraction of direct beam radiation intercepted by IPAR by a shaded or non-shaded, canopied, georeferncable object can be described mathematically in ArcGIS as IPAR = 1 - exp (-kLAI/cos 0s).Measurement of this reflective quantity and ecobiologically-related, explanatorial, endmember, fractional, interception efficiency (f_{PAR})),however, can be time consuming because of the need to constantly sample for geo-spatiotemporal variability especially when forecasting unknown, unsampled,productive, shaded, georefernced, geospectrally interpolated, canopied, *S. damnosum* s.l., riverine, larval habitat unmixed, bio-signature-related , spatial components. A method may be presented for estimation of IPAR and f_{PAR} using a commercially available hemispherical radiation sensor (e.g., Li-Coy LAI-2000) employing medium resolution, geo-spatiotemporally dependent, satellite data. These instruments can provide information on the structure of the canopy and the angular dependence of light interception for single measurements to be interpreted for qualitatively regressively quantitating all solar zenith angles of the georeferenced riverine, shade canopied, larval habitat.

Complex 3-D canopy surface covers such as geosampled, georeferenced, shaded riverine, *S. damnosum* s.l., larval habitats are known to exhibit highly anisotropic reflectance, due, in part, to effects such as self-shadowing and specular reflectance [1,3]. This implies that a explanatorily, geospectrally interpolatable canopied, geospectral, moderate resolution, endmember decomposed, NDVI, biosignature-related, hemispherical reflectance value, taken as the integral of the spectral bidirectional reflectance distribution function(BRDF) over the hemisphere value tabulated for the georeferenced riverine habitat in ArcGIS for a given sunposition, might be quite dependent on that sun position. The Li-Strahler forest canopy model [4] accounts for the anisotropic behavior of the BRDF by using geometric optics and simple principles of Boolean set theory, and provides the opportunity to explore the diurnal variation of spectral hemispherical reflectance. The model views a sparsely covered scene as an assemblage of illuminated tree crowns of ellipsoidal shape.

Thus, under a given solar illumination angle tabulated for a seasonally productive, canopied, *S. damnosum* s.l., vegetated, georeferencable, riverine, larval habitat, the areal proportions of the shadowed and sunlit moderate resolution, imaged, geosampled, riverine, *S. damnosum* s.l., larval habitat, canopy LULC and of shadowed and sunlit background may be determined for any viewing angle in ArcGIS. The NDVI decomposed, explanatorial, endmember biosignature of these areal, canopied, habitat components, as weighted by their proportions may determine the directional reflectance factor of the canopy at that viewing angle. The effects of the mutual shadowing and obscuring of canopy crowns in ArcGIS by one another may be included. This reflectance model may be extended to provide instantaneous hemispherical surface reflectance computations of discontinuous, productive habitat, shaded, vegetated, LULC canopies. Since the model would render a directional reflectance factor for each small change in viewing angle, hemispherical reflectance for a particular solar illumination angle of the georeferenced, riverine, larval habitat, canopied, seasonal, LULC cover can be calculated in ArcGIS by the numerical integration of the directional reflectance over the viewing hemisphere. At present, hemispherical reflectance for a canopied, geosampled, georeferenced, shaded, seasonally productive, riverine, *S. damnosum* s.l., larval habitat is represented as geospectrally dependent, explanatorily interpolatable, interger value which include diffuse irradiance, canopy multiple scattering, at leaf specularity effects at a 0.61m mixel resolution [3]. These may be radiometrically calibrated to moderate resolution with the introduction of sophisticated calculations of geospectrally decomposable, NDVI, endmember biosignatures.

Hemispherical radiation sensor method has been remotely tested in a millet crop and a shrub fallow area in semi-arid West Africa. For example, Hanan et al. [16] generated canopy scale vegetation net production in ArcGIS, of four canopies employing two contrasting models of photosynthesis. The vegetation canopies included the *Guiera senegalensis* shrubs of the shrub fallow site, the herb layers of the shrub fallow, grass fallow sites and the millet crop. The two LULC models were based on two factors, namely the production efficiency approach, which assumed that light was the primary limiting factor and, the CO_2 supply function approach, which assumed that the rate of CO_2 influx to the leaves was the main limiting factor. The models were generalized to apply across multiple, explanatorial, canopy, vegetation–related, LULC types through time by allowing important categorical, covariate, parameter estimators to vary according to the proportion of C_3 plants in the canopy, by addition of maintenance and growth respiration terms and, by addition of an empirical objective term related to leaf age.

The models were driven in ArcGIS employing ground verified measurements of the biophysical explanatorial variables (i.e., light interception, stomatal and canopy conductances) which summed to a ten-day temporal scale. This forecast was then fitted to harvest estimates of ten-day net production. Each term of the overall models were tested for statistical significance during the model fitting procedure at a 95 confidence interval. Despite their opposing assumptions, both models were able to explain a large proportion (>80%) of the total variance in ten-day net production period for the four canopies during the growing season. This was attributable in part to the fact that both ArcGIS models were classified based on the assessment of canopy amount (represented by light interception) which were probabilistically correlated, and because the photosynthesis functions describing the effect of the eco-environmental geosampled predictor variables (e.g., vapour pressure deficit) were also correlated. Inclusion of the maintenance respiration term was statistically significant for both modelling approaches. Leaf age was significant but this may have been related to the covariance of the day of the year with the geosampled, explanatorial, time series, geosampled, covariate, parameter estimator, coefficient values. In most cases significant differences in the average values of maximum PAR conversion efficiency (ϵ^*) and CO_2 concentration gradient (Δ) were found between C_3 and C_4 species.

Although remotely aggregated hemispherical radiation sensor data aggregated in ArcGIS may be employed to infer instantaneous direct and diffuse interception as well as the daily integrated values remotely retrived from a prolific, geo-spatiotemporally, geosampled, georeferencable, shade canopied, *S. damnosum s.l.*, rivereine, habitat, eco-epidemiological, capture point, spectrometers such as LAI-2000 (http://www.licor.com/) it may estimate PAR sensor arrays with errors in instantaneous, IPAR, simulated values. These misspecifications may be large at specific times of day. For example, quantitated hemispherical radiation values may rise only to 30 W m^{-2}at solar noon in an African riverine environment, when incident PAR is more than 400 W m^{-2}. Instantaneous f_{PAR} estimates exhibit some bias towards underestimation at small solar zenith angles, and overestimation at larger angles, particularly on shrub fallow sites [4]. Although these errors may be generally small (much less than 0.l unit of f_{PAR}) at some daily time periods ,the geosampled, *S. damnosum* s.l., riverine ,larval habitat daily IPAR may be misspecified even with a very low measure (<5%)of the direct PAR sensor measurements. Further, indirect methods including the LAI-2000 plant canopy analyzer (Li-Cor, Lincoln, Nebraska) and AccuPAR Ceptometer (Decagon Devices, Pullman, WA), two of the most commonly used devices, may be hindered by the complexity of canopy architecture in the riverine habitat and the high-cost of the instruments.

Regardless, fPAR, generated in ArcGIS may be employed extensively as an explanatorial, time series dependent, remotely sensed, explanatorial, covariate, parameter estimator, reflectance emissivity, transmittance wavelength estimators of a georeferenced, medium resolution derived, prolific, *S. damnosum* s.l., shade canopied, vegetative, riverine, larval habitat geosampled in an African environment by procuring remote proxy calculations of canopy surface photosynthesis and Net Primary Production (NPP) (e.g., the annual net growth of vegetation harvestable amount) from the satellite data indirectly. A medium resolution derived fPAR product may be for example, an fPAR value between 0.0 and 1.0 assigned to each 1-km cell of a global gridded database in ArcGIS.This geodatabase may contain corresponding larval habitat, endmember, biosignature-related, NDVI compositing intervals. Biogeochemical, explanatorial, forecasting, eco-epidemiological, risk models produce conversion-efficiency, time series dependent, covariate, paramter estimator coefficients, combined with the fPAR products to produce daily terrestrial photosynthesis and annual NPP [13]. These NDVI products may be essential in calculating terrestrial energy, carbon, water-cycle processes and biogeochemical products of geo-spatiotemporally, shade-related, vegetation-oriented, dense and sparse, canopied, LULC reflectance, emissivity, wavelenght, transmittance of prolific, *S. damnosum* s.l.,georeferenced, riverine,larval habitats.

To perform further canopy LULC research, the difference between direct and diffuse FPAR may be conducted on a geo-spatiotemporal, geosampled, productive, riverine *S. damnosum* s.l., shade vegetated, riverine, larval habitat, It may necessary to analyze the variation characteristics of direct and diffuse FPAR. Using the scattering by arbitrarily-inclined leaves (SAIL) model, the effects of background explanatorial, seasonal, geospectral reflectance and canopy habit atoptical and geometrical properties on the relationship between FPAR and a decomposed moderate resolution NDVI may be determined. A prolific *S. damnosum* s.l., riverine, shade, canopy vegetated, riverine, larval habitat SAIL model may be used to simulate radiation transfer inside the canopy. Simulating FPAR using a Monte Carlo model in ArcGIS and analyzing the influencing factors of FPAR, such as solar zenith angle and LAI for a seasonally specific (e.g., flooded) riverine, *S. damnosum* s.l., shade vegetated, riverine, larval habitat may reveal optimally explanatorily interpolatable, photosynthetic or NPV endmember, covariate, parameterized estimator coefficients. Simulating FPAR based on a Monte Carlo model and analyzing the effects of soil background and leaf angle on the riverine, larval habitat, vegetation-related LULC, canopy FPAR may also help identify unsampled, unknown, prolific, *S. damnosum* s.l., habitats in an African riverine environment. The SAIL model may simulate direct and diffuse FPAR under various weather and LAI conditions [2]. The SAIL model is a radiation transfer model developed from the SUITS model [4]. The scattering and extinction coefficients of the SAIL canopy reflectance model may be derived in ArcGIS for the case of a fixed arbitrary leaf inclination angle and a random leaf azimuth *S. damnosum* s.l., habitat endmember, distribution. The SAIL model includes the uniform model of G.H Suits as a special case, and its main characteristics are that canopy variables, such as LAI and the leaf inclination distribution function which may be used as input parameters in a time series, georeferencable, moderately resolutionary, imaged, riverine, *S. damnosum* s.l., model to provide realistic angular profiles of directional reflectance as a function of view angle or solar zenith angles.

A way of estimating nadir reflectance from off-nadir views for remotely qualitatively regresssively quantitating various solar zenith angles may help interpolate a decomposed, moderate resolution, NDVI, biosignature of canopy vegetation, LULC of a productive, geo-spatiotemporally, geosampled, shade, canopied, *S. damnosum* s.l., riverine, larval habitat. Geospectral measurements were made with a Mark II radiometer five times during the day on each of four dates from 15° interval zenith and 45° azimuth positions for wheat canopies during the development interval stem extension to watery ripeness of the grain [6]. The ratio of off-nadir [R (Zv,Av)] to nadir [R(0)] radiance in a moderate resolution [ETM+} NIR band (0.76–0.90 µm) was described for generating photosynthetic and NPV, variables from a time series, regression equation:

$$R\left(Z_{V,}A_V\right)\Big/R(0) = 1.0 + \left[\beta_o + \beta_1 \sin\left(\frac{A_V}{2}\right) + \beta_2\left(1/\cos Z_V\right)\right]\sin Z$$

where Av was view azimuth angle relative to the sun position, Zs was solar zenith angle, and Zv was view zenith angle. The coefficient of determination was 0.70 or higher. The equation described the observations that the ratio of off-nadir to nadir radiance increased or decreased as view zenith angle increased depending on view azimuth angle. Canopy backscattering was stronger than forward scattering and the pattern was azimuthally symmetric about the principal plane of the sun. The rate of change in the radiance ratio increased with increasing solar zenith angle. The coefficients, β0, β1 and β2, changed as the canopies grew.

Thus, in a SAIL geo-spatiotemporal, moderately resolutionary, imaged, riverine, *S. damnosum* s.l., larval habitat, eco-epidemiological, forecasting, risk model constructed in ArcGIS, the proportions of direct and diffuse radiation may be changed by means of the visibility parameter and solar zenith angles. The results may reveal that when visibility is set to 5 km, 10 km and 15 km, in a spatially probabilistic, geospatiotemporal, risk model, aggregated, endemic, onchocerciasis, transmission zones may be calculated based on autoregressed, eco-epidemiological, capture point immature, *Similium* productivity count data. The contributions of diffuse FPAR to total FPAR may have values of more than 50% for each zone. The error between total and direct FPAR may be reduced in ArcGIS with increasing visibility and with decreasing LAI. The maximum relative error may be then regressively remotely quantitated. Canopy simulation analyses may reveal that direct and diffuse FPAR varies with seasonal changes in meteorological variables. Especially when visibility is low, diffuse FPAR may be an important part of total FPAR, for robustly explanatorily, geospectrally interpolating a moderate resolutionary, derived, NDVI, endmember, umixed, interpolated, biosignature of a productive, geosampled, georeferencable, shade, canopied, *S. damnosum* s.l., riverine, larval habitat.

Photosynthetically active radiation may be seasonally defined in ArcGIS in terms of photon quantum flux, specifically, the number of moles of photons in the radiant energy between 400 and 700 nanometer (nm) for a geo-spatiotemporal, geosampled, prolific, *S. damnosum* s.l., georeferenced, canopied, riverine, larval habitat. One mole of photons is 6.0222 x 10^{23}photons(Avogadro's Number) [17]. When the responsivity of a medium resolution, sensor-derived, proxy, graphical indicator such as a decomposed explanatorial, endmember, geo-spatiotemporally dependent, NDVI, reference biosignature is plotted in ArcGIS with respect to its sensitivity to the energy content of decomposed, canopy-related, photons of a georeferenced, shade, vegetated, *S. damnosum* s.l., prolific, riverine, canopied, larval habitat, the function may reveal an increasing trend with a value of 400/700 = 0.571 at 400 nm, and 1 at 700 nm.

The reason for the lower responsivity at 400 nm in proxy, decomposed, explanatorial, ecogeographical, ecohydrological, ecobiophysical, operationizable, sub-mixel, forecasting, time series dependent, eco-epidemiological, canopy risk model regressed variables constructed in ArcGIS employing an empirical dataset of medium resolution, NDVI-derived, shade, canopy-vegetated, georeferenced, *S. damnosum* s.l., riverine, larval habitat, reference, unmixed, endmember, biosignature-related, photosynthetic and NPVcovariate, parameter reflectance emissivity, wavelenght, transmittance estimator, coefficient values can be explained, since photons at 400 nm are more energetic than photons at 700 nm (4). This light reaction would be such as the energy of a photon $Q_p$would be inversely proportional to its wavelength λ: $Q_p = (hc)/\lambda$, where *h* is the Planck constant and *c* is the speed of light. To qualitatively, remotely, regressively quantize the same number of photons at 400 nm than at 700 nm (i.e., to get the desired constant quantum response), the source radiation would have to be more energetic at the shorter wavelength. For example, the medium resolution, imaged, spectral irradiance emitted by a geo-spatiotemporally, geosampled, explanatorial, vegetated, georeferenced, riverine, *S. damnosum* s.l., productive, shaded, larval habitat canopy, needs to be larger by a factor of 700/400= 1.75 at 400 nm than for 700 nm. As a consequence, a medium resolution, fPAR sensor derived, decomposable, NDVI, endmember, target biosignature may be sensitive in terms of energy conversion rates at the shorter wavelengths emitted by the geosampled, interpolatable, canopied, larval habitat, vegetated LULC, surface regressors such that the product of spectral irradiance and sensor responsivity is constant. As such, two relevant bands, along the solar radiation spectrum may be remotely, qualitatively, regressively quantitated in ArcGIS from the operationizable, shade, vegetated, georeferenced, sub-mixel, canopied, riverine, larval habitat red and IR decomposed, endmember data. This quantization may be expressed either in terms of photosynthetic photon flux density (PPFD) measured in m^{-2} s^{-1}, since photosynthesis is a quantum process, or in terms of photosynthetic radiant flux density (PAR irradiance, W m^{-2}).

The PPFD is measured by a cosine (180°) quantum sensor [4,13]. This radiation comes from the sun and its intensity is characterized as PPFD in units of micromoles of photons per μmol/m^2/sin ArcGIS. Experiments may be conducted using PPFD to determine exact photosynthetic rates (PN) for a georeferencable, *S. damnosum* s.l., larval habitat, eco-epidemiological, geosampled, canopy model. Diurnal changes in net PN, evapotranspiration rate (ET) and water use efficiency (WUE=PN/ET) for the geosampled, riverine, larval habitat may be then optimally determined in ArcGIS. The maximum photosynthetic rate (PN max) increases from the initial vegetative phase to pod formation and declines at a rapid rate from pod filling to maturity [2]. The response of PN to PPFD may occur between 400-700 nm, for the georefernced, riverine, larval habitat which may be temperature-dependent during the day. Thus,on cool days the PN rates for a geo-spatiotemporally- geosampled, seasonally productive, *S. damnosums.l.*, georeferenced, riverine, larval habitat may be lower than for certain quanta of PPFD tabulated during the first half than during the second half of the rainy season. Evapotranspiration may be also affected by the larval habitat canopy cover and evaporative demand up to flowering, but thereafter it may be independent of the canopy and may simply follow the course of evaporative demand. ET is related to air temperature during the day while PN is related to PPFD [4]. There may be a lag of two to three hours between PNmax (around noon) and ETmax (around 2 p.m.) during the dry season when remotely, quantitatively, regressing productive, georeferenced, *S. damnosum* s.l., larval habitat, covariate, paramter estimators, geosampled in African riverine environments since categorical independent variables eco-geographically representing WUE may increase from the vegetative stage through flowering but then decrease thereafter to maturity.

If the exact spectrum of the light is known in a georeferenced, geosampled, explanatorial, operationizable, medium resolution-derived, NDVI, endmember, shade, canopy, vegetated LULC, prolific, *S. damnosum* s.l., riverine, larval habitat, decomposed, interpolatable, biosignature the PPFD values in μmol/s in ArcGIS can be modified by applying different weighting factors to different band wavelengths. This alteration would result in a quantity called the yield photon flux (YPF) being formulated, which weighs photons in the range from 360 to 760 nm according to plant photosynthetic response [13]. Medium resolution, PAR, sensor-derived, geospectrally decomposed, NDVI, explanatorial, endmember, biosignature reflectance emissivity, transmittance values in ArcGIS may be employed to measure photon flux density (YPFD or YPF), sub-mixel yield as emitted from a georeferenced, geosampled, canopy vegetated, *S. damnosum* s.l., seasonally prolific, riverine, larval habitat. This absorption density estimate may be expressed in units of m^{-2} s^{-1}which may be based on the photosynthetic action spectrum of the canopy. Photosynthesis produces signatures that can be detected at the global scale [13].

Although YPFD derived in ArcGIS from an empirically regressed dataset of time series, medium resolution, sub-mixel, geospectrally georeferencable, *S.damnosum* s.l., riverine, larval habitat, NDVI endmember, biosignature-oriented, explanatorial, continuous independent variables, the photosynthetic and NPV, covariate, parameter estimator reflectance emissivity, wavelenght, transmittance, coefficient values may be a more accurate measure of the amount of light available when robustly, remotely, interpreting, explanatorily interpolatable, time series dependent, geosampled, decomposable, canopy, habitat values. For predictive modeling purposes, however, the PPFD may be more simpler to remotely define employing the shaded canopy habitat components. Photosynthetic photon flux density is a more widely accepted measurement in the field of plant physiology [18]. To measure YPFD in sunlight the slope of the calibration equation needs to be decreased by 10% (e.g., from 500 to 450nm) [13].

Photosynthetic photon flux density as remotely qualitatively regressively quantified from a, medium resolution-derived, canopied, endmember, NDVI sub-mixel, decomposed, explanatorial, shaded, biosignature may be illuminated in ArcGIS by reflections from the bottom surface and particles suspended in the water surrounding a prolific, georeferenced, shade, *S. damnosum* s.l., vegetated, canopied, riverine, larval habitat. By modeling the PPFD in a geosampled, georeferenced, riverine, larval habitat,the direct beam and diffuse sky radiation components of the global irradiance may reflect decomposed, ecohydrologically-related, geospectral, eco-geographic, explanatorial, time series dependent, sub-mixel, covariate, parameter estimator, reflectance emissivity, transmittance, wavelenght, coefficient values.

Irradiance data software developed by the NREL Solar Radiation Laboratory [Simple Model of Atmospheric Radiative Transfer of Sunshine, (SMARTS) has been employed for modeling canopy photosynthesis. Spectra and total irradiance can then be expressed in terms of quanta [mol m−2 s−1, PPFD (400–700 nm)] [13]. Using the SMARTS software it may be possible to: (1) calculate the solar spectrum for a prolific, georeferencable, planar, shade canopied, *S. damnosum* s.l., riverine, larval, habitat surface for any given solar elevation angle, allowing for the attenuating effects of the atmosphere on extraterrestrial irradiance at each wavelength in the 400–700 nm range, (*2*) calculate PPFD *vs.* solar time for any latitude and date for the georeferenced habitat; and, (*3*) estimate total daily irradiance for any latitude and date and hence calculate the total photon irradiance for a whole year or for a growing habitat season [4]. Gross photosynthesis

(*Pg*) and PPFD characteristics of single leaves compared to that of a canopy of leaves in the habitat may be different. It may be shown in ArcGIS that that the optimum irradiance for a leaf (i.e., Iopt) is the half-saturation irradiance for a battery of empirically regressable, *S. damnosum* s.l., larval habitat,canopy, leaf-related covariates in series. A C3 plant, with leaves having an optimum photosynthetic rate at 700 μmol m−2 s−1 may be employed to determine overall PPFD in the shaded portions of the riverine larval habitat canopy. By so doing, the model may render robust estimates of *Pg* for a given date and latitude for remotely qualitatively regressively quantitating geo-spatiotemporally, geosampled, canopied, riverine, larval habitat, wavelenght emmisvities. Seasonal and annual estimates of *Pg* can be parsimoniously determined for the habitat canopy thereafter.

Many PPFD models have simulated water-related components separately basing the diffuse components on quantified semi-empirical relationships. However, semi-empirical modeling, could introduce additional sources of probabilistic error in a shaded geo-spatiotemporally, geosampled, medium resolution-imaged, *S. damnosum* s.l., riverine, larval habitat, canopied, endmember, interpolatable, georeferencable, risk forecasting, eco-epidemiological, model since the fraction of diffuse radiation and direct beam radiation would vary with cloud cover and wavelength band. Spitters et al. [14] determined that the diffuse fraction of the PPFD was 1.4 times that of the diffuse fraction. However, for a medium resolution- imaged, canopy, shaded, geosampled, georefernced, prolific, *S. damnosum* s.l. riverine larval habitat, the direct beam PPFD may vary (e.g.,from 0.2 to 0.4 m^{-2} s^{-1}) depending on cloud conditions. Taking cloudiness into account, the model may eco-geographically, ecohydrologically, predict maximum *Pg* rates of about 10 g(C) m−2 d−1 for a prolific, *S. damnosum* s.l., larval habitat, riverine, canopy cover remotely geosampled in an African riverine environment.

As such,the diffuse fractions remotely tabulated between the PAR and UV wavebands, with the partitioning of solar radiation largely would have to be determined by the scattering of the cloud particles with little wavelength dependency.However, an ecologist or experimenter may remotely qualitatively quantitate common radiation sources and measure YPF and PPFD emitted from a georeferenced, geosampled, shade, vegetated, prolific, clouded, *S. damnosum* s.l. riverine, larval habitat using an ecohydrological-related, ecogeographic, decomposable medium resolution-derived, NDVI, spectroradiometer index in ArcGIS. The vegetation index can be developed from an empirically regressed dataset of unmixed, geo-spectrally explanatorily, interpolatable, endmember, biosignature-related, photosynthetic, covariate, parameter estimator, reflectance emissivity, transmission-oriented, probabilistic, coefficient values, for example. Comparisons of these measurements may be then made with calculated measurements from quantum sensors designed to measure precise YPF and PPFD values from the georefernced, geosampled, riverine, larval habitat covariates.

Quantum refers to the amount of energy carried by a photon [13]. Quantum meters approximate the quantity of photons between 400 and 700 nms [4]. Photosynthesis is largely driven by the number of photons between these wavelengths.Quantum sensors may be employed to quantify canopy light available in geosampled, seasonal, prolific, *S. damnosum* s.l., georeferenced, shade canopy, vegetated, larval riverine habitats in African riverine settings. The line quantum sensor may be especially helpful, as it can provide a spatial average. Quantum Sensors and Quantum Meters measure PPFD inμmol m^{-2} s^{-1}[4].

Quantum sensor data in ArcGIS may exploit correlations, such as geospatial quantum entanglement in calculations of geospectrally decomposable, geosampled, prolific, *S. damnosum* s.l., riverine, larval habitat, endmember datasets so as to achieve robust forecastable, sensitive, sub-mixel, explanatorily interpolatable, empirical, absorption-related rates. Quantum entanglement is a physical phenomenon that occurs when groups of particles are generated or interact in way such that the quantum state of each particle cannot be adequately described independently—instead, a quantum state may be given for the system as a whole (e.g., amount of radiance canopy flux in a medium resolution-imaged,georeferenced, *S. damnosum* s.l., larval habitat geosampled in an African riverine environment).

A quantum sensor can measure the effect of the quantum state of another system on itself [14,17]. The mere act of measurement will influence the quantum state in ArcGIS and uncertainties can alter the quantitated probability and uncertainty associated with geo-spatiotemporally remotely quantized states during measurement. There may be only a few differences among moderate resolution sensors (e.g., <5%). YPF values as remotely tabulated from these image sensors may be consistently lower (e.g.,3% to 20%) than YPF values as determined from explanatorily interpolated, vegetative, spectroradiometric measurements decomposed, from an empirical dataset of probabilistic, geo-spatiotemporal, geosampled, biosignature-related, endmember NDVI values as rendered in ArcGIS from a georeferenced, decomposed shade, canopied, prolific,*S. damnosum* s.l., riverine larval habitat.

Additionally, quantum sensor measurements of PPFD may be consistently the same as PPFD values calculated from medium resolution, vegetation-related, endmember, LULC sub-mixel, decomposed, spectroradiometric measurements, but differences may exist for qualitatively regressively and remotely quantizing red-light-emitting (e.g., canopy dense stands) biomass products. For these reasons, an accurate measurement of PAR should optimally follow the quantification of relative quantum efficiency (RQE) curves as originally developed by McCree [18], who weighed the explanatorial, time series dependent, photosynthetic, covariate coefficient, reflectance values of all photons with wavelengths from 360 to 760 nm. A medium resolution sensor that responds according to this curve may measure YPF in μmol m^{-2} s^{-1} which is the same units as for PPFD in a georeferenced, seasonal, *S. damnosum* s.l., prolific, geosampled riverine larval habitat.

The Stark-Einstein Law states that one absorbed photon excites one electron regardless of the photon's energy between 400 and 700 nm; this law is the basis for weighting photons equally. The law stating that in a photochemical process (such as a photochemical canopy reaction in a georeferenced, seasonal, *S. damnosum* s.l., prolific, shade canopied, riverine, larval habitat) one photon is absorbed by each molecule causing the main photochemical process. In some circumstances, one molecule, having absorbed a photon, initiates a process involving several molecules. However, although >90% of blue photons are absorbed, » 20% of these photons are absorbed by inactive pigments; thus, their energy is not transferrable to energy-collecting pigments (i.e., canopy reaction centers) and is lost as heat and fluorescence. This loss means that the quantum yield of absorbed blue photons in a geo-spatiotemporal, geosampled, canopy, shaded, georeferencable, spectrally, explanatorily interpolatable, productive, *S. damnosum* s.l., shade vegetated, riverine, larval habitat may be typically less (e.g., » 20%) than the quantum yield of absorbed red photons. However, seasonal canopy changes in these geosampled, geo-spatiotemporal, larval habitats may differ in their proportion of inactive pigments.

Phytochrome is a photoreceptor, a pigment that plants, and some bacteria and fungi, use to detect light [4,17]. It is sensitive to light in the red and far-red region of the visible spectrum. Many flowering plants use it to regulate the time of flowering based on the length of day and night (i.e., photoperiodism) and to set circadian rhythms. It also regulates other responses including the germination of seeds (i.e., photoblasty), elongation of seedlings, the size, shape and number of leaves, the synthesis of chlorophyll, and the straightening of the epicotyl or hypocotyl hook of dicot seedlings.

Phytochromes in ArcGIS can be characterized by a red/far-red photochromicity [2]. Photochromic pigments change their "colour" (spectral absorbance properties) upon light absorption [13]. In the case of phytochrome the ground state would be $P_r$indicating red light absorption is particularly strong. The absorbance maximum is a sharp peak (e.g., 650–670 nm), so concentrated phytochrome solutions look turquoise-blue to the human eye [4]. But once a red photon in an explanatorial, geospectrally decomposable, prolific, shade, canopied, *S. damnosum* s.l., vegetated, riverine, larval habitat has been absorbed, the pigment will undergo a rapid conformational change in an ArcGIS geodatabase to form the P_{fr} state. By so doing, P_{fr} would indicate that far-red (i.e., "NIR"; 705–740 nm) is more preferentially absorbed than red in the habitat canopy. This shift in absorbance would be apparent to the human eye as a greenish colour. When P_{fr} absorbs far-red light it is converted back to P_r. [13]. Hence, the absorbed red light would makeP_{fr}while far-red light would render $P_r$during regressive, time series qualitative quantification of the geosampled, geo-spatiotemporal, *S. damnosusm* s.l., georefernced, riverine, larval habitat, eco-epidemiological, capture point reflected waveband data. In plants at least P_{fr} is the physiologicallyactive or "signalling"state [4]. Biochemically, phytochrome is a protein with a bilin chromophore [17].

Inada [19] found that both radiation absorption and quantum yield in the middle wavelengths (i.e., 500-600 nm) in ArcGIS were substantially lower in purple, field grown leaves than in green ones because of inactive absorption by anthocyanin during seasonal summer sampling frames. Clark and Lister [20] found that blue and blue-green Colorado spruce species had high concentrations of inactive carotenoids, which reduced blue light (400-500 nm) absorption and quantum yield during colder temperatures. Environment can also influence the concentration of inactive pigments in a shade, canopy vegetated, prolific, *S. damnosum* s.l., georeferenced, geosampled, riverine, larval habitat. McCree [21] found that growth-chamber-grown plants tended to use ultraviolet and blue radiation more efficiently than field-grown plants which may have been due to a lower concentration of inactive pigments remotely tabulated in ArcGIS of non-stressed growth chamber grown plants. In spite of these genetic and environmental influences on quantum yield, McCree [18] found that the spectral quantum yield of healthy, green leaves of 22 crop plant species differed by less than ±5%, which he defined employing an average YPF curve derived from an empirical dataset of decomposed, medium resolution-derived, endmember, observational explanatorial, predictors. Inada [22] then obtained a second set of comprehensive quantum yield data from 33 species and confirmed McCree's [21] measurements.

Phytochromes, cryptochromes, phototropins, and the UV-B photoreceptor UVR8 are sensory photoreceptors that are able to perceive specific light signals and provide information about the dynamic status of canopy architecture [20,22-24]. The simulation of selected signals of canopy, shaded light and/or the analysis of photoreceptor mutants employing medium resolution-derived,georeferenced, geo-spatiotemporally,geosampled, *S. damnosum* s.l. ,riverine,larval habitat, endmember,decomposed data variables in ArcGIS may reveal that canopy light signals exert significant influence on immature productivity. The main effects of the photoreceptors on the riverine habitat could include the control of (a) the number and position of the canopy leaves and their consequent capacity to intercept light, via changes in stem height, leaf orientation, and branching; (b) the photosynthetic capacity of green tissues, via stomatic and nonstomatic actions ;and, (c) the plant defenses against herbivores and pathogens [25]. Because both YPF and PPF sensors are imperfect integrators, and because medium resolution spectroradiometers in ArcGIS can measure PAR accurately (www.esri.com), ecologists or experimenters may consider developing calibration factors from an empirical datasets of unmixed, geosampled, explanatorial, shade, vegetated, *S. damnosum* s.l., riverine, canopied, larval habitat, NDVI-related, spectroradiometric, explanatorily interpolatable, endmember,geo-spectrally decomposable, biosignature-oriented, absorption-related, covariate, parameter estimator, coefficient values in ArcGIS. By so doing,residual quantitation of endmember specific radiation sources may improve the accuracy of integrating geo-spatiotemporally dependent, medium resolution-derived, sensor data for identifying unknown, unsampled, georeferenced, prolific, canopy, shaded, riverine, seasonal larval habitats.

Photosyntetic Photon Flux Fluence rate is defined as the photon of the fluence rate of PAR [13].The total number of photons incident on a point (e.g., georeferenced, geosampled, shade, vegetated, prolific, *S. damnosum* s.l., canopied, riverine larval habitat ground coordinate overlaid onto medium resolution satellite imagery) from all directions could be qualitatively quantitated by the Photosynthetic Photon Flux Fluence Rate (PPFFR), also measured in units of $\mu mol/m^2/s$. This rate would be based on the integral of photon flux radiance in all the direction about the georeferenced, larval habitat, eco-epidemiological, capture point. PPFFR is the same as PPFD for normal incident collimated radiation and is 4 times that of PPFD in totally diffuse radiation [26]. The ideal medium, resolution-derived, PPFFR, time series dependent, moderate sensor derived data from the endmember, decomposition algorithm in ArcGIS may have a spherical collecting surface which may exhibit the property of a cosine receiver at every productive, shade, vegetated, *S. damnosum* s.l., canopied, larval habitat geo-spatiotemporally, geosampled in an African riverine environment.

A PAR sensor in ArcGIS with a flat receiver can measure medium resolution-derived, PPFD operationzable values, (e.g., the photosynthetic photon irradiance and/or "photosynthetic quantum irradiance of a georeferenced, vegetated, shade,canopied, *S. damnosum* s.l., interpolatable riverine, larval habitat) as Einstein's($m^{-2}\ s^{-1}$) which can remotely designate the spectral range (i.e., waveband) of diffuse solar radiation that contains specific photosynthetic materials(www.esri.com).The Einstein has been used in photochemistry, photobiology and radiation physics as the quantity of radiant energy in Avogadro's number of photons. For example, in Hogewoning et al. [27], the mechanisms underlying the wavelength dependence of the quantum yield for CO_2 fixation (α) and its acclimation to the growth-light spectrum were quantitatively remotely addressed in ArcGIS by combining vivo physiological and in vitro molecular methods. Cucumber (*Cucumis sativus*) was grown under an artificial sunlight spectrum, shade light, and blue light employing the quantum yield for photosystem I (PSI) and photosystem II (PSII) electron transport and α which were subsequently simultaneously measured in vivo at 20 different moderate resolution wavelengths. The wavelength dependence of photosystem excitation balance was calculated from both vivo and in vitro data from the photosystem composition employing spectroscopic properties. Measuring wavelengths of overexciting PSI produced a higher α for leaves grown under the shaded light spectrum (i.e., PSI light), whereas wavelengths of overexciting PSII produced a higher α for the sun and blue leaves. The canopied spectrum produced the lowest PSI:PSII ratio. The photosystem excitation balance calculated from both in vivo and in vitro data was substantially similar and was shown to determine α at those wavelengths where absorption by non-photosynthetic absorption-related pigments was insignificant (i.e., >580 nm).

Hence, it may be shown remotely and quantitatively in ArcGIS, that a georeferenced, geosampled, empirical probabilistic, seasonal dataset of medium, resolution-derived, NDV-related, *S.damnosum, s.l.,* larval habitat,shade,vegetated,decomposed,canopy biosignature,endmember absorption emissitivites acclimate their photosystem composition to their growth light spectrum and, by so doing, geospectrally change wavelength dependence of the photosystem excitation balance. As such, quantum tabulations in ArcGIS yielding optimal photosynthetic processes such as CO_2 fixation may be optimally regressively determined. Combining different proxy, graphical,explanatorial, time series dependent, medium resolution wavelengths in ArcGIS may also reveal diffuse,fractionalized,solar radiation estimates emitted by the unmixed datset of, geospectrally decomposed,geospatially explanatorily interpolatable, georeferenced,shade, canopied, geosampled riverine, larval, habitat endmembers.

Diffuse solar radiation (i.e., sky radiation) is the downward scattered and reflected radiation coming from the whole hemisphere, with the exception of the solid angle subtended by the sun's disc [4]. Diffuse radiation can be measured by a pyranometer mounted on a shadow band, or be calculated employing explanatorily, qualitatively, probabilistically, regressively quantitated, globalized solar radiation and direct solar radiation-related, predictor variables in ArcGIS where the metric units would be W m^{-2}. One Einstein is one mole of quanta [17].Conversely, direct solar radiation would be the radiation emitted from the solid angle of the sun's disc, received on a surface perpendicular to the axis of this cone, comprised mainly of unscattered and unreflected solar radiation which is commonly measured by a pyrheliometer [4]. The units of measure would be Wm^{-2}.A PAR sensor with a spherical receiver is equally sensitive to photons from all direction measures [e.g., Quantum Scalar Irradiance (QSI)].

Quantum Scalar Irradiance may be defined in ArcGIS as the integral photon flux of photons in the 400–700 nm wavelength interval for medium resolution derived, geo-spatiotemporal,eco-epidemiological, capture point (e.g., a canopy shaded, productive,*S. damnosum* s.l. larval habitat) georeferenced in space from all directions around the point. Measurements of PAR sensors can then be remotely expressed in a variety of units including quanta $m^{-2}.s^{-1}$, quanta.$cm^{-2}.s^{-1}$, $\mu E.m^{-2}.s^{-1}$ and $\mu E.cm^{-2}.s^{-1}$ (μE stands for microEinstein). Vertical quantum diffuse attenuation coefficients (Kq0) of (PAR) in shade, canopied, African riverine environments where prolific, *S. damnosum* s.l., larval habitats proliferate may be geospectrally estimated from vertical profiles of PAR collected throughout a sampling frame. Quantitating temporal vertical profiles in ArcGIS of density may reveal that riverine waters are divided into two periods: a stratified period with an upper layer 10 m thick of turbid waters (e.g., $0.05 \le Kq0 \le 1.00$ m−1) (e.g., rainy flooded season), or a lower layer of more transparent waters (e.g., $0.01 \le Kq0 \le 0.50$ m−1) (dry drought-filled season) with an intervening short period. This non-stratified period may consist of a homogenous layer with less turbid seasonal waters (e.g., $0.01 \le Kq0 \le 1.00$ m^{-1}). Horizontally, the distribution of Kq0 may also optimally reveal nearshore riverine water conditions around immersed hanging vegetation of a georeferenced, shade, canopied, productive, *S. damnosum* s.l., geo-spatiotemporally, geosampled, larval habitat. The Kq0 distribution may reflect the water influx from the neighboring tributaries which may cause turbid surface trapped river plumes. These meteorological features may geophysically contribute to the ensuing mixing of unmixed, biosignature-related, moderate resolution, explanatorial, endmembers.

To investigate Kq0in ArcGIS, an ecologist or experimenter must employ regression models involving suspended particulate matter and water depth for quantizing and geospatially associating seasonal, immature productivity with geospectrally decomposed NDVI, explanatorial, canopy biosignature-related canopy-oriented,shaded,explanatorial, predictor variables during flooded, riverine, geosampled, time frames. The best statistical model may explain the observed Kq0 variability while remotely qualitatively quantitating the reciprocal of water depth for a prolific, geosampled, georeferenced, medium-resolution-imaged, shaded, *S. damnosum* s.l., canopy vegetated larval habitat.

However, a more bio-optically relevant model constructed in ArcGIS from an empirical geosampled, dataset of geo-spatiotemporally dependent, remotely retrieved, medium resolution-imaged, explanatorily operationizable, photosynthetic and NPV canopied, covariate, parameter estimator, coefficient values selected from a georeferenced, prolific, *S. damnosum* s.l., canopy, shade vegetated, riverine, larval habitat, decomposed endmember, NDVI biosignature may explain higher percentage of the observed Kq0 seasonal variability. Absorption estimates of Kq0 for the upper layer canopy cover may indicate compensation depths in riverine flooded waters deeper than 50 m, for example, which also may help account for the presence of productive, georeferencable, shaded, riverine, larval habitat communities on submerged banks of near the shore edge [1,3]. The observed temporal and spatial distribution of Kq0 may agree qualitatively with that of moderate resolution-derived, NDVI, canopy endmember decomposed, diffuse, attenuation coefficients which may also be calculated in ArcGIS over the geosampled larval habitats. PAR may then be calculated by integrating the weighted visible channels from the moderate resolution-derived, multi-wavelength instrument which would then subsequently optimally decompose an explanatorial, geospectrally interpolatable, operationizable, time series dependent, medium resolution-derived, NDVI sub-mixel, reference, target biosignature.

Nearly all endmember canopied, NDVI biosignature decompositions in ArcGIS initially employ difference formulas to remotely qualitatively quantify the density of plant growth on the Earth — NIR radiation minus visible radiation divided by NIR radiation plus visible radiation, for example. Calculations of NDVI for a given extracted mixel always result in a number that ranges from minus one (-1) to plus one (+1); however, no green leaf would render a value close to zero [2]. Vegetation indices are mathematical combinations of various bands [4, 28].Negative values of NDVI correspond to water. Values close to zero generally correspond to barren areas of rock, or sand. Positive values represent shrub and grassland (approximately 0.2 to 0.4μm), while high values indicate temperate rainforests (values approaching1) (http://earthobservatory.nasa.gov/). A zero means no vegetation and close to +1 (0.8 - 0.9μm) indicates the highest possible density of green leaves.

By transforming an empirical dataset of raw, unmixed, medium resolution-derived, operationizable, explanatorily decomposable, medium resolution, satellite, radiance estimates into individual NDVI, canopy endmember, biosignature, time series reflectance in an ArcGIS-derived, parameter estimator reflectance emissivity, wavelenght, transmittance coefficient values, ecologists or experimenters may create, robust, georeferencable shade, vegetated, *S. damnosum* s.l., canopied, riverine, larval habitat sub-images. These images may provide a rough measure of canopy architecture, light absorption, and photosynthetic and NPV activities based on decomposed, explanatorial, time series, canopy vegetation LULC-oriented reflectance surfaces associated to georeferenced, geosampled, prolific, riverine, canopied habitats. NDVI in ArcGIS is especially useful for continental to global-scale canopy vegetation monitoring as it can compensate for changing illumination conditions, surface slope, and viewing angle (http://phenology.cr.usgs.gov). The basic idea of decomposing a spectroradiometric index is to collapse the multispectral or hyperspectral remote sensing values to a particular measure, which is related to some characteristics (i.e. vegetation LULC cover and greenness) of a georeferenced object [2,4,28].That said, a time series dependent, explanatorial, operationizable, medium resolution-derived, explanatorial, NDVI, unmixed,endmember,*S. damnosum* s.l., larval habitat, reference, canopy biosignature generated in ArcGIS would not tend to saturate over dense and/or sparse shaded, vegetation-oriented observational, predictor (e.g., immersed hanging vegetation) and would be sensitive to underlying dissimilarities (i.e., spatial non-homogeneity) in background canopy (i.e. substrate) reflectance, such as the presence of leaf litter, senescent (i.e. standing dead vegetation) and woody materials (e.g., twigs). Such differences in vegetation LULC coverage can influence accurately forecasting endmember, canopy shaded, biomass density-related, geometrically log-transformed, time series dependent integers and phenological variables tabulated from an, empirically, probabilistically regressed, eco-epidemiological dataset ofunmixed, georeferenced, geosampled, medium resolution-derived, geospectrally decomposable,*S. damnosum* s.l. larval habitat, photosynthetic or NPV covariate, parameter estimator reflectance emissivity, transmittance, wavelenght coefficient values.

Based on the currently applied moderate resolution remote sensing proxy methodologies, the following broad,endmember LULC categories of georeferenced, geo-spatiotemporal, medium resolution-derived, shade, vegetated, *S. damnosum* s.l.,prolific, riverine larval habitats (e.g., sparse canopy) may be identified in ArcGIS, employing a explanatorily geo-spectrally interpolatable, field operational, NDVI, reference biosignature for: (1) geo-spatiotemporally mapping the structural properties of geosampled, seasonally prolific larval habitats, based on the geophysical structure of the canopy vegetation

(2) conducting spatial heterogeneity assessments based on primary productivity that affect the absorption of light energy in the habitat's surrounding immersed hanging, floating and dead vegetation

(3) temporal heterogeneity assessment of stress factors that interfere with photosynthesis (and thus alter the reflectance spectrum of habitat vegetation)

(4) biomapping plant chemical attractants while summarizing the influence of LULC attractants of fauna, and canopy illumination quality as emitted from the riverine larval habitat.

These latter categories would enclose the range from the most frequently employed methodologies applied to other terrestrial taxa to the latest approaches found in literature. Thus, direct and indirect measurements in ArcGIS of explanatorial, shade-related, vegetated, geo-spatiotemporally dependent, georeferenced, productive, *S. damnosum* s.l., geosampled riverine, larval habitat, immature productivity and habitat, health diversity and distribution may be optimally illustrated from an empirically regressed, operationizable, dataset of unmixed, medium resolution, NDVI-derived, stochastically/deterministically, geospectrally, explanatorily interpolatable, decomposed ,reference biosignature-related, photosynthetic and NPV, canopy endmember, covariate, parameter estimator, reflectance emissivity, transmittance wavelenght, coefficient values.

The recent success in applying hyperspectral mapping data in ArcGIS to endmember vegetation-related canopy LULC, geo-spatiotemporal field eco-epidemiological, forecast, risk mapping has shown promise in rangeland classification. Rolfson [29] focused on acquiring a seasonal inventory of in-situ reflectance spectra of medium resolution-derived, rangeland, decomposed, plant species endmembers employing OBIA in ENVI and ArcGIS to evaluate their separability for a risk-related, hyperspectral, image classification analysis. The goals of the research also included determining the separability of species endmembers at different times of the growing season. Reflectance spectra were collected for three shrub species (*Artemisia cana, Symphoricarpos occidentalis*, and *Rosa acicularis*) and five rangeland grass species native to southern Alberta, Canada (*Koeleria gracilis, Stipa comata, Bouteloua gracilis, Agropyron smithii, Festuca idahoensis*) and one invasive grass species (*Agropyron cristatum*). A library, built using the spectral database software the object-based classifier, which was subsequently populated using the decomposed explanatorial measurements with a primary focus ontime series dependent, shade, vegetated canopy reflectance values. Average extracted endmembers of canopied spectra acquired during the peak of sample greenness were compared employing three separability SMA measures [i.e., normalized Euclidean distance (NED), correlation separability measure (CSM) and Modified Spectral Angle Mapper (MSAM)] to establish the degree to which the species were remotely separable].

Spectral Angle Mapper (SAM) is a physically-based spectral classification that uses an *n*-D angle to match mixels to reference spectrain an OBIA (http://www.exelisvis.com/). Spectral Angle Mapper Classification is an automated method for directly comparing image spectra to aknown spectra (usually determined in a lab or in the field with a spectrometer) or an endmember [2]. This method treats both (the questioned and known) spectra as vectors and calculates the spectral angle between them. This method is insensitive to illumination since the SAM algorithm uses only the vector direction and not the vector length. The optimal result of the SAM classification for a prolific, georeferencable, geosampled, medium-resolution–imaged, canopied, productive, *S. damnosum* s.l., riverine, larval habitat would be a datset showing the best match at each extracted shade canopy-related mixel. This method is typically used as a first cut for determining the mineralogy and works well in areas of homogeneous regions. (http://www.exelisvis.com/).

In Rolfson [29] the authors geo-spatiotemporally mapped hydrothermally altered rocks employing proxy medium resolution data. Absorption features were highlighted in the 2 μm region, for remotely diagnosing carbonate minerals and hydrothermal alteration minerals such as alunite, kaolinite, and calcite. The NED and CSM provided mineral indices that was insensitive to the grain size of minerals and topography. The Modified Spectral Angle Mapper (MSAM) method avoided misidentification due to mixture of the target mineral with different materials such as shade, canopied vegetation-oriented, time series dependent, explanatorial, canopied, LULC covariates. The mineral index images derived employing the MSAM method also exhibited a clear boundary between areas of contrasting mineralogy in the geosampled Cuprite region and Northern Grapevine Mountains region; this result was consistent with a previously published geologic map and hyperspectral data. Further, investigation by the MSAM method identified several types of hydrothermal alteration zones associated with porphyry ore deposits near the Yerington District, Nevada. These results demonstrate the usefulness of MSAM method in terms of lithologic, medium resolution-derived,time series dependent, forecast-related, endmember, interpolatable risk mapping.

Findings such as in Rolfson [29] suggest that the choice of separability measures may be an important factor when analyzing decomposed empirically regressable, geosampled, geospectrally decomposable, explanatorily interpolatable, reference biosignature, photosynthetic and NPV canopy endmember, reflectance components. The differences observed in the separability results over time may suggest that the consideration of phenological patterns in planning data acquisition for optimum riverine classification of georeferenced, *S. damnosum* s.l., riverine, larval habitats, geospectrally decomposed, endmember, NDVI-related, biosignatures. Subsequently, this sub-mixel, remote dataset of stochastically/deterministically, interpolated, geopredictive variables may have a high level of importance for geo-spatiotemporally, remotely, probabilistically regressively, targeting prolific, unknown, unsampled, *S. damnosum* s.l., larval habitats in African riverine environments based on field-geosampled, interpolated count data.

While global explanatorial geo-classifications have relied mostly on multi-temporal, canopied, endmember, LULC dynamics for geospectrally explanatorily interpolating, sub-mixel, decomposed medium resolution-imaged, immature, *S. damnosum* s.l., habitat, reference-related, gaseous biosignatures have not ever been used.There are currently no known remotely detectable canopy endmember, gaseous biosignatures strictly associated with oxygenic and anoxygenic photosynthesis [13]. In the absence of gaseous biosignatures, a geosampled, georefernced, prolific, *S. damnosum* s.l., canopy-related, vegetation associated, LULC, shaded surface reflectance features would be the only possibly detectable biosignature. An oxygenic photosynthesizers and chemosynthetic pigment would have to be generated and diagnostically tested employing their own surface, time series, canopied, end member, reflectance biosignatures which may reflect more strongly in medium resolution wavelengths where their pigment absorption occurs.

In particular, investigations of canopied, vegetation-related LULC phenology in the hyperspectral domainshave been limited in African riverine environments. Vegetation phenology can provide a useful signal for geo-classifying geo-spatiotemporal LULC, but phenology can cause spectral misspecifications in stochastic/deterministic explanatorial interpolators especially when complex unmixed geospatial objects such as, red, green and blue (RGB),decomposed, *S. damnosum* s.l., riverine, larval habitat, canopy, emissitivity values are generated from vegetation-related, LULC components(e.g., immersed hanging vegetation, floating dead vegetation, turbid water).Remotely sensed changes in sub-mixel, canopy vegetation, LULC, time series, spectral responses caused by phenology can conceal longer term changes in the landscape [30,31]. Multi-temporal data that captures these spectral differences in ArcGIS can improve separability of vegetation landscape types over endmember geo-classifications based on single-date imagery [www.esri.com]. Global-scale explanatorial, time series dependent, LULC endmember classifications have utilized differences in vegetation phenology derived from multi-temporal empirical datasets to map the distribution of ecoregions [32-34].

While global-scale monitoring of phenology has been successful, operationizable, hyperspectral, endmember, sub-mixel, decomposed, risk–related, vegetation-oriented, forecastable, geo-spectrally interpolatable, data variables of seasonal changes in explanatorial, LULC have been limited due to the restricted abilities of coarse resolution aerial platforms to repeatedly geosampled large areas [35-38]. The spectral detail provided by medium resolution-derived data may allow classification of vegetation and monitoring of the LULCand NPV components of seasonal, prolific, canopied, *S. damnosum s.l.*, georeferenced, larval habitats geosampled in an African riverine environment in ArcGIS. The effects of vegetation phenology on endmember selection and LULC species mapping employing average RMSE may then robustly explore geo-spatiotemporal changes in the characteristics of selected, unmixed, decomposable, shade, vegetated, explanatorily interpolatable, operationizable, time series dependent, NDVI, canopied, biosignature-related, explanatorial, geospatial objects. Multiple endmember spectral mixture analysis is a linear mixing model that uses a RMSE metric [4].

The images modeled by these medium resolution-derived, operationizable, time series dependent, absorption-related, canopy endmembers in ArcGIS may demonstrate geo-spatiotemporal changes between canopy vegetation species in a prolific, georeferenced, *S damnosum* s.l., riverine, larval habitat based on field geosampled, spectral explanatorial, count data. The extensive diffuse multi-scattering reflected by medium resolution imaged, shade vegetated, georeferenced, canopied, riverine, larval habitat geo-spatiotemporally dependent, decomposed, canopy endmember objects may prevent conducting invasive regression analyses of explanatorial, geosampled photosynthetic materials (e.g., percentage of floating shaded vegetation) and NPV (e.g., canopy twigs) thus, causing error in unmixed NDVI, biosignature, endmember, interpolation calculations. As mentioned previously explicit mathematical relationships of the light–canopy interaction have been developed exclusively for sub-meter resolution, imaged canopies with non-reflective backgrounds. Therefore, an empirical, operationizable dataset of light sensitive explanatorial, proxy, covariate, coefficient values in ArcGIS, composed of medium resolution-derived, geo-spectrally unmixed,time series dependent, NDVI,canopied endmember,reference biosignature,values as temporally rendered from a georeferenced, shade, canopied, prolific, *S damnosum* s.l., riverine, larval habitat geosampled in an African riverine environment, may have the disadvantage of unquantifiable scattered spectra where image correction is not trivial and, as such, noise may be introduced during mixel decomposition.

Importantly, time series dependent, NDVI spectral libraries for maintaining decomposed, medium, resolution-derived, sub-mixel, endmember data products in object based classifiers are generally derived in laboratory conditions for example, employing controlled situations using artificial irradiance and minimalized atmospheric effects. However, the spectral reflectance of temporally dependent, canopied, georeferenced, S. *damnosum* s.l., riverine, larval habitat, vegetated, LULC, ecogeographically classified, explanatorial, surface data, topographic, feature attributes represent elements that have experienced extensive chemical, physical and biological weathering and, as such, might contain moisture. Conventional medium resolution satellite maps of intertidal sediment domains employing point samples can be spatially unrepresentative, due to errors introduced through moisture-ridden sediment geosampling and subsequent interpolations [35,39]. Light from the canopy, soil, LULC surfaces can influence decomposability of geospectrally explanatorily, interpolatable, unmixed, NDVI, endmember, reflectance values by a large degree. This is of concern in forecast, vulnerability, eco-epidemiological, risk endmember mapping productive, georeferncable, seasonal vegetated, canopy, shaded, *S damnosum* s.l., larval habitat, photosynthetic and NPV regressors for identifying unsampled, unknown habitats since in many African semi-arid and arid riverine environments tend to have higher cover of bare ground. Heute and Jackson [40] found that the soil reflectance LULC surface impact on NDVI values in ArcGIS was greatest in areas with between 45% and 70% vegetative cover. The unmixed endmember reflectance spectrum of a whole canopy is influenced by factors such as the effects of leaf area, the orientation of leaves, ground coverage, and presence of non-leaf elements, areas of shadow and soil surface reflectance [41].

Overall as Jiang et al. [42] reported, there exist many perspectives and discrepancies between decomposed endmember, NDVI, unmixed, fractional, LULC-, vegetation cover, absorption-related reflectance values for optimally remotely discriminating the scale effect of any canopy object. The principle behind derivation of endmember, fractional vegetation, medium resolution, LULC-related, radiance cover aggregated from NDVI, canopy-related, ArcGIS data is to relate the decomposed, biosignature information to reference values, such as dense vegetation and bare soil, assuming the individual component, NDVI, sub-mixel, data can be represented by the reference data [1,3,4].

However, even if component, medium resolution-derived, NDVI, decomposed, endmember data in ArcGIS and in ENVI technology can be estimated without error, there would still be sources of spectral, sub-mixel, probabilistic uncertainty caused by the scale effect of the NDVI especially when retrieving canopy-oriented, vegetation-related, radiance LULC fractions from the original synthesized, moderate resolution, decomposed, NDVI biosignature. It remains unclear the extent to which the sub-mixel scale, moderate resolution-derived, unmixed NDVI corresponds to the scales and what possible relationships exist between the unmixed material for any type of seasonal, *S. damnosum* s.l., riverine,larval habitat-related, explanatorial, probabilistic, time series dependent, explanatorily interpolatable, forecast-oriented, eco-epidemiological, risk mapping. The relationship between medium solution-derived NDVI and radiance fractional, LULC specified, vegetation-related, canopy cover in ArcGIS may be directly influenced by the scale effect of the decomposed, riverine, larval habitat endmember NDVI. Understanding this residual forecast effect may be essential to understanding the relationship between fractionalized, NDVI, biosignature, endmember, absorption radiance estimates in ArcGIS and for accurate retrievals of operationizable, interpolatable, seasonal, shade, canopy, decomposed reflectance emissivity, transmittance data (remove period) in ENVI. These geospectral, ecobiological explanatorial, time series dependent, covariate parameter, estimator attributes may limit the general use of medium resolution, spectral libraries in the unmixing procedures(e.g., sub-mixel decomposition) of a georeferenced, shade, vegetated, prolific, geosampled, seasonally canopied, *S. damnosum* s.l., riverine,larval habitat.

A discontinuous, geospectrally decomposed, within canopy–related, medium resolution imaged, prolific, *S. damnosum* s.l., riverine, larval habitat, NDVI, explanatorily interpolatable biosignature target in ArcGIS may also cause extensive endmember confusion among known light sensitive, photosynthetic and NPV covariate coefficient measured values in a regression equation. As Rundquist [43] reported NDVI has been criticized because of substrate reflectivity, as well as its insensitivity to increases in vegetation LULC-related biomass past particular thresholds. For example, discontinuous, dense, canopy endmembers can cause an increase of the blue/red radiation ratio in vegetated canopies generating higher photosynthetic rates per unit leaf area [44].Vegetation have distinctive spectral characteristics as was observed by Gates [45] who noted that canopy vegetation LULC in ArcGIS leaf reflects and transmit incident radiation in a manner that is uniquely characteristic of pigment cell containing water by solution.

Reflectance also will vary with wavelengths for within medium resolution imaged, geosampled, explanatorial, georeferencable, prolific, *S. damnosum* s.l., riverine, larval habitat, shade, canopied, endmember, unmixed, biosignature-related, fractionalized, vegetated materials in ArcGIS as energy at certain wavelengths may be scattered or absorbed to different degrees. These sub-mixel, reflectance, covariate parameter estimator coefficient value variations may not be evident when time series-dependent, geospectral reflectance curves (i.e., plots of reflectance versus wavelength) are employed for different sized, decomposable, medium resolution imaged, georeferencable, riverine,larval habitat–related, explanatorial, time series dependent, canopied, geospatially, probabilistically regressable objects. Thus, the explanatorial shaded, canopy endmember, explanatorial, time series biometrical properties of vegetated LULC in different medium resolution wavelengths of the electromagnetic spectrum may not be analyzed thoroughly for efficiently monitoring prolific, *S. damnosum* s.l., larval habitats geosampled in African riverine environments nor, utilized for ecogeographic and ecohydrologic, forecast,eco-epidemiological, risk, modelling of explanatorial, ecobiophysical, georeferencable processes (e.g., presence of chorophyll canopy pigments)related to vegetative vigor and physiognomy characteristics of these habitats.

Tucker [46] tested various combinations of the red, NIR, and green bands to predict biomass, water content, and chlorophyll content of grass plots in ArcGIS. The NDVI was strongly correlated with chlorophyll content and crop characteristics that were directly related to chlorophyll content, such as green biomass and leaf water content. Monteith and Unsworth [47] conducted a theoretical analysis which revealed that vegetation indices (VIs) are uniquely related to the amount of incident light reflected and therefore absorbed by a canopy, assuming a low and constant value for soil absorption. Myneni et al. [48] showed that NDVI was near-linearly related to the chlorophyll content of single soybean leaves and were curvilinearly related to the chlorophyll content of soybean canopies.This reflux relationship may have been due to surface leaves intercepting more light than leaves deeper in the canopy.

Since most photosystems includes the first steps of the *Z-scheme*, delineating oxidized chlorophyll *a* molecules in OBIA it may be vital for uncertainty diagnostic testing non-normal endmember, wavelenght transmittance errors in ArcGIS may when generating an optimal, unmixed, empirical,time series dependent, geospectrally interpolatable, medium resolution-derived, proxy, explanatorial, biophysical, photosynthetic or NPV covariate, parameter estimator dataset of decomposed, canopied biosignature-related regression values. It is called the Z scheme because it links the two photosystems in a way that resembles the letter"Z". (http://commons.wikimedia.org/wiki/File:Z-scheme.png).The "Z-scheme" describes the oxidation/reduction changes during the light reactions of photosynthesis. All photosynthetic organisms have chlorophyll *a* [4,13].

Chlorophyll *a* is a type of chlorophyll that is most common and predominant in all oxygen-evolving photosynthetic organisms such as higher plants, red and green algae. Foliar pigments such as chlorophyll *a* play a crucial role in plant photosynthesis through the conversion of solar radiation into stored chemical energy and can provide important information on gross primary productivity [4,7]. The amount of solar radiation absorbed by a leaf is largely a function of foliar concentrations of photosynthetic pigments, therefore low concentrations of chlorophyll can directly limit photosynthetic potential and hence primary production [2].Chlorophyll *a* is best at absorbing wavelength in the 400-450 nm and 650-700 nm of the electromagnetic spectrum. Its molecular formula is $C_{55}H_{72}O_5N_4Mg$. Chlorophyll *a* is a specific form of chlorophyll employed in oxygenic photosynthesis which absorbs most energy from wavelengths of violet-blue and orange-red light: It also reflects green/yellow light and, as such, contributes to the observed green color of most plants [49]. If these wavelengths are spectrally unmixed improperly in an OBIA, they will generate a false, non- interpolatable, eco-explanatorial, shade, canopy, vegetated, *S damnosum* s.l., larval habitat, NDVI, endmember, biosignature-oriented, explanatorial risk map in ArcGIS.

Further, during photosynthetic activities of canopy, shade vegetated, geosampled, georeferencable, *S damnosum* s.l., riverine, larval habitats in ArcGIS, two compounds are commonly generated: nicotinamide adenine dinucleotide phosphate (NADPH) and adenosine triphosphate (ATP).The NADPH is the main reducing agent in chloroplasts, providing a source of energetic electrons to other reactions. Its production leaves chlorophyll with a deficit of electrons (i.e., oxidization), which must be then obtained from some other reducing agent. The excited electrons lost from chlorophyll in a medium resolution imaged, shade, canopy, vegetated, seasonal-geosampled, georeferenced, prolific, *S damnosum* s.l., riverine, larval habitat must then be remotely captured in order to generate a robust, geospectrally, explanatorily interpolatable, sub-mixel, robustifiable, decomposable, field and remote, operationizable, NDVI, canopy biosignature but, it may be confused with an electron transport chain such as plastocyanin for example, during decomposition. In photosynthesis, plastocyanin functions as an electron transfer agent between cytochrome f of the cytochrome b_6f complex from photosystem II and P700+ from photosystem I [50]. Cytochrome b_6f complex and $P700^+$ are both membrane-bound proteins with exposed residues on the lumen-side of the thylakoid membrane of chloroplasts [26]. The thylakoid membrane is the site of the light-dependent reactions of photosynthesis with the photosynthetic pigments embedded directly in the membrane [51] which may be remotely inaccessible at moderate resolution.

Besides chlorophyll, canopy, shade, vegetated, remotely explanatorial, geospatiotemporally, geosampled, productive *S. damnosum* s.l., riverine, larval habitats geosampled in African riverine ecosystems also use pigments such as carotenes and xanthophyll [1]. Algae use chlorophyll, but various other pigments are present as phycocyanin, carotenes, and xanthophylls in green algae, phycoerythrin in red algae (rhodophytes) and fucoxanthin in brown algae as well as diatoms resulting in a wide variety of colors that may be geospectrally associated with a georeferenced, geosampled, shade, vegetated, remotely explanatorial, prolific, medium resolution imaged,*S damnosum* s.l., shade canopied, riverine, larval habitat. Canopy reflectance results from a complex interaction between pigment concentrations, canopy structure, background signal and illumination conditions (e.g., sun-sensor-target geometry) [52].These light harvesting biosignature endmembers may render fractionalized radiance misspecifications during geospectral interpolation in ArcGIS of explanatorily decomposed, medium solution-imaged, canopy-oriented, stomata conductance-related, reflectance emissivity, wavelenght, transmittance data feature attributes.

Leaf reflectance is controlled by the presence of foliar constituents such as chlorophyll, nitrogen, carotenoids, and water [2] In visible wavelengths, chlorophyll absorbs strongly in red and blue spectral regions, with maximum absorbance between 660 and 680 nm and maximum reflectance in green wavelengths (560 nm) [2,4]. Internal leaf structure also affects the amount of incident radiation absorbed, scattered and reflected through the upper epidermis, due to refractive discontinuities between intercellular air spaces and cell walls [46]. Broadleaves have a thin epidermal layer, long palisade cells and more air spaces surrounding spongy mesophyll cells, whereas cylindrical needle leaves have an undifferentiated, densely packed mesophyll and thick cell walls [13]. Research has suggested that NIR reflectance is controlled by the ratio of mesophyll cell surface to intercellular air spaces. As such, differences in broadleaf reflectance spectra in a prolific, geo-spatiotemporally-resampled, medium-resolution imaged, shade, canopied, *S. damnosum* s.l., riverine habitat analyzed in ArcGIS, could exist even with the same chlorophyll content; making chlorophyll content estimation across plant functional types complex.

At the canopy level, reflectance is also governed by leaf architecture, clumping, leaf angle distribution, tree density, NPV canopy elements [46], along with solar/viewing geometry, ground cover and understory vegetation [28]. Conifer canopies reflect less NIR radiation than broadleaf canopies, which is a function of the optical properties of the leaves, non-photosynthetic elements and leaf angle distribution [2]. Vertical leaves promote a deeper penetration of incident radiation within the canopy, where multiple scattering within the crown allows for a higher probability of photon absorption [47]. It is also therefore possible that reflectance factors from two georeferenced, explanatorial, medium-resolution-derived, prolific, rieverine, larval habitat, seasonal, decomposed canopies are different in ArcGIS even if the spectral reflectance of the constituent leaves are the same.

Although, the chloroplastic carotenoid, zeaxanthin has been shown to act as a blue radiation sensor mediating guard-cell movement [4], precisely geospectrally capturing and modulating gas exchange between the leaf cells and the surrounding canopy architecture in a medium resolution-derived, time series dependent, endmember, NDVI-related, empirical dataset of georeferenced, geosampled, decomposable, interpolatable, unmixed, *S. damnosum* s.l., riverine, larval habitat, canopy biosignature variables may be remotely tedious. Further, a geo-spatiotemporally dependent, empirical dataset of georeferenced, medium resolution-derived, geospectrally decomposable, NDVI-oriented, canopy, endmember biosignature covariate parameter estimator, reflectance emissivity, transmittance coefficient, fractionalized, radiance values may be more difficult to interpolate accurately due to an inability to define scale, leaf-level, gas exchange component variables in the geosampled, seasonal, riverine larval habitat, sub-mixel, empirical dataset. Unfortunately, the changes observed within medium resolution-derived, shade, canopy-related, riverine,*S. damnosum* s.l., vegetated,larval habitat, NDVI-related, explanatorial, endmember, canopied, profiles may compromise quantification of multiple, ecobiological, geo-spatiotemporally and non-ecogeographically dependent, photosynthetically-oriented and NPV operationizable, explanatorial, time series dependent parameter estimators. Scaling and interpolating leaf-level fluxes are essential at the canopy level [2,4].

Amongst the most relevant issues on scaling fluxes in a canopy-oriented, explanatorial, vegetated-related LULC, geospatiotemporally-dependent, medium resolution-derived, shaded or non-shaded, NDVI-related, productive, *S. damnosum* s.l., riverine, larval habitat, decomposed, biosignature, endmember-related regressors may be the multiple representations of canopy light levels and assimilation capacities of the unmixed photosynthetic and NPV covariates. Light utilization is a primary factor determining plant ecosystem productivity [53,54] and is a function of light interception by the plant canopy and the response of photosynthesis to irradiance. Increasing leaf mass per unit ground area increases light interception by the canopy and is positively correlated with NPP across a range of ecosystems [55]. However, the cumulative interception of light through a prolific, georeferenced, geo-spatiotemporally-geosampled, shade, vegetated, *S. damnosum* s.l., riverine larval habitat canopy may cause light limitation of photosynthesis in the lower canopy. To maximize seasonal, canopy-level, carbon uptake, changes in photosynthetic light response that maximize leaf-level carbon uptake under prevailing light conditions should optimally occur through the canopy crown [56].During photosynthesis in green plants, light energy is captured and used to convert water, carbon dioxide, and minerals into oxygen and energy-rich organic compounds [13].

Although geospectrally extracted,medium resolution-derived, seasonal,vegetated, *S. damnosum* s.l., georeferencable, prolific, riverine, larval habitat, explantorily shade canopied, time series dependent, canopy biosignature-related reflectance emissivity, wavelenght, transmittance components in ArcGIS and ENVI may play an important role in revealing mass exchange and controlling factors in the energy and atmosphere, the medium resolution, sub-mixel, radiance endmember response from the stomatal conductance for the whole canopy may be misrepresented in the unmixed model as one empirical function. Such a non-mechanistic representation of multiple imaged, endmember, radiance fractionalized, shaded and canopied, spectral conductance may contain erroneous, residual, multicollinear, *S. damnosum* s.l., riverine, larval habitat, or autocorrelation coefficients. Unmixed medium-resolution, shade, canopy, vegetated, *S. damnosum* s.l., riverine, larval habitat, canopy endmembers involved in multicollinearity can be combined into a single variable, however, this formulation may not be appropriate for resolving non-independence in geosampled,photosynthetic and NPV reflectance, covariates.

There are four principal assumptions which justifying the use of linear regression models for purposes of inference or prediction: (1) linearity and additivity of the relationship between dependent and independent variables: (2) statistical independence of the errors (in particular, no correlation between consecutive errors in the case of time series homoscedasticity (i.e, constant variance) of the errors (a) versus time (in the case of time series data)(b) versus the predictions (3) versus any independent variable; and, (iv) normality of the explanatorial, time series, dependent error distribution [29]. For conducting a robustifiable, time series, geospectral, explanatorial, geosampled interpolation on an empirical dataset of decomposed endmember, georeferencable,o perationizable, geo-spatiotemporal, geosampled, *S. damnosum* s.l., larval habitat,canopy,biosignature-related,covariates parsimoniously, the photosynthetic and NPV , LULC, predictor variables must reveal independence,homoskedacisty, and normal distribution of errors [1].

Several methods have been described to reduce collinearity and other violations of regression assumptions in moderate resolution remote sensing in ArcGIS models by applying iterative approaches to unmixing and endmember selection. Based on a suggestion made by Bateson and Curtiss [57] on manual endmember selection, several follow-up papers [58,59] were published to automate and refine procedures for iterative unmixing, but currently in literature, statistics such as scale and local variance and theoretical models based on convolution have not been proposed to support resolving multicollinearity in medium resolution-derived, NDVI, endmember, time series dependent, canopy biosignature-related, reference, explanatorial, forecasting-related categorical and continuous variables. In addition, in unmixing operationizable, geospectrally, stochastically/deterministically, explanatorily, interpolatable, medium resolution data applications, canopy endmember selection and the resulting abundance image errors are often associated with RMSE without a critical review of the level of accuracy and uncertainty in decomposed, temporally dependent, biosignature-oriented, unmixed datasets.

Regarding the collinearity problem in a geospectrally-oriented, explanatorial, time series, eco-epidemiological, explanatorily geo-spatiotemporally dependent, empirical datasets of shade, canopied, *S. damnosum* s.l., vegetated, biosignature-oriented, riverine, larval habitat, canopy endmember decomposed, geopredictive variables, predictorvariables, classical multivariate, explanatorial, residual, uncertainty, probabilistic, non- normality diagnostic models may resolve any non-independence employing Euclidean geometrical algorithms. In Euclidean geometry this relation is intuitively visualized by points (e.g., geo-spatiotemporal prolific, larval habitats ,geosampled in an African riverine environment based on immature count data) lying in a row on a "straight line". However, in most current seasonal, entomological-related, remotely sensed, aggregated geometries (e.g., Euclideanized habitat measurements) a line is typically a primitive (i.e., undefined) object type, so such visualizations will not necessarily be appropriate [7,60].

An explanatorily, geo-spatiotemporal, resampled, risk, forecasting eco-epidemiological, model in ArcGIS for remotely qualitatively quantitating Euclidean geometry may offer an interpretation of how resampled, georeferenced, *S.damnosum s.l.* riverine, larval habitat, explanatorial, time series reflectance points, lines and other object types become collinear within the context of that model [61-63]. For instance, in spherical geometry, where lines are represented in the standard model by great circles of a sphere [61-63], sets of explanatorily, collinear, decomposable, geo-spatiotemporally, resampled, shade, canopied, prolific, *S. damnosum* s.l., vegetated, riverine, larval habitat reflected points may lie in a circle. Such points would not lie on a "straight line" in the Euclidean sense, and would not be thought of as being in a row. A mapping of a geometry to itself which sends lines to lines is called a collineation; it preserves the collinearity property [2]. The rendered *S. damnosum* s.l., vegetated, larval habitat operational radiance maps (or linear functions) of the vector spaces may then be viewed as geometric maps, (i.e., map lines to lines), that is, the map habitat collinear point may be set to collinear point sets (i.e., collineations) in ArcGIS. In projective geometry these linear larval habitat reflectance mappings would be homographies.

In ArcGIS projective geometry, a homography is an isomorphism of projective spaces, induced by an isomorphism of the vector spaces from which they are derived (www.esri.com). Thus, geo-spatiotemporally dependent, decomposable, geospatially interpolatable, explanatorily, resampled, shade, canopied prolific, medium-resolution-imaged, *S. damnosum* s.l.,georefernced, riverine, larval, habitat bijections that map lines to lines in Geostatistical Analyst ™ in ArcGIS for example, would be a collineation. In mathematics, a bijection (or bijective function or one-to-one correspondence) is a function between the elements of two sets, where every element of one set is paired with exactly one element of the other set, and every element of the other set is paired with exactly one element of the first set [2]. Hence, there are no unpaired elements. A bijective function $f: X \rightarrow Y$ is a one-to-one (injective) and onto (surjective) mapping of a set X to a set Y [64]. In ArcGIS there are collineations which are not homographies, but the fundamental theorem of projective geometry asserts that it is not so in the case of real projective spaces of dimension at least two.

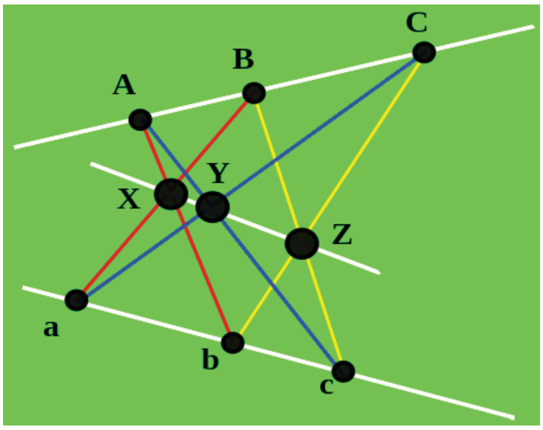

Figure 2: The Levi graph of the Pappus configuration of a bipartite distance-regular graph in Arc GIS with 18 vertices and 27 edges.

Historically, ArcGIS homographies and projective spaces have been introduced to study perspective and projections in Euclidean geometry, and the term "homography", which, etymologically, roughly means "similar drawing" date from a specific time period. At the end of 19th century, formal definitions of projective spaces were introduced, which differed from extending Euclidean or affine spaces by adding points at infinity. The term "projective transformation" originated in these abstract constructions. These ArcGIS data products may divide classes for any explanatorial, empirical entomological dataset (e.g., decomposed, endmember, medium resolution-derived, NDVI reflectance eco-geographic or non eco-geographic wavelenght-oriented, endmember, covariate, parameter estimators) that have been shown to have equivalent numbers of time series dependent, empirically geosampled explanatorial regressors.

A projective space may be thus constructed in ArcGIS as the set of the lines of a vector space over a given field for parsimoniously, geospectrally, interpolating an empirical operationizble, datatset of geosampled, stochastically/deterministically georeferncable, explanatorily, decomposable, *S. damnosum* s.l. riverine, larval habitat-related, canopy endmember, biosignature-oriented, time series dependent, forecasting independent variables geosampled over a African riverine community. This construction could facilitate using tools from linear algebra for the study of the ArcGIS homographies. The alternative approach consists in defining the projective space through a set of axioms which do not involve explicitly any field (e.g., incidence geometry, synthetic geometry). In this context, geo-spatiotemporally dependent, ArcGIS-related seasonal geosampled, riverine, larval habitat explanatorily interpolated, time series dependent collineations would be easier to define than remotely tabulated, medium-resolution-derived, *S. damnosum* s.l. related homographies (i.e, "projective collineations").

Equivalently Pappus'shexagon theorem and Desargues' theorem may be generalized in ArcGIS for remotely qualitatively, probabilistically, regressively quantitating empirical, geosampled, operationizable, eco-epidemiological, datasets of georeferncable, projective, geospectrally decomposable, endmember, medium resolution-derived,explanatorily interpolatable, shaded, *S. damnosum* s.l. riverine, larval habitat, canopy reflected, fractionalized geometries. In mathematics, Pappus' hexagon theorem states that given one set of collinear points *A, B, C,* (e.g., endmember, riverine, larval, habitat geocordinates) and another set of collinear points *a, b, c*, then the intersection points *X, Y, Z* ofline pairs *Ab* and *aB*, *Ac* and *aC*, *Bc* and *bC* are collinear, lying on the Pappus line. Projective planes in which the "theorem" is valid are called Pappian planes[64].These three points would be the points of intersection of the "opposite" sides of the hexagon *AbCaBc* which would hold in a projective plane over anycanopied biosignature-related, decomposed, radiance-related, geo-spatiotemporally, geosampled, ArcGIS *S. damnosum* s.l., larval habitat, georeferencable, medium resolution field. However, this model would fail for projective planes over any noncommutative division ring.

A choosen set of projective ArcGIS imposed, geospectrally, interpolatable, geo-spatiotemporally fractionalized, canopy radiance endmember, explanatorial, empirical dataset of operationizable, medium resolution-derived, shade, canopied, *S. damnosum s.l.* riverine, larval habitat reflux coordinates may be optimally geo-represented as C=(1,0,0), c=(0,1,0), X=(0,0,1), A=(1,1,1). Then the lines *AC*, *Ac*, *AX* may be given by $x_2=x_3$, $x_1=x_3$, $x_2=x_1$, by cartographically delineating the georeferenced,geosampled,points *B*, *Y*, *b* to be$B=(p,1,1)$, $Y=(1,q,1)$, $b=(1,1,r)$for some p, q, r. The three lines *XB*, *CY*, *cb* in ArcGIS would then be ecogeographically and/or ecohydrologically seasonally represented as$x_1=x_2p$, $x_2=x_3q$, $x_3=x_1r$, so they would pass through the same canopy-related, eco-epidemiological, capture point (e.g., prolific, geosampled, shade canopied, *S. damnosum* s.l., georefernced, riverine,larval habitat) *a* if and only if rqp=1. The condition for the three lines *Cb*, *cB* and *XY* $x_2=x_1q$, $x_1=x_3p$, $x_3=x_2r$in ArcGIS would pass through the same geosampled endmember point *Z* which could be subsequently quantized when rpq=1. So this last set of three lines in a canopy, endmember, mapped georefernced, productive, seasonally shaded, *S. damnosum* s.l., larval habitat geosampled in an African riverine environment would be concurrent if all the other eight sets are defined in ArcGIS and since multiplication is commutative, thus $pq=qp$. Equivalently, *X*, *Y*, *Z* in the medium resolution-derived, time series dependent, explanatorial, shade, canopied, *S. damnosum s.l.*, larval habitat,empirical dataset would be diagnosed as collinear.

The dual of this incidence theorem states that given one set of concurrent lines *A*, *B*, *C*, and another set of concurrent lines *a*, *b*, *c*, then the lines *x*, *y*, *z* defined by pairs ofexplanatorial, *S. damnoum* s.l., endmember, geo-spatiotemporal, decomposed, canopy biosignature, seasonal, reflectance points resulting from pairs of intersections $A\cap b$ and $a\cap B$, $A\cap c$ and $a\cap C$, $B\cap c$ and $b\cap C$ would be concurrent[4]. Pappus's theorem is a special case of Pascal's theorem for a conic—the limiting case when the conic degenerates into 2 straight lines[27]. The Pappus configuration is the configuration of 9 lines and 9 points that occurs in Pappus's theorem, with each line meeting 3 of the points and each point meeting 3 lines [2]. In general, the Pappus line does in ArcGIS not pass through the point of intersection of *ABC* and *abc* [65]. This configuration is self-dual. Since, in particular, the lines *Bc*, *bC*, *XY* will have the properties of the lines *x*, *y*, *z* of the dual theorem, the collinearity of *X*, *Y*, *Z* in an ArcGIS explanatorial, empirical, dataset of operationizable, time series dependent, shade canopied, prolific, riverine,*S. damnosum* s.l. larval habitat explanatorial, georeferencable, biosignature, endmember reflectance emissitivty, transmittance wavelenght-oriented, geopredictive variable would be equivalent to concurrence of *Bc*, *bC*, *XY* (Figure 2).

Suppose an ecologist or experimenter chooses projective, temporally dependent, *S. damnosum* s.l., shade, canopied, riverine larval habitat decomposed, explanatorial reflectance coordinates with C=(1,0,0), c=(0,1,0), X=(0,0,1), A=(1,1,1) in ArcGIS.On the lines *AC*, *Ac*, *AX*, given by $x_2=x_3$, $x_1=x_3$, $x_2=x_1$, the points *B*, *Y*, *b* would then be $B=(p,1,1)$, $Y=(1,q,1)$, $b=(1,1,r)$for some p, q, r.

The three lines *XB*, *CY*, *cb* could then be optimally graphed as $x_1=x_2p$, $x_2=x_3q$, $x_3=x_1r$, so they would pass through the same *S. damnosum* s.l. riverine larval habitat reflectance pathway *a,* if and only if $rqp=1$. The condition for the three lines *Cb*, *cB* and *XY* $x_2=x_1q$, $x_1=x_3p$, $x_3=x_2r$ to pass through the same point *Z* then would be $rpq=1$. So this last set of three lines would be concurrent if all the other explanatorial, empirical, probabilstically regressable, decomposed endmember reflectance ArcGIS datasets for example are concurrent since multiplication is commutative; thus, $pq=qp$ again. Equivalently, *X*, *Y*, *Z* would be collinear. Projective space [i.e., $P(V)$] of dimension *n* over a field *K* in ArcGIS may be defined as the set of the lines in a *K*-vector space of dimension $n+1$. If a basis of *V* has been fixed, a canopy, reflected, medium resolution-derived, productive, canopied, *S. damnosum s.l,.* riverine, larval habitat, geo-spatiotemporally geosampled time series, parameter estimator of *V* may be cartographically represented by a point $\left(x_0,\ldots,x_n\right)$ ofK^{n+1}. A point of $P(V)$, being a line in *V*, may thus be represented by the coordinates of any nonzero point of this line, which would be homogeneous coordinates of the projective point in ArcGIS.

Given two projective spaces $P(V)$ and $P(W)$ of the same dimension inArcGIS, a homography is a mapping from $P(V)$ to $P(W)$, which is induced by an isomorphism of vector spaces f: $f: v \to W$ [65]. Such an isomorphism in a canopy, shaded, riverine, *S. damnosum* s.l, riverine, larval habitat, decomposition, canopy endmember, biosignature-related, eco-epidemiological, geospectral, forecasting, risk model would induce a bijection from P(V) to P(W) because of the linearity of f. Thus, if two georefernced, *S. damnosum* s.l., larval habitat canopy reflectance points in an ArcGIS geodatabase are geo-spatiotemporally dependent isomorphisms, f and g could optimally define the same homographic delineation if and only if there is a nonzero element a of K such that $g=af$. This may be written in terms of a dataset of temporally dependent, shade canopied, *S. damnosum* s.l, riverine, larval habitat, decomposed, forecasting endmember, biosignature homogeneous coordinates in the following way.

A homography φ in ArcGIS may be defined by a nonsingular $n+1 \times n+1$ matrix $[a_{i,j}]$ (i.e., the matrix of the shade, canopied, georeferenced, *S. damnosum* s.l. larval habitat homography. This matrix may be defined up to the, multiplication by a nonzero element of K. Hence, the endmember, homogenous, geospectrally interpolated, explanatorial, canopy reflux coordinates $[x_0 : \ldots : x_n]$ of the unmixed medium resolution derived, georefernced, riverine, larval habitat and its geo-spatiotemporally-geosampled, operationizable, image coordinates would be realized by $\left(y_0 : \ldots\ldots : y_n\right)$ and φ. Coincidentally this optimally regressable, residually forecasted, canopy reflectance would be geospatially related to $y_0 = a_{0,0}x_n + a_{0,n}x_n \;\; y_n = a_{n,0}x_0 + a_{n,n}x_n$ by simply adding points (i.e., other geosampled, prolific, riverine, larval habitats, reflected canopy points) at infinity to affine spaces (i.e., projective completion) in ArcGIS and adding the preceding formulas which would then become affine geocoordinates, employing

$$y_1 = \frac{a_{1,0} + a_{1,1}x_1 + \ldots + a_{1,n}x_n}{a_{0,0} + a_{0,1}x_1 + \ldots + a_{0,n}x_n} = \frac{a_{n,0} + a_{n,1}x_1 + \ldots + a_{n,n}x_n}{a_{0,0} + a_{0,1}x_1 + \ldots + a_{0,n}x_n}.$$

The residualeco-epidemiological, forecasts from this model could then generalize the expression of the homographic function. By so doing, the endmember shade, canopied, *S. damnosum* s.l. larval habitat mixed decomposition and subsequent interpolation of the geospectrally, explanatorily, decomposed, canopy endmember, biosignature reflectance could define a partial function between affine spaces, which would be outside the hyperplane where the denominator is zero.

Conversely, in ArcGIS, an isomorphism is a homomorphism (or more generally a morphism) that admits an inverse. Two mathematical objects are isomorphic if an isomorphism exists between them [64]. An automorphism is an isomorphism whose source and target coincide [2]. The interest of isomorphisms for resolving endmember collinearity in a decomposed, explanatorial, geo-spatiotemporal dataset of *S. damnosum* s.l. larval habitat medium resolution, sub-mixel, biosignature-related, reflectance –oriented, predictive variables would be based on the fact that two isomorphic objects cannot be distinguished by using only the properties employed to define morphisms; thus, isomorphically geospectrally interpolated, larval habitat, canopy endmember reflectance objects geosampled in an African riverine environment must be considered extensively heterogeneous as long as one considers only these properties and their consequences. For most algebraic structures, including groups and rings, a homomorphism is an isomorphism if and only if it is bijective [65].

In topology, where the morphisms are continuous functions, isomorphisms are also called bicontinuous functions [64] In ArcGIS, where the morphisms are differentiable functions, isomorphisms are also called diffeomorphisms (www.esri.com). A canonical isomorphism is a canonical map that is an isomorphism [2]. Two objects are said to be canonically isomorphic if there is a canonical isomorphism between them. For example, a canonical, explanatorial, operationalizable, shade canopied, *S. damnosum* s.l. larval habitat geospectrally interpolatable, forecast, eco-epidemiological, risk map, regressively remotely targeting, productive, unsampled, unknown, immature habitats from a finite-dimensional vector space *V* to its second dual space is simply a canonical isomorphism in ArcGIS; on the other hand, *V* is isomorphic to its dual space but not canonical in general, in most commercial cartographic software. Isomorphisms are formalized using category theory [5]. A morphism $f: X \to Y$ in a category in a ArcGIS constructed *S. damnosum* s.l. larval habitat, eco-epidemiological, geospectral endmember, forecasting, risk model is an isomorphism if it admits a two-sided inverse, meaning that there is another morphism $g: Y \to X$ in that category such that $gf=1_X$and $fg=1_Y$, where 1_X and 1_Y are the identity morphisms of *X* and *Y*, respectively in the model, resdiual forecasts.

Further, in coordinate geometry, in *n*-dimensional ArcGIS eco-geographical space, a set of three or more distinct reflectance points from a remotely sensed, medium resolution derived, decomposed, georeferenced, geosampled empirical dataset of shade, canopied, riverine –related, geo-spatiotemporal, *S. damnosum* s.l., vegetated, larval habitat, time series explanatorial, endmembers are collinear if and only if, the matrix of the coordinates of these vectors is of rank 1 or less. For example, given three geosampled, *S. damnosum* s.l., larval habitat, sub-mixel reflectance points $X=(x_1, x_2, .. , x_n)$, $Y=(y_1, y_2, .. , y_n)$, and $Z=(z_1, z_2, .. , z_n)$ where the matrix $\begin{vmatrix} x_1 & \mathrm{x}_2 & \ldots & \mathrm{x}_\mathrm{n} \\ y_1 & \mathrm{y}_2 & \ldots. & \mathrm{y}_\mathrm{n} \\ z_1 & \mathrm{z}_2 & \ldots. & \mathrm{z}_\mathrm{n} \end{vmatrix}$ is of rank 1 or less, the points would be collinear. Equivalently, for every subset of three decomposed, explanatorial, operationizable, time series dependent, *S. damnosum* s.l., riverine, vegetated, explanatorial, larval habitat, shade-related, canopyreflectance points $X=(x_1, x_2, .. , x_n)$, $Y=(y_1, y_2, .. , y_n)$, and $Z=(z_1, z_2, .. , z_n)$, could be remotely quantized by the matrix $\begin{bmatrix} 1 \, x_1 & \mathrm{x}_2 & \ldots & \mathrm{x}_\mathrm{n} \\ 1 \, y_1 & \mathrm{y}_2 & \ldots & \mathrm{y}_\mathrm{n} \\ 1 \, z_1 & \mathrm{z}_2 & \ldots & \mathrm{z}_\mathrm{n} \end{bmatrix}$ which would be of rank 2 or less when the points are collinear. In particular, for three geosampled, decomposed, larval habitat, explanatorial, time series dependent, reflux points in the plane (n=2), the above matrix would be square and the points collinear if and only if its determinant is zero; since 3 × 3 determinant is plus or minus twice the area of a triangle whose three points are vertices. This then would be equivalent in ArcGIS to the statement that the three reflux geosampled, georefernced, riverine, larval habitat, endmember, covariate points are collinear if and only if the triangle with those points as vertices has zero area.

Three distinct, decomposed, georeferenced, geosampled, geospectrally, explanatorily interpolatable shade, canopied, *S. damnosum* s.l., vegetated, larval habitat, endmember, reflectance points in ArcGIS may be defined as straight, meaning all the points are collinear, if and only if, for every three points A, B, and C, and the following determinant of a Cayley–Menger determinant is zero (with $d(AB)$. Equivalently, a set of at least three distinct, decomposable, shade, canopied, *S. damnosum* s.l., larval habitat, explanatorial geosampled points are collinear if and only if, for every three points A, B, and C with $d(AC)$ are greater than or equal to each of $d(AB)$ and $d(BC)$. If so the triangle inequality $d\ (AC) \leq d\ (AB) + d(BC)$ in ArcGIS will hold with equality. In this approach, deconvolving an uncertainty-oriented,ArcGIS or SAS (i.e., AUTOREG) second-order autocorrelation matrix into linear operationizable, explanatorial, combinations of field-level, geo-spatiotemporally, geosampled, shade, canopied, vegetated LULC-oriented, *S. damnosum* s.l. larval habitat endmember, georeferenced decomposed biosignature-oriented, medium resolution imaged, ecohydrological, ecogeographic, predictor variables may simplify some of these problems. Remotely sensed entomological data, as a result, is often highly geospatially auto correlated [2].

To enable data collection by medium resolution remote sensing instruments the Earth's continuously varying surface is regularized into a grid of consistently sized and shaped mixels [4]. The remote characterization and quantification of explanatorial, operationizable, time series dependent, latent, autocorrelation coefficients can provide a valuable source of information for both theoretical and applied studies in remotely sensed, empirically, probabilistically regressed canopy endmember, decomposed, biosignature-oriented, geosampled, time series dependent, field explanatorial, predictor variables [12,65-70]. A measure of the degree to which a set of explanatorial, decomposed, geospatial, medium resolution derived, biosignature-related, time series and their geospatially associated ,sub-mixel, data values cluster together in space (i.e., positive spatial autocorrelation) or dispersed (negative spatial autocorrelation) can be measured in ArcGIS. For example, an HTML file summarizing results from global Morans *I*, for example maybe generated in ArcGIS Geospatial Analyst™ which may reveal slight negative autocorrelation ('cold spot') in the geosampled, canopy, decomposed endmembers.

Consequently, various techniques may be developed in ArcGIS to assess the spatial dependence characteristics of distance–related, field-level, geosampled, explanatorial, empirical datasets of georeferenced, shade-related, vegetated,*S. damnosum* s.l., riverine, larval habitat, time series dependent, operationizable canopy, endmember-related, geospectral, biosignature-oriented, decomposed,redictor variables .An autocorrelation error covariance matrix and a spatial eigendecomposition algorithmic, orthogonal, filter analyses was employed in Jacob et al. [71,] for example, for providing a computationally attractive and feasible description of variance-related, time series-oriented, probabilistic, regressive, uncertainty estimates for correctly identifying sub-resolution clusters of georeferenced, geosampled, prolific, malaria mosquito -related, canopied, aquatic, larval habitats of *Anopheles arabiensis s.s.* based on larval/pupal productivity. Autoregressive regression coefficients for a spectrally decomposable, aquatic, larval habitat, time series model were assessed using global error techniques which were reported as error covariance matrices. A global statistic summarizes error estimates from multiple geographic locations [62,72].

A method of probabilistic, regression error estimation for geospatial explanatorial, time series simulation *An.arabiensis s.s.,* models was then demonstrated employing the autocorrelation indices and multiple, synthetic, decomposed, orthogonal, eigenfunction-related, spatial filters to distinguish among the effects of the geosampled, biophysical, canopied covariate, parameter estimator uncertainties. The residual forecasts were based on a stochastic simulation of the ecological geosampled, time series dependent, immature, canopied, *Anopheles,* aquatic larval habitat geosampled decomposed endmember covariates. The authors assumed that a test for normalized diagnostic checking error residuals in a seasonal geosampled, *An. arabiensis s.s.* geo-spatiotemporal, aquatic, larval habitat, autoregressive, endmember, decomposable, eco-epidemiological, forecasting, diagnostic, risk model may enable suitable intervention efforts (e.g., targeting productive, aquatic, habitat, geospatial clusters), based on seasonal, geosampled, larval/pupal productivity rates. The authors employed the asymptotic distribution of the time series dependent, covariate, parameter estimator, reflectance emissitivty, wavelenght transmittance coefficients from probabilsitic, a residualizable autocovariance matrix in ArcGIS. The models considered extended any normal regression analysis previously considered in the literature.

Field and remote-related explanatorial geosampled data were collected during July 2006 to December 2007 in Karima rice-village complex in Mwea, Kenya. SAS 9.1.4® was used to explore univariate statistics, correlations, distributions. ArcGIS then generated global autocorrelation statistics from the ecological geosampled, time series dependent, explanatorial, empirical,canopied, *An. arabiensis s.s.* –related, eco-epidemiological, caovariate, parameterized datasets. A local autocorrelation index was also generated using spatial covariance estimators (i.e., Moran's *I*).

The Moran's statistic was explanatorily decomposed into orthogonal and uncorrelated, eco-epidemiological, vulnerbility-based endemic transmission (e.g., mesoendemic) geoclassified LULC, topographic patternized components using a Poisson model with a gamma-distributed mean (i.e. negative binomial regression). The eigenfunction values rendered from the spatial configuration matrices were then used to define expectations for qualitatively, regressively, quantitating, prior distributions. A set of posterior means were defined. After the model had converged, samples from the conditional distributions were used to summarize the posterior distribution of the explanatorial-related, geospatiotemporally-geosampled, canopy-oriented, *An. arabiensis s.s.* -related parameter estimators. Thereafter, a time series dependent, geospatial, residual trend analyses was employed to evaluate variance uncertainty propagation in the model using a autocorrelation, time series, uncertainty-oriented, ecogeographically, probabilistically weighted, diagnonalized, ArcGIS matrix.

By specifying uncertainty, regressive, coefficient estimates in an Bayesian-related, probabilistic estimation algorithmic, regression-based, residualized eco-geographic framework, the canopy covariate, parameter estimator Number of tillers was found to be a significant predictor, positively associated with the geosampled, clustering, seasonally-oriented, *An. arabiensis s.s.,* aquatic,larval habitats. The goal of Bayesian inference is to compute a distribution over the most plausible parameter estimator values [73,74]. This "posterior" distribution was obtained by combining the likelihood with a "prior" distribution P (θ) over the field and remotely explanatorily, geosampled, malarial, larval habitat, parameter values θ. The spatial filter model output accounted for approximately 19% redundant information in the empirically, decomposed, ecological, *An. arabiensis s.s.,* geosampled, larval habitat, eco-epidemiolgical data. In the residual, probabilistic, error estimation model there was significant positive autocorrelation (i.e., clustering of habitats in geographic space) based on log-transformed larval/pupal data and the geosampled canopy covariate Depth of habitat.

On occasion a time series probabilistic, diagnostic, autocorrelation-related, error-prone, error covariance, geo-spatiotemporally dependent weighted matrix and/or an eigenfunction decomposition, orthogonizable, spatial filter analyses may not be able to prioritize control strategies for correctly identifying an empirical, decomposable eco-epidemiological, probabilistically regressable, geopredictor dataset of georeferencable clustering covariates, parameter estimators ecogeographically, cartographically representing explanatorily geosampled, prolific, entomological, operationizable, canopied endmember, explanatorial, covariate coefficients. For example, Jacob et al. [75] generated a sub-resolution malarial larval habitat, regression-related, seasonal forecasting, canopy-related, unmixed, endmember, interpolated, vulnerability map for Uganda which involved the analysis of disease incidence using a prevalence-associated, responsible-oriented, explanatorial, geo-spatiotemporally-dependent, variable which was available as aggregate counts over a geographical region subdivided by administrative boundaries (e.g., districts).

Cases as counts were employed as a response variable in a Poisson regression-related, auto-probability, eco-epidemiological, model framework in GEN MOD for quantitating the empirical explanatorial, operationizable, dataset of time series dependent, district-level covariates paramter estimators. (i.e., meteorological data, densities and spatialdistribution of Health Centers, etc.) geo-spatiotemporally, geosampled from 2006 to 2012. Results from both a Poisson and a negative binomial regression with a non-homogenous, gamma, distributed mean revealed that the canopy estimators rendered from the model were significant but the regressors provided virtually had no predictive power. Inclusion of multiple entomological-related indicator variables denoting the time sequence and the georeferenced, explanatorial, district-level, quantitated, geolocational, spatial structure was then articulated in ArcGIS with Thiessan polygons which also failed to reveal meaningful geospatially interpolatable covariates. Thereafter, an Autoregressive Integrated Moving Average (ARIMA) model was constructed in ArcGIS which revealed a conspicuous but not very prominent, first-order,geo-spatiotemporal, autoregressive structure in the individual district–level,eco-epidemiological, time series dependent, risk-related, forecasting,canopy models which were thereafter subsequently fitted to the time series, explanatorial district-level data to better understand the geosampled data and to predict future points. Univariate (i.e., single vector) ARIMA is a forecasting technique that projects the future values of a series based entirely on its own inertia [12,73].

A random effects term was then specified employing the monthly time series, geosampled, Ugandan malarial data. This specification included a district-level intercept term that was a random deviation from the tabulated intercept term which was based on a normalized frequency distribution. The random effects specification revealed a non-constant mean across the explanatorily, time series probabilistically regressed, canopied, geospatial, geosampled, malarial data across the districts. This random intercept geographically represented the combined effect of all the omitted covariates that caused districts to be prone to the malaria prevalence than other districts.

Additionally, inclusion of a random intercept in ArcGIS assumed random heterogeneity in the districts' propensity or underlying risk of malaria prevalence which persisted throughout the entire duration of the time sequence under study. This random effects term displayed no spatial autocorrelation, and failed to closely conform to a bell-shaped curve. The model's variance however, implied a substantial variability in the prevalence of malaria across the districts. The estimated model contained considerable overdispersion (i.e., excess Poissonized variability); the quasi-like hood scale was 76.565. The following equation was then employed to forecast the expected value of the prevalence at the district level; prevalence =exp [-3.1876= (random effect)]. This research proved compilation of remotely sensed georeferencable, explanatorial, geosampled, geo-spatiotemporal, eco-geographical, ecohydrological and cartographical data can allow continual updating of random effect term estimates in cases where zero autocorrelation (i.e., chaotic landscapes) are reported in spatially dependent error matrices in ArcGIS.

Hence, when geospatially interpolating decomposed ,explanatorial, sub-mixel, canopied endmember, reflectance values in place of scene-invariant values to estimate FVC in a medium resolution-derived image, for example, the accuracy of FVC estimates may be increased, providing evidence that it may be useful to consider the effects of geospectral autocorrelation when conducting a robust endmember, unmixed, biosignature-oriented, NDVI-related.geo-classified, LULC,regression-based, vulnerability, mixture analysis of georeferenced, shade-oriented, canopy vegetated, decomposed, *S. damnosum* s.l., larval habitats geosampled in African riverine environments.

However, medium-resolution, remotely sensed, endmember reflectance spectra may be biased by several intervening factors, and the biases may be propagated into estimations of the FVC by algorithms based on a linear mixture model (LMM) [12].The errors propagated in FVCs generated from a Sub-mixel, vector entomological, aquatic, immature habitat, LULC composition estimation in ArcGIS and ENVI commonly employ a linearizable mixture model and fuzzy membership functions. The membership function of a Fuzzy set is a generalization of the truth values of variables may be any real number between 0 and 1.;by contrast, in Boolean logic, the truth values of variables may only be 0 or 1 [2]. shade, vegetated, *S. damnosum* s.l., georeferenced, canopied, larval habitat may depend on the retrieval algorithm due to differences in the assumptions of the model as well as constraints employed in the algorithm. Optimally, these differences may be fully understood in ArcGIS prior to algorithm selection for practical forecasting LMM mapping of unknown, unsampled, prolific *S. damnosum s.*l. shade, canopied, riverine larval habitats based on FVC-induced geo-spatiotemporal ecogeographic, ecohydrological, explanatorial, covariates, parameter estimators.

Although numerous studies have investigated the relationships between errors propagated by different algorithms, these relationships have not been fully understood from a stochastic/deterministic, probabilistic algorithmic, perspective. Introducing techniques for deriving the analytical underpinnings residual endmember uncertainty propagation in FVC based on several unmixing algorithms may enable robust, parsimonious, geospectral, explanatorial, interpolation of an decomposed, empirical dataset employing estimation FVC-induced algorithms based on a, medium resolution-derived, NDVI, endmember, sub-mixel, reference, canopy biosignature-related, decomposed, photosynthetic or NPV covariate, parameter estimator, wavelenght, reflectance emissivity, transmittance coefficient values. The derivation would assume that measurement noise is band-correlated additive noise. The bias errors propagated in a tabulated FVC from the medium resolution-derived, NDVI decomposed, georeferenced, shade, vegetated, S. *damnosum* s.l., canopied, riverine, larval habitat biosignature may then optimally be deduced as being geo-spatiotemporally dependent on the canopy endmember spectra assumed in the algorithm, the target spectrum, and the empirically geosampled, photosynthetic and NPV covariate, parameter estimator, coefficient values of the vegetation index. These covariate coefficient values may be employed as constraints, for also regressively probabilistically quantitating magnitude of the input error. It may be found, for example that the relationships among the propagated errors in ArcGIS assume asymmetric elliptical forms with absorption coefficients that are determined by the input variables. Such results can suggest that the relationships of the shade, canopy, vegetated, biosignature-related, canopy, endmember, geospatial, explanatorial, time series interpolation of the extracted, riverine, larval habitat, sub-mixel data variables depends heavily on the choice of unmixed spectra as well as the spectrum of the target decomposed mixel and the vegetation index employed as a constraint. Such findings should assist in the selection of an optimum geospatial algorithm in ArcGIS based on prior knowledge of the target field for identifying unknown, unsampled, seasonally, shaded and non-shaded, productive, canopied, *S. damnosum* s.l. riverine larval habitats.

Theoretically, remotely, qualitatively, probabilistically regressively, explanatorily quantitating geospectrally dependent, explanatorial error and latent autocorrelation functions in a geo-spatiotemporally dependent, medium resolution-derived, shade, canopied, *S. damnosum* s.l. vegetated, riverine, larval habitat, NDVI, endmember,biosignature-related, reference, signature for forecasting, eco-epidemiological, optimizable, risk, model residual reflectance emissivity, wavelenght, transmittance output would require employing cost-effective, non-Gaussian ensemble of weighted matrices in ArcGIS. A direct comparison of the prediction of these ensembles within experimentally measured, seasonal,*S. damnosum* s.l., larval habitat, canopy spectra may be possible for a georeferenced, medium resolution-derived, decomposed, NDVI, sub-mixel, eco-epidemiological, geosampled datsets. Also the time autocorrelation function of an initially prepared non-stationary state in a medium resolution derived *S. damnosum s.l.,* larval habitat, NDVI, endmember, reference, biosignature may be efficiently geospectrally qualitatively quantitated by post- decomposition techniques. By so doing, the repulsion of eigenstates in a particular time domain may be clearly manifested in a georeferencanle, riverine larval habitat sub-mixel decomposition results. An eigenstate is the measured state of some object possessing explanatorily quantifiable characteristics such as position, momentum [73].

Jacob et al. [76] adjusted second moment bias in eigenspace employing a Bayesianistic, explanatorial, empirical, operationizable, time series dependent, geoparametric paradigm in ArcGIS. Dirichlet Tessellations and Worldview1 (WV-1) 0. 41m remove space please(.41) spatial resolution data was initially employed for ecogeographically geolocating productive, aquatic larval habitats of West Nile mosquito vector *Culex quinquefasciatus* in Trinidad. Optimal, observational, explanatorily, interpolatable observational, eco-epidemiological, probabilistic predictors associated to prolific, geosampled, georeferencable, habitats were also determined. The design of the mixed model incorporated spatial autocorrelation whilst including the influence of other aspatial georeferenced, temporally dependent, photosynthetic and NPV explanatorial, time series dependent, predictor variables. The authors employed geospatially lagged, simultaneous, autoregressive, uncertainty-oriented, models based on multiple bio-ecological, environmental-related, parameter estimators of geosampled immature *Cx. quinquefasciatus* data overlaid onto WV-1 data to help implement a remote, habitat-based ArcGIS cyberenvironment surveillance system in Trinidad geospectrally specific for remotely targeting prolific larval habitats.

The authors employed Geomatica Ortho Engine® v. 10.2 for extracting a Digital Elevation Model (DEM) from the WV-1 raw imagery. Results of the DEM analyses indicated a statistically significant, inverse, linear relationship between total immature, geosampled, *Cx. quinquefasciatus* data and elevation (m) ($R^2 = -0.439$; $p < 0.0001$), with a standard deviation of 10.41. Additional geo-spatiotemporally, field-geosampled, eco-epidemioloigcal, information was derived employing data from an orthogonal, algorithmic, grid-matrix constructed in an ArcGIS geodatabase and overlaid onto the WV-1 data. A unique identifier was placed in the centroid of each 1km x1km grid cell. Univariate statistics and Poisson probability regression models were then constructed in PROC REG employing the time series dependent, covariate, paramter estimator, time series dependent, coefficient values in SAS/GIS®.The *Cx. quinquefasciatus* eco-epidemiological, forecasting, endmeic, transmission-oriented, geospectral, risk model was over dispersed. Hence, we employed a negative binomial regression with a non-homogenous, gamma, distributed mean in PROC REG to compensate for the overdispersion (i.e, over-Poissian variation) due to embedded outliers in the empirical, geo-spatiotemporally-geosampled dataset and to compensate for the violation of the Poisssion assumption that the variance was equal to the mean in the dataset. By so doing, the authors were able to achieve a final model that was checked for robustness using a step-wise backward elimination process to normalize any heteroskedastic and/or multicolinear emissivity. wavelenght, endmember, forecasters.

Regression coefficient estimates were then employed to define expectations for parsimoniously simulating prior distributions in a Generalized Bayesian Hierarchical probabilistic matrix employing Markov Chain Monte Carlo (MCMC) specifications in ArcGIS. One of the most popular methods for simulations is Markov Chain methods which are a class of sampling algorithms for quantitatively iterating a probability distribution based on a chain that has the desired distribution as its equilibrium distribution [70]. The state of a MCMC chain can be used as a sample of the desired distribution especially where the quality of the sample improves as a function of the number of steps [73, 76].The Bayesian regression model geospatially and aspatially adjusted the model estimates employing a Wishart matrix. In Bayesian statistics, in the context of the multivariate normal distribution, the Wishart distribution is the conjugate prior to the precision matrix $\boldsymbol{\Omega} = \boldsymbol{\Sigma}^{-1}$, where $\boldsymbol{\Sigma}$ is the covariance matrix [2].

A geospatial, time series, explanatorial, residual, probabilistic, trend analyses was then performed using latent autocorrelation indices which linked tabular data in SAS PROCLMIXED® with *Culex* egg-raft count in an ArcGIS, cyberenvironment. The probabilistic estimation matrix identified prolific habitats based on the operationizable, covariate Distance to the nearest house. An Ordinary kriged-based, time series, stochastic interpolator was then constructed in Geostatistical Analyst Extension of ArcGIS based on the adjusted Bayesianized, explanatorial, regression estimates. For total *Cx. quinquefasciatus* egg-raft count, first order trend was fitted to the semivariogram at a partial sill of 5.931

km, nugget of 6.374 km, lag size of 7.184 km, and a range of 31.02 km using 12 lags. The semivariogram depicts the spatial autocorrelation of the measured sample points [73]. Once each pair of predicted habitat geolocations was cartographically plotted, an empirical semivariogram, was also fit through various interpolator-based diagnostic statistics (sill, nugget etc) [12,73].

The authors then assessed the performance accuracy of the interpolation procedures based on the magnitude and distribution of errors between observed and model-predicted values employing Voroni tessellations in ArcGIS. In mathematics, a Voronoi diagram is a partitioning of a plane into regions based on distance to points in a specific subset of the plane [73]. That set of points (called seeds, sites, or generators) is specified beforehand, and for each seed there is a corresponding region consisting of all points closer to that seed than to any other (i.e., Voronoi cells) [12]. The Voronoi diagram of the geo-spatially, probabilistically, empirically, regressed , eco-epidemioloigcal dataset of *S. damnosum* s.l., endmember, interpolated, covariate, parameter estimators points was found to be operationizable, in a plane is a triangulation DT(P)].The model was aggregated such that no point in P was inside the circumcircle of any triangle in DT(P) [4]. The Voroni residuals divided the ecogeographic and non-ecogeographic space between the individual georeferenced, geosampled, *Cx. quinquefasciatus* larval habitats by XY explanatorial coordinates in 2-dimenisional space which revealed that the uncertainty-oriented, geophysical, parameter estimator, endmember residuals in the interpolation model were within normal statistical limitations.

Delaunay triangulations constructed in ArcGIS may maximize the minimum angle of all the angles of the triangles in the triangulation while avoiding skinny triangles in a post-stochastic, explanatorial, geospectral, interpolation of an empirically regressed georeferncable eco-epidemiological, dataset of geosampled, seasonal, medium resolution-derived, shade canopied, *S. damnosums s.l.* riverine, vegetated, larval habitat, NDVI unmixed, submixel, canopied, endmember reflectance emissitivty, wavelenght, unmixed, biosignature-related, transmittance constituents. The state being measured and described (e.g., the photosynthetic capacity or productivity of the plant canopy may be then qualitatively, remotely, probabilistically, regressively quantized. By so doing, the actual influence of chlorophyll content of materials, for example, in a georeferncable, geo-spectrally decomposable, riverine, *S. damnosum* s.l., larval habitat, for example, may be also parsimoniously, regressively, quantitated and potential optimizable, regressable predictor variables (i.e. position or momentum) may be seasonally identified. Therefore, an eco-epidemiological dataset of operationizable, geo-spectrally-oriented, explanatorial, geo-spatiotemporally, interpolated, residual forecasts rendered from a shade canopied, *S. damnosum s.l.* georeferencable, riverine shade, vegetated, larval habitat, NDVI unmixed, endmember, unmixed, ENVI model, for example, can be experimentally measured either directly and/or indirectly, for tabulating a definite computable, operationizable, spatialized value, (i.e., eigenvalue). "Eigenvalue" refers to a mathematical property of square matrices [77]. In medium-to-coarse geospatial resolution satellite images, single decomposed mixels often contain a mixture of different types of LULCs [4]. Use of very high resolution imagery can mitigate this mixel problem in ArcGIS to some degree, but the relatively higher cost and lower frequency at which high resolution imagery is typically acquired can be an issue when implementing control strategies of IVM such as remotely targeting, georeferenced, shade, vegetated, canopied, seasonally prolific, *S. damnosum* s.l. larval habitats geosampled in African riverine environments.

RapidEye™ is a constellation of 5m medium resolution satellites each offering five spectral bands of information at a cost effective price of 1.28 U.S. dollar / kilometre (km) which can provide imagery over relatively large areas (swath of 77 km) and a temporal resolution of 1 day, increasing the successful acquisition of cloud-free data. Each sensor is capable of collecting image data in five distinct bands of the electromagnetic spectrum: Blue (440-510 nm), Green (520-590 nm), Red (630-690 nm), and NIR (760-880 nm). The nominal resolution on the ground is 5m (http://www.satimagingcorp.com/satellite-sensors/other-satellite-sensors/rapideye/).

Further, RapidEye adds a fifth band, the Red-Edge (690-730 nm) to the traditional, multispectral, set of blue, green, red and NIR. The Red Edge is a region in the red-NIR transition zone of vegetation reflectance spectrum and marks the boundary between absorption by chlorophyll in the red visible region, and scattering due to leaf internal structure in the NIR region. This way, vegetation cellular structure in an empirical geosampled, dataset of shade, canopied, georeferenced, explanatorial, unmixed, NDVI, biosignature-related, ggeospatiallly explanatorily interpolatable, *S. damnosum* s.l. larval habitat geo-spectrally decomposed, phosotosynthetic and NPV covariate, parameterized estimators, reflectance, wavelenght, emissitivty, transmittance coefficients values in ArcGIS may be remotely, qualitatively, regressively quantized as each canopy plant cell which would act like an elementary corner reflector. For example, quantitating, endember probabilsitic, spectral irradiance effects of rapid, seasonal, canopy changes in a georeferencable, riverine, prolific, *S. damnosum* s.l., larval seasonal LULC habitats, may be determined from 5% to 50% reflectance, which may be remotely captured between 680 nm to 730 nm. RapidEye's traditional broadband and Red-Edge indices have been evaluated for grassland nitrogen and biomass [78, 79], crop canopy chlorophyll content [80], Forest Leaf Area Index (LAI) [81], and wheat ground cover and LAI [82].

Leaf Area Index (LAI) is defined in ArcGIS as a simple ratio between the total one side leaf surface of a plant and the surface area of the LULC on which the plant grows (www.esri.com). LAI is a dimensionless value, typically ranging from 0 for bare ground to 8 for dense vegetation [2]. LAI is one of the most important LULC explanatorial, time series dependent, predictor variable governing the canopy processes [83] and is related to leaf and canopy chlorophyll contents, photosynthesis rate, carbon and nutrient cycles, dry and fresh biomass, and growing stages [84]. Hence, LAI has been applied in plants and environmental studies of evaporation, transpiration, light absorption, yield estimation, growth stages of crops and chemical element cycling [85-88]. A common non-destructive surrogate for LAI, which is based on reflectance of red and NIR bands, is using the NDVI [89].

Effective LAI is routinely quantified with optical instruments that measure gap fraction through the probability of beam penetration of sunlight through the vegetation-related LULC in ArcGIS. However, there have been few efforts to obtain theoretically consistent effective leaf area indices from those measurements. For example, to apply the Beer–Lambert law, multiple gap fraction measurements may be averaged in two ways: (1) by taking the mean of the logarithms of the individual gap fraction values or (2) by taking the logarithm of the mean gap fraction. The Beer–Lambert law, or the Beer–Lambert–Bouguer law relates the attenuation of light to the properties of the material through which the light is traveling [4].

Interestingly, studies have established relationships between VIs and LAI [90,91] and biomass yield using moderate resolution data in ArcGIS [92-94]. Overall, these VIs showed variable sensitivity to different levels of LAI and biomass. NDVI is sensitive to low LAI (i.e. LAI < 2–3), but saturates at medium to high LAI [91]. A similar pattern is observed for the relationship between moderate-resoluion- derived NDVI and biomass, with NDVI saturating at medium to high (fresh) biomass (around 2 kg/m^2) [93].

Since the RapidEye^{TM} constellation's Red Edge band is sensitive to chlorophyll status and leaf and canopy structure, it is expected that this band would contribute to the characterization of different LULC plant cover types (e.g., vegetated, canopy, shaded, prolific, *S. damnosum s.l.,* larval habitat, geosampled in an African riverine environment). Schuster, Förster and Kleinschmidt [94] tested the Red Edge band in an LULC classification project in ArcGIS. Sixteen classes including two forest classes (deciduous and coniferous) were assessed. They found that the Red Edge band provided an overall classification accuracy that was consistently higher than without it. In terms of individual classes, the most significant improvements were obtained with classes comprised of open landscape vegetation. Recio et al. [95], found that optimal could be achieved by involving endmember biosignature-related, NDVI, decomposable illumination variables derived from the Red Edge band. Conrad et al. [96] employed multiple indices in ArcGIS combining the Red Edge, Red and NIR bands in a multi-temporal approach to separate several crop types. The authors concluded that using the three bands as a way to characterize this sensitive portion of the sub-mixel reflectance spectrum permitted an accurate separation of the crop types under investigation.

Recent studies support the hypothesis that a broad Red Edge band, as employed in the RapidEye sensors, is also suitable for obtaining information about the chlorophyll and nitrogen content of plants in ArcGIS [97,98]. Crop management yield strongly depends on an adequate supply of nitrogen [99,100]. This study assessed whether vegetation indices derived from broadband RapidEye™ data containing the Red Edge region (690–730 nm) were equal to those computed from narrow band data in predicting nitrogen status and other canopied products in a geo-spatiotemporally, geosampled, prolific, *S. damnosum* s.l., riverine, larval habitat.

The application of endmember algorithms at broad spatial extents may enable the production of foliar 5m Rapid Eye^{TM} geosampled *S. damnosum* s.l larval habitat ArcGIS chlorophyll maps, which are powerful tools for promoting a better understanding of riverine-related, chlorophyll, canopy dynamics over space and time. These spatially continuous maps are vital for monitoring vegetation stress and for enhancing understanding of habitat canopy plant-environment interactions and the controlling mechanisms on chlorophyll content. The ability of this technique to characterize variations in endmember chlorophyll content across different canopy-oriented, vegetation LULCs may help identify riverine habitat species and structures which would be important for making the method operational across multiple seasonal extents, and for its inclusion in photosynthesis and carbon cycle Rapid Eye ^{TM},*S. damnosum* s.l, larval ecogeographic and non-ecographic, forecasting, eco-epidemioloigical, endemic, transmission-oriented, risk models. Various single and combined indices have been computed from in-situ spectroradiometer data and simulated RapidEye™ data. For example, Schelling [101] found a combination of the RedEdge NDVI was able to predict chlorophyll concentration in wheat with a coefficient of determination of R^2=0.77.In statistics, the coefficient of determination, denoted $R^2$is a number that indicates how well data fit a statistical model [102]. This transition zone may be the basis of accurately interpolating a decomposed, Red Edge, chorophyll ,unmixed NDVI-related, biosignature as determined cartographically from an empiricial dataset of decomposed explanatorily, georeferenced, shaded, *S. damnosum* s.l. vegetated riverine ,larval habitat canopy pigment covariate, parameter estimator, reflectance emissivity, wavelenght transmitatnce coefficients. This procedure may be synthesized optimally in ArcGIS employing the normalized difference between the reflectance in the red visible (0.6µm) and the NIR (0.8µm) reflectance spectrum.

Thus, a seasonal endmember, unmixed, spectral analyses of a prolific, canopied, *S. damnosum* s.l., riverine, larval habitat biosignature, employing RapidEye^{TM} can reveal whether seasonal, canopy, chlorophyll concentration increases, the typical slope in the Red Edge spectral region and shift towards the NIR. Further the Red Edge inflection point wavelength (λi) may be employed as an indicator for this shift. Accordingly, several 5m spectral indices employing narrow bands, both from ground-based RapidEye^{TM} measurements have been successfully applied to also determine green biomass, water content, chlorophyll content and nitrogen status [12,100]. Knowledge about nitrogen status may represent an important factor for accurately explanatorily geospectrally interpolating a decomposed, RedEdge, NDVI, endmember sub-mixel biosignature for identifying unknown, unsampled, shade, vegetated, canopied prolific ,*S. damnosum s.l.,* riverine, larval habitats, in African riverine environments.

Also the Red Edge position (REP) may be employed to estimate the chlorophyll and other light sensitive pigments content of leaves in a decomposable, Red Edge, NDVI biosignature in an OBIA which may be a way to also remotely assess canopy health of a georeferenced, canopy, shaded, *S. damnosum* s.l., vegetated, riverine, larval habitat. Red Edge NDVIs may reveal higher correlations with field measurements of seasonal canopy plant health (http://www.satimagingcorp.com/satellite-sensors/other-satellite-sensors/rapideye/). Further, a dataset of remotely regressive, explanatorial, decomposed, unmixed endmember-specified, Red Edge, NDVI, decomposed, biosignature-related, photosynthetic and NPV, sub-mixel, covariate, parameter estimator, reflectance emissivity transmittance coefficients values may measure and monitor plant growth (vigor), vegetation LULC cover, and biomass production of seasonally productive, geosampled, georeferencable, *S. damnosum* s.l. canopied riverine larval habitats.

Here we present the mathematical basis which is linked to a Red Edge geospectrally extracted, NDVI-related, endmember, sub-mixel, biosignature decomposition for generating a three-dimensional (3-D) shade, vegetated, canopy-based, riverine, *S. damnosum* s.l., larval, habitat-related, ecogeographic and non-ecogeographic, forecasting, time series dependent, eco-epidemiological, risk model forecasts of unknown, unsampled seasonally interpolated habitats in ArcGIS. The differential form of the radiative transfer equation [i.e.,] $\frac{1}{C}\frac{\partial}{\partial_t}I_V+\Omega.\Delta I_V+\left(K_{V,S}+K_{V,a}\right)I_V=J_V+\frac{1}{4\prod C}K_{v,S}\int_{\Omega}I_V d\Omega$ was employed where j_v was the emission coefficient, $k_{v,\,s}$ was the scattering cross section, and $k_{v,\,a}$ was the absorption cross section of the cost-effective, 5m satellite system, data products. The differences in the geospectral, explanatorial, georeferenced, canopy, endmember parameter estimators in the Red Edge, NDVI, *S. damnsoum s.l.,* reflectance, response model was then qualitatively assessed employing various forms for the emission and absorption coefficients. A general solution in terms of the these coefficients was then written as: $I_V\left(S\right)=I_V\left(S_o\right)e^{-\Gamma v(So,S)}+\int_{S_o}^{S}j_V\left(S'\right)e^{\Gamma_{V(S',S)}}dS'$ employing the data products where $\tau_v(s_1,\ s_2)$ was the optical depth of the medium between positions s_1 and s_2: $\Gamma_V\left(S_1, S_2\right) = \int_{S1}^{S2} \alpha_{V(S)} ds$. Properly remarginalize please Thereafter, a robust, time series dependent, *S. damnsoum s.l.* riverine larval habitat, shade, canopy, endmember, Red Edge, NDVI, geo-spatiotemporal, unmixed, Biosignature-related, eco-epidemiological, sub-mixel, model was constructed. Subsequently the endmember biosignature reflectance was geospectrally interpolated over two African riverine environments.

The main goal of this article was first to determine the feasibility of quantitatively geospectrally decomposing a vegetated, shade, canopied, Red Edge, NDVI,*S. damnosum s.l.,* riverine, larval habitat, canopy, endmember biosignature in ArcGIS and secondly to present a robust, cost-effective, method for accurately classifying geo-spectrally, explanatorily interpolatable, predictive, geo-spatiotemporal, eco-epidemiological, risk–based, LULC, mapping patterns. Initially, we employed data collections from an eco-epidemiological riverine, breeding, eco-epidemiological, study site in Burkina Faso. We created a Red Edge NDVI employing the 5m satellite data product in ENVI. We geospectrally decomposed a canopy endmember bundles and generated bounding fractional images for conducting a subscene simulation exercise based on computed shaded canopy surface fractional radiance values.

We assumed that geospectral changes can be partially or fully considered in a georeferenced, geosampled, shade, vegetated, riverine-related, *S. damnosum* s.l., canopied, larval habitat, atmospheric radiative transfer model for PAR estimation in ArcGIS. We also assumed that geo-spatiotemporally, probabilsitically, regressively quantitating these changes may additionally take into account the angular variability of the incident diffuse PAR in a time-series dependent, Red Edge NDVI, canopy, biosignature-oriented, endmember, sub-mixel, unmixed, eco-epidemiological, forecasting, risk-related, reflectance model. An atmospheric radiative transfer model, code or simulator calculates radiative transfer of electromagnetic radiation through a planetary atmosphere (http://circ.gsfc.nasa.gov/). Thus, we also assumed that regressively quantitated, extremely contrasting, seasonally prolific, *S. damnosum s.l.* larval habitat decomposed endmember, unmixed, interpolatable, reflectance emissivity transmisttance values for the within- canopy invariant photosynthetic and NPV eco-epidemiological, biophysical, structural attributes employing a RedEdge NDVI endmember biosignature wavelenghts in ArcGIS may determine how variations in geo-radiometric observations and structural properties of the georeferenced, geosampled, larval habitat at different red and NIR scales impact the spectrum of radiation reflected by the vegetated, geo-classifed, LULC, canopied surface. Unmixing a mixel into its component parts it is possible to enableimore accurate estimation of the areal extent of different land cover classes [2].

Currently, spectral endmember quantification of time series dependent, unmixed, canopy vegetation-related geo-classified LULCs at different red and NIR scale calculations tend to use the isotropic diffuse PAR in their absorbed PAR (APAR) and canopy-related, LULC, photosynthesis calculations only [103]. Unfortunately, this assumption regarding the radiation regime would give rise to APAR and canopy photosynthesis errors in a time series dependent, predictive, autoregressive, shade-related, canopied, *S. damnosum s.l.* riverine, larval habitat, Red Edge NDVI endmember biosignature-oriented, forecasting, eco-epidemiological, unmixed, forecasting, risk model [104]. Conversely, the spectral properties of dominant constituents within a medium resolution-derived , shade, canopied, riverine, larval habitat mixel may deconvolve, geo-spectrally decomposed, Red Edge, NDVI constituents rendering explanatorily interpolatable, canopy LULC surface, radiance fractional, abundance,endmember radiance values in ArcGIS.We also employed a SPA for unmixing the georeferencable,vegetated, shade, canopied, Red Edge, *S. damnosum s.l.,* larval habitat, NDVI, endmember biosignature as from literature it is the only spectral extraction technique that builds on convex geometry and orthogonal projections by including a constraint on the adjacency of endmember candidate mixels.

Common endmember extraction algorithms presume that the number of materials present is either known or may be predetermined by employing geospectral geodatabases or other approaches [4]. We utilized an orthogonal projection for endmember extraction of an empirical dataset of explanatorial, shade, canopied, *S. damnosum* s.l., vegetated, larval habitat imaging geospectrometric LULC and NDVI extracted endmember radiance values in ArcGIS. The unmixing algorithm was then based on a fully unsupervised approach and employed convex geometric characteristics. The subsequent extraction of the *S.damnosum* s.l., larval habitat endmembers from the Red Edge, decomposed, NDVI biosignature was based on three main stages in ENVI as follows: 1) approximate estimation of the initial number of image-based, shade, canopied endmembers employing absorption features present in the spectrum of the larval habitat mixel; 2) extraction of the initial canopy endmembers by projecting the decomposed eco-epidemiological data onto an orthogonal subspace; and 3) determination of the exact number and geolocation of each endmember. Here, the dimension of the subspace was varied until the best estimation of the subspace was achieved.

The Red Edge NDVI data was then examined within a radiative transfer model in ArcGIS. Recent studies on canopy radiative transfer functions have led to the development of the canopy spectral invariant theory [4, 105, 106], according to which variations of canopy scattering (i.e., reflectance plus transmittance) and absorptance are mainly influenced by linear-based, explanatorial, optical properties (i.e., spectral leaf transmittance and reflectance) of individual leaves and wavelength independent, canopy, structural variables (e.g., the canopy interceptance).

The theory of spectral invariants or *p* theory states that the canopy scattering coefficient at any wavelength can be related to the leaf scattering coefficient at the same wavelength through a spectrally invariant canopy structured parameter-the photon recollison probability [107]. The *p* theory has recently gained interest of the modeling community as an effective tool for characterizing scattering in clumped foliage canopy, vegetated, geo-classified LULC structures. The spectral invariant relationships have been reported for ecological canopy transmittance [108,109] and reflectance [110,111], suggesting that the canopy leaving radiation can further be broken down into its reflected and transmitted portions of an Red Edge NDVI.

We assumed that, the SPA and the radative transfer model could illustrate the influence of a new decomposed endmember on a dataset of proxy, explanatorial, shaded, spectral, canopy vegetation, LULC–related, geo-spatiotemporally- geosampled, echydrologic and non-ecogeographic structural variables as illuminated by a *S. damnosum* s.l., larval habitat, Red biosignature while providing vital information on the convergence of the algorithm. Though the rate of convergence speed can vary in unmixing algorithms with the complexity of the scene[5], we assumed the LULC patterns rendered from the larval habitat, endmember decomposition of a Red Edge, NDVI, canopied biosignature in ENVI would reveal the largest changes in volume ratio at the beginning of the image extraction process, followed by progressively smaller changes and, thereafter, followed by a convergence towards a plateau.Common endmember extraction algorithms presume that the number of materials present is either known or may be pre-determined by spectral eco-geographic databases [4]. We assumed that the SPA algorithm may extract the larval habitat endmembers from the Red Edge, *S. damnosum* s.l., larval habitat, NDVI, spectral, canopied, endmember biosignature without reducing the data dimensionality. Further, we assumed the algorithm would employ the spectral angle and the spatial adjacency of the decomposed, Red Edge, NDVI biosignature to constrain the selection of candidate mixels representing an autoregressively, forecastable, riverine, *S. damnosum* s.l., larval habitat, endmember, reflectance spectrum.

We then employed a geometric-optical risk model analysis in ArcGIS where the Red Edge reflectance was modeled as a function of the self-shadowing structure of the geo-spatiotemporally, geosampled *S. damnosum s.l.* larval habitat canopy, which treated the decomposed photosynthetic and NPV explanatorial, time series dependent, data, feature attributes as a collection of discrete objects-individual plant crowns that were arranged on a plane. The pattern of sunlit and shadowed objects and background that is seen from a particular viewing position in a geometric-optical is taken as the primary factor controlling the directional reflectance [112].We assumed that the pattern of light and shade associated with a Rapid Eye, 5m, data-derived, Red Edge, NDVI product may be modeled using geometric optics, Boolean set mathematics, and theorems from stereology. [i.e., a method that utilizes random, systematic sampling to provide unbiased and quantitative data for extracting quantitative information about 3-D material remotely derived from measurements made on two-dimensional planar sections of the material [73].

Principles of geometric optics and Boolean models for random sets of autoregressively, forecastable, riverine, *S. damnosum* s.l., larval habitat, endmember, reflectance spectrum. in 3-D space may provide the mathematical basis for constructing an eco-epidemiological forecasting, risk model in ArcGIS from bidirectional radiance. The model may be defined at two levels: whole-canopy and individual-leaf. At the whole-canopy level, the riverine Rapid Eye ™ 5m scene may be treated as a collection of discrete canopy envelopes with simple geometric shapes that are arranged on a contrasting background.

Originally developed as a practical alternative to radiative transfer models for complex, naturally-vegetated, canopied, land surfaces that cannot be approximated as plane-parallel canopies, the geometric-optical approach has been extended to leaves as objects in both plane-parallel and discrete canopies. In essence, the geometric-optical approach amounts to a careful description of single scattering with a very simplified treatment of multiple scattering [113]. A similar approach to modeling for directional reflectance of forest covers was developed independently by Estonian researchers in the former USSR [114]. Though our approach shares some similarity to this research, they are some significant differences. Notably, our objective was to clearly remotely distinguish canopy gaps and to emphasize the importance of the proportion of the sunlit and viewed crown surface of a georeferenced, geosampled, shade, vegetated, medium resolution, imaged, vector entomological-related, canopied, riverine, geospatial, seasonal object. We assumed that this process would enable us to treat mutual shadowing and the directional effect of foliage clumping properly in an explanatorial operational dataset of decomposed, RapidEye™ Red Edge, NDVI, geo-spatiotemporal, endmember biosignature, covariate, parameter estimators in an ArcGIS cyberenvironment and in ENVI via a OBIA. By so doing we assumed we would conduct a robust interpolation for identifying unknown, unsampled, prolific seasonal, S. damnosum s.l. habitats.

We also generated multiple, Rapid Eye ™ explanatorial, geomorphological, endmember, unmixed, covariate, parameter estimator, eco-epidemiological, operationizable time seriesdatasets of remotely synthesized geospectrally-dependent, explanatorial, photosynthetic and NPV canopy coefficient values from a digitized, LULC surface-based, shade vegetated, *S. damnosum s.l.* habitat, unmixed, time series, biosignature-oriented, risk model using the 5m data. Digital Elevation Models (DEM) are topographic maps that provide a geometrically correct reference frame over which other satellite data layers can be draped in ArcGIS [www.esri.com]. Since remote sensing classifications and biomass estimation algorithms of vegetation-related LULCs in rugged areas are hampered by topographic effects [4] DEMs may be used as the basis for topographic correction [115-118]. Implementing an unmixing approach on an interpolatable, Red Edge, geospectral, NDVI biosignature over a 5m DEM in an area of complex topography such as an African riverine environment may require the ability to remove anisotropic effects, (i.e., variations in the spectral response on inclined surfaces compared to that of a horizontal surface) efficiently. We assumed a horizontally homogeneous, Lambertian surface, reflecting energy equally in all shaded canopy directions of a decomposed, empirical, operationizable, dataset of geosampled, georeferenced, RapidEye™ imaged, unmixed, explanatorily interpolatable, *S. damnosum s.l.*, iverine, larval habitat, photosynthetic and NPV canopy, covariate, parameter estimator, reflectance, emissivity, wavelenght, time series dependent, transmittance series coefficients may be explicitly a part of the calculations of albedo in Red Edge NDVI decomposed endmember, geo-spatiotemporally-geosampled dataset.

Lambertian reflectance LULC is the property that defines an ideal "matte" or diffusely reflecting surface (e.g., canopied trailing vegetation) of georeferncable, productive *S. damnosum* s.l., riverine, larval habitat. The apparent brightness of a Lambertian surface to an observer is the same regardless of the observer's angle of view [4]. More technically, the surface's luminance is isotropic, and the luminous intensity obeys Lambert's cosine law. Even when lights are isotropic and distant, smooth Lambertian objects can produce infinite-dimensional sets of images [2]. But recent experimental work [11,29] has indicated that the set of images produced by an object under a wide range of lighting conditions lies near a low dimensional linear subspace in the space of all possible images. This quantitative illumination technique may be used to construct efficient recognition algorithms that handle lighting variations in a geospectrally decomposed, explanatorial, Red Edge, canopied, *S. damnsoum s.l.* larval habitat, NDVI, endmember biosignature. In this paper we explain these empirical results analytically and use this understanding to produce new recognition canopy, illumination-oriented, photosynthetic and NPV decomposition algorithms.

Interestingly, canopy vegetative LULC surfaces that are not Lambertian reflectors are the measured bidirectional reflectance distribution functions (BRDFs)which can change with illumination angle.Thus, a remotely detected, medium resolution-derived, shaded, prolific, georefernced, *S. damnosum* s.l., geosampled, vegatative, riverine, larval habitat, probabilistically regressively quantitated, decomposed, BRDF, wavelenght-related, covariate, parameter estimator, reflectance, emissivity transmittance coefficient dataset, the canopy endmembers could be attributable to seasonal shifts in the vegetative classified, LULC explantorial, geosampled, canopied structure. These changes may be caused by changes in illumination and viewing geometry of the 5m sensor. Factors which affect reflectance from canopy vegetated LULC surfaces and contribute to the non-

Lambertian nature of these surfaces include: (1) geospectral properties of canopy elements and substrate; (2) the canopy architecture (that is, leaf area index (3) illumination and viewing directions [2].

Our strategy was to divide the canopy radiation field of the georeferenced, larval habitat, 5m, Rapid Eye ™, geospectrally explanatorily decomposed, Red Edge, canopied, *S. damnsoum s.l.* larval habitat, NDVI, endmember biosignature reflectance emissivity transmittance variables employing ENIV and ArcGIS into three components: non-canopied, unscattered sunlight, single-scattering radiance, shadowing and multiple-scattering radiance. By so doing, we assumed that we would be able to regressively quantitate single-scattering radiance from the 5m, submixel, unmixed canopied biosignature components evaluated by a numerical integration as we insisted on the explicit inclusion of the "hotspot effect". Vegetation canopies often exhibit a pronounced peak in reflectance in the backscatter direction (i.e. where the sun and the sensor are at the same angular position relative to a given point on the earth surface), known as the 'hot spot' or 'opposition surge' [119].

A canopy BRDF was formulated in ArcGIS employing the various 5m, satellite data, products after creating the explicit radiance calculation formulae of all the imaged larval habitat reflectance, emissitiy transmisttance components. The bidirectional reflectance distribution function (BRDF; $f_r\left(\omega_{1,}\omega_2\right)$) is a function of ecogeographically geoclassified, LULC , canopied endmember, predictive variables that defines how light is reflected at an opaque surface. The function is employed both in the optics of real-world light, in computer graphicsalgorithms, and in computer vision algorithms [4]. The function takes an incoming light direction, $\omega_{1,}$ and outgoing direction, $\omega_{r,}$ (taken in a coordinate system where the surface normal n lies along the z-axis), and returns the ratio of reflected radiance exiting along ω to the irradiance incident on the surface from direction $\omega_{1,}$. Each direction ω is itself geospatially parameterized by azimuth angle ϕ and zenith angle θ, therefore the BRDF as a whole is a function of actually illumination-oriented, geo-spatiotemporal remote variables. The BRDF has units sr^{-1}, with steradians (sr) being a unit of solid angle [4]. The BRDF is an intrinsic property of a surface, which describes the angular distribution of radiation reflected by it, for all angles of existence and under any given illumination geometry [120]. The data was then exported into ENVI where a Red Edge, canopied, NDVI, endmember biosignature was subsequently created.

Canopy architecture may play a significant vital role in determining the BRDFs from a decomposed geosampled, *S. damnosum* s.l., riverine, larval, habitat, vegetative, LULC-related, canopy geolocation. Leaves are oriented at a variety of inclination angles, thereby varying effective illumination and viewing angles [10]. The result may be a complex pattern of reflected and transmitted, larval habitat, canopy, RapidEye™ radiation values. Canopy architecture in these habitats, however can seasonally change due to wind, heliotropism, and water stress. Non-Lambertian behavior of these vegetative canopies must be thus understood to relate changes in canopy reflectance to vegetative-related, explanatorial, LULC reflectance, emissivity transmittance properties rather than shadow and incoming wavelenght soley. One of the purposes of this study was to determine if the effects of leaf and substrate optical properties, canopy architecture, and illumination and viewing angles on BRDF of a geosampled, prolific, georefernced, *S. damnosum* s.l., canopied, riverine, larval habitat could be robustly decomposed and then interpolated to determine geolocations of prolific, georefernced, riverine larval habitats. The implications of these effects on Red Edge, NDVI, and the interpolated, derivative, canopy, endmember LULC spectra may reveal the fraction of absorbed, photosynthetic, covariate, wavelenght, parameter estimator coefficients is vital for identifying geolocations of prolific, riverine, shaded habitats.

Numerous studies of photosynthetic acclimation to changing environmental conditions have only focused on the top layer (young and sunlit) leaves in the canopy. However, the leaves in the low layer in a shaded, within canopy, geo-spatiotemporally, geosampled, RapidEye™ imaged, prolific, *S. damnosum* s.l., riverine, larval habitat may reveal different responses compared with young leaves for risk mapping and acclimating canopy age with immature black-fly productivity. The leafage distribution within the riverine larval canopy with varying leaf nitrogen and chorophyll content may determine the photosynthetic and NPV capacity and sink strength of the whole plant. Moreover,the change in photosynthetic and NPV capacity in regard to the elevated temperature may represent an acclimation of photosynthesis to temperature combined with the changes in African riverine phenological events. It may be found that a rise in canopy growth temperature stimulates plant development with increased photosynthesis during the peak riverine growing period. However, the ribulose- 1,5-bisphosphate carboxylase/oxygenase (Rubisco) has been found to be inactive under high temperatures which may disturb aggregating *S. damnosum* s.l., riverine, larval habitat , seasonal, canopy, photosynthetic profiles.

Ribulose-1,5-bisphosphate carboxylase/oxygenase, commonly known by the abbreviation RuBisCO, is an enzyme involved in the first major step of carbon fixation, a process by which atmospheric CO_2 is converted by plants to energy-richmolecules such as glucose [2]. In chemical terms, it catalyzes the carboxylation of ribulose-1,5-bisphosphate (also known as RuBP). It is probably the most abundant protein on Earth. As ribulose 1.5-bisphosphate carboxylase/oxygenase (i..e, Rubisco) activity limits light-saturated canopy photosynthesis under present atmospheric condition, the effects of an overexpression Rubisco content and photosynthesis may be examined in a geospectrally decomposed, Rapid Eye ™ imaged, geo-spatiotemporally, geosampled, shaded prolific, *S. damnosum* s.l. riverine larval habitat dataset of leaves at different positions in the canopy. Rubisco content in the transformant may be significantly greater in the uppermost, fully expanded canopy leaves but decreased to levels similar to those in wild-type plants in the lower leaves in the decomposed, riverine, larval habitat, geo-spatiotemporal, forecasting, eco-epidemiological, canopy, endmember, LULC derivative spectra-related, time series dependent, ecohydrological, ecogeographic and non-ecogeographic, forecasting, risk model. The mRNA levels of total Rubisco in these leaves may be much less than those in the expanding riverine larval habitat canopy.

Geospectrally decomposed, explanatorily interpolatable, *S. damnosum* s.l., riverine, larval habitat, canopy leaves, where Rubisco synthesis is active may suggest commensurately low level of synthesis. Although the activation state of Rubisco may be lower in the uppermost, fully expanded habitat canopy leaves of the transformant, may be recovered to its full level in the lower leaves. As a result, the photosynthetic rate may not differ in leaves at the same position in the habitat. Similarly, whole plant biomass may not differ between varying canopy photosynthetic plant genotypes. The enzyme ribulose bisphosphate carboxylase oxygenase (RuBisCO) would catalyze the reaction between RuBP and CO_2 in the riverine, larval, habitat canopy. The product would be the highly unstable 6-carbon intermediate known as 3-keto-2-carboxyarabinitol 1,5-bisphosphate. This six-carbon intermediate would decay virtually instantaneously into two molecules of 3-phosphoglycerate (3-PGA). RuBisCO also catalyzes

RuBP with oxygen (O_2) in a process called photorespiration, a process that is more prevalent at high temperatures [2]. RuBP is also involved in photorespiration, in which it combines with O_2 to become 3-PGA + phosphoglycolic acid. In the Calvin Cycle, RuBP is a product of the phosphorylation of ribulose-5-phosphate by Adenosine triphosphate (ATP). Ribulose-1,5-bisphosphate involved canopy photosynthesis synthesis processes in a geo-spatiotemporally, geosampled, seasonally productive, *S. damnosums*.l., riverine, larval habitat. Regarding elevation in growth CO_2, a decrease in Rubisco content may be observed in a, geosampled productive, georeferencable, canopy shaded, riverine, *S. damnosum* s.l., larval habitat coupled with lower content of chorophyll and leaf nitrogen especially when the nitrogen supply is insufficient during riverine flooding.

On the other hand, water stress is a well-knownlimiting factor for carbon uptake and growth of canopy plants. Seasonal canopy water deficiency may result in stomatal closure, decreased intercellular CO_2 content, Rubisco inactivity, accumulation of free radicals and disruption of light harvesting complexes in a geosampled, productive, georeferencable, canopy shaded, *S. damnosum* s.l., riverine, larval habitat. Moreover, the synthesis of chorophyll may be inhibited leading to decreases in the light-harvesting protein associated with photosystem II (PSII).Consequently, we attempted to model the response ofa RapidEye^{TM} imaged geosampled, *S. damnosum* s.l., riverine, larval habitat, canopy plants changes to elevation and geospectrally unmixed treatments of qualitatively regressively quantitated, geo-spatiotemporal climate and LULC explanatorial, wavelenght covariate, parameter estimator, reflectance, emissivity transmittance coefficients. Additionally we attempted to quantitate the variation in impacts according to leaf canopy position in the riverine georeferenced habitat. Based on the literature, a united measurement on gas exchange and chorophyll fluorescence we assumed would provide useful information about the ecophysiological performance of an aggregation of geosampled, productive, georeferencable, *S. damnosum* s.l., larval habitat, shaded, canopy plants under environmental stress (e.g., riverine, flooding).

Thereafter, the RapidEye^{TM}, Red Edge, NDVI, endmember biosignature, waveband data was employed as a dependent variable in a stochastic interpolator (i.e., Ordinary kriged-based algorithm). Based on an canopy endmember, kriged, probabilistic estimation technique, the data regularization framework known as stochastic interpolation recovers well-behaved functional representations of input data [12]. Our stochastic interpolation of the shade canopied, *S. damnosum* s.l., riverine, larval habitat, geo-spatiotemporally, ecohydrologially, ecogeographically, and non-ecogeographically geosampled, discontinuous, canopy endmembers split the interpolation operator into a discrete deconvolution that was followed by a discrete convolution of the decomposed data.

At the heart of the process was a row stochastic, uncertainty-oriented, matrix which represented the approximation of the larval habitat canopied, Rapid Eye ^{TM}, 5m data by a probabilistic regression weighting of the unmixed reflectance, emissivity transmittance, predictor values. It allowed the direct inclusion of various models (e.g., Voroni polygons) in to the post data regularization process. We examined connections to radial basis functions for constructing a generalized Rapid Eye^{TM} canopy endmember, algorithmic framework for providing a unique mechanism for linking the canopy endmember,*S. damnosum* s.l., riverine, larval habitat, decomposed, sub-mixel, ec-epidemiological, data with conventional interpolation which in this investigation was built on non-negative operators. Decomposed photosynthetic and NPV canopy endmembers can be implemented

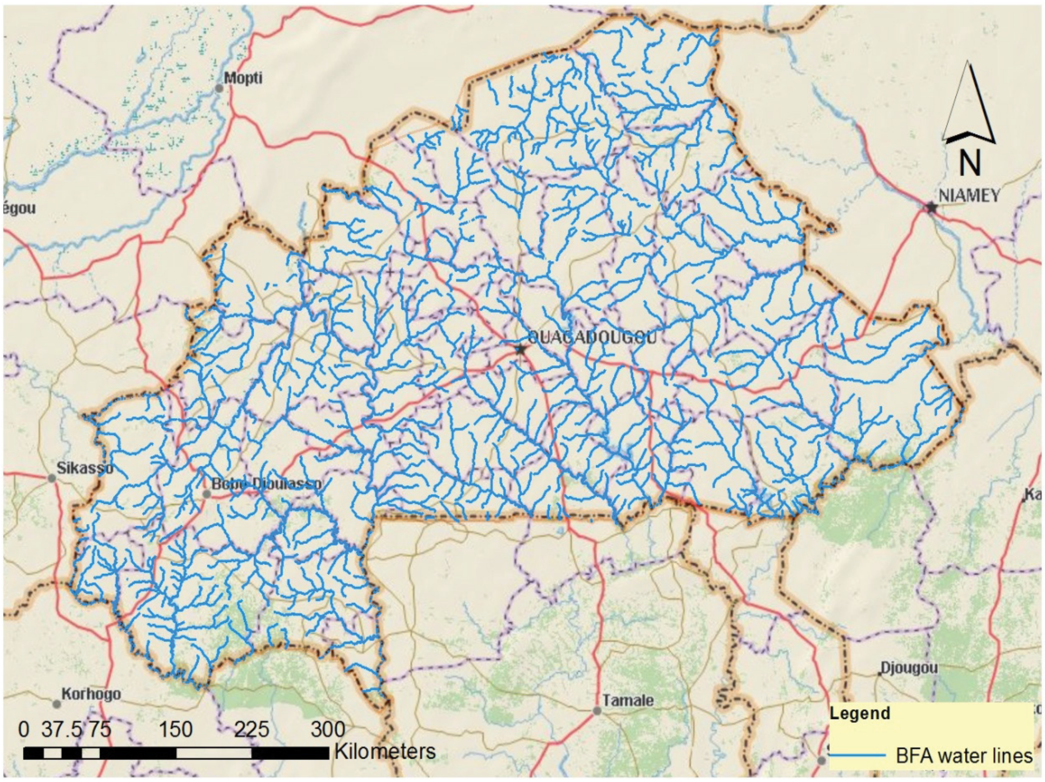

Figure 3: A map of Burkina Faso.

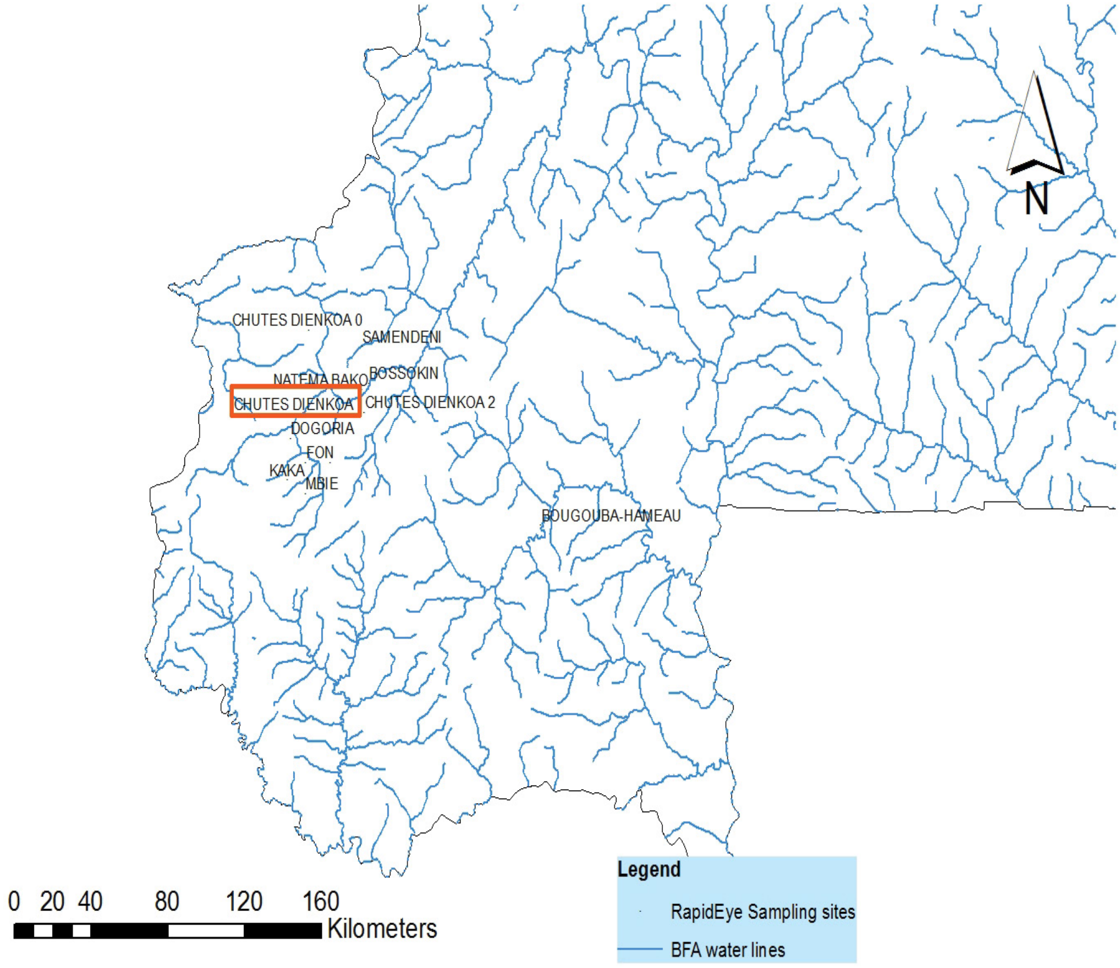

Figure 4: The Chutes Dienoka study site.

with flexibility to yield data approximation, interpolation, peak sharpening, non-linear smoothing, and all manner of hybrid schemes in a principled way by a deliberate choice of different generators of the row space of the convolution matrix[4,115].

We then investigated the explanatorily, geospectrally interpolated,unmixed,Rapid Eye ™ NDVI, canopy biosignature's ability to discriminate canopy vegetation, LULC-type and other ecohydrological, ecogeographical and non-ecogeographical, explanatorial, 5m,imaged, geospatial seasonal riverine objects (e.g., shaded floating vegetation), within the canopy *S. damnosum* s.l., riverine, larval habitat, decomposed, geo-calssifed LULC endmembers in a Boolean model. The Boolean model for a random subset of the plane or higher dimensions analogously is one of the simplest and most tractable models in stochastic geometry [4]. Our model formulation included identifying the larval habitat, canopied, LULC reflectance observed in the backscattering and forward scattering regions, respectively rendered from the Red Edge decomposed biosignature. Our assumption was that by performing an integration of the BRDF in a seasonal geosampled, vegetated, shade, canopied, *S. damnosum s.l.,* larval habitat, NDVI, canopy, endmember, photosynthetic, reflectance, response model, an instantaneous hemispherical reflectance (i.e., spectral surface albedo) could be remotely probabilistically qualitatively, regressively, resdiually quantitated and thereafter geospectrally robustly interpolated. Our assumption was that integration of the BRDF with respect to both 5m wavelength and the angle of existence would yield the albedo. By so doing, we assumed we could also employ the Red Edge, decomposed, NDVI-related, geospectral endmember, biophysical, parameter retrieval technique via BRDF over a heterogeneous northern Ugandan riverine region to target prolific unsampled, unknown, habitats based on geo-spatiotemporally field-geosampled, immature *Similium* count data.

Due to local differences in climate, LULC soil type, vegetation species, *etc.,* in African riverine environments we assumed that the geospectral, canopy, endmember, explanatorial, characteristics of soil and canopy vegetation LULC may exhibit positive geospatial autocorrelation. As such, we employed an eigenfunction decomposition algorithm (see Griffth 2003) to predict variations in the geospectral characteristics of the various Rapid Eye ™ imaged green, vegetation-related, LULC-related canopy covariate, parameter estimator, coefficient across ecogeographic space. We assumed that the algorithm would geospectrally quantize the geo-spatially, explanatorily, interpolated reflectance, emissivity transmittance values for generating robust, sub-mixel, Red Edge, NDVI, endmember, residualized forecasts. For example, we assumed that the accuracy of FVC estimates estimated in ArcGIS would increase, providing evidence that the photosynthetic canopy-related covariates may be useful when considering the effects

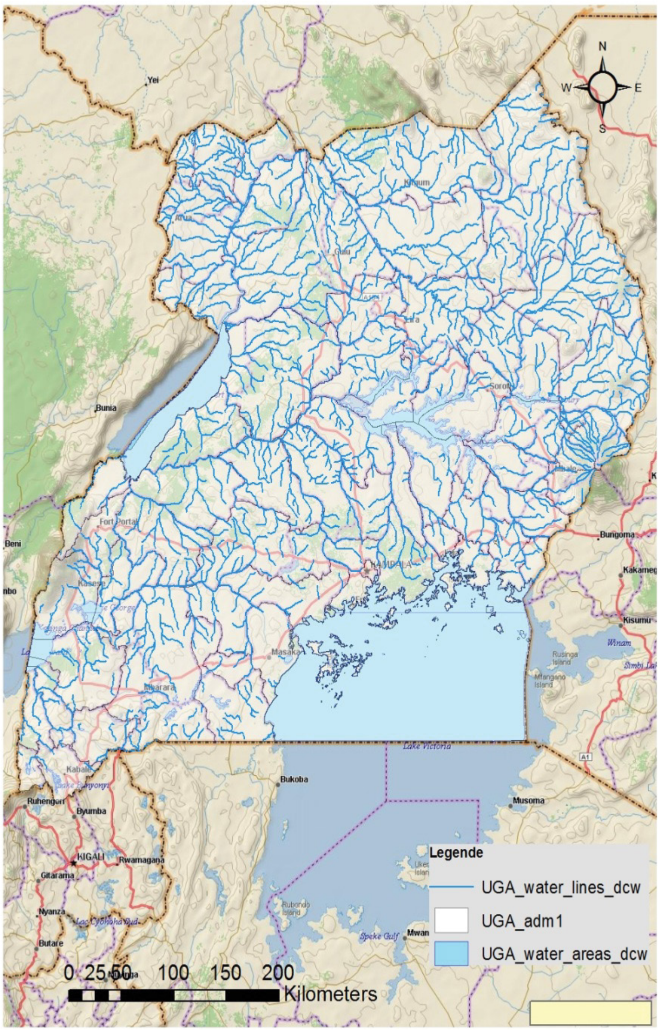

Figure 5: A map of Uganda.

of latent geospectral autocorrelation for a mixture analysis of shade canopied,empirically geo-spatiotemporally, geosampled,*S. damnosum* s.l., georeferenced, riverine, larval habitats.

Evidence-based targeting of interventions is a crucial component in the fight against vector-born, infectious disease, larval habitats as targeted interventions are more efficient and more cost-effective than untargeted interventions [8]. Environmental onchocerciasis management programs have typically implemented as "all-out" campaigns by treating all potential breeding habitats. In contrast, remotely, regressively targeted, onchocerciasis, environmental management using OBIA and ArcGIS can be based on a sound understanding of the heterogeneity in seasonal immature *Similium* productivity. However, deficiencies in field and remote methodology for measuring such productivity hamper our progress in understanding these habitats and other unknown, unsampled habitats cost effectively in African riverine communities. To address these issues, we develop a framework of habitat-based interventions by adoption of a medium resolution, remote sensing, eco-epidemiological landscape approach in ArcGIS to elucidate mechanisms underlying canopy vegetated LULC, decomposed, explanatorial components in ENVI that affect immature *Similium* productivity. The importance of vigorous quantitative estimation of this productivity is highlighted in a geospectral, stochastic, explanatorial interpolator.

In regions with riverine-based geospatial variation, the selection of a single, sub-meter, spatial resolution data product for an imaged, immature, vegetated, shade, canopied, riverine *Similium* habitat may be unnecessary. The ideal LULC-related vector arthropod-related observation depends on quantitating the process of the phenomenon and on the landscape spatial heterogeneity [2,4,115]. Further, since in African riverine ecosystems, shade canopied, geo-spatiotemporally, geosampled, *S. damnosum* s.l., riverine, larval georeferenced habitats differ in their capacity of immature production [1], intervention efforts remotely , regressively, targeting productive habitats on a geo-classified canopied LULC using a proxy, medium resolution, decomposed, NDVI, endmember-oriented biosignature encompassing geospectrally explanatorily interpolated, shade, vegetated ,canopy spectra in ArcGIS may be more efficient than mobilizing field sampling eco-epidemiological teams. Thus,our research objectives were to: a) generate a 5m, Rapid Eye^{TM}, Red Edge, probabilistic, NDVI map from a georeferenced *S. damnosum s.l.* larval habitat geosampled in a Burkina Faso riverine ecosystem b) digitally segment the, vegetated, shade, canopied habitat, NDVI mixels based on geospatial/geospectral and texture LULC characteristics within an object-based framework, c) determine the regions in which the canopied,riverine, habitat tissue optical characteristics is most significantly influence using a 3-D radiative transfer canopy wavelenght reflectance data, a successive progressive algorithm, a geometric-optical model and a BDRF function, d)determine the variability in leaf, woody stem, and standing litter emissivity and transmittance properties across a wide array of habitat canopy plant species, genera, growth forms, lifeforms, and functional groups along a strong climatic gradient and across a broad range of foliar biochemistry. f) Test the relative importance of tissue optical, canopy structural, pigments and variability in driving changes in LULC (5m mixel-level) radiance for specific, riverine, within-canopied ecosystem types (e.g., trailing vegetation) e) krige the geo-spectrally extracted decomposed, canopy immature, habitat, endmember biosignature-related, components over a northern Ugandan riverine environment and, field verify estimates derived from the interpolator for targeting productive unknown, unsampled *S. damnosum s.l.,* larval habitats based on geo- spatiotemporal, field-geosampled count data.

Material and Methodology

Study site

Burkina Faso is a landlocked country in West Africa whose geographic coordinates lie at a latitude: 13° 00´ North of the Equator and a longitude of: 2° 00´ West of Greenwich Meridia. It is surrounded by six countries: Mali to the north, Niger to the east, Benin to the southeast, Togo and Ghana to the south, and Côte d'Ivoire to the southwest (Figure 3). The size of this country, formerly called the Republic of Upper Volta, is 274,200 square kilometers (105,900 sq. mi) with an estimated population of more than 15,757,000. Of the total land area, water covers approximately 400 km^2. Burkina Faso has three distinct seasons: warm and dry (November–March), hot and dry (March–May), and hot and wet (June–October). Annual rainfall varies from about 250 mm to 1,000 mm in the country.

The eco-epidemiological riverine village study site (Chutes -Dienoka) is in the south western region of Burkina Faso about 250 kilometers from Oaugadodogu the capital (Figure 4). The terrain surrounding the study site is mostly flat with undulating plains and

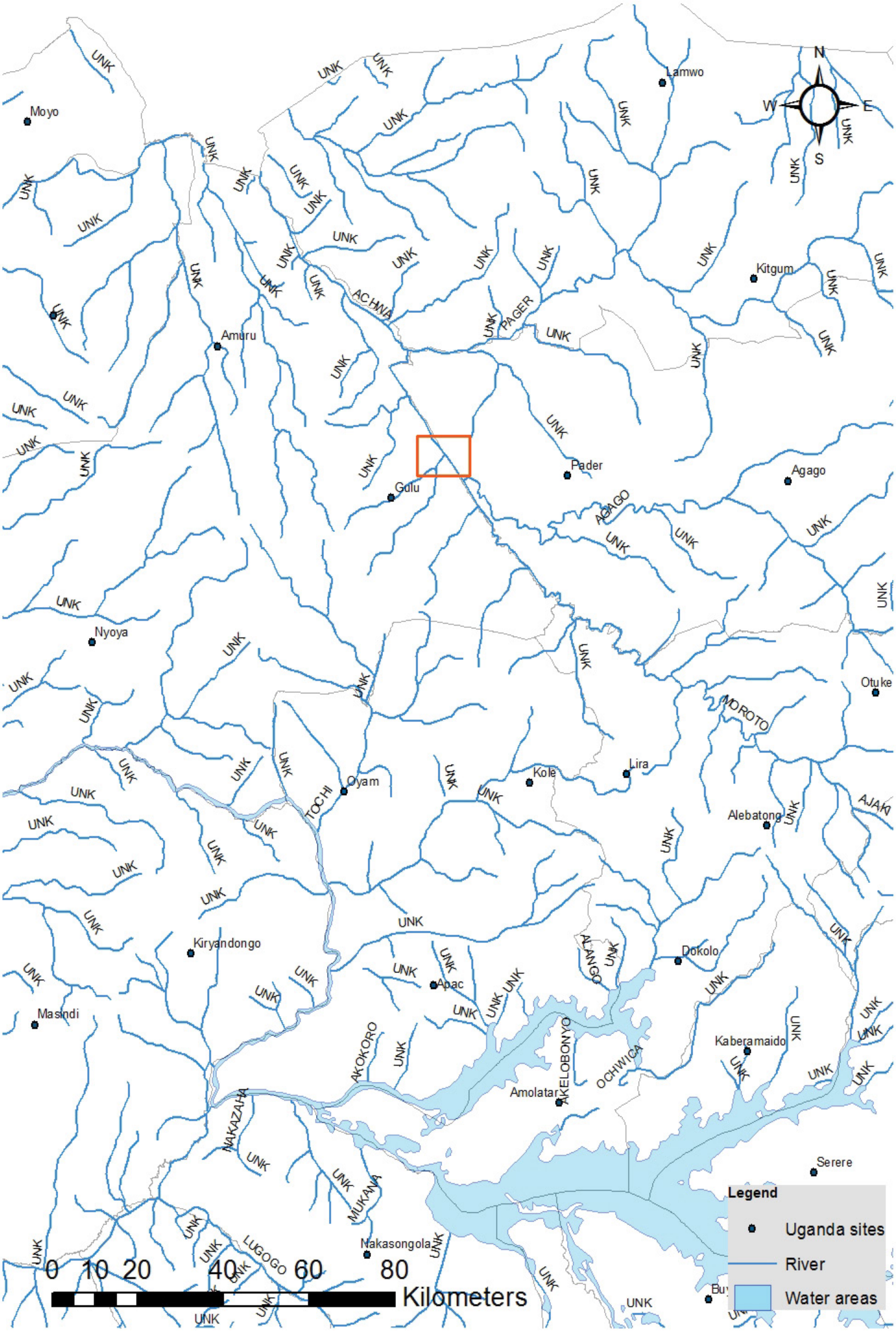

Figure 6: The Achwa river study site.

hills. Most of the region lies on a savanna plateau, with fields, brush, and scattered trees. The geological history of the study site is marked by Precambrian volcanic activity and Eburnean faulting and folding. These geological events, followed by successive erosion cycles have given rise to the basis of the relief in some portions of the study site which are comprised of peneplain and sandstone plateaux.

The Plateau of Bobo-Dioulasso is the highest part of the bedrock at the study site; its surface is rolling with gentle slopes, sometimes flat which betrays the presence of ferralitic cuirasses either at the surface or at very shallow depth. These cuirasses form gently sloping glacis with slopes of under 5 percent. There are seven main soil types in the river ecosystems which include: leached ferruginous; brown eutrophic; vertisols; ferralitic; halomorphic, hydromorphic and raw mineral soils. The first two soils cover more than two thirds of the riverine epidemiological study site.

In the study site there are four types of pasture vegetation which include:1) savannah with sparse tree cover on buttes with laterite pans including such plants as *Butyrospermum paradoxum, Burkea africana, Loudetiopsis scaëttae* and *Schizachyrium sanguineum*; 2) treed savannas with *Isoberlinia doka* and *Andropogon ascinodis;* and, 3) grassy savannah on bowal with *Loudetia togoensis* and *Diheteropogon hagerupii*; savannas in temporarily flooded riverine areas with *Imperata cylindrica* and*Schizachyrium brevifolium*; and, grasslands of land flooded for long periods with *Oryza barthii* and *Acroceras amplectens*. The basin of the Niger Riverdrains 27% of the study site surface area. The Niger's tributaries – the Béli, the Gorouol, the Goudébo and the Dargol – are seasonal streams and flow for only four to six months a year.

The Niger River (is the principal river of western Africa, extending about 4,180 km (2,600 mi). Its drainage basin is 2,117,700 km^2 (817,600 sq. mi) in area. Its source is in the Guinea Highlands in southeastern Guinea. It runs in a crescent through Burkina Faso Niger, on the border with Benin and then through Nigeria, discharging through a massive delta, known as the Niger Delta or the Oil Rivers, into the Gulf of Guinea in the Atlantic Ocean. The Niger is the third-longest river in Africa, exceeded only by the Nile and the Congo River (also known as the Zaïre River). Its main tributary is the Benue River which runs directly through the Chutes-Dienkoa epidemiological study site.

Figure 7: Rapid Eye 5 m data for the Chutes-Dienkoa study site.

Uganda is a landlocked country in East Africa. The country is located on the East African plateau, lying mostly between latitudes 4°N and 2°S (a small area is north of 4°), and longitudes 29° and 35°E (Figure 5). It averages about 1,100 meters (3,609 ft.) above sea level, and this slopes very steadily downwards to the Sudanese Plain to the north where the Gulu study site is located. Although generally equatorial, the climate is not uniform as the altitude modifies the climate. Southern Uganda is wetter with rain generally spread throughout the year. At Entebbe on the northern shore of Lake Victoria, most rain falls from March to June and in the November/December period. Further to the north a dry season gradually emerges, for example, at the Gulu epidemiological study site which is located about 120 km from the South Sudanese border where November to February is much drier than the rest of the year.

The main soil types are 18 divided into 7 groups based on their occurrence and agricultural productivity. The Uganda surfaces cover most areas south of Lake Yoga. This group embraces five types of deep, sandy clay loams with medium to high productivity. The Tanganyika surfaces cover most areas north of Lake Kyoga, West Nile and some parts of the South Western tip of Uganda, embracing five types of sandy clay loam with low to medium productivity. The Karamojong surfaces cover the North Eastern part of the country and embrace two soil types of sandy clay loams and black clays with very low productivity. Rift valley soils in the Western and Northern parts of the country, bordering on the Western Rift Valley, embracing two types of mainly sandy clay loams with alluvial parent rock of medium to high productivity. Volcanic soils are dominant in Mt. Elgon, Northern Karamoja, and the extreme South Western tip of Uganda (Kabale and Kisoro) with medium to high productivity except in N. Karamoja where their productivity is low. Alluvial soils are found outside the Rift Valley, mainly in Central Northern Uganda (Lango and Acholi) as well as West of Lake Victoria. The productivity of these sandy soils is very low. The last group of soil types is in Northern Uganda and their productivity is low.

Based on topography, Uganda has been divided into four relief regions: - 1) Above 2 000 meters - 2% of the land area,2)1 500 - 2 000 meters - 5% of the land area 3)900 - 1 500 meters - 84% of the land area and 4) Below 900 meters - 9% of the land area. The rainfall pattern resembles that of the northern system, with more rain at higher altitudes. Mixed cropping is common with a wide variety of crops. The system is in the sub-humid zone where the vegetation community is moist *Butyrospermum/Combetrum/Terminalia* grassland. Livestock activities are limited by the presence of tsetse fly. As in the northern system, tobacco and cotton are major cash crops.

The Achwa River is a river of Uganda where our study site is geolocated (Figure 6). The river begins in hills in the northwestern part of Katakwi Province and flows through Lira Province and becomes the border between the provinces of Pader and Gula where the Agago River and then the Pager River flow into it. The Achwa River forms most of the border between the provinces of Atiak and Gitgum before crossing into Sudan east of the border town of Nimule and joining the White Nile about ten miles northwest of Nimule. That particular section of the White Nile is known as Bahr el Jebel or "River of the Mountain", or Mountain Nile. The Achwa drains much of the northeastern highland and northern plateau of Uganda. Like most rivers in the region the flow of the Achwa is strongly influenced by the season and weather. It is prone to flooding at times [121].

Variable	Description	Units
GCP	Ground control points	Decimal-degrees
FlOW	flowing water	Presence or absence
TURB	Turbidity of water	Formazin Turbidity Unit
AQVEG	Aquatic vegetation	Percentage
HGVEG	Hanging vegetation	Percentage
DDVEG	Dead vegetation	Percentage
MMB	Man-made barriers	Type (e.g., dams, bridges)

Table 1: Environmental predictor variables geosampled of the *S. damnsoum s.l.* habitat.

The distance from the Achwa's headwaters to the White Nile is about 185 miles. The river flows through East Sudanian savannah which encompasses much of northeastern Uganda. This hot, dry, wooded savannah at the Gulu study site is composed mainly of *Combretum* and *Terminalia* shrub and tree species and tall elephant grass which has been adversely affected by agricultural activities, fire, clearance for wood and charcoal. Presently however, large blocks of relatively intact habitat remain outside protected areas.

Remote sensing data

RapidEye satellite sensor was successfully launched from the DNEPR-1 Rocket on August 29th, 2008 at Baikonur Cosmodrome in Kazakhstan. The RapidEye constellation of five Earth Observation satellites has been in operation since February of 2009. The system images a 77 kilometer wide swath, which produces more than 5 km^2 five of earth every day for its archive and over one billion km^2 every year (www.satimagingcorp.com*).*

The RapidEye Basic (1B) products are geometrically corrected to an idealized sensor and satellite model, and band aligned. They are delivered as NITF (National Imagery Transmission Format) files together with Rapid Positioning Capability (RPC) described by rational functions. The horizontal accuracy of Level 1B products is determined by satellite attitude (which is adjusted by pre-marking Ground Control Points during image cataloging) and ephemeris as well as terrain displacement, since no terrain model is used in the processing of the 1B products. The worldwide RapidEye Ground Control Point database has been mainly populated with GCPs derived from the GeoCover 2000 Landsat mosaic, along with other reference data of higher accuracy to create the available GCPs used during cataloging and processing. Moving into the future, the GCPs created from the GeoCover 2000 mosaic will be replaced with points derived from the GLS 2000 Lands at mosaic. The replacement process with start in areas with the largest deviation between the two datasets. The default accuracy of the Basic product, using GCPs derived from the Landsat mosaic, is 45m CE90 (RMSE 1-D = 21m) or better. In the case where GCPs of better accuracy are available, this accuracy will not exceed 23m CE90 (RMSE 1-D = 11.00m) These geo-location accuracies are valid for image collected at Nadir over flat (< 10^{o}slope) terrain.

Over 70% of RapidEye's imagery has a view angle of less than 10°, as the view angle of RapidEye™ imagery is always less than 20°. The system also has the capability for daily revisit to any point on earth. RapidEye™ products are collected by a 12 bit imager. During on-ground processing, radiometric corrections are applied and all image data are scaled up to 16 bit dynamic range. The scaling is done with a constant factor that converts the (relative) pixel digital numbers (DNs) from the sensor into values directly related to absolute radiances. The scaling factor was originally determined pre-launch. However, absolute radiometric calibration for each sensor element of each band is now continually monitored and adjusted. This factor is applied so that the resultant single DN values correspond to 1/100th of a Watt/m^2 sr^{-1} µm.

The focal plane of the RapidEye sensors is comprised of five separate CCD arrays, one for each band. This means that the bands have imaging time differences of up to three seconds for the same point on the ground, with the blue and red bands being the furthest apart in time. During processing, every 1B and L3A product isband co-registered using a DEM to roughly correlate the bands to the reference band (red-edge), then a final alignment is done using an auto-correlation approach between the bands. For areas where the slope is below10°, the band co-registration should be within 0.2 pixels or less (1-sigma).

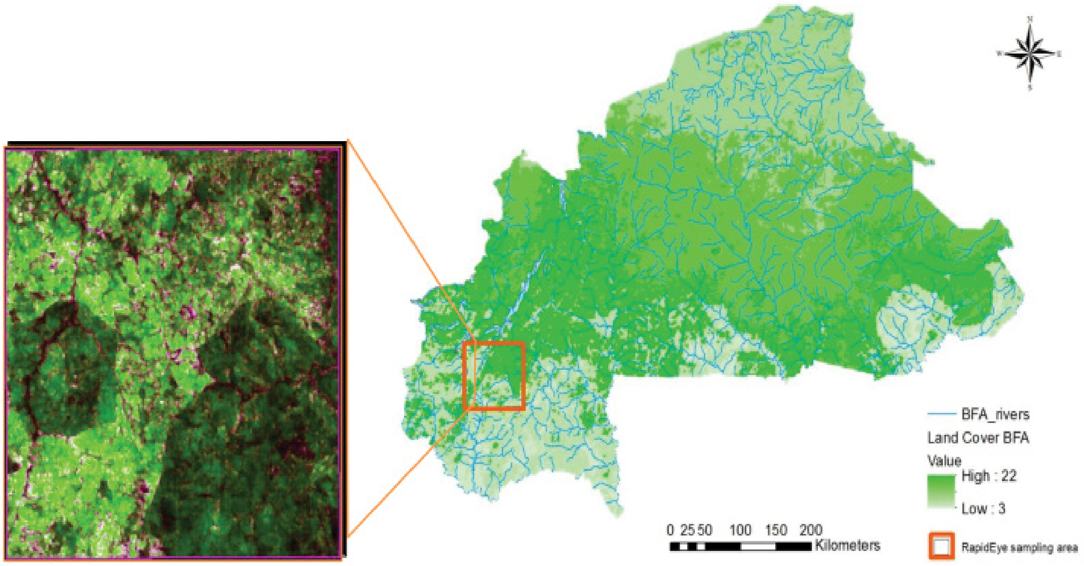

Figure 8: Red Edge NDVI for a shade canopied *S. damnosum* s.l. larval habitat.

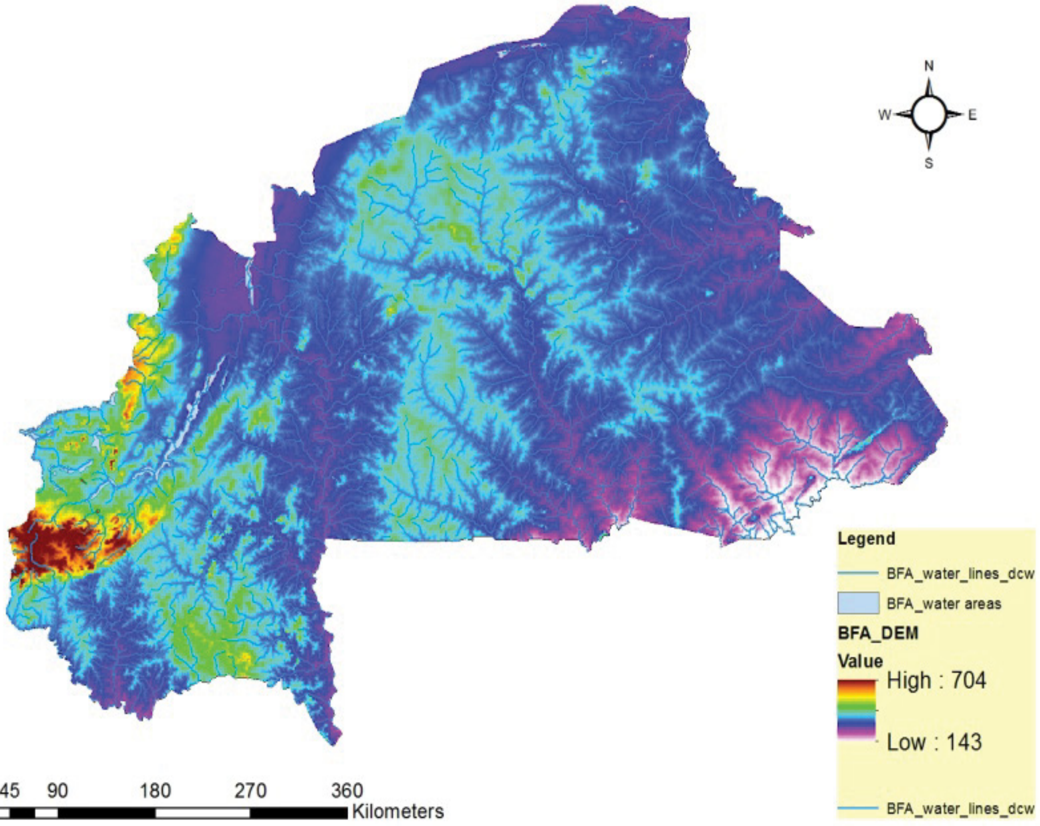

Figure 9: A Rapid Eye 5 m Digital elevation model for the Dienkoa study site.

The image was atmospherically corrected using the quick atmospheric correction (QUAC) procedure in ENVI 4.8 (ENVI, 2006). The QUAC procedure in ENVI is based on the empirical finding that the average reflectance of diverse material spectra is not dependent on each scene, thus processing is much faster compared to first-principles methods (ENVI, 2006). QUAC determines atmospheric compensation parameters directly from the information contained within the image (mixel spectra) thereby. letting the retrieval of accurate reflectance spectra (ENVI, 2006). QUAC determines average baseline (darkest channel) and endmembers by using both vegetation and bright spectral filter in any particular image (http://exelisvis.com).

In this research the Order Polygon contained 5 vertices consisting of longitude/ latitude (decimal degrees) geographic coordinates using a WGS-84 ellipsoid. The Rapid Eye data contained 64 km^2 of the land cover in the study sites (Figure 7). The Rapid Eye imagery was classified using the Iterative Self-Organizing Data Analysis Technique (ISODATA) unsupervised routine in ERDAS *Imagine* v.8.7™ (ERDAS, Inc., Atlanta, Georgia). Unsupervised classifications are commonly employed for the identification of sub-meter resolution-derived time series dependent, LULC classes associated with explanatorial, prolific vector insect habitats based on geo-spatiotemporal, field-geosampled count data [1,3,75,76]. The clearest, cloud-free images available of the contiguous sub-areas of the study sites were used to identify land cover and other spatial features associated with the georeferenced *S. damnosum s.l.* habitats.

Habitat mapping

Initially, base maps were generated using the 5m RapidEye in ArcGIS 10.3^{tm} with differentially corrected global positioning systems (DGPS) ground coordinates of a prolific, seasonal, vegetated canopy, shaded, *S. damnosum s.l.*, riverine, habitat geosampled, at the Chutes-Dienkoa study site village in Burkina Faso. The DGPS ground coordinates were acquired from a CSI max receiver which has a positional accuracy of +/- .178 (84). Using a local DGPS broadcaster can compensate for ionospheric and ephemeris effects which can improve horizontal accuracy significantly and can bring altitude error down in a geo-spatiotemporal-sampled, predictive, entomological, larval habitat distribution model [1,3,75,76].

The georeferenced, riverine, shade, canopied, geosampled, *S. damnosum s.l.*, larval habitat, remote attributes was entered into the VCMS™ relational database software product (Clarke Mosquito Control Products, Roselle, IL). The VCMS™ database supports a mobile field data acquisition component module, called Mobile VCMS™ that synchronizes field-geosampled data from industry standard Microsoft Windows Mobile™ devices and can support add-on DGPS data collection [http://store.elecdata.com/field_data_collection/vcms.aspx]. Mobile VCMS™ and its corresponding FieldBridge® middleware software component were used to support both wired and wireless synchronizing of the seasonal field-sampled data collected from the georeferenced, *S.damnsoum* s.l., larval habitat, discontinous canopy. The data collected with the Mobile VCMS™ was then synchronized directly into a centralized VCMS™ relational repository database.

Thereafter, geocoded spatial display of the geo-spatiotemporal, geosampled, *S.damnosum s.l.*georeferenced, larval habitat data attributes was mapped using the embedded VCMS™ GIS Interface

```
e = ENVI()

; Open an input file
File = Filepath('_burkinafaso ', $
 Root_Dir=e.Root_Dir)
Raster = e.OpenRaster(File)

; Process a spatial subset
Subset = ENVISubsetRaster(Raster, Sub_Rect)

; Get the task from the catalog of ENVITasks
Task = ENVITask('QuerySpectralIndices')

; Define inputs
Task.INPUT_RASTER = Subset

; Run the task
Task.Execute

; Get the task from the catalog of ENVITasks
Task2 = ENVITask('SpectralIndices')

; Define inputs
Task2.INPUT_RASTER = Subset
Task2.INDEX = Task.

; Run the task
Task2.Execute

; Get the fielddata' data collection
DataColl = e.Data

; Add the output to the data collection
DataColl.Add, Task2.OUTPUT_RASTER

; Display the result
View1 = e.GetView()
Layer1 = View1.CreateLayer(Task2.OUTPUT_RASTER)

; Print the available indices to the
; ENVI command line
Task.AVAILABLE_INDICES
Start the application
e = ENVI()

; Open an input file
File = Filepath(burkinafaso Subdir=['data'], $
 Root_Dir=e.Root_Dir)
Raster = e.OpenRaster(File)

; Process a spatial subset
Subset = ENVISubsetRaster(Raster, Sub_Rect])

; Get the task from the catalog of ENVITasks
Task=ENVITask('SpectralIndices')

; Define inputs
Task.INDEX = ['Normalized Difference Vegetation Index',]
Task.INPUT_RASTER = Subset

; Define outputs
Task.OUTPUT_RASTER_URI = e.
; Run the task
Task.Execute

; Get the data collection
DataColl = e.Data

; Add the output to the data collection
DataColl.Add, Task.Output_Raster

; Display the result
View1 = e.GetView()
Layer1 = View1.CreateLayer(Task.Output_Raster)
```

Table 2: ENVI Query Spectral Indices Task routine for separating geosampled, georeferenced, vegetated, canopy shaded, *S. damnosum s.l.* larval habitat mixels.

```
Start the application
e = ENVI()

; Open an input file
File = Filepath(, Subdir=' S. damnosum s.l.data'], $
 Root_Dir=e.Root_Dir)
Raster = e.OpenRaster(File)

; Process a spatial subset
Subset = ENVISubsetRaster(Raster, Sub_Rect=[600,200,799,399])

; Get the task from the catalog of ENVITasks
Task=ENVITask('SpectralIndices')

; Define inputs
Task.INDEX = ['Normalized Difference Vegetation Index',]
Task.INPUT_RASTER = Subset

; Define outputs
Task.OUTPUT_RASTER_URI = e.

; Run the task
Task.Execute

; Get the data collection
DataColl = e.Data

; Add the output to the data collection
DataColl.Add, Task.Output_Raster

; Display the result
View1 = e.GetView()
Layer1 = View1.CreateLayer(Task.Output_Raster)
```

Table 3: Refining the shade canopied *S. damnosum* s.l. larval habitat spectral indexusing the ENVI Spectral Indices Task API routine.

Accuracy measure%	No Red Edge	Only Red Edge	W=1	W=10	W=20	W=50	W=100
Overall Accuracy	90.92	83.13	92.42	90.35	81.45	91.99	89.97
Kappa	87.81	77.78	87.33	88.12	75.24	86.51	84.41
Dense Vegetation	98.31	98.43	98.21	96.91	99.24	96.58	99.21
Sparse vegetation	83.11	74.29	89.69	87.81	66.42	71.29	68.66
Bare land	82.55	72.18	81.57	82.36	55.72	85.21	79.25
Water	100	100	100	100	100	100	100

Table 4: An accuracy assessment comparing different weights assigned to the Red edge spectral band.

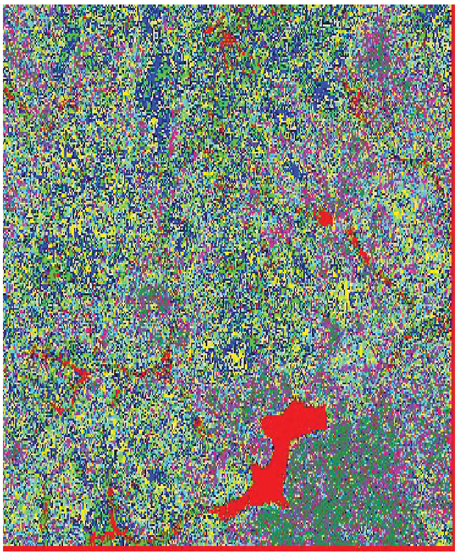

Figure 9: Red Edge *S. damnosum* s.l. NDVI signature with hot spot.

Kit™ which was developed utilizing ESRI's MapObjects™ 2 technology. VCMS including connectivity with hand held computers and field data collection devices including DGPS receivers. PalmOS and Windows PocketPC handhelds have been used for malaria [48] and, eastern equine encephalitis virus (EEEV) mosquito habitat monitoring [122]. The VCMS™ database supported the export of all the geo-spatiotemporally, geosampled, spectral parameters using any combination of the time-series dependent, georeferenced, riverine larval habitat remotely sensed, covariate, parameter, estimators in order to further process and display specific, explanatorial, LULC georeferencable, data explanatorial, feature attributes in a stand-alone desktop GIS software package (i.e., ArcGIS 10.3®). A polygon layer outlining the georeferenced *S. damnosum s.l.* habitat was then created by digitizing the RapidEye visible and NIR imagery.

Grid-based algorithm

A digitized matrix was constructed by applying a mathematical algorithm in order to fit the continuous and bounded, riverine, larval, habitat surfaces from a field and canopy-geosampled operationizable, attribute in ArcGIS. Each digitized grid cell within the matrix contained an attribute value as well as the *S. damnosum s.l.* larval habitat geocoordinates. As such, the geospatial location of each cell was implicitly contained within the ordering of the matrix. GIS grid-based data files consist of columns and rows of uniform cells coded according to georeferenced data values [4,115].Multiple data layers were then created using different coded values for the various field explanatorial attributes which were related to the same grid cell.

Each polygon was assigned a unique identifier. Field attribute tables were then linked to the polygons. The georeferenced, polygons were used to define the sampling frame, which was extended to include a 5 km buffer from the external boundary of the geo-spatiotemporal, geosampled, riverine larval habitat, eco-epidemiological study sites. This allowed for multiple interactions enabling retrieval and transformation of the geosampled *S. damnosum s.l.* larval habitat canopy parameters efficiently, regardless of spatial dimensionality of the habitat canopy.

Environmental parameters

Multiple georeferenced, photosynthetic, canopy-related, covariate, parameter estimators were then examined extensively employing longitude, latitude, and altitude data. The data was also comprised of individual geo-spatiotemporal geosampled empirical, observations of the georeferenced *S. damnosums*.l larval habitat together with a battery of categorical canopy attributes (Table 1).

Vegetation indices

The different modules in ENVI 5.2 were employed to perform the Red Edge NDVI calculations. Red edge NDVI differs from other NDVIs by employing bands along the Red Edge, instead of the main absorption and reflectance peaks (http://www.satimagingcorp.com/satellite-sensors/other-satellite-sensors/rapideye/). This index is a modification of the traditional broadband NDVI.

The RedEdge NDVI was computed directly without any bias or assumptions regarding plant physiognomy, canopy cover class, soil type, or climatic conditions, within a range from -1.0 to 1.0 employing the 5 m visible and NIR reflectance, (p), in ENVI using the expression: $RENDVI = \frac{\rho_{750} - \rho_{705}}{\rho_{750} + \rho_{705}}$. The difference of the RapidEye visible and NIR bands was divided by their sum, successfully in ENVI which formed the functionally equivalent NDVI, over the canopy and terrestrial surfaces of the georeferenced, vegetated, shade, canopied, *S. damnosum s.l.* eco-epidemiological. Chutes Dienkoa, study site.

Narrowband greenness VIs are combinations of reflectance measurements sensitive to the combined effects of foliage chlorophyll concentration, canopy leaf area, foliage clumping, and canopy architecture[4]. Similar to the broadband greenness VIs, narrowband greenness VIs are designed to provide a measure of the overall amount and quality of photosynthetic material in vegetation, which is essential for understanding the state of vegetation. Narrowband greenness VIs are intended for use with imaging spectrometers [2]. Use of NIR measurements, with much greater penetration depth through a geo-spatiotemporally, geosampled, *S. damnosum* s.l., riverine, larval habitat canopy than red, allowed quantitating the total amount of green vegetation, geoclassified LULCs in the column until the signal saturates at very high levels (Figure 8). QuickBird applications include vegetation phenology (growth) studies, land-use and climatological impact assessments, and vegetation productivity modeling (www.digitalglobe.com).

The following steps were then employed in ENVI in order to create the Red Edge NDVI. From the Toolbox, we selected Band Algebra > Spectral Indices. In the Spectral Index dialog, we chose an input image. The image contained wavelength metadata. We then employed ENVI to runk multiuple tasks on the 5m Rapid Eye™ data.

We selected an output filename and location. By so doing, this enabled the Preview check box to see a preview of the settings in ENVI. We clicked OK to process the data. The preview was calculated only on the area in the Image window. We selected the Display result option to display the output image when the processing was complete. We noted that the Red Edge NDVI image that consisted of multiple indices (i.e., where each Rapid Eye band was a different index.

The image was then segmented with a multi-resolution segmentation algorithm employing a fine scale parameter and 4 different weights (from 0 to 100) which were assigned to the Red Edge spectral band to evaluate its influence in the segmentation and classification process. Each canopy weight generated a segmented 5m image. Explanatorial, data feature attributes related to spectral information, geometry and texture were then calculated for each image segment employing the ENVI which was performed along with field data to select 'classes (Dense vegetation, Sparse vegetation, Bare land, and Water).A decision tree approach was then applied to the samples to select the attributes that provided the best separation among the classes within the scenes.

Spatial hydrological model

The latest version of PCI Geomatics Orthoengine® software was then used to generate a RapidEye DEM from the geo-spatiotemporal, geosampled, canopied, S. *damnosum s.l.* habitat data. A DEM is a raster representation of a continuous surface, usually referencing the surface of the earth [4]. The accuracy of this georeferenced, data is determined primarily by the resolution (the distance between sample points). Other factors affecting accuracy are data type (integer or floating point) and the actual sampling of the surface when creating the original DEM. PCI software supports automatic overlay of vector insect habitat DGPS collections, geometric modeling using Toutins rigorous model, Rationale Polynomial Coefficients (RPC) models, automatic DEM generation, orthorectification and automatic mosaicking [www.pcigeomatics.com] (Figure 9).

The vegetation canopied, *S. damnosum* s.l. riverine larval habitat

QuickBird DEMwas initailly represented as a e represented as a raster [i.e, a grid of squares, also known as a heightmap when representing elevation] and as a vector-based triangular irregular network (TIN). The TIN DEM dataset is also referred to as a primary (measured) DEM, whereas the Raster DEM is referred to as a secondary (computed) DEM [4]. While a sub-resoltuin 3-D DEM may be useful for landscape modeling and visualization applications, they are most commonly employed for flood or drainage modeling, land-use studies, geological applications, and other applications [2]·

Object-oriented classification

Before applying spectral index to the imagery, raw mixel values (i.e., DN values), we calibrated the Rapid Eye™data into physically meaningful units. The top-of-atmosphere (ToA) reflectance was employed to correct the noisy variables. Image products delivered in an integer format can be rescaled to the TOA reflectance using radiometric rescaling coefficients provided in the product metadata file (MTL file), The following equation is used to convert DN values to TOA reflectance for OLI data as follows: $\rho\lambda'=M\rho Qcal+A\rho$ where: $\rho\lambda'$ = TOA planetary reflectance, without correction for solar angle. Note that $\rho\lambda'$ did not contain a correction for the sun angle.$M\rho$ = Band-specific multiplicative rescaling factor from the metadata (REFLECTANCE_MULT_BAND_x, where x was the band number),$A\rho$ = Band-specific additive rescaling factor from the metadata (REFLECTANCE_ADD_BAND_x, where x is the band number),Qcal = quantized and calibrated standard product mixel values (DN), TOA reflectance with a correction for the sun angle is then:$\rho\lambda=\rho\lambda'\cos(\theta sz)=\rho\lambda'\sin(\theta se)$ where: $\rho\lambda$ = TOA planetary reflectance θse = Local sun elevation angle. The scene center sun elevation angle in degrees is provided in the metadata (SUN_ELEVATION).θsz = Local solar zenith angle; $\theta sz = 90° - \theta se$.

The ENVI software easily converted the optical Red Eye band data to ToA reflectance values. A file was opened that ended with "_MTL.TXT". From the ENVI main menu bar, "Open Image File" was selected. ENVI automatically opened the canopy shaded *S. damnosum* s.l. larval habitat image as multiple files. For creating a reflectance data file from the ENVI main menu bar, the Basic Tools, Preprocessing and Calibration Utilities was used. The optical data file and the *ENVI Calibration* dialog opened all the filled in calibration parameters. By clicking the Reflectanceradio button an output file name (i.e., *S. damnosum* s.l.) was entered. The reflectance values ranged from 0.0 to 1.0 which was stored in floating point data format.

Digital Numbers were converted to radiance vegetated, shade, canopied *S. damnosum s.l* larval habitat georeferenced values. Thereafter, these radiance values were converted to reflectance values. The formula to convert DN to radiance values of the geosampled, larval habitat data was based on gain and bias within $L_\lambda = gain^* DN + bias$ where: L_λ was the cell value (i.e., radiance estimate) and DN was the cell value. It was noted that DN gain was the gain value for a specific Rapid Eye band and bias was the deviated value for any specific, canopy, shaded, *S. damnosum* s.l. reflectance band. The ENVI formula in Band Math as 0.05518 * (B1) + 1.2378 was calculated using a scene specific gain value of 0.05518 and an offset value of 1.2378. In the Band Pairing dialog B1 was matched with the appropriate optical band. The formula employed in this process was as follows:

$$L_{L\lambda} = ((LMAX_\lambda - LMIN_\lambda / (QCALMAX - QCALMIN))$$

$*(QCAL - QCALMIN) + LMIN_\lambda$ where:L_λ was the cell value as radiance, QCAL was the DN, LMIN was the spectral radiance scales to QCALMIN, $LMAX_\lambda$ was Rapid Eye spectral radiance scales to QCALMAX, QCALMIN was the minimum quantized calibrated 5 m mixel value and QCALMAX was the maximum quantitated calibrated mixel value (i.e.,255) radiance to ToA reflectance.

The formula $\rho_\lambda = \pi * L_\lambda * d^2 / ESUN * \cos\theta_S$ was then employed to quantitate multiple illumination, viewing angle, reflectance, wavelenght coefficients where: ρ_λ was the unitless $\rho_\lambda = \pi * L_\lambda * d^2 / ESUN * \cos\theta_S$ plantary reflectance; L was the RapidEye spectral radiance; d was the Earth-Sun distance in astronomical units; $ESUN_\lambda$ was the mean solar exoatmospheric irradiances and θ_s was solar zenith angle. Solar exoatmospheric irradiance and Rayleigh optical thickness within pass band of each space borne sensor were then estimated for calculating the most basic physical parameter, namely ground reflectance.

For calculating the solar exoatmospheric irradiance and Rayleigh optical thickness within the Rapid Eye band data, modern Rayleigh scattering calculations were employed in AreGIS. Spectral data on extraterrestrial solar radiation, Rayleigh scattering, ozone absorption and absorption by the uniformly mixed gases are critically evaluated and used for computing the integral Rayleigh optical thickness of the clean and dry atmosphere for a given relative optical air mass or solar elevation angle [2]. The results are commonly compared to the corresponding values calculated with the help of the three parameterization formulae. We used the Penndorf [122] method for calculating Rayleigh optical thickness of the geosampled, georefernced, *S. damnosum* s.l. riverine larval habitat canopy. In Penndorf's paper, the refractive index of air was calculated using the equation of Edlén [123]: $(n_S - 1)\times 10^8 = 6432.8 + \frac{2949810}{146-\lambda^{-2}} + \frac{25540}{41-\lambda^{-2}}$ where n_s was the refractive index of air and λ is the wavelength of light in micrometers. This equation is for "standard" air, which is defined as dry air at 760 mm Hg (1013.25 mb), 15°C (288.15 K), and contains 300 ppm CO_2. It is an empirical relationship derived by fitting the best available experimental data and is dependent on the composition of air, particularly CO_2 and water vapor. Next, Penndorf [122] calculated the Rayleigh scattering coefficient for standard air using the classic equation that is presented in many textbooks [124,125]: $\sigma = \frac{24\Pi^3 (n_S^2 - 1)^2}{\lambda^4 N_S^2 (n_S^2)^2}\left(\frac{6+3\rho}{6-7\rho}\right)$ where σ was the scattering cross section per molecule; N_s was molecular density; the term $(6 + 3\rho)/(6 - 7\rho)$ was the depolarization term, *F*(air), or the King factor; and ρ was the depolarization factor or depolarization ratio, which described the effect of molecular anisotropy. The *F* (air) term is the least known for purposes of Rayleigh scattering calculations and is responsible for the most uncertainty [4].

In the calculations of the *S. damnosum* s.l., riverine, larval habitat, canopy in in ArcGIS derived Rayleigh optical thickness, the depolarization term did not depend on temperature and pressure, but did depend on the shade mixture within the geosampled, georeferenced shaded, vegetated, canopied, *S. damnosum* s.l. explanatorial, larval habitat geosampled at the Chutes Dienkoa, eco-epidemiological, riverine, study site. Also, we assumed in the habitat N_s was dependent on temperature and pressure, but not depend on the gas mixture. The resulting value of σ, in the model was the scattering cross section per molecule of the gas which would then we assumed was independent of temperature and pressure, but not dependent on the composition of the gas.

Note in the *S. damnosum* s.l. model, N_s depended on Avogadro's number and the molar volume constant, and was expressed as molecules per cubic centimeter, and that values. However, since $(n^2_s - 1)/(n^2_s + 2)$ is proportional to N_s, Bucholtz [126], the resulting expression for σ in the shade, vegetated canopied, model was independent of temperature and pressure. Note that the usual approximation $n^2_s + 2 \approx 3$ was not included in the interest of keeping all calculations as accurate as possible. Results of such calculations were presented and the table of values employed over particular Rapid Eye™ wavelength ranges emitted from the georeferenced, geosampled, shaded, and vegetated canopied, *S. damnosum* s.l. larval habitat.

We used the general formula for calculating the shaded canopied, *S. damnosum* s.l. larval habitat.ground reflectance where (r) was *tv Eo stz EdLs Lp d*+-=qpr(cos) . In this equation *Lp* denoted path radiance, *d*-earth to sun distance in astronomical units, *Eo* –bandpass exoatmospheric irradiance, *Ed* - down welling spectral irradiance from the atmosphere, *tv* – atmospheric transmittance along the path from the *S. damnosum* s.l. larval habitat to the Rapid Eye sensor, and *tz* – atmospheric transmittance along the path from the sun to ground. The transmittance terms were then calculated using the equations: *tv*= exp (-t secq *v*) *and tz* = exp (-t secq *s*). Here *v*q and *s*q were, respectively, the zenith angles of the sun and sensor. The parameter t was the total optical thickness of the atmosphere, which included the effect of aerosol particles, ozone, water vapor and atmospheric, molecules. Out of these, the canopy illumination contribution was calculated which depended strongly on the Rapid Eye™ wavelength which we estimated from *r* = exp (-0.1188* *h* - 0.00116* *h*2) {0.00859 *l-4 (1 + 0.0013*l-2 + 0.00013*l-4)} where h was the height of the georeferenced, canopy, shaded, *S. damnosum* s.l.,canopy vegetated, larval, habitat surface above sea level.

The solar zenith angle was then calculated employing the Solar Position Calulator. The solar zenith angle is the angle measured from directly overhead to the geometric centre of the sun's disc, as described using a horizontal coordinate system [2]. The horizontal coordinate system is a celestial coordinate system that employs the observer's local horizon as the fundamental plane. It is expressed in terms of altitude (or elevation) angle and azimuth. The solar elevation angle is the altitude of the sun, the angle between the horizon and the centre of the sun's disc [2,4,115]. If we write θ_s for the solar zenith angle, then the solar elevation angle α_s=90° – θ_s. [127]. The calculator program returns solar zenith angle, declination, Julian day, equation of time, hour angle, instantaneous and daily extraterrestrial radiation values, and sunrise and sunset times (http://solardat.uoregon.edu/SolarPositionCalculator.html).

Next, ENVI's Radiometric Calibration tool calibrated the Rapid Eye 5 m imagery from spaceborne sensors to radiance and ToA reflectance. An atmospheric correction tool Fast Line-of-sight Atmospheric Analysis of Spectral Hypercubes (FLAASH®) then removed the effects of atmospheric scattering and gas absorptions to produce optimal surface reflectance of the geosampled, riverine, S. larval habitat data. FLAASH automatically scales reflectance data by 10,000 to produce integer data, which consumes less disk space (www.Ittvis.com/portals). Other tools in ENVI such as Dark Subtraction, Empirical Line Correction, Flat Field Correction, and Internal IAR Reflectance Correction also helped correct for atmospheric effects for preparing the multispectral data for generating the Red Edge spectral index.

Once a dataset of the explanatorial, remotely-dependent, operationizable, covariate, parameterized, estimator coefficients was constructed, ENVI spectral tools were used to analyze the 5m satellite image of the shade, vegetated, *S. damnosum s.l.,* riverine habitat canopy.

F^0	extraterrestrial solar radiance
$F(\bullet)$	Fresnel reflectance function
$f(\Omega',\Omega)$	BRDF of soil
$gl(\Omega)$	distribution function of the leaf normal orientation
$\Gamma(\Omega',\Omega)$	area scattering transfer function of canopy
H	height of canopy in meters
i^0	extraterrestrial solar net flux incident on the top of atmosphere
$I^0(\tau,\Omega)$	unscattered solar radiance
$I^1(\tau,\Omega)$	single scattering radiance
$I^M(\tau,\Omega)$	multiple scattering radiance
$J^M(\tau,\Omega)$	source function of radiative transfer
κ	leaf dimension parameter
λ	wavelength
LAD	leaf angle distribution
LAI	leaf area index
μ_0	cosine of solar zenith angle
η	leaf wax refractive index
N	total Lumber of layers of the coupled medium split for multiple scattering calculation, each of thickness $\Delta\tau$
$\Omega(\mu,\phi)$	solid angle consisting of cosine of zenith angle μ and azimuth angle ϕ
$P(\Omega',\Omega)$	phase function of atmosphere
ϕ_0	solar azimuth angle
rl	leaf reflectance
$R^s(\Omega',\Omega)$	bidireccional reflectance factor of soil surface
R^s	reflectance of Lambertian surface
τ	optical depth of medium
τ_α	atmospheric optical depth
$\tau_{\alpha e}$	aerosolopticaldepth
τ_Γ	molecularopticaldepth
τ_t	total optical depth of the coupled atmosphere-canopy medium
$u_l($	leaf transmittance
$u_l(z)$	leaf area density
ω	single scattering albedo

Table 5: Theradiative transfer equation predictor covariatecoefficients in thedecomposition of theradiationfield of thegeorefrenced*S.damnosum s.l.*riverine larval habiatmodel.

We input the data into ENVI® technology using the GeoTIFF format. ENVI supports Input File functions including GeoTIFF, NITF and Tile Product (.til) (www.ittvis.com/portals). In ENVI a spectrum plot, known as a *z*-profile, of the mixel under the cursor was run through all bands of the 5m image. The basic workflow involved importing the decomposed data collected at the Chutes –Dienkoa riverine study site from the explanatorial, operationizable, geospatially interpolatable, geosampled, shade, vegetated, canopied, *S. damnosums.l.,* larval habitat habitat data into a spectral library. A spectral library was used in the endmember collection workflow to perform a supervised classification, based on the reflectance values of each image attribute and the habitat data. Binary Encoding, Spectral Angular Mapping (SAM) and Spectral Feature Fitting were then employed to rank and match any unknown spectrum to the materials in the library.

The image endmembers of the georeferenced, shade, vegetated, canopied, *S. damnosum s.l.* habitat and its associated attributes were then extracted them from ENVI®'s spectral library. Several spectra corresponding to the different backgrounds in the geosampled, explanatorial, *S. damnosum s.l.,* riverine, larval habitat (i.e., rippled water mixel components) scene had to be included, since multiple scatterings between floating leaves in the habitat, for example, and a bright soil background increased the NIR reflectance of eachsatellite data product generated in the object-based classifier. Leaf cells have evolved to scatter (i.e., reflect and transmit) solar radiation in the NIR spectral region [4,75].

After the calibration of all the spectrally dependent explanatorial, *S. damnosum s.l.* habitat canopy covariate coefficient estimates, we then determined if the images could be converted to match spectral contents within the ENVI library. Analogously, the reference endmembers spectra in the library were transformed into the endmembers spectra of thegeoreferenced larvalhabitat Red Eye image. We employed a random selection of mixels to assess the satellite classification accuracy. Each image class representative mixels were then selected and compared to a reference training dataset. During the segmentation procedure, image objects were generated based on several adjustable criteria of homogeneity such as colour, shape, and texture

Data pre-processing involved converting DN to radiance atmospheric correction using FLAASH™, and co-registration techniques. Image classification was then performedemploying an object-oriented approach. FLAASH™ generated multiple models (.gmd file). We then converted the Red Eye, georeferenced riverine *S. damnosum* s.l. habitat image DN to at-sensor radiance and computed at-sensor reflectance for normalizing the solar elevation angle. The equation we used was as follows: $\rho BandN = \frac{\prod\left(LBandN * GainBandN + BiasBandN\right) * D^2}{EBandN * \left(COS((90-\theta) * \pi / 180)\right)}$ where, $_{\text{BandN}}$=Reflectance for Band NL_{bandN}=Digital Number for Band N D=Normalized Earth-Sun DistanceE_{bandN}=Solar Irradiance for Band N. Most surfaces are not perpendicular to the Sun, and the energy they receive depends on their solar elevation angle. The maximum solar elevation is 90° for the overhead Sun.(http://www.britannica.com/ / solar-elevation-angle).

The reference data was the "ground truth" data of the explanatorial, geo-spatiotemporal-geosampled, shade, canopied, *S. damnosum* s.l., riverine, georeferenced, larval habitat, within-canopy-related, spectrally dependent, explanatorial, predictor variables (e.g., floating vegetation fractionalized radiance values). Selected random image mixels from the thematic map were compared to the reference data. The estimated accuracy for the spectrally extracted data was then calculated using: $P = \left[-Z_{\alpha/2} \angle \frac{x - n\theta}{\sqrt{n\theta(1-\theta)}} \angle Z_{\alpha/2}\right] = 1 - \alpha$ where, x=number of correct identified mixels, n=total number of pixels in the sample, θ=the map accuracy, (1-α)=a confidence limit.

The successive projection algorithm (SPA)

The SPA was then employed in ArcGIS to generate canopy-based, shaded, Red Edge, *S. damnosum* s.l., larval habitat, NDVI, endmember signature. *P*(*i, j*) denoted the spectrum for the spectrally extracted 5m mixels using the image coordinates (*i, j*), as the foundation of the unmixing algorithm which was defined by using $\overline{p}_{(i,j)} = \sum_{k=1}^{m} f_{(i,j)k^{\vec{e}_k}} + \vec{\varepsilon}_{(i,j)}$ and also where *m* was the number of the canopy endmembers, $\vec{e}_k$ was the *kth* endmember, $\vec{\varepsilon}_{(i,j)}$ was the approximation error term (i.e., residual), and *f* (*i j*) *k*, was the fractional abundance for the *kth* endmember of 5 m mixel (*i, j*). The error term in $\overline{p}_{(i,j)} = \sum_{k=1}^{m} f_{(i,j)k^{\vec{e}_k}} + \vec{\varepsilon}_{(i,j)}$ computed the possible linear mixtures from $\overline{p}_{(i,j)} = \sum_{k=1}^{m} f_{(i,j)k^{\vec{e}_k}} + \vec{\varepsilon}_{(i,j)}$ and $f_{(i,j)k} \geq 0, K = 1, \ldots m, \sum_{k=1}^{m} f_{(i,j)k} = 1$ which formed a simplex *Cm* defined by *m* vertices which corresponded to the Red Edge NDVI decomposed biosignature shade,canopied, unmixed endmembers, $\vec{e}_1, \vec{e}_2, \ldots., \vec{e}_m$. According to Jacob et al. [5] the volume of the simplex *Cm* can be calculated from the equation $V\left(C_m\right) = \frac{1}{(m-1)}\left\lceil \det\left(WW^{\tau}\right)\right\rceil^{\frac{1}{2}}$ where $W = \left\lceil \vec{e}_2 - \vec{e}_1, \vec{e}_3 - \vec{e}_1, \ldots., \vec{e}_n - \vec{e}_1 \right\rceil$ is the volume of the simplex defined by *m* endmembers, and where det (·) denotes the determinant of a matrix representing the operation of an absolute value. In this research, once the Red Edge, shade canopied, georeferenced, *S. damnosum s.l.,* larval habitat, Red Edge, NDVI endmembers $\vec{e}_1, \vec{e}_2, \ldots., \vec{e}_m$ were determined their fractional abundance was estimated through the least squares method which was equivalent to the projection $W = \left\lceil \vec{e}_2 - \vec{e}_1, \vec{e}_3 - \vec{e}_1, \ldots., \vec{e}_n - \vec{e}_1 \right\rceil$ ion on the simplex.

Radiative transfer model

We then focused on the radiation field of the atmosphere and canopy as a single coupled medium, and the radiative transfer models of atmosphere and canopy which was separately described because of their different attenuating properties in ArcGIS. The coupled mediums illustrated the Red Edge, NDVI, *S. damnosum s.l.*, larval habitat, decomposed, sub-mixel, endmember biosignature on various equations in which optical depth replaced the geometric altitude values. The top of atmosphere was set to -r=0 while the bottom was set to Ta, and the total optical depth to Tt. Therefore, the optical depth of the larval habitat canopy was calculated using Tt—Ta, which was interpreted employing LAI which was calculated using $P = P_{\max}\left(1 - e^{-c.LAI}\right)$ where $P_{\max}$ designated the maximum primary production and C designated a growth coefficient. This inverse exponential function then generated a primary production function.

Next, in order to geospatially characterize the shade, vegetated, canopied, *S. damnosum s.l.,* riverine, larval habitat, hotspot phenomenon effectively and obtain stable solutions of within-canopy, multiple scattering, we decomposed the spectrally extracted, Red Edge, unmixed biosignature signature into three parts; unscattered radiance $\mathrm{I}^0(\tau,\Omega)$, single scattering radiance, and multiple scattering radiance $\mathrm{I}^{\mathrm{M}}(\tau,\Omega)$ $\mathrm{I}(\tau,\Omega) = \mathrm{I}^0(\tau,\Omega) + \mathrm{I}^1(\tau,\Omega) + \mathrm{I}^{\mathrm{M}}(\tau,\Omega)$ in ArcGIS. A simple scheme was then represented by $\mathrm{I}^0(\tau,\Omega)$ which was denoted by 1, which was not scattered by the atmosphere, but was reflected directly by the within canopy surface features. In this research, $\mathrm{I}^1(\tau,\Omega)$ was the various Red Edge, NDVI, canopy, biosignature radiance values either scattered once by the atmosphere, denoted by 2, or once by the within canopy, structural, explanatorial, spectral variables which was denoted by 3. Also $\mathrm{I}^{\mathrm{M}}(\tau,\Omega)$ was the most complicated component, which included all of other imaged, riverine, larval habitat, canopied, explanatorial, operationizable, georeferenced components in the radiation field of the coupled medium. Unscattered sunlight radiances $\mathrm{I}^0(\tau,\Omega)$ were then characterized by the following radiative transfer equation and corresponding boundary conditions. When T< Ta the radiative transfer model rendered:

$$\begin{cases} -\mu\dfrac{\partial \mathrm{I}^0(\tau,\Omega)}{\partial\tau}+\mathrm{I}^0(\tau,\Omega)=0 \\ \mathrm{I}^0(0,\Omega)=\delta(\Omega-\Omega_0)i_0 \qquad \mu<0 \quad \text{where } \tau_a^{bot} \text{ the result was} \\ \mathrm{I}^0\left(\tau_\alpha^{bot},\Omega\right)=\mathrm{I}^0\left(\tau_c^{top},\Omega\right) \qquad \mu>0 \end{cases}$$

τ_c^{top} where the optical depths was at the bottom of the atmosphere and the ToA of the larval habitat canopy, respectively. Here different notations from the 5m imager were used to indicate the physical meaning of the canopy boundary conditions. The model provided the upper boundary condition, which meant only parallel sunlight illuminated the atmosphere at the top of the riverine, larval habitat, shaded, canopy in the direction Ω_0. When $\tau>\tau_\alpha$, the residuals were:

$$\begin{cases} -\mu\dfrac{\partial \mathrm{I}^0(\tau,\Omega)}{\partial\tau}+h(\tau,\Omega)G(\Omega)\mathrm{I}^0(\tau,\Omega)=0 \\ \mathrm{I}^0\left(\tau_c^{top},\Omega\right)=\mathrm{I}^0\left(\tau_\alpha^{bot},\Omega\right) \qquad \mu<0 \\ \mathrm{I}^0(\tau_t,\Omega)=fs(\Omega_0,\Omega)|\mu_0|\mathrm{I}^0(\tau_t,\Omega_0) \qquad \mu>0 \end{cases}$$

Jointly solving the above equations with these boundary conditions rendered:

$$\mathrm{I}^0(\tau,\Omega)=$$

$$\begin{cases} \mathrm{I}_{d1}^0(\tau,\Omega)=i_0\exp(-\tau/|\mu|)\delta(\tau,\Omega_0) \qquad \mu<0,\tau\le\tau_\alpha \\ \mathrm{I}_{d2}^0(\tau,\Omega)=\mathrm{I}_{d1}^0(\tau,\Omega) \\ \cdot\exp\left[-C(\Omega)(\tau-\tau_\alpha)/|\mu|\right] \qquad \mu<0\tau_\alpha<\tau\le\tau_t \\ \mathrm{I}_{u2}^0(\tau,\Omega)=i_0 \\ \cdot\exp\left[-\dfrac{\tau_\alpha+(\tau_t-\tau_\alpha)G(\Omega_0)}{|\mu_0|}\right] \\ \cdot fs(\Omega_0,\Omega)|\mu_0|\exp\left[-\varepsilon(\tau,\Omega)\right] \qquad \mu>0,\tau_\alpha<\tau\le\tau_t \\ \mathrm{I}_{u1}^0(\tau,\Omega)=\mathrm{I}_{u2}^0(\tau_\alpha,\Omega) \\ \cdot\exp\left[-(\tau_\alpha-\tau)/\mu\right] \qquad \mu>0,\tau\le\tau_\alpha \end{cases}$$

The Red Edge, NDVI, biosignature, sub-mixel information was expressed as $\mathrm{I}_{u2}^0(\tau,\Omega)$ which represented the upwelling sunlight radiance within the georeferenced geosampled, vegetated, *S. damnosum* s.l. larval habitat canopy, and the function $\varepsilon(\tau,\Omega)$. We modified the extinction coefficients of the canopy endmembers. We then incorporated the extracted, within-canopy, radiance values including the floating, hanging and surrounding dead vegetation canopy geospectral components employing:

$$\varepsilon(\tau,\Omega)=\frac{1}{\pi}\int_\tau^{\tau_t}\mathrm{h}(\mathrm{t},\Omega)\mathrm{G}(\Omega)\mathrm{dt}=\mathrm{G}(\Omega)\frac{\tau_\mathrm{t}-\tau}{\mu}-\left[\sqrt{\frac{\mathrm{G}(\Omega_0)\mathrm{G}(\Omega)}{\mu|\mu_0|}}\frac{\mathrm{kH}}{\Delta(\Omega_0,\Omega)}\right]\mathrm{t}_0$$

where t0 was defined as $t_0=\exp\left[-\dfrac{\Delta(\Omega_0,\Omega)\tau}{k\mathrm{H}}\right]-\exp\left[-\dfrac{\Delta(\Omega_0,\Omega)\tau_t}{k\mathrm{H}}\right]$

The Red Edge, NDVI, endmember, unmixed, biosignature model in ArcGIS revealed that for single scattering radiances, unscattered sunlight became the scattering source, and the boundary conditions. These conditions were then determined based on the fact that no incident single scattering radiances originated from above ToA or below the bottom of the canopy. When T<Ta occurred in the model, the residuals rendered:

$$\begin{cases} -\mu\dfrac{\partial \mathrm{I}^l(\tau,\Omega)}{\partial\tau}+\mathrm{I}^l(\tau,\Omega)= \\ \dfrac{\omega i_0}{4\pi}p(\Omega_0\to\Omega)\exp\left(-\dfrac{\tau}{\mu_0}\right) \\ r^1(0,\Omega)=0 \qquad \mu<0 \\ \mathrm{I}^1\left(\tau_\alpha^{bot},\Omega\right) \qquad \mu>0 \end{cases}$$

Additionally, when T >T the decomposition, *S. damnosum* s.l., larval hábitat, eco-epidemiological, risk model rendered:

$$\begin{cases} -\mu\dfrac{\partial \tau^1(\tau,\Omega)}{\partial\tau}+h(\tau,\Omega)G(\Omega)\mathrm{I}^1(\tau,\Omega) \\ \dfrac{i_0'}{\pi}\Gamma(\Omega_0,\to\Omega)\exp\left[-(\tau-\tau_\alpha)\dfrac{G(\Omega_0)}{|\mu_0|}\right] \qquad \text{where } i_0' \text{ was the} \\ \mathrm{I}^1\left(\tau_c^{top},\Omega\right)=\mathrm{I}^1\left(\tau_\alpha^{bot},\Omega\right) \qquad \mu<0 \\ \mathrm{I}^1(\tau_t,\Omega)=0 \qquad \mu>0 \end{cases}$$

incident solar net flux arriving at the top of the habitat canopy, $i_0'=i_0\exp\left(-\tau_\alpha/|\mu_0|\right)$ In the downward direction $\mu<0$, the solution was easily derived. When T < Ta, the riverine, larval habitat, Red Edge, NDVI, endmember, biosignature, risk decomposition model was solved using :

$$\mathrm{I}^l(\tau,\Omega)=$$

$$\begin{cases} \dfrac{\omega Fop(\Omega_0\to\Omega)|\mu_0|}{4(|\mu_0|\leftarrow|\mu|)}\left[\exp\left(-\dfrac{\tau}{|\mu_0|}\right)-\exp\left(-\dfrac{r}{|\mu|}\right)\right] \qquad \Omega\ne\Omega_0 \\ \dfrac{\omega F_0\tau}{4|\mu_0|}P(\Omega_0\to\Omega)\exp\left(-\dfrac{\tau}{\mu_0}\right) \qquad \Omega=\Omega_0 \end{cases}$$

Then $\tau_\alpha<\tau<\tau_t$ was solved using the equation:

$$\mathrm{I}^1(\tau,\Omega)=$$

$$\begin{cases} \dfrac{i_0'|\mu_0|\Gamma(\Omega_0\to\Omega)}{\pi\left[G(\Omega)|\mu_0|-G(\Omega_0)|\mu|\right]}t_1+\Delta\mathrm{I}^1(\tau,\Omega) \qquad \Omega\ne\Omega_0 \\ \dfrac{(\tau-\tau_\alpha)i_0'\Gamma(\Omega_0\to\Omega)}{\pi|\mu_0|}\exp\left[-G(\Omega_0)\dfrac{\tau-\tau_\alpha}{|\mu_0|}\right] \\ +\Delta\mathrm{I}^1(\tau,\Omega) \end{cases}$$

where t_1 was defined by the equations

$$t_1=\exp\left[-G(\Omega_0)\frac{\tau-\tau_\alpha}{|\mu_0|}\right]-\exp\left[-G(\Omega)\frac{\tau-\tau_\alpha}{|\mu|}\right]\text{and}$$

$$\Delta \mathrm{I}^1(\tau,\Omega)=\mathrm{I}^1(\tau_\alpha,\Omega)\exp\left[-G(\Omega)(\tau-\tau_\alpha)/|\mu|\right]$$

which represented the single scattering riverine larval habitat canopy radiances emerging from the atmosphere without scattering in the riverine *S. damnosum s.l.* larval habitat canopy.

$$\mathrm{I}^1(\tau,\Omega)=\begin{cases} \dfrac{1}{\mu}\displaystyle\int_r^{\tau_t} F(\tau',\Omega) & \\ \cdot\exp\left[-\dfrac{1}{\mu}\displaystyle\int_\tau^{\tau'} h(\varepsilon,\Omega)G(\Omega)\,d\varepsilon\right]d\tau' & \tau_\alpha\le\tau\le\tau_t \\ \dfrac{\omega F_0 p(\Omega_0\to\Omega)|\mu_0|}{4(\mu+|\mu_0|)}t_2 & \\ +\mathrm{I}^1(\tau_\alpha,\Omega)\exp\left(\dfrac{\tau-\tau_\alpha}{\mu}\right) & \tau<\tau_\alpha \end{cases}$$

In the upward direction (p > 0), the solutions were a little more complicated because of the hotspot effect which was determined by

where t_2 was: $t_2=\exp\left[-\dfrac{\tau}{|\mu_0|}\right]-\exp\left[\dfrac{\tau}{\mu}-\left(\dfrac{1}{\mu_0}+\dfrac{1}{\mu}\right)\tau_\alpha\right]$ and the second integration at Ta < T < Tt. This equation was then explicitly obtained by means of an alternative integer and range, which was solved using $F(\tau',\Omega)=\frac{i_0'}{\pi}\Gamma(\Omega_0\to\Omega)\exp\left[-G(\Omega_0)(\tau-\tau_\alpha)/|\mu_0|\right]$. The radiance $\mathrm{I}^1(\tau,\Omega)$ at Ta < T <Tt derived for the Red Edge, NDVI, endmember, unmixed biosignature signature material was then numerically evaluated without further assumptions. An explicit approximation to $\mathrm{I}^1(\tau,\Omega)$ was then derived and used for inversion in the canopy, biosignature-related, decomposition, eco-epidemiological, risk model.

Inverted geometric-optical model

We then employed the Li-Strahler geometric-optical model based on the assumption that the BRDF would retrieve georeferneced, *S. damnosum s.l.,* habitat, shaded, canopy-oriented, structural variables from the decomposed, Red Edge, NDVI, endmember, biosignature variables in ArcGIS. The Li-Strahler geometric-optical model [113] is based on the assumption that the BRDF is a purely geometric phenomenon resulting from a scene of discrete 3-dimensional objects being illuminated and viewed from different positions in the hemisphere.

The unmixing technique in this algorithm has been previously described in Jacob et al. [1]. Briefly, the BRDF was first defined by $f_r(\omega_i,\omega_r)=\dfrac{dL_r(\omega_r)}{dE_i(\omega_i)}=\dfrac{dL_r(\omega_r)}{L_i(\omega_i)\cos\theta_i d\omega_i}$ where *L* was the radiance, *E* was the irradiance, and θ_i was the angle made between ω_i and the georeferenced, vegetated, shade, canopied,riverine, *S. damnosum* habitat and its associated floating, vegetation, LULC, surface reflectance emissivities. Because the BRDF is a four-dimensional function that defines how light is reflected at an opaque surface (2), the function took an incoming light direction, ω_i, and outgoing direction, ω_o, which were both defined in the Red Edge, NDVI, canopy, endmember signature with respect to the georeferenced, *S. damnosum,* larval habitat and its neighboring floating vegetation, hanging, floating and dead vegetation geoclassified LULC, and returned the ratio of reflected radiance exiting along ω_o to the irradiance incident from direction ω_i. Note, each direction ω was itself parameterized by azimuth angle φ and zenith angle θ, therefore, the BRDF was 4-dimensional. The BRDF had units sr^{-1}, with steradians (sr) being a unit of solid angle.

We also employed Lambertian reflectionin ArcGIS. In computer graphics, Lambertian reflection is often used as a model for diffuse reflection [2]. This technique causes all closed polygons (such as a triangle within a 3D mesh) to reflect light equally in all directions when rendered [128]. In effect, a georeferenced, shade, vegetated, *S.*

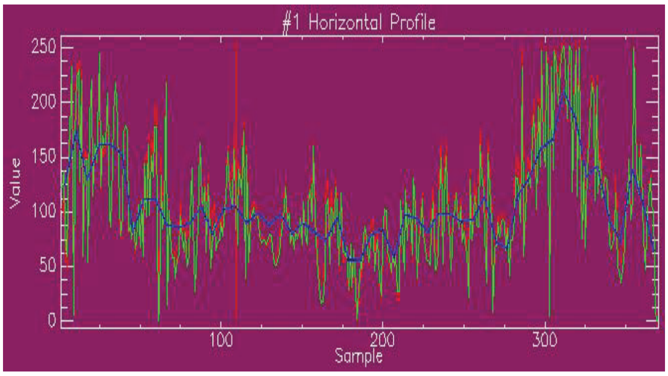

Figure 10: A decomposed Red Edge *S. damnosum s.l.* larval habitat NDVI signature.

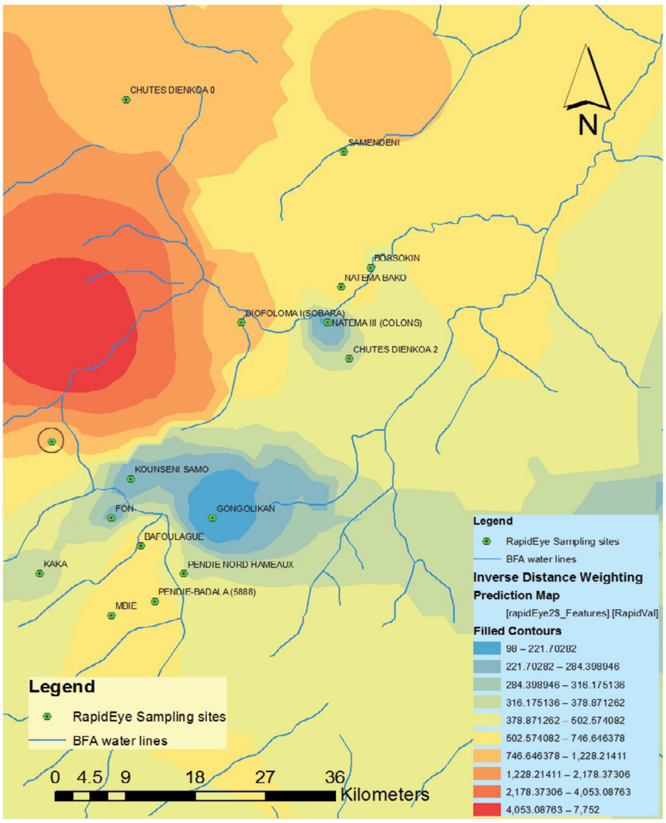

Figure 11: A Geospectrally interpolated Red Edge *S. damnosum* s.l. larval habitat NDVI signature at the Dienkoa study site.

damnosum s.l. canopied, larval habitat rotates around its normal vector will not change the way it reflects light [3]. However, the habitat canopy will change the way it reflects light if it is tilted away from its initial normal vector since the area is illuminated by a smaller fraction of the incident radiation [5]. Here the reflection was calculated by taking the dot product of the surface's normal vector, **N**, and a normalized light-direction vector, **L**, pointing from the surface to the light source.

The canopy reflection was calculated by taking the dot product of the surface's normal vector, **N**, and a normalized light-direction vector, **L**, pointing from the surface of the georeferenced habitat and its light sources. This number was then multiplied by the color of the surface and the intensity of the light of the canopy surface: $l_D = L.NCI_L$ where I_D was the intensity of the diffusely canopy reflected light (i.e., surface brightness), C was the color and I_L was the intensity of the light. Because $L.N = |N||L|\cos\alpha = \cos\alpha$, where α was the angle between the direction of the two vectors, the illumination intensity wasthe highest when the vector pointed in the same direction as the light vector (i.e., $\cos(0) = 1$).When the surface is perpendicular to the direction of the light), the normal vector is perpendicular to the light vector (i.e., $\cos(\prod/2) = 0$, the surface runs parallel with the direction of the light) [12].

The inverted geometric-optical model was then used to retrieve specific spectral Red Edge, NDVI, canopy biosignature canopied, georeferenced, operationizable, riverine, larval habitat, explanatorial, wavelenght ,emissivity, reflectance, covariate, coefficient estimates. The reflectance associated with a georeferenced habitat was treated as an area-weighted sum of four fixed reflectance components: sunlit canopy, sunlit background, shaded canopy, and shaded background. In the georeferenced shade, vegetated, *S. damnosum s.l.* canopied, larval habitat, geometric-optical model these four components were simplified to three: sunlit canopy–C, sunlit background–G and shadow–T . The endmember spectral components were derived using G, C, T components' classes which were initially estimated by the 5m Rapid Eye image using ENVI®. For inverting the model, parts of the three spectral canopied, larval habitat, shaded components were represented by (Kg) which was calculated using:

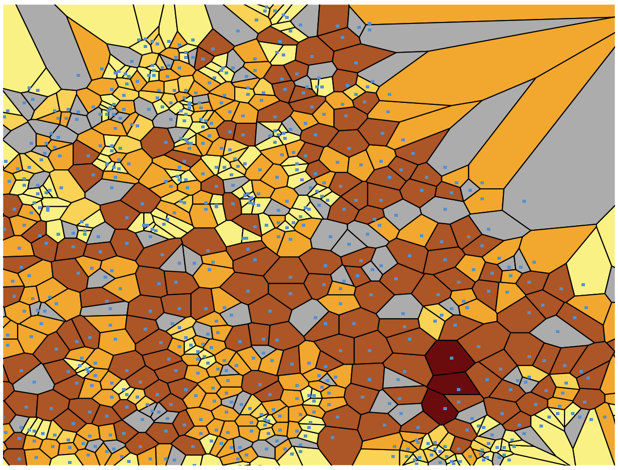

Figure 12: Voroni Tesselations for the geospectral interpolation of the decomposed Red Edge *S. damnosum* s.l. habitat signature of the Dienkoa study site.

$$K_g = e^{-\Pi.M.\left[Sec(\theta_i)+Sec(\theta_V)-o(\theta_i+\theta_V)\phi\right]} \tag{2.1}$$

$$O(\theta_i,\theta_v,\phi) = 1/\pi\left(\sec\theta_i + \sec\theta_v\right)\left(t - \sin t\cos t\right) \tag{2.2}$$

$$\cos t = \frac{h\left|\tan\theta_i - \tan\theta_v\cos\phi\right|}{r\left(\sec\theta_i + \sec\theta_v\right)} \tag{2.3}$$

$$M = \frac{-\ln\left(K_g\right)}{\left(\sec\theta_i + \sec\theta_v\right)\left(\pi - t + \cos t\sin t\right)} \tag{2.4}$$

$$CC = 1 - e^{-\pi\cdot M} \tag{2.5}$$

where, *I q u q* were the zenith angles of illumination and viewing.*O* was the average of the overlap function between illumination and viewing shadows of the Rapid Eye imagers, sub-mixel, endmember, spectral version of the decomposed, Red Edge, NDVI, *S. damnosum s.l.*, habitat, unmixed, biosignature and their associated canopy floating, hanging dead vegetation-related LULC components as projected onto the background. *j* was the difference in azimuth angle between illumination and viewing in each model.

Boolean models were then generated in ArcGIS. The equation $R(i,v) = K_g G + \frac{C}{A}\iint_{A_c}\frac{\langle i,s\rangle}{\cos\theta_i}\frac{\langle v,s\rangle}{\cos\theta_v}ds$ was employed where K_g was expressed as $K_g = e^{-\lambda\prod R^2\left[Sec\theta_i'+Sec\theta_V'-\bar{o}(\theta_i,\theta_V,\psi)\right]}$ and where $\bar{O}(\theta_i,\theta_v,\varphi,)$ was the average of the overlap function $O(\theta_i,\theta_v,\varphi,h)$ between illumination and viewing shadows of the georeferenced, geosampled, *S. damnosum* s.l. riverine larval habitat and its associated data feature attributes. The Boolean model for a random subset of the plane or higher dimensions, analogously is a common tractable models in stochastic geometry [4].

Further, ϕ was the difference in azimuth angle between viewing and illumination positions of the 5 m Rapid Eye™ imaged objects associated to the riverine, georeferenced, geosampled, *S. damnosum* s.l., riverine habitat. To simplify the equation, the overlap function was approximated by the overlap area and center positions of the ellipses. This approximation is justified when solar zenith and viewing zenith angles are not too large [10]. In the case of long ellipsoidal shadows, however, this approximation could have overestimated the width of the *S. damnosum s.l.*, riverine, habitat hotspot in the azimuthal direction and underestimated the width of the hotspot in the azimuthal direction. To improve the accuracy and preserve the proper hotspot width information, another approximation was developed as follows; $\varphi = 0$ *or* $\varphi = \pi$. First, the overlap function was determined in the principal plane. W $\varphi = 0$ and π were employed as the elliptical illumination estimates and then the viewing shadows were aligned in the same direction. The overlap area was approximated by an ellipse with one axis equal to the overlap length and the other equal to the *S. damnosum* s.l. geospatiotemporally-geosampled, habitat width encompassing hanging, floating and dead vegetation spectral explanatorial components which yielded

$$O(\theta_i,\theta_v,\varphi) = \frac{1}{2}\left[\sec\theta_i' + \sec\theta_v' - \frac{h}{b}\left|\tan\theta_i' - \tan\theta_v'\cos\varphi\right|\right].$$

Our Boolean analyses represented the decomposed, Red Edge, endmember, NDVI biosignature, riverine, larval, habitat canopy endmembers as a vector model. Vector space is an algebraic model for representing text documents and any objects, in general as vectors of identifiers, such as, for example, index terms [4].The goal of an ArcGIS Boolean analysis is to detect deterministic dependencies between items or similar data-structures in observed response patterns. These deterministic dependencies have the form of logical formulas connecting the items. Assume, for example, that a questionnaire contains items *i*, *j*, and *k*. Examples of such deterministic dependencies are then $i \rightarrow j$, $i \wedge j \rightarrow k$, and $i \vee j \rightarrow k$. Here each *I* dimension corresponded to a separated endmember (e.g., floating shaded vegetation). A final signature was generated (Figure 10).

Interpolation analyses

Spatial linear waveband predictors were then generated from the *S. damnosum* s.l. habitat Red Edge NDVI biosignature employing an Ordinary kriged-based equation in ArcGIS Geospatial Analyst. We geospectrally interpolated the decomposed biosignature values over the northern Ugandan riverine ecosystem. The algorithms for our interpolation have already been described in Jacob et al. [1]. Briefly, the dependent variable was the spectral illumination estimates generated from the decomposed, Red Edge, biosignature emissitives which was transformed to fulfill the diagnostic normality test prior to performing the kriging. The Ordinary kriged-based algorithm was then used to generate predictive maps. In order to to parsimoniously interpolate the value $Z(x_0)$, the decomposed, *S. damnosum s.l.* habitat, shaded, canopy, spectral values and its associated vegetation components, $Z(x)$, the canopy biosignature $x_0$was used where $z_i = Z(x_i)$, i = 1..., *n* represented forecasted, georeferenced, prolific, riverine, habitat,geolocations, x_1, xn.

Ordinary kriging was computed as a linear unbiased explanatorial estimator, $\check{Z}(x_0)$ of $Z(x_0)$ based on a stochastic-based model of the dependence quantified by the variogram $\gamma(x, y)$ and by the expectation $\mu(x)=E\,[Z(x)]$ and the covariance function$c(x, y)$ of the random field (Figure 11).

The kriging estimator was given by a linear combination of the algorithm: $\hat{Z}(x_o) = \sum_{i=1}^{n} w_i(x_o)Z(x_i)$ employing the decomposed, Red Edge, NDVI, biosignature, shaded canopy, endmember datasets of $z_i=Z(x_i)$ with weights $w_i\,(x_o)$, i=1,.., *n* chosen, such that the variance in the spectral autoregressive model residuals was calculated by

$$\sigma_k^2(x_0) := Var(\hat{Z}(x_0 o) - Z(x)) = \sum_{i=1}^{n}\sum_{j=1}^{n} w_i(x_0)w_j(x_0)c(x_i, x_j) + Var(Z(x)) - 2\sum_{i=1}^{n} w_i(x_0)c(x_i, x_0)$$

which was further minimized using:

$$E[\hat{Z}(x) - Z(x)] = \sum_{i=1}^{n} w_i(x_0)\mu(x_i) - \mu(x_0) = 0 \cdot$$

A Voronoi diagram was also constructed in ArcGIS with the geosampled, explanatorial, riverine, larval habitat, georeferenced points as the centers of the decomposed, Red Edge, NDVI, biosignature polygons employing the Weighted Voronoi Diagram Extension in ArcGIS 10.3® for the Chutes Dienkoa eco-epidemiological riverine study site. Using the Generate tab in ArcGIS spatial Analyst a weighted Voronoi diagram was generated from the forecasted point features. The Graphical User Interface (GUI) has two tabs: Generate and Update (www.esri.com).

The Voronoi Diagram was generated in ArcGIS, whereby, a predicted *S. damnosum* s.l. habitat was associated with p_i (i.e., spectral explanatorial canopy covariate coefficient) in each model using $P=\{p_1,.., p_n\}$ where $2 \leq n \leq \infty$ and $x_i \neq x_j$ for $i \neq j$, i, j I_n (Figure 12). The region was given by $V(p_i)=\{x\colon \| x - x_i\| \leq \| x - x_j \|$ for $j \neq i,\ iI_n\}$ which was the Ordinary Voronoi polygon associated with *p* where the set given by $V=\{ V(p_i),.., V(p_n)\}$ was the planar Ordinary Voronoi diagram generated by *P*. A planar ordinary Voronoi diagram was then defined with half planes as follows where we let $P=\{ p_i,.., p_n \} \subseteq R^2$, where $2 \leq n \leq \infty$ and $x_i \neq x_j$ for $i \neq j$, $i, j\, \mathcal{E}\, I_n$. We called the region $V(P_i) = \bigcap_{j \varepsilon In \setminus \{i\}} H(P_i P_j)$ which was the ordinary Voronoi polygon in each model associated with p_i and set $V(P)=\{V(p_1),.., V(p_n)\}$. The planar Ordinary Voronoi diagram was then generated by P. A raster image showing normal Euclidean distance and adjusted Euclidean distance was then created as well as a Voronoi polygon shapefile. The riverine, larval, *S. damnosum s.l.*, shade canopied, habitat, data, feature attributes predicted by the Red Edge, NDVI, unmixed, biosignature variables were then transferred to Voronoi polygons automatically by appending the spatial attributes of one layer to another.

Results

The Red Edge, NDVI, geospectral, explanatorial parameters were generated in, ENVI using the Rapid Eye™ 5m, data. For each NDVI value, the total areas were determined for specific, ArcGIS, geoclassified LULC, surface, vegetation-related cover endemic, transmission-oriented zones associated to the geosampled, *S. damnosums.l.*, riverine, larval, habitat canopy, (e.g., floating and emergent vegetation) and for a few hybrid, vegetation-cover classes consisting of open water and submersed vegetation surrounding the georeferenced riverine habitat. The vegetation LULC cover classes (dense canopy, sparse canopy, bare rock and water) comprised the largest total area of the NDVI value. The equation Image Server employed to generate the output produced a single-band dataset from each 5m data product. The differential reflection in the red and IR bands from the 5m imager enabled quantifying density and intensity of canopy, green, vegetation growth using the geospectral reflectivity of solar radiation. Our model revealed green leaves surrounding the shaded, *S. damnosum* s.l. habitat had better reflection in the NIR wavelength range than in visible wavelength ranges. When leaves are water stressed, diseased, or dead, they become more yellow and reflect significantly less in the NIR range [4,115].

The Red Edge NDVI produced in ENVI was subsequently exported into ArcMap. The NDVI was filtered in ArcMap for determining the lowest NDVI value that was associated to healthy, canopy green riverine, geo-classified LULC-relted vegetation of the geosampled, georeferenced, riverine *S. damnosum s.l.* larval habitat.To decide this value, the natural Rapid Eye color imagery as the top layer was color balanced and then added to the RedEdge NDVI canopy layer. By clicking on multiple 5m mixels with the Identity Tool, the edge of live/dead canopy LULC-related vegetation the imaged georefernced, *S. damnosum* s.l., riverine, larval habitat, gesoampled at the Chutes – Dienkoa, eco-epidemiological, study site wasvisually detected on a risk map.

A Red Edge NDVI vale of 0.1 was determined for the brownish/green (i.e, unhealthy sparse canopy) of the larval habitat canopy. Subsequently, a NDVI value of 0.9 was presumed to be associated with healthy, living, canopy vegetation. Thereafter, sequential classes of Red Edge, NDVI, quantitated values were created and then color coded accordingly. The Symbology Tab was employed to complete this step which was navigated to by using Layer Properties of the NDVI TIFF file. The symbology type was switched to "Classified" Histograms. Pressing the Classify button, set the exclusion values to -1.0 to 0.09.

ArcMap subsequently filtered out all values in this range for geo-classifying the *S. damnosum s.l.* larval habitat 5m Rapid Eye^{TM} data into operationizable, georeferenced clusters of similar values. The Red Edge NDVI Natural Breaks (i.e.jenks) was then created with 3 LULC classes (i.e., densed green vegetation, bare soil and water). By so doing, a schema was generated that separated stressed vegetation LULC (e.g., sedge) from the more vigorous vegetation LULC in the habitat canopy (e.g., emerging floating vegetation).We then created a copy of this NDVI layer and exported it back to ENVI.

We then generated a correlation time series dependent, geospectral error matrix to determine the accuracy of the decomposed, Red Edge, NDVI, biosignature, parameter estimators. The row in the matrix cartographically represented the Red Edge NDVI data constructed from the decomposed, Rapid Eye data, 5m products, while the columns represented the reference data (i.e.,*in-situ* geosampled data). Measures of thematic accuracy were also generated including overall classification accuracy and percentage of omission, forecasting, explanatorial, predictor variables. The georeferenced, riverine, larval habitat, explanatorial, canopy-related, non-reflective, NPV, covariate, paramter estimator, coefficient, indicator, measurement values were the percentage of 5m mixels that were in a given Red Edge NDVI class, but were not eco-geographically or non-ecogeographically classified.

Predicted sizes of open-water, submersed, and floating-and-emergent canopy vegetation-related LULC cover areas were closely inspected for observed sizes in the polygonized dataset. An explanatorial, residualized, normalized, uncertainty-oriented output was then generated using the Kappa measures and the field-verified, geo-spatiotemporally dependent, photosynthetic, covariate, paramter estimator, coefficient values regressively devised from the Red Edge, NDVI, *S. damnosum s.l.*, immature habitat, shade, canopied, geo-spatiotemporally-geosampled, randomized variables. As primary accuracy measures, these canopy-related, biophysical, explanatorial change measures were normalized by the arithmetic mean of the calculated canopy entropies generated by the time series, geosampled, mapping variables.

A mixel-based classification of the geo-spatiotemporally, geosampled, shaded, *S. damnosum s.l.* georeferenced, riverine, larval habitat canopy, geo-classifed LULC vegetationwas thereafter undertaken employing ENVI technology. A standard unsupervised classification was performed using an ISODATA classification system and a maximum likelihood (ML) algorithm respectively. The ISODATA unsupervised classification calculated the class means in the georeferenced, riverine, larval habitat, Red Edge, NDVI, 5m,canopy, endmember variables evenly distributed in data space which were then subsequently iteratively clustered. The remaining endmembers were then regressively quantitated employing minimum distance techniques. Each iteration recalculated the means and reclassified the 5m, canopy, endmember, forecasted data with respect to the new calculated mean values. This process continued until the number of canopy endmembers in each designated vegetated, shade-oriented, operationizable, georefernced larval habitat, explanatorial, LULC class changed by less than the selected mixel change threshold in the object based classifier.

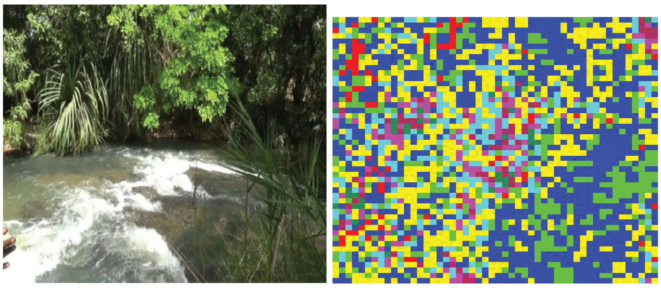

Figure 13: A digital picture of a large *S. damnosum* s.l large habitat with ENVI window of raw biosignature mixel count.

ENVI technology then automatically categorized individual 5m, endmember feature attributes of the Red Edge NDVI based on canopy, floating hanging and dead vegetation geospectral LULC classes. The object classifier converted the remotely-sensed raster layers to vector coverages which were then classified as shapefiles. ENVI provided interactive spatial/spectral mixel editing for the image components in the RedEdge, riverine, larval habitat, mapped NDVI.

The ENVI Feature Extraction module automated the process of performing accurate segmentations. For example, the FLAASH model included a method for retrieving selected "dark" pixels (e.g., shaded, canopy, floating LULC, vegetation) in the scene. The spectral profile based on the image endmembers were then extracted using a spectral angle mapper (SAM) algorithm. The algorithm determined the spectral similarity between the geo-spectrally extracted, RedEdge, NDVI, *S. damnosum* s.l., larval habitat, remotely quantitated, radiance estimates, by calculating the angle between the canopy reflux emissivitives and by treating the reflectance spectra as vectors in eco-geographic space where the dimensionality was equal to the number of Rapid Eye^{TM} bands.

The FLAASH model output and the SAM algorithm compared the angle between the endmember spectrum vector and the 5m spectrum vector in *n*-D space. Spectral Angle Mapper calculated the spectral similarity between the RedEdge, NDVI, image spectrum and the reference reflective spectra which revealed that the RedEdge, NDVI, *S. damnosum s.l.,* larval habitat, covariate, paramter estimator, coefficients was affected by solar illumination factors as the angle between the vectors was not independent of the vectors length. Smaller angles between the unmixed reference spectrum in the endmember spectral library. Shade canopied, larval habitat, endmembers that were further away than the specified maximum angle threshold in radians were not classified.

We also employed the Spectral Information Divergence (SID) classification in ENVI to compare the similarity between the selected RedEdge, NDVI, *S. damnosum s.l.,* georeferenced, riverine, larval habitat, shade-related, canopy-oriented, trailing vegetation–assocated LULC, endmember components by measuring the probabilistic discrepancy between their corresponding reflux emissivities. Initially, the ToolBox Classification in ENVI was selected to perform the classification chores. From the Enmember Collection dialogue menu bar, the SID algorithm was then selected. The Classification Input File dialog then appeared. An input file was selected which performed the spatial and geospectral subsettings and masking.

From the Endmember Collection SID dialog we selected Import > *spectra_source* for collecting and archiving the NDVI geo-classified data.The SID, RedEdge, endmember, explanatorial, parameter estimator dialog appeared. Thresholding options were selected from the Set Maximum Divergence Threshold area. The Single Value parameterization was employed.A single threshold was choosen for the unmixed, canopied, *S. damnosum s.l.,* larval habitat, shade-oriented, canopied, floating, hanging and dead vegetation-related, geo-classifed, LULC classes in the NDVI. A value was then entered in the Maximum Divergence Threshold field. This was the minimum allowable variation between the shade canopied, explanatorial, vegetation-related LULC endmember spectrum vector and the mixel vector. The default value was .05. Multiple values were then entered into a different divergence to test each LULC class against its corresponding maximum spectral divergence. A class was selected to assign threshold larval habitat, vegetation, endmember, probabilistic, radiance values which subsequently edited the value in the Edit Selected Value field employing the Maximum Divergence Threshold dialog.

Subsequently, classification output was selected to Memory. The Output Rule Images was selected to determine whether or not to create rule images. The rule images was employed to create intermediate classification image results before final assignment of the RedEdge, NDVI,*S. damnosum s.l.,* georeferenced, riverine, larval habitat, LULC classes. The Rule Classifier was used to create a new classification image without having to recalculate the entire classification.

In Preview a 256m x 256m spatial subset was generated from the center of the output RedEdge, NDVI, *S. damnosum s.l.,* georeferenced, riverine, larval habitat, classified image. The explantorial parameter estimators were changed as needed. In Preview the display was updated. ENVI added the resulting output to the Layer Manager. The output from SID was a classified 5m image and a set of classified sub-images (one per shade canopied, larval habitat endmember). The values of the rule images represented the SID value. The output of the equation that defined SID in ENVI for a pair of spectral vectors was identified. Lower spectral divergence measures represented better matches to the unmixed, endmember, canopied, larval habitat, derivative spectra. Areas that satisfied the Maximum Divergence Threshold criteria were carried over as classified areas into the classified larval habitat endmember spectrum vector image. The SID successfully calculated all the time series dependent, geospectral, error probabilities of the canopied, endmember, biosignature data in the library.

The spectral library accounted for all processes and factors influencing the explanatorial, geo-spatiotemporal, reflectance-related, endmember, spectral data collection as rendered from the decomposed, RedEdge, *S. damnosum s.l.,* georeferenced, canopied, riverine,larval habitat, NDVI, which was subsequently converted to match the library-based data. Analogously, the reference endmembers spectra in the library were transformed into the canopy endmembers spectra of the habitat biosignature. We expressed these unmixed, endmember, shade, canopy, vegetated, linear combinations as image endmembers. A function incorporating the calibration and the alignment was repeatedly evaluated for different candidate groups of the unmixed, Red Edge, NDVI, canopied, biosignature endmembers until a suitable representation of the image endmembers was determined.

Before applying the spectral index to the Rapid Eye imagery, raw mixel values [i.e., digital numbers (DN)] were converted into physically meaningful units to differentiate endmember reflectance spectra and immature *Similium* productivity based on habitat size in ENVI. The digital numbers of the RapidEye™ image mixels represented absolute calibrated radiance values in ecogeographic space where non-atmospheric corrected images reflectance values were generated. To convert the DN of the georeferenced, geosampled, *S. damnosum* s.l. riverine, larval habitat,extracted mixel to radiance values it was necessary to multiply the DN value by theradiometric scale factor, as follows: RAD(i) = DN(i) * radiometric ScaleFactor (i). The resulting value was the ToA radiance of the larval habitat mixel in W/m^{2}sr µm. The formula used in this process were as follow:

$$L_\lambda = ((LMAX_\lambda - LMIN_\lambda / (QCALMAX - QCALMIN))*$$

$$(QCAL - QCALMIN) + LMIN_\lambda$$

where: L_λ was the quantitated Rapid Eye™ cell value and where radiance QCAL was equal to DN, while $LMIN_\lambda$ was the 5m spectral radiance scales to QCALMIN, $LMAX_\lambda$QCALMIN which was the minimum quantized calibrated mixel value. QCALMAX was the maximum quantized calibrated mixel value (i.e., 255). The small habitat had a DN of 68 while the larger habitat had a DN of 117. The larger, georeferenced, riverine, larval habitat had a larger immature count than the smaller larval habitat (Figure 13).

A canopy, Red Edge, NDVI,*S. damnosum s.l.,* larval habitat was then created employing the ENVI spectral library. A standard ENVI spectral library (.sli) was selected. By so doing, ENVI's Spectral Library Viewer was launched. The left side of the Spectral Library Viewer dialog listed the Red Edge, NDVI, larval habitat, endmember biosignature within the selected library. The right side of the viewer used tabs to display the metadata for selected canopied biosignature variables and queried selected endmember, covariate, parameter estimator, coefficient values. Metadata for the selected biosignature appeared in the Metadata tab.the area.We noted that the factor LAI/cosθ_s represented the riverine, larval habitat, canopy vegetative, optical thickness. Thus, the proportion of incident fPAR that was intercepted by the geosampled, georefernced, shade, canopied, habitat was dependent on the canopy structure (LAI). Asrar et al. (1984) demonstrated that NDVI and APAR are functions of LAI.

A successive projection algorithm (SPA) in Asrar et al. (1984) was built for decomposing the Red Edge, NDVI,*S. damnosum* s.l. habitat,canopy endmember, riverine LULC, biosignature employing convex geometry and orthogonal projection.The extraction Asrar et al. (1984) shade, canopied, sub-mixel, operationizable,image endmembers from the decomposed biosignature without having to reduce the sampled data dimensionality. SPA built on the convex geometry search algorithm by including a constraint on the spatial adjacency of the endmember candidate, Red Edge, *S. damnosums.l.,* endmember, larval

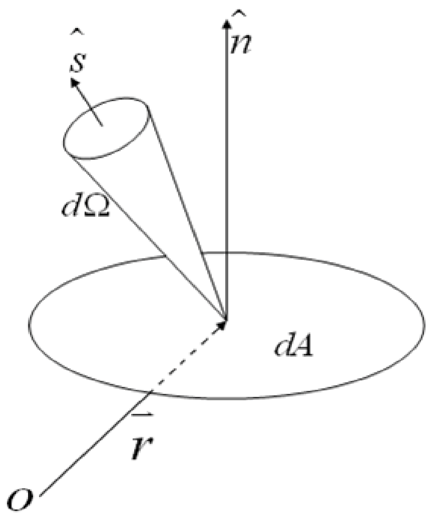

Figure 14: Red Edge *S. damnosum s.l.*larval habitat biosignature canopy energy flux as calculated by $\vec{J}(\vec{r},t) = \int_{4\pi} \hat{S}L(\vec{r},\hat{S},t)\,d\Omega\left(\frac{W}{m^2}\right)$.

habitat, unmixed, NDVI-related, biosignature decomposed variables with its associated explanatorial, georeferncable sub-mixel, reflectance components. The SPA reduced the susceptibility for searching for outliers. The algorithm described how a vertex was identified based on its spectral uniqueness in the simplex. The algorithm measured the vector Euclidean norm and the distance of the RedEdge, NDVI, larval habitat, derivative spectra to the subspace which was defined by selected canopy endmembers. A meaningful canopy endmember for this vertex was the multiple candidate LULC endmembers that were spectrally distinct (e.g., those that were geolocated on the habitat canopy at or near one of the corners of the simplex).

The convex geometry SPA provided information on the convergence of the algorithm.This property was employed in the SPA algorithm to determine the main step in thegeorferenced, riverine, larval habitat,end member, biosignature decomposition for quantitation of the RedEdge, NDVI,canopy, spectral heterogeneity at the vertices of the simplex. For the given geosampled, canopy endmember, riverine, larval habitat, unmixed, biosignature point in the simplex, a point with maximum distance was at the vertex of the simplex.

Based on the SPA residual algorithmic output, the affine transformation (i.e., orthogonal projection) of the simplex generated was also a simplex.This output revealed that the shade, canopied, decomposed, Red Edge, NDVI, canopy, LULC-oriented, vegetation-related, biosignature endmembers were located in the vertices of the new simplex after the transformation. This transformation allowed the use of the orthogonal subspace projections as the core mechanism for parsimoniously conducting the decomposition endmember extraction exercise.

A vector with maximum Euclidean norm (i.e., magnitude) was generated at the vertices of the simplex. In linear algebra, functional analysis and related areas of mathematics, a norm is a function which assigns a positive length or size to all vectors in a vector space, other than the zero vector [27]. A semi-norm was then allowed to assign zero length to some non-zero vectors. We employed the 2-dimensional Euclidean space R^2 equipped with the Euclidean norm for analyzing the initially decomposed, *S. damnosum* s.l., larval habitat, canopy, biosignature endmembers. Euclidean space is a particular metric space that enables the investigation of topological LULC geo-classified properties such as compactness [4]. An inner product space is a generalization of a Euclidean space [2]. Both inner product spaces and metric spaces of the riverine, larval habitat, canopied, endmember model was explored within a functional analysis. Elements in this vector space are usually drawn as arrows in a 2-dimensional cartesian coordinate system starting at the origin (0,0) [12]. The Euclidean norm assigns to each vector the length of its arrow [2].

By including a constraint on the geospatial, Euclidean, subspace adjacency of the shaded, explanatorily, geospectrally decomposed, vegetated, *S. damnosum* s.l riverine, larval habitat LULC dataset and their individual canopy-related, endmember reflectance, geospectral values, the SPA algorithm captured the contiguous 5m-mixel VI in red, IR and NIR bands, employing data pre-processing applications in the sensor data. The georeferenced, shade, canopied, immature data was able to describe the change of the simplex volume ratio between successive iterations during the endmember extraction process. Further, the algorithm reduced the susceptibility to outlier 5m-mixel, geospectrally-oriented, erroneous, resdiualized covariate coefficients which allowed for optimizing the unmixed, camopied, canopy endmember, LULC, reflectance spectra and eco-geographically classifying them based on their actual reflection attributes.

Although, the decomposed, Red Edge, NDVI, geospectral, canopied, biosignature, endmember, decomposed LULC, explanatorial were extracted, the final dataset did not include any treatment of diffuse irradiance, canopy multiple scattering or leaf specularity. This decomposition exercise required the selection of individual wavelength information for each unmixed, wavelenght-oriented, canopy, vegetated, endmember, photosynthetic and NPV data, feature attribute which was calculated by a radiative transfer equation. An analytical was then derived for the inclination angle density function which was $g(\alpha) = \dfrac{2\chi^3 Sin\alpha}{\lambda(Cos^2\alpha + \chi Sin^2\alpha)^2}$ where α was the leaf inclination angle, *X* was the ratio of vertical to horizontal projections of canopy elements, and *A* was a normalized ellipse area, approximated by $\lambda=\chi+1.774(\chi+1.182^{-0.733}$

We employed a three-dimensional 3-D radiative transfer model in ArcGIS to decompose the Red Edge,*S. damnosum s.l.,* larval habitat, canopied biosignature. FLAASH, was based on theoretical model atmospheres using radiative transfer codes derived from optical characteristics of the atmosphere in our Rapid Eye TM 5m image. The software categorized the atmosphere in our image (riverine humidity, dry, etc.) and provided sun elevation angle, Image-based methods (e.g. dark object subtraction) are far less computationally intensive, but radiative transfer codes (e.g. FLAASH) can sometimes provide more reliable results when comparing images across space and/or time. (https://geonet.esri.com/).

The process of solar radiative transfer in ArcGIS at the land surface is important to energy, water, and carbon balance, especially for vegetated, geoclassifed, LULC areas [1]. We used a two-stream model to consider the riverine, habitat, canopy plant, functional types within a gridded matrix to determine independence of each other and their leaves (i.e., horizontal homogeneous tendencies). The model revealed an increase of canopy absorption within sparse vegetation LULC with multi layered canopied area with a large sun zenith angle θ_{sun} which may have been due to increases of the ground and sky shadows and of the optical pathlength .This phenomenon may have been also due to shadow overlapping between the georeferenced, shaded habitat, canopy layers.

The flow of radiation energy through a small area element in the radiation field was characterized by radiance employing $L\left(\vec{r},\hat{S},t\right)\left(\dfrac{W}{m^2 Sr}\right)$. Radiance is defined as energy flow per unit normal area per unit solid angle per unit time [4]. We mathematically modeled the transfer of energy based on assumed photon movement in the geo-spatiotemporally, geosampled, shade canopied, prolific, *S. damnosum* s.l., riverine, larval habitat where $\vec{r}$ denoted position, *S* denoted unit direction vector and **t** denoted time. Several other important physical habitat quantities were remotely quantized based on the canopy radiance including fluence [i.e., $F(\vec{r}) = \int_{-\infty}^{+\infty} \Phi(\vec{r},t)dt(\dfrac{J}{m^2})$] and fluence intensity [i.e., $\Phi(\vec{r},t) = \int_{4\pi} L(\vec{r},\hat{s},t)d\Omega(\dfrac{W}{m^2})$]. The vector counterpart of fluence rate in the prevalent direction of energy was then calculated (Figure 14)

A differential equation describing radiance [i.e., $L(\vec{r},\hat{s},t)$] was generated in ArcGIS. The model was based on conservation of energy. Briefly, this theory states that a beam of light loses energy through divergence and extinction (including both absorption and scattering away from the beam) and gains energy from light sources in the medium and scattering directed towards the beam [2]. Coherence, polarization and non-linearity are neglected. Optical properties such as refractive index η, absorption coefficient μ_a, scattering coefficient μ_s, and canopy scattering anisotropy **g** are taken as time-invariant but may vary spatially [12]. Scattering is assumed to be elastic [27]. A georeferenced, *S. damnosum* s.l., riverine, larval habitat, shaded, vegetation-related ,LULC, canopy-related, regression-related equation was then written from the NDVI data as:

$$\frac{\partial L(\vec{r},\hat{s},t)/c}{\partial t} = -\hat{s}.\nabla L(\vec{r},\hat{s},t) - \mu_t L(\vec{r},\hat{s},t)$$

$$\frac{\partial L(\vec{r},\hat{s},t)/c}{\partial t} = -\hat{s}\cdot\nabla L(\vec{r},\hat{s},t) - \mu_t L(\vec{r},\hat{s},t) + \mu_s \int_{4\pi} L(\vec{r},\hat{s}',t) P(\hat{s}'\cdot\hat{s}) d\Omega' + S(\vec{r},\hat{s},t)$$

where **C** was the relative refractive index, $\mu_t = \mu_a + \mu_s$ was the extinction coefficient, $P(\hat{s}',\hat{s})$ was the phase function, representing the probability of habitat canopy light with propagation direction $\hat{s}'$ being scattered into solid angle $d\Omega$ around $\hat{s}'$. In most cases, the phase function depends only on the angle between the scattered $\hat{s}'$ and incident $\hat{s}'$ directions, i.e. $P(\hat{s}',\hat{s}) = P(\hat{s}'\cdot\hat{s})$ [4,115] the scattering canopy anisotropy was then expressed as $g = \int_{4\pi} (\hat{s}'\cdot\hat{s}) P(\hat{s}'\cdot\hat{s}) d\Omega$ and $S(\vec{r},\hat{s},t)$.

Radiance was expanded on a basis set of spherical harmonics $\mathbf{Y}_{n,\,m}$. In diffusion theory, radiance is taken to be largely isotropic, so only the isotropic and first-order anisotropic terms are used [2]. Here we defined the riverine larval habitat canopy radiance using $L(\vec{r},\hat{s},t) \approx \sum_{n=0}^{1} \sum_{m=-n}^{n} L_{n,m}(\vec{r},t) Y_{n,m}(\hat{s})$ where $L_{n,\,m}$ were the expansion coefficients. Radiance was expressed with 4 terms; one for n=0 (the isotropic term) and 3 terms for n=1 (the anisotropic terms). Using properties of spherical harmonics and the definitions of fluence rate $\Phi(\vec{r},t)$ and tabulated canopy densities from $\vec{J}(\vec{r},t)$, the isotropic and anisotropic terms were respectively thereafter expressed as follows:

$$L_{0,0}(\vec{r},t) Y_{0,0}(\hat{s}) = \frac{\Phi(\vec{r},t)}{4\pi} \text{ and}$$

$$\sum_{m=-1}^{1} L_{1,m}(\vec{r},t) Y_{1,m}(\hat{s}) = \frac{3}{4\pi} \vec{J}(\vec{r},t)\cdot\hat{s} \text{ Hence,}$$

we approximated the riverinehabitat canopy radiance as

$$L(\vec{r},\hat{s},t) = \frac{1}{4\pi}\Phi(\vec{r},t) + \frac{3}{4\pi}\vec{J}(\vec{r},t)\cdot\hat{s}\cdot$$

Substituting the above expression for radiance, the geo-spatiotempoally, geosampled, prolific, *S. damnosum* s.l. georeferenced canopied, riverine larval habitat forecasting, eco-epidemiological, risk model estimators were respectively rewritten in scalar and vector forms. The scattering term integrated over the complete 4π solid angle. For the vector form, the photosynthetic and NPV covariate coefficients were multiplied by direction $\hat{S}$ before evaluation. The forecasts rendered revealed two outcomes: $\frac{\partial\Phi(\vec{r},t)}{c\partial t} + \mu_a\Phi(\vec{r},t) + \nabla\cdot\vec{J}(\vec{r},t) = S(\vec{r},t)$ and $\frac{\partial\vec{J}(\vec{r},t)}{c\partial t} + (\mu_a + \mu_{s'})\vec{J}(\vec{r},t) + \frac{1}{3}\nabla\Phi(\vec{r},t) = 0\cdot$ The diffusion approximation is limited to systems where reduced canopy scattering coefficients is much larger than their absorption coefficients and minimum layer thickness of the order of a few transport mean free path [4].

Using the second assumption of diffusion theory, we noted that the fractional change in canopy density $\vec{J}(\vec{r},t)$ over one transport mean free path in the geosampled riverine, larval habitat was negligible.

The vector representation of the diffusion theory reduces to Fick's law $J(r,t)\ \frac{-\nabla\Phi(r,t)}{3(\mu_a\ \ \mu_{s'})}$ [4] which we then employed to define canopy density in terms of the gradient of fluence rate. Substituting Fick's law into the scalar representation of the geosampled, *S. damnosum* s.l., larval habitat regressable residual estimates gave the diffusion equation $\frac{1}{c}\frac{\partial\Phi(\vec{r},t)}{\partial t} + \mu_a\Phi(\vec{r},t) - \nabla\cdot[D\nabla\Phi(\vec{r},t)] = S(\vec{r},t)$ The model revealed $D = \frac{1}{3(\mu_a + \mu_{s'})}$ which was the diffusion coefficient and $\mu'_s = (1\text{-}g)\ \mu_s$ which was the canopy scattering coefficient.

Notably, there was no explicit dependence on the scattering coefficient in the diffusion equation. Instead, only the reduced scattering coefficient appeared in the expression for *D*. This lead to an important relationship; diffusion in the geo-spatiotemporally-geosampled, shade canopied, prolific, *S. damnosum* s.l., georeferenced, riverine, larval habitat was unaffected if the canopy anisotropy was changed while the reduced scattering coefficient remained constant. For qualitatively quantitating various configurations of boundaries (e.g. layers of canopy and light sources), a diffusion equation was solved.

The source term in the diffusion equation became $S(\vec{r},t,\vec{r}',t') = \delta(\vec{r}-\vec{r}')\delta(t-t')$, where $\vec{r}$ was the position at which fluence rate was measured and $\vec{r}'$ was the position of the source. The pulse peaked at time t'. The diffusion equation was solved for fluence rates which yielded

$$\Phi(\vec{r},t;\vec{r}',t) = \frac{c}{[4\pi Dc(t-t')]^{3/2}} \exp\left[-\frac{|\vec{r}-\vec{r}'|^2}{4Dc(t-t')}\right] \exp[-\mu_a c(t-t')]$$

The term $\exp\left[-\mu_a c(t-t')\right]$ represented the exponential decay in the geosampled, shade canopied, prolific, *S. damnosum* s.l., georeferenced, riverine, larval habitat, fluence rate due to absorption in accordance with Beer's law. The other terms represented broadening due to canopy scattering. Given the above solution, an arbitrary source was characterized as a superposition of short-pulsed point sources. Taking time variation out of the diffusion equation rendered the following for a time-independent,, canopied, eco-epidemiological, capture point source: $S(\vec{r}) = \delta(\vec{r}) : \Phi(\vec{r}) = \frac{1}{4\pi Dr}\exp(-\mu_{\text{eff}} r)$ We noted that $\mu_{\text{eff}} = \sqrt{\frac{\mu_a}{D}}$ was the effective attenuation coefficient and indicatedthe rate of spatial decay in fluence.

Consideration of the habitat, shaded, boundary conditions permitted use of the diffusion equation output to characterize light propagation in the canopy. To begin to address a boundary, one can consider what happens when photons in the medium reach a boundary (i.e. a surface) [12]. The direction-integrated the riverine habitat canopy radiance at the boundary and directed it into the mediumwhich was equal toquantitating the direction-integrated radiance at the boundary and directed out of the medium multiplied by reflectance $R_F : \int_{\hat{s}\cdot\hat{n}<0} L(\vec{r},\hat{s},t)\hat{s}\cdot\hat{n}d\Omega = \int_{\hat{s}\cdot\hat{n}>0} R_F(\hat{s}\cdot\hat{n})L(\vec{r},\hat{s},t)\hat{s}\cdot\hat{n}d\Omega$ where $\hat{n}$ was normal to and pointing away from the boundary. The diffusion approximation then rendered an expression fordetermine the riverine larval habitat canopy radiance L in terms of fluence rate Φ and current density $\vec{J}$. The steps in representing a beam incident on the semi-infinite canopy habitat anisotropically scattering medium was based on two isotropic point sources: $\frac{\Phi(\vec{r},t)}{4} + \vec{J}(\vec{r},t)\cdot\frac{\hat{n}}{2} = R_\Phi \frac{\Phi(\vec{r},t)}{4} - R_J\vec{J}(\vec{r},t)\cdot\frac{\hat{n}}{2}$ where $R_\Phi = \int_0^{\pi/2} 2\sin\theta\cos\theta R_F(\cos\theta)d\theta$. Therefater $R_J = \int_0^{\pi/2} 3\sin\theta(\cos\theta)^2 R_F(\cos\theta)d\theta$ was tabulated. Substituting Fick's law ($\vec{J}(\vec{r},t) = -D\nabla\Phi(\vec{r},t)$) then rendered a distance from the riverine, ,immature, habitat, canopy boundary where z=0 $\Phi(\vec{r},t) = A_z \frac{\partial\Phi(\vec{r},t)}{\partial z}$ and where $A_z = 2D\frac{1+R_{\text{eff}}}{1-R_{\text{eff}}}$. Solutions to the equation of radiative transfer. equation included $I_\nu(s) = I_\nu(s_0)e^{-\tau_\nu(s_0,s)} + \int_{s_0}^{s} j_\nu(s')e^{-\tau_\nu(s',s)}ds'$ The differences were essentially due to the various forms of thehabitat emission and canopy absorption coefficients

A decrease of canopy absorption occured in densely vegetated, LULC ccanopy georeferenced, riverine, larval habitat areas with small θ_{sun}. in ArcGIS For a one-layer canopy, these decreases may have been due to crown shape effects that enhanced the transmission through the canopy edge [12]. For the multilayer canopy portion of the georeferenced, riverine, larval habitat, aside from the shape effects, transmission may have been increased by the decreased ground shadow due to the shadow overlapping between layers. Ground absorption usually changes with opposite sign as that of the canopy absorption [25]. Somewhat lower albedos are found over most vegetated areas throughout the year [7]. The 3D model quantitated the affects of the fraction of sunlit canopy leaves and their corresponding absorption values in the geosampled, productive, georefernced, *S. damnosum* s.l., riverine, larval habitat.

The Pareto frontier, *P(Y)*, was formally described by considering a system with function $f : R^n \rightarrow R^m$, where *X* was a compact set of feasible decisions in the metric space R^n, and *Y* was the feasible set of criterion vectors in R^m, such that $Y = \{y\varepsilon R^m : y = f(x), x\varepsilon X\}$. This equation was constructed employing all the empirical photosynthetic and NPV, *S. damnosum* s.l., riverine, larval habitat, geosampled, canopy covariates. Assumptions were determined of the preferred directions of known criteria values. A geosampled habitat point [i.e., $y''\varepsilon R^m$] was determined which was then written as $y'' < y'$. The Pareto frontier for the empirical geosampled, geo-spatiotemporal *S. damnosum* s.l. larval habitat was then $P(Y) = \{y'\varepsilon Y : \{y''\varepsilon Y : y'' < y', y'' \neq y'\} = \theta\}$.

In the geometric optical model the shape of the hotspot function of the georefernced, geosampled, *S. damnosum s.l.,* canopied, endmember biosignature was found to be based on the viewing and illumination positions in the model, which were diverged due to the shape and height of the spheroids. The equation was helpful to understand how the shape of the geosampled, georeferenced, riverine, larval habitat, and geospectally/geospatially associated floating, hanging and dead vegetation LULC, canopied components governed the shape of overlap functions. The exact overlap function on the principal cone was also captured employing the hybrid of the geometric optical model which revealed canopy bidirectional reflectance values over the decomposed explanatorial, endmember biosignature data featureattributes.

In the model the viewing zenith was the viewing direction which had a different azimuth than the illumination position. Rather than computing the overlap of ellipses rendered from the decomposed, canopy, biosignature, endmember, NDVI components at arbitrary inclinations, a linear function was instead employed which robustly quantitated the diminution of the overlaps rendered from the model residuals using azimuth angles. The azimuthal cut off of the hotspot in the georeferenced, geosampled, *S. damnosum* s.l. riverine, larval habitat canopy was then geolocated.

The shape of the hotspot functions was found to be based on the viewing and illumination positions in the Red Edge, NDVI, larval habitat, canopy, reflectance model which diverged due to the shape and height of the spheroids. The equation $K_g = e^{-\lambda\pi R^2\left[\sec\theta_i' + \sec\theta_v' - \bar{O}(\theta_i,\theta_v,\varphi)\right]}$ was helpful to understand how the shape of the decomposed endmember canopy, biosignature's shaded, riverine, larval, habitat components governed the shape of the overlap functions. Since it is important to have an exact solution for overlap function on the principal plane [2,3], the equation $O(\theta_i,\theta_v,\varphi) = (t - \sin t\cos t)(\sec\theta_i' + \sec\theta_v')/\pi$ was employed where $\cos t = \frac{h\left|\tan\theta_i' - \tan\theta_v'\cos\varphi\right|}{b\left(\sec\theta_i' + \sec\theta_v'\right)}$. Exact overlap function on the principal cone was obtained for the model where $\theta_v' = \theta_i'$ and φ varied from 0 to 2π. The hybrid of geometric opticality for the canopy biosignature model was then determined for qualitatively quantizing habitat canopy, unmixed, bidirectional reflectance over the decomposed, *S. damnsoum s.l.,* larval habitat, Red Edge, NDVI, endmember values.

In the Red Edge, NDVI, *S. damnosum s.l.,* larval habitat, canopy endmember, biosignature model the viewing zenith was θ_v, but the viewing direction had a different azimuth than the illumination position. Rather than computing the overlap of ellipses rendered from the georeferenced, riverine, larval habitat canopy floating, hanging and dead vegetation-related, explanatorily temporally dependent, endmember NDVI components at arbitrary inclinations and distances directly, a linear function was instead fit to the diminution of the overlaps generated employing azimuth angles.

$\Phi = \frac{4R}{h\left(\tan\theta_v + \tan\theta_i\right)}$ was then approximated by the azimuthal cut-off of the hotspot as determined by the Red Edge, NDVI, *S. damnosum* s.l., larval habitat, canopy, endmember, biosignature model. Linearly interpolated, explanatorial, time series forecasts were employed for defining φ between 0 and Φ or . For the case $\Phi < \pi$, we assigned $O(\theta_i, \theta_v, \varphi) = O(\theta_i, \theta_v, \varphi = \pi)$ for all φ between Φ and π. Though this approximation we were able to quantify any small errors in canopy overlapping areas. The residual output from the equation [i.e. $O(\theta_i, \theta_v, \varphi) = \frac{1}{2}\left[\sec\theta_i' + \sec\theta_v' - \frac{h}{b}\left|\tan\theta_i' - \tan\theta_v' \cos\varphi\right|\right]$] was then employed to determine if the model quantitated azimuthal width effectively for adequately determining the riverine, S. *damnosum* s.l., larval habitat, canopy,"hotspot" effect as determined by the R/h ratio. The outward width of hotspot on the principal plane was then determined by b/h ratio; and, the inward width was determined by both [129-135].

Exact contribution of sunlit, georeferenced, geosampled, canopied, riverine, larval habitat, surface, predictor variables and their shading effects were then quantized. The effect of sunlit canopy on the bidirectional reflectance was explanatorily quantified employing the second term in equation $R(i,v) = K_g G + \frac{C}{A}\iint_{A_c} \frac{\langle i,s\rangle}{\cos\theta_i}\frac{\langle v,s\rangle}{\cos\theta_v} ds$ [3.1]. This variation depended on both the density and angular distribution of *ds* in the equation [3.1]. Strahler and Jupp [136] assumed that each object in a scene could be modeled as a sphere without mutual illumination shading between *ds* elements. As such, a second term for quantitating the decomposed, *S. damnosum* s.l., canopy, biosignature, sub-mixel data was approximated by $K_c C = \frac{1}{2}\left(1 + \langle i,v\rangle\right)\left(1 - e^{-\lambda\pi R''^2 \sec\theta_v}\right)C$. In this expression, the first term was the illuminated proportion of the area of a single sphere viewed at position *v* which was also illuminated at position i. This was weighted by the second term which was the proportion of the area of spheres visible from zenith angle $\langle i, v$. Since both terms varied smoothly between zero and one, this contribution to the riverine larval habitat canopy hotspot was quite flat. In the case of a spheroid, we simply then replaced $\langle i, v\rangle$ by $\langle i', v'\rangle$, where $\langle i', v'\rangle = \cos\theta_i' \cos\theta_v' + \sin\theta_i' \sin\theta_v' \cos\varphi$.

The first term in equation $K_c C = \frac{1}{2}\left(1 + \langle i,v\rangle\right)\left(1 - e^{-\lambda\pi R''^2 \sec\theta_v}\right)C$ in ArcGIS ignored the problem of mutual shading of the *S. damnosum* s.l., riverine, larval habitat, canopy floating, hanging and dead vegetation endmember, NDVI components in the model. We handled this problem by employing a multiple integration, in which the mutual shadowing of the riverine larval habitat canopy and other associated wihin-canopy habitat objects were treated in the same way as the mutual shading of the leaves. Our objective was to derive a simple approximation to describe the effect of the shaded, larval habitat, canopy cover based on collections of individual, discrete, endmember, reflectance, surface values (i.e., trailing vegetation components) as rendered from the model forecasts. To carry this out, we developed an approach that applied one-stage geometric optics to deal with the geospatial relationship between the endmember reflectance spectra of the riverine, habitat, canopied, surface components that was mutually shaded in the illumination direction and the georeferenced explanatorial parts mutually shaded in the view direction. Quantification of the mutual shadowing larval habitat proportions generated from the decomposed, geo-spatiotemporally, geosampled, *S. damnosum* s.l., larval habitat, riverine, canopy and its associated georeferenced, vegetation-related, LULC, endmember components revealed no collinearity**.** In Li and Strahler [113] simulation and mathematics simplified to the one-dimensional case which was proved so that for the nadir-viewed cone model, mutual shadowing of illumination would not change the ratio $K_c/(1-K_g)$. In the georefernced, riverine, larval habitat, canopy reflectance, forecasting, eco-epidemiological, risk model, this ratio was itself denoted K_c which we employed to generate u A_c/A for parsimoniouslyquantitating consistency with K_g where the mutual shadowing in illumination and viewing directionswas deemed independent (i.e., A_c/A) for consistency with K_g.

We then considered the proportion of the riverine, georeferenced, *S. damnosum s.l.,* larval habitat canopy which was mutually shadowed by the georefernced, vegetation -related LULC endmember components in the model regressors. In the direction of illumination, there was some photosynthetic and NPV geospectral, endmember, reflectance commponents which had an area (e.g., $\pi R^2 \sec\theta_i'$) only in specific areas of the Red Edge, NDVI, endmember, canopied biosignature. For example, the total projected area of the immersed canopy endmember LULC vegetation components was $\lambda\pi R^2 \sec\theta_i'$, if there was no mutual shadowing.

If there was mutual shadowing inthe Red Edge NDVI, canopy, endmember biosignature, the net projected area in the larval habitat canopy was $1 - e^{\lambda\pi R^2 \sec\theta_i'}$. The difference indicated the total mutual shadowing of the entire canopy cover. The quantity M_i, was the mutual derived canopy shadowing proportion in the illumination direction which was calculated as $M_i = 1 - \frac{1 - e^{-\lambda\pi R^2 \sec\theta_i'}}{\lambda\pi R^2 \sec\theta_i'} M_i$. The product revealed the degree of mutual canopy shadowing in the illumination direction. Next a spheroid, was determined, which on average, had a proportion M_i of the Red Edge, NDVI, *S. damnsoum s.l.*, habitat, canopy biosignature, surface area that was not sunlit. This part of the habitat canopy was concentrated at the lower part of the spheroid. We then generated a boundary drawn on the habitat canopy surface of the spheroid with the area comprising M_i located below it.

Similarly, we defined M_v as the mutual shadowing proportion of the floating, hanging and dead vegetation-related, LULC-oriented, sub-mixel, explanatorial, components in the view direction as $M_v = 1 - \frac{1 - e^{-\lambda\pi R^2 \sec\theta_v'}}{\lambda\pi R^2 \sec\theta_v'}$. The viewing shadows were concentrated at the lower part of the spheroid so the M_v boundary was definable. The proportion of sunlit in the Rapid Eye sensor captured corresponded to the area above both $M_1$and M_v boundaries which was dependent on both zenith and azimuth differences between the illumination and view directions. At the hotspot, M_i and $M_{v\,t}$ boundaries overlapped and the RapidEye ™ data revealed no mutual shadowing of the geosampled, larval habitat, canopy, vegetation-related, LULC, endmember components. Interestingly, when the view zenith angle was larger than the illumination zenith angle, M_v was greater than M_i and little or no mutually-shaded canopy habitat area was visible, based on the azimuth differences between the imaged objects. Thus, the 5m, Red Edge, canopy biosignature was able to capture the essence of the mutual-shading effects of the canopy, floating, hanging and dead vegetation, decomposed, endmember, unmixed, geospectral components.

We then quantified the *f*-Ratio of nonnadir-viewed, canopy-based habitat spheroids employing the decomposed, Rapid Eye™ data. First, we considered a single spheroid in the riverine, larval habitat, canopy sub-mixel, unmixed, geospectral data. For the spheroidal case, it is necessary to show whether the *f*-Ratio is still independent of density, as in the

Citation: Jacob BG, Novak RJ, Toe LD, Sanfo MS, Lassane K, et al. (2016) Ecogeographically and Non-Ecogeographically Forecasting Discontinuous Canopied *Simulium damnosum* s.l. Habitats by Interpolating Metrizable Sub-Mixel Mean Solar Exoatmospheric Quantum Scalar Irradiance where θ_i is a Zenith Angle and Diatomically Etiolated Xanthophylls with Azimutally Isotropic Sources of Chloroplastic Carotenoid Zeaxanthins Spectrally Extracted from a Decomposed RapidEye™ Red Edge Normalized Difference Vegetation Index Reference Biosignature: A Case Study in Burkina Faso and Uganda. J Remote Sensing & GIS 5: 152. doi:10.4172/2469-4134.1000152

case of the nadir-viewing cones [58,105]. From the view direction, the spheroid had a projected area $\Gamma_v = \pi R^2 \sec\theta_v'$; however, onlythe portion $\frac{1}{2}\left(1+\langle i',v'\rangle\right)$ of the larval habitat canopy cover was sunlit. Similarly, the illumination shadow on the ground occupied the habitat canopy area (i.e., $\pi R^2 \sec\theta_i'$). The compound area of viewed riverine, larval habitat, floating, hanging and dead vegetation, LULC-related, endmember, sub-mixel components plus illumination shadow projected onto the background was $\Gamma = \pi R^2\left[\sec\theta_i' + \sec\theta_v' - O\left(\theta_i',\theta_v',\varphi\right)\right]$. We defined the *f*- ratio for the spheroidal and its eoc-geospectrally associated explanatorial, covariate, parameter estimator, coefficients as $F = \frac{\Gamma_c}{\Gamma} = \frac{\frac{1}{2}\left(1+\langle i',v'\rangle\right)\sec\theta_v'}{\sec\theta_i' + \sec\theta_v' - O\left(\theta_i',\theta_v',\varphi\right)}$, where Γ_c was the sunlit area of the georeferenced riverine, larval habitat, shade, canopied, floating, hanging and dead vegetation, LULC-related, canopy, endmember components. The corresponding ratio $f = \frac{K_c}{1-K_g}$ for the endmember selection was then defined for the Red Edge, decomposed canopy, biosignature, NDVI, endmember emissivities.

In the unmixing model *n* represented the shadow parameters generated from the unmixed, Red Edge, canopied, endmember biosignature, NDVI, *S damnsoum s.l.,* riverine, larval habitat decomposed mixel. If there was no mutual shadowing, the model rendered *f* = *F*. As *n* increased, however, mutual canopy shadowing occurred and, as such, $K_g = e^{-\lambda\pi R^2\left[\sec\theta_i' + \sec\theta_v' - O\left(\theta_i,\theta_v,\varphi\right)\right]}$. We then defined the mutual canopy shadowing proportion *M* as $M = 1 - \frac{1-K_g}{\lambda\Gamma}$, which was the fraction of total shadowing cast from the floating, hanging and dead vegetation-related, LULC, endmember relection components that fell onto the larval habitat canopy cover instead of the background. The sunlit and viewed shade, canopy-related, riverine, larval habitat, explanatorial, surface data feature attributes were then reduced by hiding either from viewing or from illumination.

The *f*-Ratio with mutual habitat canopy shadowing was $f = \frac{n\Gamma_c - \sum\Delta_{A_c}}{A\left(1-K_g\right)}, = F\frac{1-\sum\Delta_{A_c}/\left(n\Gamma_c\right)}{1-M}$ where $\sum\Delta_{A_c}$ was the total decrement from $n\Gamma_c$ to A_c (i.e., the background-projected area of viewed, sunlit, larval habitat, canopied surface). $\sum\Delta_{A_c}$ was expressed employing three terms: a decrement due to mutual canopy shading in the view direction plus a decrement due to mutual canopy shading in the sun direction, minus those elements shaded in both directions using $\sum\Delta_{A_c} = n\Gamma_v\left(P_v M_v + P_i M_i - P_o\right)$, where P_v was the conditional probability that the geosampled, riverine, canopied, larval habitat faced the sun given that it was mutually shaded from view. *Pi* was the probability that the floating, hanging and dead vegetation -related LULC, canopy endmember surface elements faced the viewer given that it was mutually canopy shaded from illumination. Both P_i and P_v were average proportions of the larval habitat, canopy-related, gridded areas projected in the view direction.

P_o, the third term in the model was the overlapped part of the first two terms, expressed as a fraction of Γ_v. We noted that the P_o, contained three parts derived from the Rapid Eye™ imaged 5 m, explanatorial, geo-spatiotemporally, geosampled, canopy-related, riverine larval habitat, surface elements(i.e., floating, hanging and dead vegetation-related LULCs). This collection contributed to the georeferenced, riverine, larval habitat, canopy hotspot due to the spatial correlation of the shadows. Since the probabilities of being hidden in multiple directions were not independent, we were able to substitute $\sum\Delta_{A_c} = n\Gamma_v\left(P_v M_v + P_i M_i - P_o\right)$ into $f = \frac{n\Gamma_c - \sum\Delta_{A_c}}{A\left(1-K_g\right)}, = F\frac{1-\sum\Delta_{A_c}/\left(n\Gamma_c\right)}{1-M}$ which yielded a single expression for $f = F\frac{1-\Gamma_v\left(P_v M_v + P_i M_i - P_o\right)/\Gamma_c}{1-M}$. We then modelled, P_v, P_i and P_o. We employed all illumination or viewing canopy shadows incorporating M_i or M_v where the Red Edge, NDVI, reflected, canopy boundaries respectively. In our model, P_v,, P_i and P_o, were used to visualize the M_v and M_i boundaries. Since, viewing and illumination canopy-related shadows fell strictly below M_v and M_i boundaries, P_v, the conditional probability that a geospatiotemporal, geosampled, seasonal, habitat canopy surface element facing the sun given the mutually shadowed areas, was the ratio of the illuminated portion of the projected surface below the M_v boundary.

Correspondingly, P_i was the conditional probability that the explanatorial, operationizable, geo-spatiotemporally, geosampled, riverine, *S. damnsoum s.l.,* larval habitat, riverine canopy directly faced the viewer and was mutually shaded from illumination. The ratio of the viewed portion of the projected, Red Edge, NDVI, delineated georefernced, riverine, larval habitat canopy area below the M_i boundary was subsequently quantitated. Note, that M_i was the proportion of mutually-shaded, Red Edge, NDVI, delineated, larval habitat, canopy surface projected to the direction of illumination, but $P_i M_i \Gamma_v$ was the area of this fraction of the habitat canopy surface with floating hanging and dead vegetation-related, LULC endmember components projected to viewing direction. Proper calculation of this portion of the riverine, larval habitat, geosampled canopy and its associated attributes involved some projection change. We then used P_o as the quantized variable representing all the overlapping areas (i.e., o), which was represented as a fraction of Γ_v.

We then considered the case in the principal plane for further geospectrally decomposing the geosampled, riverine, *S. damnsoum s.l.,* larval habitat biosignature. For simplicity, we assumed that all shadows from the Red Edge, canopied, *S. damnosum s.l.* larval habitat, floating, hanging and dead endmember vegetation, LULC components fell below the boundaries M_v and M_i, which were the traces of planes intersecting the spheroid at its center. The angle between the planes of the M_i and the illumination boundary was $\theta_{M_i} = \cos^{-1}\left(1-2M_i\right)$.We defined θ_{M_v} similarly. At the larval habitat hotspot, the M_i and M_v boundaries coincided when $P_v = P_i = 1$, $P_o = M_v = M$, and $f = F = 1$. We then assumed that the viewing zenith angle increased to $\theta_v > \theta_i$. In usual cases when mutual shadowing of an entomological-related, seasonal-geosampled, larval habitat is to be considered, the M_v boundary is higher than the M_i boundary [73].

In the Rapid Eye™ sensor's view, P_v was the ratio of the riverine habitat's surface area between M_v boundary and the illumination boundary to the whole area under the M_v boundary. That is, $P_v = \frac{M_v\Gamma_v - \left(\Gamma_v - \Gamma_c\right)}{M_v\Gamma_v}$ while P_i was one, and P_o cancelled the M_i term. Then, the equation become $f = F\frac{1-P_v M_v \Gamma_v/\Gamma_c}{1-M} = F\frac{\left(1-M_v\right)\Gamma_v}{\left(1-M\right)\Gamma_c} = \frac{1-e^{-\lambda\Gamma_v}}{\left(1-K_g\right)}$. This result suggested that when the viewing direction in the principal plane deviated from

($\theta v > \theta i$), the f-ratio changed in the riverine, *S. damnsoum s.l.,* larval habitat, canopy reflectance model forecasts. When the coverage is very low, the increment of θ_m may be also so small that M_v will be under the M_i boundary [75]. As such, we simply ignored mutual shadowing in the riverine, larval habitat. We did however, realize that when θ_v moved inward on the principal plane but had not reached nadir, the M_i was higher than M_v: hence, $P_v = 1$, $P_o = M_v$, and $P_i = \frac{1-\cos\left(\theta_{M_i} - \theta'_i + \theta'_v \cos\varphi\right)}{1-\cos\theta_{M_i}}$

After θv passed the nadir, the M_v boundary went to the opposite side of the spheroid from M_i. In this case, the Red Edge, NDVI, sub-mixel, geospectral data revealed the horizontal projection of the larval habitat canopy and its floating, hanging and dead vegetation, canopy LULC, explanatorial, endmember decomposed components at $\varphi = \pi/2$. We then used *Pi* just as in Strahler and Jupp [129], with φ equal to π where P_v was the fraction of M_v over the illumination boundary, i.e.,

$$P_v = \left\{ \begin{array}{ll} \dfrac{1-\cos\left(\theta_{M_v} - \theta'_v + \theta'_v \cos\theta\right)}{1-\cos\theta_{M_v}}, & \left(\theta_{M_v} - \theta'_v + \theta'_v \cos\theta\right) \ge 0 \\ 0, & \left(\theta_{M_v} - \theta'_v + \theta'_v \cos\theta\right) < 0 \end{array} \right\}.$$

Note when θ_v was between the riverine, explanatorial, georeferenced, geosampled, larval habitat hotspot and nadir, P_v was always 1 and a discontinuity of P_v appeared at the nadir. This discontinuity arose from the assumption that all the riverine larval habitat shadow components fell under the M_v boundary. Additionally, the M_v at $\theta_v = 0$ was the physical intersection of the canopy boundaries between the larval habitat floating, dead and the hanging immersed, canopy endmember NDVI components, which did not change with viewing geometry: thus, $P_v M_v$ was still continuous at nadir, and equal to P_o. In other words, the *S. damnsoum s.l.* riverine larval habitat canopy formula had a very large viewing zenith, so that $\theta_{M_v} - \theta'_i + \theta'_v \cos\varphi) > 0$. Our decomposed, Red Edge, NDVI, canopy, endmember biosignature model revealed that when M_i and M_v were independent in $\sum \Delta_{A_c}/(n\Gamma_c) = M$, $f = \frac{n\Gamma_c - \sum \Delta_{A_c}}{A\left(1-K_g\right)}, = F\frac{1-\sum \Delta_{A_c}/(n\Gamma_c)}{1-M}$. If all the spatial objects are at the same height, the situation will be very close to the "uniform height case" – mutual, time series, canopy-related shadows will always fall on the lower part of the objects and the object top-viewing effect will be strong [115]. However, when canopy heights are distributed over a wide range, the top layer of the canopy will play a more important role in determining the BRDF of the canopy than the lower layer [112,113]. Therefore, when the *S. damnsoum s.l.* riverine larval habitat canopy structural height in the decomposed, Red Edge, NDVI biosignature was geospectrally quantified by their distribution estimates, the BRDF was apparent.

The BRDF was determined by the size, shape, and height of the geo-spatiotemproally, geosampled, riverine, larval habitat canopy and the floating, hanging and dead vegetation, endmember components in the top layer. Restrictions were exercised when quantitation of a single top layer was conducted, employing the range of distribution of height of the unmixed, geosampled, explanatorial, geosampled, riverine, larval habitat, shade canopied, physical elements in the biosignature and its geosampled attributes when the regressors did not exceed twice the vertical axis of the spheroid. To share the weighting between the geospatiotemporal, geosampled, 5m resolution-derived, covariate, parameter estimator coefficient estimates, the equation $\beta = \left(1 - \frac{h_2 - h_1}{4b}\right)^2$ was employed, if $\left(h_2 - h_1\right) > b$. When $\left(h_2 - h_1\right) > b$, β is forced to be zero there is a requirements to redefine the layers [106]. By so doing, both P_v and P_i were optimally calculated as a weighted sum of corresponding terms $P = \beta P_1 + \left(1-\beta\right)P_2$, where P_1 and P_2 were the spectral time series probabilities associated with the spatial dimensions of the geosampled habitat canopy.

The space of canopy realization was generated by randomly drawing each radiative transfer model input, Red Edge, NDVI, explanatorial variables in ArcGIS within distribution laws. The radiative transfer equations and their boundary conditions were given by:

$$\begin{cases} -\mu\dfrac{\partial \mathrm{I}^{\mathrm{M}}(\tau,\Omega)}{\partial\tau} + \mathrm{I}^{\mathrm{M}}(\tau,\Omega) = \\ \dfrac{\omega}{4\pi\int_{4\pi} p(\Omega'\to\Omega)\mathrm{I}^{\mathrm{M}}(\tau,\Omega')d\Omega'} \\ +Q_1(\tau,\Omega) \qquad \tau \le \tau_\alpha \\ -\mu\dfrac{\partial \mathrm{I}^{\mathrm{M}}(\tau,\Omega)}{\partial\tau} + G(\Omega)\mathrm{I}^{\mathrm{M}}(\tau,\Omega) = \\ \dfrac{1}{\pi}\int_{4\pi} \Gamma(\Omega'\to\Omega)\mathrm{I}^{\mathrm{M}}(\tau,\Omega')d\Omega' \\ +Q_2(\tau,\Omega) \qquad \tau_\alpha < \tau < \tau_t \end{cases}$$

$$\begin{cases} -\mu\dfrac{\partial \mathrm{I}^{\mathrm{M}}(\tau,\Omega)}{\partial\tau} + \mathrm{I}^{\mathrm{M}}(\tau,\Omega) = \\ \dfrac{\omega}{4\pi\int_{4\pi} p(\Omega'\to\Omega)\mathrm{I}^{\mathrm{M}}(\tau,\Omega')d\Omega'} \\ +Q_1(\tau,\Omega) \qquad \tau \le \tau_\alpha \\ -\mu\dfrac{\partial \mathrm{I}^{\mathrm{M}}(\tau,\Omega)}{\partial\tau} + G(\Omega)\mathrm{I}^{\mathrm{M}}(\tau,\Omega) = \\ \dfrac{1}{\pi}\int_{4\pi} \Gamma(\Omega'\to\Omega)\mathrm{I}^{\mathrm{M}}(\tau,\Omega')d\Omega' \\ +Q_2(\tau,\Omega) \qquad \tau_\alpha < \tau < \tau_t \end{cases}$$

where

$$\begin{cases} Q_1(\tau,\Omega) = \dfrac{\omega}{4\pi}\int_{2\pi+} p(\Omega'\to\Omega) \\ \cdot\mathrm{I}^0(\tau,\Omega')d\Omega + \dfrac{\omega}{4\pi}\int_{4\pi} p(\Omega'\to\Omega) \\ \cdot\mathrm{I}^1(\tau,\Omega')d\Omega' \qquad \tau \le \tau_\alpha \\ Q_2(\tau,\Omega) = \dfrac{1}{\pi}\int_{2\pi+} \Gamma(\Omega'\to\Omega) \\ \cdot\mathrm{I}^0(\tau,\Omega')d\Omega' + \dfrac{\omega}{\pi}\int_{4\pi} \Gamma(\Omega'\to\Omega) \\ \mathrm{I}^1(\tau,\Omega')d\Omega' \qquad \tau_\alpha < \tau < \tau_t \end{cases} \tag{3.2}$$

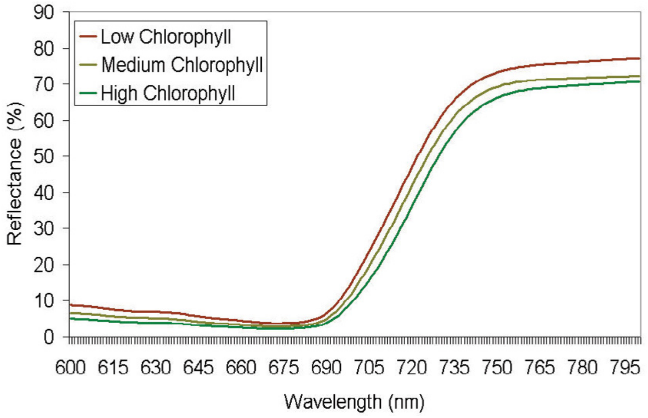

Figure 15: The Red Edge position (REP) estimatation of the chlorophyll content of the geosampled, canopied *S. damnosum* s.l. larval habitat shaded leaves.

Notice that the correction function is not used in the second equation in [3.2], since no hotspot effect was taken into account in the multiple scattering calculations. It was obvious that no closed solution could be derived.The input variables were assumed initially independent as no information was available about their possible covariance. The distribution law of each within a canopied, *S. damnsoum s.l.*, larval habitat, decomposed variable was selected so that the density of probability was set to be proportional to the sensitivity of the shade reflectance to the variable considered. This customizaton allowed qualitatively quantitating sample canopied habitat domains where the reflectance was more sensitive to the spectrally-dependent, Red Edge, NDVI, reflectance, covariate, parameter estimator, coefficients. We achieved this by applying transformations for each decomposed, Red Edge,*S. damnsoum s.l.*, larval habitat, NDVI, biosignature, canopy-related, sub-mixel, explanatorial, predictor variable where the sensitivity of the reflectance was quantitated as constant transformed variable. The transformations were selected employing a trial and error process which was applied directly for quantitating the geo-spatiotemporal red and NIR nadir observations. Then, uniform random drawing was completed over the transformed,Red Edge,*S. damnsoum s.l.*, larval habitat, NDVI, endmember ,unmixed, biosignature-related variables.

In the explanatorial, geometric-optical model, the bidirectional reflectance was modeled as a purely phenomenon that resulted as scenes of discrete, three-dimensional objects (i.e., hanging and floating vegetation, endmember, sub-mixel LULC components) of the geosampled, *S. damnosum s.l.,* riverine, habitat canopy which was viewed from different positions in the hemisphere. The resulting scene was broken down into their canopy fractions specifically sunlit and shadowed background and scene brightness. Illumination direction was calculated by a linear combination of the canopy fractions and their respective radiance estimates. The shape of the 5m-derived, canopied hanging, dead and floating vegetation, endmember patterns of the diffuse ripple water components were among the driving regressors in the model. These *S. damnosum s.l.* riverine habitat canopy spectral, Red Edge, sub-mixel emissivities conditioned the mixture of sunlit and shaded objects and background data that was observed from multiple viewing directions thus quantitating all directions of illumination. This mixture, in turn, controlled the brightness in the image. Corrections of the effects from varying sun sensor target canopy geometries in the multitemporal decomposed datasets were described by the BRDF. Measuring the spread of the corrected results from the desired equal reflectance line provided a measure of the accuracy of our method. After correction, the root mean square (RMS) reflectance errors were approximately 0.01 in the visible and 0.02 in the NIR.

An expression for additional azimuthal variation was also derived from the geometric-optical model. This azimuthal variation differed fundamentally in canopy radiance for each layer of the Red Edge, *S. damnsoum s.l.*, larval habitat, NDVI, riverine, endmember, unmixed, biosignature model. It was observed that all non-zero polar angles were most evident in the larval habitat canopy when vertical and nearly opaque components of the habitat canopy and its floating, dead and trailing vegetation components were illuminated and viewed along polar sun angles. For the variation of the directional reflectance of the canopy cover with azimuthual view angle, shade-related, explanatorial parameters were qualitatively quantified when the illuminated area of the Rapid Eye^{TM} imaged canopied, riverine larval habitat (i.e., georeferenced areas that was affected by the sun at large angles from the zenith) was remotely identified. The 5m model characterized the geometric patterns of the first derivative reflectance spectra in the Red Edge region of the georeferenced, geosampled, *S. damnosum* s.l., riverine, larval habitat. The ratio of the Red Edge area was less than 731 nm to the entire Red Edge area which was negatively correlated with canopy chorophyll count. This finding allowed the construction of a new Red Edge parameter, defined by Red Edge symmetry (RES).

Compared to the commonly used Red Edge parameters (i.e., Red Edge position, Red Edge amplitude, and Red Edge area), RES was a better predictor of low chorophyll content in the riverine larval habitat canopy. RES was easily calculated using the reflectance of Red Edge boundary wavebands at 675 and 755 nm (R675 and R755) and reflectance of Red Edge center wavelength at 718 nm (R718), employing the equation RES = (R718-R675)/(R755- R675). Compared to the commonly used Red Edge parameters RES may be a better operationizable predictor of, shade, canopied, geo-spatiotemporal, prolific, *S. damnsoum* s.l., riverine, larval habitats geosampled in African riverine environments.

The Red Edge position was also used to exactly estimate the chlorophyll content of leaves and over the canopy RES of the geosampled, *S. damnosum* s.l. riverine, canopied, larval habitat which was easily calculated using the reflectance of Red Edge boundary wavebands at 675 and 755 nm (R_{675} and R_{755}) and reflectance of Red Edge center wavelength at 731nm (R_{718}), with the equation RES = (R_{718}-R_{675})/(R_{755}- R_{675}). The close relationships between the simulated RES and riverine, larval habitat canopy chorophyll count indicated a high feasibility of forecasting the phosynthetic pigment with simulated RES from the Rapid Eye^{TM} data. We summized that the Red Edge was a region in the red-NIR transition zone of the riverine, habitat, canopy, vegetation, LULC-related, reflectance, spectrum marked the boundary between absorption by chlorophyll in the red visible region, and scattering due to leaf internal structure in the NIR region (Figure 15).

The distance between two large sun angles *A* and *B* were then used as representive canopy explanatorily, decomposed, georeferenced, geosampled, geospectrally, shade, canopied, *S. damnosum* s.l., vegetated, larval habitat, reflectance points which were quantized by $\det\begin{bmatrix} 0 & \mathrm{d}(\mathrm{AB})^2 & \mathrm{d}(AC)^2 & 1 \\ \mathrm{d}(\mathrm{AB})^2 & 0 & \mathrm{d}(BC)^2 & 1 \\ \mathrm{d}(AC)^2 & \mathrm{d}(BC)^2 & 0 & 1 \\ 1 & 1 & 1 & 0 \end{bmatrix} = 0$. The first few spectrally decomposed *S. damnosum* s.l. canopy, endmember coefficients for j=0,..was then calculated as, 2, -16, 288, -9216, 460800,..For j=2, where the matrix became $-16\Delta^2 = \begin{vmatrix} 0 & 1 & 1 & 1 \\ 1 & 0 & c^2 & b^2 \\ 1 & c^2 & 0 & a^2 \\ 1 & b^2 & a^2 & 0 \end{vmatrix}$ which, then subsequently rendered areas for a plane triangle with side lengths a, b, and c, (i.e., a form of Heron's formula).

Given the lengths of the georeferenced, geosampled, *S. damnsoum* s.l. riverine larval habitat canopy reflected sides a, b, and c, and the semi perimeter $S \equiv \frac{1}{2}(a+b+c)$ of a triangle, Heron's formula of the area Δ of a triangle was remotely quantited as $\Delta = \sqrt{S(S-a)(S-b)(S-c)}$ The Heron's formula then employed a Cayley-Menger determinant as $-16\Delta^2 = \begin{vmatrix} 0 & a & b & c \\ a & 0 & c & b \\ b & c & 0 & a \\ c & b & a & 0 \end{vmatrix} = \begin{vmatrix} 0 & 1 & 1 & 1 \\ 1 & 0 & c^2 & b^2 \\ 1 & c^2 & 0 & a^2 \\ 1 & b^2 & a^2 & 0 \end{vmatrix}$. Another highly symmetrical form of the reflected larval habitat canopy points was then rendered by

$$\left(4\Delta^2\right) = \left[a^2 \ b^2 \ c^2\right] \begin{vmatrix} -1 & 1 & 1 \\ 1 & -1 & 1 \\ 1 & 1 & -1 \end{vmatrix} = \begin{vmatrix} a^2 \\ b^2 \\ c^2 \end{vmatrix}.$$

For j=3, the content of the 3-simplex (i.e., volume of the general tetrahedron) was then given by the determinant $288\,V^2 = 2\begin{vmatrix} 0 & 1 & 1 & 1 & 1 \\ 1 & 0 & d_{12}^2 & d_{13}^2 & d_{14}^2 \\ 1 & d_{21}^2 & 0 & d_{23}^2 & d_{24}^2 \\ 1 & d_{31}^2 & d_{32}^2 & 0 & d_{34}^2 \\ 1 & d_{41}^2 & d_{42}^2 & d_{43}^2 & 0 \end{vmatrix}$ where the georefernced, geosampled *S. damnosum* s.l. canopy edge between vertices *i* and *j* had length d_{ij}. Setting the left side equal to 0 (corresponding to a tetrahedron of volume 0) rendered a relationship between Euclideanized distances of the highly reflected, prolific, canopied, riverine, habitat geosampled points in ArcGIS from the less reflective canopied points (i.e., vertices of a planar quadrilateral) [65]. This determinant used the Heron's formula which was equal to −16 times the square of the area of a triangle with side lengths *d* (*AB*), *d* (*BC*), and *d* (*AC*). If this determinant equaled zero our assumption was that the procedure was equivalent to checking whether the triangle with vertices *A*, *B*, and *C* had zero area. Thereafter, the vertices in the shade, canopied, explanatorial, *S. damnosum s.l.* riverine, larval habitat endmember, geospectrally, temporally dependent, forecasting, explanatorial, risk model was diagnosed as collinear.

We employed a residual autocorrelation matrix in ArcGIS to treat the *S. damnosum* s.l. riverine, larval habitat, endmember, spectral collinearity. It consisted of elements of the discrete autocorrelation function, $R_{xx}(j)$ arranged in the following manner:

$$R_x = E\left[XX^H\right] \begin{vmatrix} R_{xx}(0) & R^*_{xx}(1) & R^*_{xx}(2) & \ldots R^*_{xx}(N\text{-}1) \\ R_{xx}(1) & R_{xx}(0) & R^*_{xx}(1) & \ldots R^*_{xx}(N\text{-}2) \\ R_{xx}(2) & R_{xx}(1) & R_{xx}(0) & \ldots R^*_{xx}(N\text{-}3) \\ . & . & . & . \\ . & . & . & . \\ R_{xx}(N-1) & R_{xx}(N-1) & R_{xx}(N-3) & \ldots R_{xx}(0) \end{vmatrix}$$

This was clearly a Hermitian matrix. In mathematics, a Hermitian matrix (or self-adjoint matrix) is a square matrix with complex entries that is equal to its own conjugate transpose—that is, the element in the *i*-th row and *j*-th column is equal to the complex conjugate of the element in the *j*-th row and *i*-th column, for all indices *i* and *j*: $a_{ij} = \overline{a}_{ij}$ or $A = A^{\overline{T}}$, in matrices that can be understood as the complex extension of real symmetric matrices [1].

In spherical coordinates, the scale factors are $h_r = 1$, $h_\theta = r \ sin \ \phi$, $h_\theta = r$, and the separation functions are $f_1(r) = r^2$, $f_2(\theta) = 1$, $f_3(\phi) = sin\phi$, giving a Stäckel determinant of S=1. The Laplacian we used in this model was $\nabla^2 = \frac{1}{r^2}\frac{\partial}{\partial r}\left(r^2 \frac{\partial}{\partial r}\right) + \frac{1}{r^2 Sin^2}\frac{\partial}{\partial \phi}\left(Sin \ \phi \ \frac{\partial}{\partial \phi}\right)$ To solve Laplace's equation in spherical coordinates, we attempt separation of the geosampled, georeferenced, *S. damnosum* s.l. –related, larval habitat, predictor variables by writing $F = (r,\theta,\phi) = R(r)\Theta(\theta)\Phi(\phi)$. Then the Helmholtz differential equation becames

$$\frac{d^2R}{d\ r^2}\Phi\Theta + \frac{2}{r}\ \frac{d\ \mathrm{R}}{d\ \mathrm{r}}\Phi\Theta + \frac{1}{r^2 Sin^2\phi}\frac{d^2\Theta}{d\ \theta^2}\Phi R + \frac{Cos\phi}{r^2 Sin^2\phi}\frac{d\Phi}{d\ \phi}\Theta R + \frac{1}{r^2}\frac{d^2\Phi}{d\ \phi^2}\Theta R = 0$$

We then divided the product be by $\mathrm{R}\Theta\Phi$,

$$\frac{r^2 Sin^2\ \phi}{\Phi R\ \Theta}\Phi\Theta + \frac{d^2\ \mathrm{R}}{d\ \mathrm{r}^2} + \frac{2}{r}\frac{r^2 Sin^2\phi}{\Phi R\Theta}\Phi\Theta\frac{d\ \mathrm{R}}{d\ \mathrm{r}} + \frac{1}{r^2 Sin^2\phi}\frac{r^2 Sin^2\phi}{\Phi R\Theta}\frac{d^2\Theta}{d\ \theta^2}$$

$$+\left(\frac{\cos\phi\sin\phi}{\Phi}\frac{d\Phi}{d\Phi} + \frac{\sin^2\Phi}{\Phi}\frac{d^2\Phi}{d\Phi^2}\right) = 0$$

The solution to the second part of the decomposition was sinusoidal for quantitating the *S. damnosum* s.l. larval habitat risk model predictors so we used differential equation $\frac{d^2\Theta}{d\ \theta^2}\frac{1}{\Theta} = -m^2$ which then rendred solutions which were defined either as a complex function with, $m = -\infty,\ldots,\infty\Theta(\theta) = A_m e^{im\theta}$ or as a sum of real sine and cosine functions with $m = -\infty,\ldots,\ \infty_T\Theta(\theta) = S_m \sin(m\theta) + c_m \cos(m\theta)$ By so doing, the equation created was delineated as

$$\frac{r^2}{R}\frac{d^2\ \mathrm{R}}{d\ \mathrm{r}^2} + \frac{2r}{R}\frac{d\ \mathrm{R}}{d\ \mathrm{r}}\frac{1}{Sin^2\phi}\left(\frac{\cos\phi\sin\phi}{\Phi}\frac{d\ \Phi}{d\ \phi} + \frac{Sin^2\phi}{\Phi}\frac{d^2\Phi}{d\phi^2} - m^2\right) = 0$$

The radial part must be equal to a constant

$$\frac{r^2}{R}\frac{d^2\,\mathrm{R}}{d\,\mathrm{r}^2}+\frac{2r}{R}\frac{d\,\mathrm{R}}{d\,\mathrm{r}}=l(l+1)r^2\frac{d^2\,\mathrm{R}}{d\,\mathrm{r}^2}+2r\frac{dR}{dr}=l(l+1)r$$

But this is the Euler differential equation (see Appendix 2), so we tried a series solution of the form $R+\sum_{n=0}^{\infty}a_n r^{n+c}$ Then $r^2+\sum_{n=0}^{\infty}(n+c)(n+c-1)a_n r^{n+c-2}+2r\sum_{n=0}^{\infty}(n+c)a_n r^{n+c-1}$ and there after

$$-l(l+1)\sum_{n=0}^{\infty}a_n r^{n+c}=0 \text{ and } \sum_{n=0}^{\infty}(n+c)(n+c-1)-a_n r^{n+c}+$$

$$2\sum_{n=0}^{\infty}(n+c)a_n r^{n+c}-l(l+1)\sum_{n=0}^{\infty}a_n r^{n+c}=0$$

$$\sum_{n=0}^{\infty}\left[(n+c)(n+c+1)-l(l+1)\right]a_n r^{n+c}=0$$

The general nonhomogeneous differential equation was given by $x^2\frac{d^2y}{dx^2}+\alpha x\frac{dy}{dx}+\beta y=S(x)$ and the homogeneous equation is $x^2y''+\alpha xy'+\beta y=0^{y''}+\frac{\alpha}{x}y'+\frac{\beta}{x^2}y=0\ y''+\frac{\alpha}{x}y'+\frac{\beta}{x^2}y=0$ We attempted to convert the equation from $y''+p(x)y'+q(x)y=0$ to one with constant coefficients $\frac{d^2y}{dz^2}+A\frac{dy}{dz}+By=0$ by using the standard transformation for linear second-order ordinary differential equations. Comparing the equation functions *p(x)* and *q(x)* are $p(x)\equiv\frac{\alpha}{x}=\alpha x^{-1}q(x)\equiv\frac{\beta}{x^2}=\beta x^{-2}$ We let B$\equiv\beta$ and define z= $B^{-\frac{1}{2}}\int\sqrt{q(x)}dx=\beta^{-\frac{1}{2}}\int\sqrt{\beta x^{-2}}\ \mathrm{dx}=\int x^{-1}dx=l\eta x$ =Then A was given by A=

$$\frac{q'(x)+2p(x)q(x)}{2\left[q(x)\right]^{3/2}}B^{1/2},=\frac{-2\beta x^{-3}+2\left(\alpha x^{-1}\right)\left(\beta x^{-2}\right)}{2\left[\beta\left(x^{-2}\right)\right]^{3/2}}B^{1/2}=\alpha-1$$

which was a constant. Therefore, the equation became a second-order ordinary differential equation with constant coefficients $\frac{d^2y}{dz^2}+(\alpha-1)\frac{dy}{dz}+By=0$

We then defined $r_1={}^{1/2\left(-A+\sqrt{A^2-4B}\right)}={}^{1/2\left[1-\alpha+\sqrt{(\alpha-1)^2-4\beta}\right]}$,

$r_2={}^{1/2\left(-A-\sqrt{A^2-4B}\right)}={}^{1/2\left[1-\alpha+\sqrt{(\alpha-1)^2-4\beta}\right]}$ and a $^{1/2(1-\alpha)}$ The solutions were and

$$y=\begin{cases}c_1e^{r_1z}+c_2e^{r_2z} & (\alpha-1)^2>4\beta\\(c_1+c_2z)e^{az} & (\alpha-1)^2=4\beta\\e^{(az)}[c_1cos(bz)+c_2sin(bz)] & (\alpha-1)^2<4\beta\end{cases}$$

In terms of the original variable *x*, the model revealed:

$$y=\begin{cases}c_1|x|^{r_1}+c_2|x|^{r_2} & (\alpha-1)^2>4\beta\\(c_1+c_2\ln|x|)|x|^a & (\alpha-1)^2=4\beta\\|x|^a[c_1cos(b\ln|x|)+c_2sin(b\ln|x|)] & (\alpha-1)^2<4\beta\end{cases}$$

Zwillinger (1997, p. 120) gives two other types of equations known as Euler differential equations, $y=\pm\sqrt{\frac{ay^4+by^3+cy^2+dy+e}{ax^4+bx^3+cx^2+dx+e}}$ (Valiron 1950, p. 201) and $y'+y^2=ax$.

The r^c term (with n=0), c(c+1)=l(l+1), in the risk model was true only if c=l, l-1 and all other terms were not present. So $a_n=0$ for n≠l,–l–1. Therefore, the solution of the ***R*** component had to be be given by $Rl(r)=A_lr^l+B_lr^{-l+1}$ Plugging the output back into (◇) rendered, $l(l+1)-\frac{m^2}{Sin^2\phi}+\frac{Cos\phi}{Sin\phi}\frac{1}{\phi}\frac{d\Phi}{d\phi}+\frac{1}{\Phi}\frac{d^2}{d\phi^2}=0$ and $\Phi''\frac{Cos\phi}{Sin\phi}\Phi'+\left[l(l+1)-\frac{m^2}{Sin^2\phi}\right]\Phi=0$ which is the associated Legendre differential equation for $x=Cos\phi$ and m=0,.., l The general complex solution was therefore $\sum_{i=0}^{\infty}\sum_{m=-l}^{i}A_lr^l+B_lr^{(-l-1)})P_l^m(cos\phi)e^{(-im\theta)}\equiv\sum_{i=0}^{\infty}\sum_{m=-1}^{\infty}(A_lr^l+B_lr^{(-l-1)})Y_l^m(\theta,\phi),$ where $Y_l^m(\theta,\phi)=P_l^m(cos\phi)e^{-im\ \theta}$ were the spherical harmonics. The generalized real solution was $\sum_{i=0}^{\infty}\sum_{m=0}^{l}\left(A_lr^l+B_lr^{-l-1}\right)p_l^m(Cos\phi)\left[S_l^m(m\theta)+C_l^mCos(m\theta)\right]$ Some of the normalization constants of p_l^m were absorbed by S_m and C_m, so this equation appeared in the form where $Y_l^{m(o)}(\theta,\phi)\equiv P_l^m(Cos\phi)Sin(m\theta)$ and $Y_l^{m(e)}(\theta,\phi)\equiv P_l^m(Cos\phi)Sin(m\theta)$ were the even and odd (real) spherical harmonics. If azimuthal symmetry is present, then $\Theta(\theta)$ is constant and the solution of the Φ component is a Legendre polynomial $P_l(Cos\phi)$. The general solution would then be then

$$F(r,\phi)=\sum_{i=0}^{\infty}\left(A_lr^l+B_lr^{-l+1}\right)P_l(Cos\phi)$$

A Bayesian probabilistic estimation matrix was then employed in PROC MCMC consisting of *n* the dependent, shade canopied,

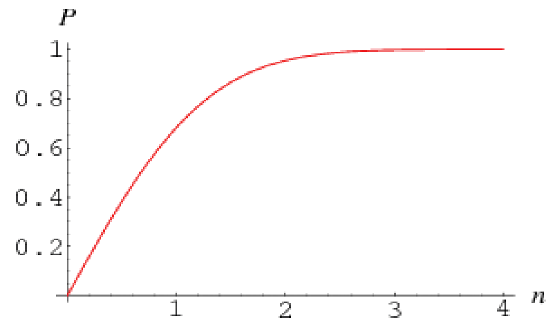

Figure 16: The confidence interval symmetrically placed around the mean, so a 50% confidence interval for a symmetric probability density function would be the interval [-*a*, *a*] such that $\frac{1}{2}=\int_{-a}^{a}P(x)\,dx.$

explanatorial, *S. damnosums.l.,* riverine, larval habitat endmember, sub-mixel, observations $x_1,..,x_n$ and a p-dimensional random vector$X\in\mathbf{R}^{p\times 1}$ (i.e, a $p\times1$ column-vector) and an unbiased stimator of the ($p\times p$) covariance matrix $\operatorname{cov}(X)=\operatorname{E}\left[\left(X-\operatorname{E}[X]\right)\left(X-\operatorname{E}[X]\right)^{\mathrm{T}}\right]$. The sample covariance matrix $\mathbf{Q}=\frac{1}{n-1}\sum_{i=1}^{n}(x_i-\overline{x})(x_i-\overline{x})^{\mathrm{T}}$, was generated where X_i was the i-th endmember, explanatorial, riverine, larval habitat observation of the p-dimensional random vector, where $\overline{x}=\begin{bmatrix}\overline{x}_1\\ \vdots\\ \overline{x}_p\end{bmatrix}=\frac{1}{n}\sum_{i=1}^{n}x_i$ was the sample mean. The reason for the factor $n-1$ being employed in the *S. damnsoum* s.l., endmember, spectral, uncertainty model rather than n was because a factor appeared was biased in the estimates of sample variances and sample covariances, a maximum likelihood estimator. Thereafter a sample mean was generated.

Next a maximum likely hood estimator (MLE) of the *S. damnsoum* s.l. endmember uncertainty covariance matrix was constructed which rendered an unbiased estimate which was subsequently given by $\mathbf{Q_n}=\frac{1}{n}\sum_{i=1}^{n}(x_i-\overline{x})(x_i-\overline{x})^{\mathrm{T}}$. in SAS. The unbiased uncertainty estimate of the covariance matrix provides an acceptable estimate when the data vectors in the observed dataset are all complete: that is they contain no missing elements [12]. The approach for estimating the shade, canopied, explanatorial, *S. damnosums*.l., riverine, larval habitat, endmember, Bayesian, covariance matrix was to treat the estimation of each variance separately, and to use all the decomposed observations for which both variables had valid values. Assuming the missing data were missing at random resulted in an estimate for the covariance matrix bein biased. When estimating the cross-covariance of a pair of signals that are wide-sense stationary, missing samples do not need be random (e.g., sub-sampling by an arbitrary factor is valid) [69]. Confidence intervals were generated corresponding to a given *S. damnsoum* s.l. endmember uncertainty probability estimate T (Figure 16).

For a normal distribution, the probability that a given *S. damnsoum* s.l. larval habitat canopy end member measurement falls within **n** standard deviations ($n\sigma$) of the mean u (i.e., within the interval $\left[u-n\sigma,u+n\sigma\right]$) was given by

$$P\left[u-n\sigma<x<u+n\sigma\right]=\frac{1}{\sigma\sqrt{2\pi}}\int_{u-n\sigma}^{u+n\sigma}e^{-(x-u)^2/\left(2\sigma^2\right)}dx$$

$$=\frac{2}{\sigma\sqrt{2\pi}}\int_{u}^{u+n\sigma}e^{-(x-u)^2/\left(2\sigma^2\right)}dx$$

We then let $u\equiv\left(x-u\right)/\sqrt{2\sigma}$, so $du=dx/\sqrt{2\sigma}$. Then= $P\left[u-n\sigma<x<u+n\sigma\right]=$

$$\frac{2}{\sigma\sqrt{2\pi}}\sqrt{2}\,\sigma\int_{0}^{n/\sqrt{2}}e^{-u^2}du\,\frac{2}{\sqrt{\pi}}\int_{0}^{n/\sqrt{2}}e^{-u^2}du\ \operatorname{erf}\left(\frac{n}{\sqrt{2}}\right)$$ where

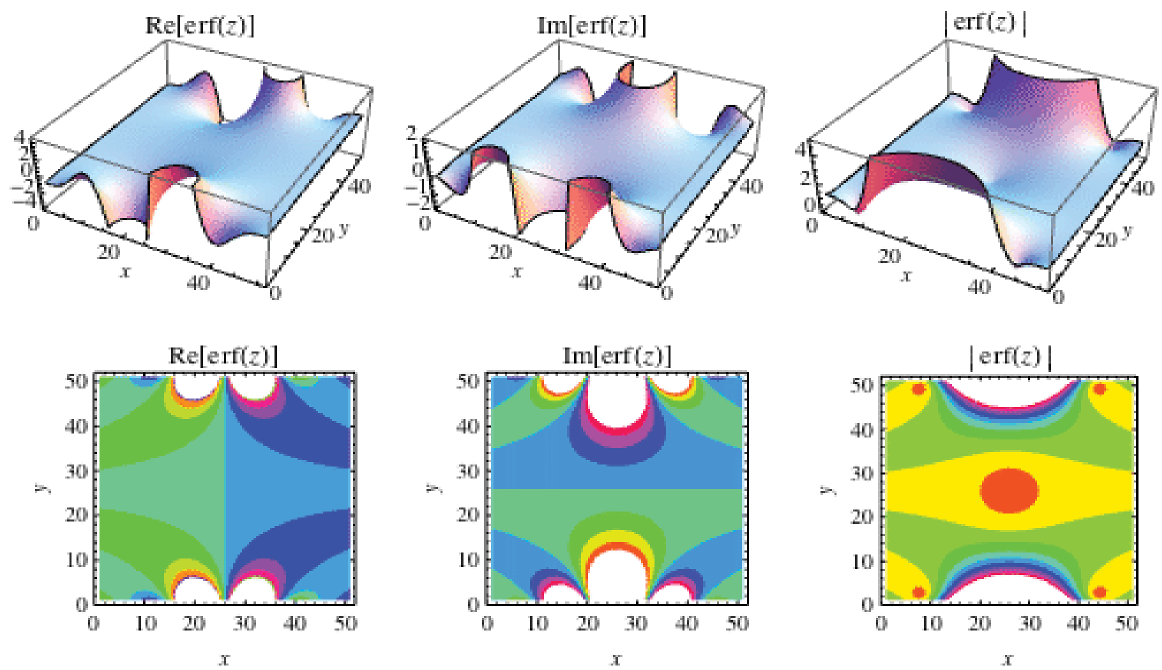

Figure 17: The *S. damnsoum* s.l. larval habitat Erf expressed in terms of a hyper geometric function of the first kind ***M*** as $erf=\left(Z\right)=\frac{2Z}{\sqrt{\pi}}M\left(\frac{1}{2},\frac{3}{2},-Z^2\right)$ $=\frac{2Z}{\sqrt{\pi}}e^{-Z^2}M\left(1,\frac{3}{2},Z^2\right)$ with the derivative $\frac{d^n}{dz^n}erf\left(Z\right)=\left(-1\right)^{n-1}\frac{2}{\sqrt{\pi}}H_{n-1}\left(Z\right)e^{-Z^2}$

erfr(x) was the so-called erf function. erf(z) is the "error function" encountered in integrating the normal distributionwhich is a normalized form of the Gaussian function. In the *S. damnosum* s.l., canopied endmember, forecasting, eco-epidemiological, risk model entire function defined by $erf(Z) \equiv \frac{2}{\sqrt{\pi}} \int_0^Z e^{-r^2} dt$ [4]. Erf is implemented in the Wolfram Language as erf [*z*]. A two-argument form giving $erf(Z_1) = erf(Z_0)$ was also implemented as erf [*z0, z1*]. *S. damnsoum* s.l. larval habitat endmember erf satisfied the identities $erf(Z_1) = 1 - erf(Z) \frac{2_Z}{\sqrt{\pi}} 1F_1\left(\frac{1}{2}; \frac{3}{2}; -Z^2\right) = \frac{2_Z e^{-Z^2}}{\sqrt{\pi}} 1F_1\left(1; \frac{1}{2}; \frac{3}{2}; -Z^2\right)$ where erfc(z) was erfc, the complementary error function, and 1 $F_1(a;b;z)$ was a confluent hypergeometric function of the first kind. For Z>0, $erf(Z) = \pi^{-1/2} \gamma\left(\frac{1}{2}, Z^2\right)$ where γ (a, x) was the incomplete gamma function.

We also defined a *S. damnsoum* s.l. larval habitat endmember erf can as a Maclaurin series where $erf(Z_1) = 1 - erf(Z) \frac{2_Z}{\sqrt{\pi}} 1F_1\left(\frac{1}{2}; \frac{3}{2}; -Z^2\right)$ $= \frac{2_Z e^{-Z^2}}{\sqrt{\pi}} 1F_1\left(1; \frac{1}{2}; \frac{3}{2}; -Z^2\right)$ Similarly, we noted that $erf^2(Z) = \frac{4}{\pi}\left(Z^2 - \frac{2}{3}Z^4 + \frac{14}{45}Z^6 - \frac{4}{35}Z^8 + \frac{166}{4725}Z^{10} + \ldots\right)$ For x<<1, erf(x) from $erf(x) = \frac{1}{\sqrt{\pi}} e^{-x^2} \sum_{n=0}^{\infty} \frac{(2x)^{2n+1}}{(2n+1)!!}$ was computed. For x>>1, $erf(x) = \frac{2}{\sqrt{\pi}}\left(\int_0^{\infty} e^{-t^2} dt - \int_x^{\infty} e^{-t^2} dt\right) -= 1 - \frac{2}{\sqrt{\pi}} \int_x^{\infty} e^{-t^2} dt$ was computed employing the integration the forecast derivatives rendered

$$\int_x^{\infty} e^{-t^2} dt = -\frac{1}{2} \int_x^{\infty} \frac{1}{t} d\left(e^{-t^2}\right) = -\frac{1}{2}\left[\frac{e^{-t^2}}{t}\right]_x^{\infty} - \frac{1}{2} \int_x^{\infty} \frac{e^{-t^2}\, dt}{t^2} =$$

$$\frac{e - x^2}{2x} + \frac{1}{4} \int_x^{\infty} \frac{1}{4} \int_x^{\infty} \frac{1}{t^3} d\left(e^{-t^2}\right)$$

$$\frac{e^{-x^2}}{2x} - \frac{e^{-x^2}}{4x^3} - \ldots, \text{ so} \qquad erf = (x) 1 - \frac{e^{-x^2}}{\sqrt{\pi x}}\left(1 - \frac{1}{2x^2} - \ldots\right)$$

x_n	$p(\mu - x_n < x < \mu + x_n)$
σ	0.6826895
2σ	0.9544997
3σ	0.9973002
4σ	0.9999366
5σ	0.9999994

Table 6:summarized probabilities $p(\mu - x_n < x < \mu + x_n)$ of*S. damnsoum*s.l. larval habitat endmember measurements from a normal distribution fall within $[\mu - x_n, \mu + x_n]$ for $x_n = n\sigma$.

x_n	$p(\mu - x_n < x < \mu + x_n)$
σ	0.6826895
2σ	0.9544997
3σ	0.9973002
4σ	0.9999366
5σ	0.9999994

Table 7:summarized probabilities $p(\mu - x_n < x < \mu + x_n)$ of*S. damnsoum*s.l. larval habitat endmember measurements from a normal distribution fall within $[\mu - x_n, \mu + x_n]$ for $x_n = n\sigma$.

and continuing the procedure gave the asymptotic series $erf = (x) 1 - \frac{e^{-x^2}}{\sqrt{\pi x}} \sum_{n=0}^{\infty} \frac{(-1)^n (2n-1)!!}{2^n} x^{-(2n+1)}$ $1 - \frac{e^{-2}}{\sqrt{\pi}}\left(x^{-1} - \frac{1}{2}x^{-3} + \frac{3}{4}x^{-5} - \frac{15}{8}x^{-7} + \frac{105}{16}x^{-9} + \ldots\right)$ Erf had the values erf(0) and erf (∞) (Figure 17). The erf had an odd function [i.e., erf (-Z)=-erf(Z) and satisfied erf (Z)+erf(Z)=1.where H_n was the prolific, shade , canopied, geo-spatiotemrpoally geosampled, *S. damnsoum* s.l. larval habitat Erf expressed in terms of a hypergeometric function of the first kind with a confluent Hermite polynomial. The first derivative was $\frac{d}{dZ} erf(Z) = \frac{2}{\sqrt{\pi}} e^{-z^2}$, and the intergral was

$$\int erf(Z) dz = z\ erf(Z) + \frac{e^{-z^2}}{\sqrt{\pi}}$$

The multivariate normal distribution of a *k*-dimensional random vector $\mathbf{x} = [X_1, X_2, \ldots, X_k]$ was written in the following notation using the *S. damnosum* s.l., larval habitat specified regressors $\mathbf{x} \sim \mathcal{N}(\mu, \Sigma)$, to make it explicitly known that *X* is *k*-dimensional, $\mathbf{x} \sim \mathcal{N}_k(\mu, \Sigma)$ with *k*-dimensional mean vector $u = \left[E[X_1], E[X_2], \ldots, E[X_K]\right]$ and K*Kcovariance matrix $\Sigma = \left[Cov\left[X_{i,} X_j\right]\right], i = 1, 2, \ldots, K; 1, 2, \ldots, K$. The multivariate normal distribution was "non-degenerative" since the symmetric covariance matrix $\sum$ was positive definite. The distribution of the geosampled, canopied, riverine, larval habitat, shaded, covariate coefficients was $f_{\mathbf{x}}(x_1, \ldots, x_k) = \frac{1}{\sqrt{(2\pi)^k |\boldsymbol{\Sigma}|}} \exp\left(-\frac{1}{2}(\mathbf{x} - \mu)^{\mathrm{T}} \boldsymbol{\Sigma}^{-1} (\mathbf{x} - \mu)\right)$, where X was a real *k*-dimensional column vector and $|\Sigma|$ was the determinant of $\boldsymbol{\Sigma}$. Note the equation reduced the univariate normal distribution if $\boldsymbol{\Sigma}$ was a 1 × 1 matrix. A table was generated (Table 6).

Conversely, to find the probability **P** confidence interval centered about the mean for a normal distribution in units of σ, we solved $\frac{2}{\sqrt{\pi}} \int_0^{n/\sqrt{2}} e^{-u^2} du$ **n** to obtain $n = \sqrt{2} erf^{-1}(P)$, where $erf^{-1}(x)$ was the inverse erf function (Table 7). These values were returned by Normal CI [0, 1, Confidence Level ->*P*] in the Wolfram Language package HypothesisTesting`.

A random vector $X \in \mathbf{R}^p$ (i.e., a $p \times 1$ "column vector"), multivariate, normal distribution with a nonsingular covariance matrix Σ was then generated. We noted that $\Sigma \in \mathbf{R}^{p \times p}$ was a positive-definite matrix and the probability density function of *X* was $f(x) = (2\pi)^{-p/2} \det(\Sigma)^{-1/2} \exp\left(-\frac{1}{2}(x - \mu)^{\mathrm{T}} \Sigma^{-1} (x - \mu)\right)$ where $\mu \in \mathbf{R}^{p \times 1}$ was the expected value of *X*. The shade, canopied, *S. damnosum* s.l. riverine, larval habitat, endmember, sub-mixel, decomposed, covariance matrix Σ was the multidimensional analog of what in one dimension was the variance, and $(2\pi)^{-p/2} \det(\Sigma)^{-1/2}$ which normalized the density $f(x)$ so that it was integrated to 1. We also noted that the dataset of the unmixed *S. damnosums*.l. riverine, larval habitat endmembers $X_1, \ldots, X_n$ were independent and identically distributed samples. Based on the observed values $x_1, \ldots, x_n$ of this sample, we estimated Σ.

The likelihood function of the unmixed *S.damnosum* s.l. riverine, larval habitat, eco-peidemiological, forecasting, risk model was then calculated as $\mathcal{L}(\mu,\Sigma)=(2\pi)^{-np/2}\prod_{i=1}^{n}\det(\Sigma)^{-1/2}\exp\left(-\frac{1}{2}(x_i-\mu)^{\mathrm{T}}\Sigma^{-1}(x_i-\mu)\right)$. It was then readily shown thereafter that the MLE of the mean vector μin the canopied, explanatorial, S. *damnosums*.l. riverine, larval habitat, endmember, covariance matrix was "sample mean" vector: $\overline{x}=(x_1+\cdots+x_n)/n$. Since the estimate $\overline{\mathrm{X}}$ did not depend on Σ, we substituted it for μ in the likelihood function which rendered $\mathcal{L}(\overline{x},\Sigma)\propto\det(\Sigma)^{-n/2}\exp\left(-\frac{1}{2}\sum_{i=1}^{n}(x_i-\overline{x})^{\mathrm{T}}\Sigma^{-1}(x_i-\overline{x})\right)$, Thereafter, the value of Σ that maximized the likelihood of the autorgressive sub-mixel decomposed data was saught.

We regarded the scalar $(x_i-\overline{x})^{\mathrm{T}}\Sigma^{-1}(x_i-\overline{x})$ as the trace of a 1×1 matrix. This made it possible to employ the identity tr(*AB*)=tr(*BA*) as *A* and *B* matrices. We then obtained

$$\mathcal{L}(\overline{x},\Sigma)\propto\det(\Sigma)^{-n/2}\exp\left(-\frac{1}{2}\sum_{i=1}^{n}\mathrm{tr}((x_i-\overline{x})^{\mathrm{T}}\Sigma^{-1}(x_i-\overline{x}))\right)$$

$$=\det(\Sigma)^{-n/2}\exp\left(-\frac{1}{2}\sum_{i=1}^{n}\mathrm{tr}((x_i-\overline{x})(x_i-\overline{x})^{\mathrm{T}}\Sigma^{-1})\right)$$

$$=\det(\Sigma)^{-n/2}\exp\left(-\frac{1}{2}\mathrm{tr}\left(\sum_{i=1}^{n}(x_i-\overline{x})(x_i-\overline{x})^{\mathrm{T}}\Sigma^{-1}\right)\right)$$

$$=\det(\Sigma)^{-n/2}\exp\left(-\frac{1}{2}\mathrm{tr}\left(S\Sigma^{-1}\right)\right)\text{where}$$

$S=\sum_{i=1}^{n}(x_i-\overline{x})(x_i-\overline{x})^{\mathrm{T}}\in\mathbf{R}^{p\times p}$. was the scatter matrix. Since it follows from the spectral theorem of linear algebra that a positive-definite symmetric matrix *S* has a unique positive-definite symmetric square root $S^{1/2}$, we usedthe "cyclic property" of the trace to write $\det(\Sigma)^{-n/2}\exp\left(-\frac{1}{2}\mathrm{tr}\left(S^{1/2}\Sigma^{-1}S^{1/2}\right)\right)$.in the canopied, explanatorial, S. *damnosums*.l. riverine, larval habitat, endmember covariance matrix. We then let $B=S^{1/2}\Sigma^{-1}S^{1/2}$. Then the expression became $\det(S)^{-n/2}\det(B)^{n/2}\exp\left(-\frac{1}{2}\mathrm{tr}(B)\right)$. The positive-definite matrix *B* can be diagonalized, and then the problem of finding the value of *B* that maximized $\det(B)^{n/2}\exp\left(-\frac{1}{2}\mathrm{tr}(B)\right)$ [12]. Since the trace of a square matrix equaled the sum of S. *damnosums*.l., riverine, larval habitat, sub-mixel, eigenvalues ("trace and eigenvalues"), the equation reduced to the problem of finding the eigenvalues λ_1,.., λ_p that maximized $\lambda_i^{n/2}\exp(-\lambda_i/2)$. When we solved the equation we obtained $\lambda_i=n$ for all *i*.

Finally we obtained $\Sigma=S^{1/2}B^{-1}S^{1/2}=S^{1/2}\left(\frac{1}{n}I_p\right)S^{1/2}=\frac{S}{n}$, [i.e., the *p*×*p* "sample explanatorial, S. *damnosums*.l. riverine, larval habitat, canopy endmember, covariance uncertainty matrix"(i.e., $\frac{S}{n}=\frac{1}{n}\sum_{i=1}^{n}(X_i-\overline{X})(X_i-\overline{X})^{\mathrm{T}}$)] which was the MLE of the decomposed, population covariance matrix" *Σ*. The random matrix *S*was shown to have a Wishart distribution with *n*-1 degrees of freedom. That is: $\sum_{i=1}^{n}(X_i-\overline{X})(X_i-\overline{X})^{\mathrm{T}}\sim W_p(\Sigma,n-1)$. The Wishart distribution is a member of the family of probability distributions defined over symmetric, nonnegative-definitematrix-valued random variables (i.e.,"random matrices") [12].

Our results indicated that the cause of the azimuthual variation could be traced to solar flux illumination of the vertically-oriented hanging floating and dead endmember LULC-related, larval habitat components. The variation of the Rapid Eye™ reflectance was moderated by azimutually isotropic sources of flux from sky light and the habitat canopy reflectance values unbiasedly. The geospectral unmixing yielded abundance estimates for each canopy endmember together summing-up to the 100% reflectance measured in the image. A scattergram representing the canopy endmember reference biosignature of shade, canopied, riverine, *S. damnosum s.l.* habitat and its associated hanging and floating vegetation, sub- mixel, geospectral, reflectance values was then generated. The biosignature was found to be characteristic of the Red Edge *S. damnosum s.l* larval habitat was red 134.67, 145.24 blue and 114.101 greenThe images were analyzed to predict potential *S. damnosum s.l.* larval habitats.

We then used an Ordinary kriged-based algorithm in ArcGIS® for predicting *S. damnosum s.l.* riverine larval habitatsemploying the decomposed Red Edge NDVI reference signature from the Chutes-Dienkoa study site for geolocating prolific habitat at the Achwa study site.A map was generated (Figure 18).

For determining optimal S. *damnsoum s.l.* habitat explanatorial canopied predictors, a semivariogram was constructed which expressed the variation in the spectral, Red Edge, NDVI, endmember, covariate coefficients. The semivariogram was nonnegative [i.e.,$\gamma(x,y)\geq 0$,]. The semivariogram $\gamma(x,x)=\gamma_i(0)=E\left((Z(x)-Z(x))^2\right)=0$at distance 0 since at zero the residual forecast $Z(x)-Z(x)=0$. A semivariogram if and only if it is a conditionally negative definite function, (i.e. for all weights $w_1,\ldots,w_N$ subject to $\sum_{i=1}^{N}w_i=0$and locations $x_1,\ldots,x_N$

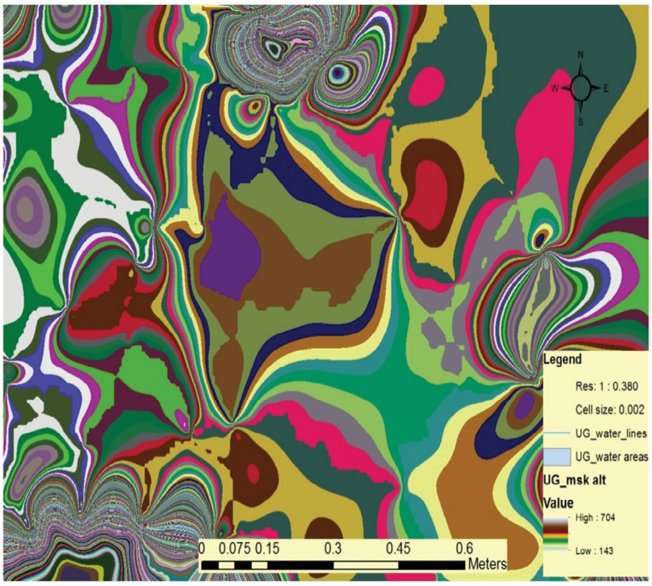

Figure 18: Unmixed Red Edge NDVI *S. damnosum s.l.* habitats signature interpolated over a Rapid Eye DEM of the Achwa study site.

it holds: $\sum_{i=1}^{N}\sum_{j=1}^{N} w_i\gamma(x_i, x_j)w_j \leq 0)$ [1]. The geospectrally explanatorial, interpolated, operationizable, decomposed, *S. damnosum s*.l., riverine, larval habitat, canopy, endmember, unmixed, biosignature variables corresponded to the variance $var(X)$ of $X = \sum_{i=1}^{N} w_i Z(x_i)$ which was given by the negative of this double sum. As a consequence the explanatorily, interpolated, geo-spatiotemporally dependent, riverine, larval habitat semivariogram was non-continuous only at the origin. The height of the jump at the origin is sometimes referred to as *nugget* or nugget effect [12,73]. The variogram [i.e., $2\gamma(x, y)$] was a function describing the degree of dependence between the predicted, prolific, shade, canopied, *S. damnosum s.l.* riverine habitats [i.e., $Z(x)$]. This was defined as the expected squared increment of the forecasted values between the georeferenced habitat locations.

The geospectrally interpolated, operationizable, explanatorial decomposed, *S. damnosum* s.l. riverine, larval habitat endmember model output was nonnegative since it was the expectation of a square. The covariance function was related to semiovariogram by $2\gamma(x, y) = C(x, x) + C(y, y) - 2C(x, y)$. Interestingly, $\gamma(x, y)=E(| Z(x) - Z(y) |^2)=\gamma(y, x)$ was a symmetric function, consequently, $\gamma_s(h)=\gamma_s(-h)$ was an even function. Coincidentally the function was also a semivariogram as it was a conditionally negative definite function, for all weights in the, habitat, model, forecasted, prolific geolocations.

Since the covariance function of the stationary process existed in the model, we related it to a semiovariogram by $2\gamma(x, y) = C(x,x) + C(y, y) - 2C(x, y)$. But since our geosampled, stochastic, endmember, geospectrally interpolated, explanatorial, *S. damnosum* s.l., riverine, larval habitat, forecasting, eco-epidemiological, canopy risk model reflected a non-stationary process the square of the difference between the expected values was quantitated by $2\gamma(x, y) = C(x,x) + C(y, y) - 2C(x, y) + (E[Z(x)] - E[Z(y)])^2$. For quantitating a random field [i.e., stochastic process] $Z(x)$ on the domain D employing a covariance function $C(x, y)$, we used the covariance of the interpolated endmember, *S. damnosum* s.l., RedEdge, NDVI, decomposed, biosignature values of the random field at two model forecasted prolific geolocation sites x and y as $C(x, y) := \operatorname{cov}(Z(x), Z(y))$.

The following parameters described the shade canopied, geospectrally interpolated, *S. damnosum* s.l., riverine, larval habitat variograms: The *nugget* represented the height of the jump of the semivariogram at the discontinuity at the origin.The *sill* was the limit of the variogram tending to infinity lag distances.We also computed the range which was the distance in which the difference of the semiovariogram from the sill becamenegligible. In geospectrally/geospatially, interpolated, shade, canopied, explanatorial, operationizable, *S. damnosum* s.l. riverine, larval habitat, eco-epidemiological, forecasting, risk models with a fixed sill, it is the distance at which this is first reached; for models with an asymptotic sill, it is conventionally taken to be the distance when the semivariance first reaches 95% of the sill [1,3].Theoretically, at zero separation distance (lag = 0), the semivariogram value is zero in a predictive, autoregressive,entomological-related, larval habitat,eco-epidemiological, risk model, however, at an infinitesimally small geosampled habitat distances, the semivariogram often exhibits a nugget effect (i.e., measurement errors or spatial sources of variation at distances smaller than the sampling interval), which is some value greater than zero [12]. In addition to the constant E[z(s)] and the assumption of intrinsic stationarity, ergodicity was defined in the *S. damnosum* s.l., riverine, larval habitat, eco-epidemiological models to estimate the empirical semivariance.

Using the geosampled, georfernced decomposed Red Edge *S. damnosum* s.l. riverine larval habitat NDVIvalues of LAGDISTANCE=8 and MAXLAGS=10 was run in PROC VARIOGRAM without the NOVARIOGRAM option in order to compute the empirical semivariogram. We specifed the CL option in the COMPUTE statement to calculate the 95% confidence limits for the classical semivariance. The section COMPUTE Statement described how to use the ALPHA= option to specify a different confidence level.

We rquested a robust version of the semivariance with the ROBUST option in the COMPUTE statement. PROC VARIOGRAM produced a plot of the explanatorily interpolated, unmixed, *S. damnosum* s.l., riverine, larval habitat, unmixed, biosignature canopy endmembers and then revealed both the classical and the robust empirical semivariograms. In addition, the autocorrelation Moran's *I* and Geary's *c* statistics was tabulated under the assumption of randomization using binary weights. The following statements implement all of the preceding requests:

```
proc variogram data=blackfly outv=outv;compute lagd=7 maxlag=10 cl robust; autocorr(assum=random);

coordinates xc=East yc=North;var blackfly; run;ods graphics off;
```

The VARIOGRAM procedure computed the empirical semivariogram from a set of point measurements. Semivariograms are used in the first steps of spatial prediction as tools that provide insight into the spatial continuity and structure of a random process [2]. Naturally occurring randomness is accounted for by describing a process in terms of the spatial random field (SRF) concept [130]. An SRF is a collection of random variables throughout your spatial domain of prediction [13]. Based on our sample, spatial prediction aimed to provide georferenced, highly, productive, habitat coordinate values of the SRF at unknown, unsampled habitat geolocations where no measurements were available. Prediction of the SRF values at unsampled locations by techniques such as ordinary kriging requires

Lag Class	Pair Count	Average Distance	Semivariance				
			Robust	Classical	Standard Error	95% Confidence Limits	
0	7	3.61	0.0414	0.0235	0.0119	0.000	0.06317
1	83	7.61	0.3569	0.3118	0.05702	0.573	0.4751
2	141	17.84	1.0674	1.1229	0.1962	0.889	1.3877
3	173	22.08	3.6398	2.3975	0.2879	2.312	3.5347
4	226	27.13	4.8580	4.5824	0.3896	3.759	5.4208
5	216	33.89	5.9904	5.7508	0.5378	4.865	7.1864
6	219	41.29	8.1376	7.5337	0.4896	6.189	8.9376
7	254	43.38	7.5478	7.2216	0.6449	5.952	8.4833
8	278	59.13	9.079	8.1337	0.6348	5.948	8.4268
9	281	64.81	8.2733	8.8447	0.5718	5.747	7.5323
10	293	72.93	8.1440	5.3577	0.8647	5.243	7.4722

Table 8: Geospectrally interpolatd decomposed, *S. damnosum s*.l. riverine, larval habitat endmember model output from the Variogram Procedure**.**

Coefficient	Observed	Expected	Std Dev	Z	Pr>|Z|
Moran's I	1.0657	-0.0335	0.168	6.34	<0.0001
Geary's c	0.0159	1.0000	0.548	-5.37	<0.0001

Table 9: The autocorrelation statistics from the resdiual spectral endmember *S. damsnosum* s.l. larval habitat eco-epidemiological, forecasting, risk model.

the use of a theoretical semivariogram or covariance model [115]. Due to the randomness involved in quanting the stochastic processes in the *S. damnosum* s.l., larval habitat, forecasting, eco-epidemiological, risk-related model, the theoretical semivariance could not be computed. Instead, we generated an empirical semivariance which provided an estimate of the theoretical semivariance, which was then used to characterize the spatial structure of the riverine larval habitat processes (Table 8).

Table 4 shows the output from the requested autocorrelation analysis. This included the observed (computed) Moran's *I* and Geary's *c*coefficients, the expected value and standard deviation for each decomposed, explantorily interpolated, *S. damnosum* s.l., larval habitat, shade, canopied, georeferenced ,sub-mixel, bisoignature coefficients, the corresponding **Z** score, and the ***p***-value in the Pr $> \lfloor Z \rfloor$ column. The low ***p***-values suggested strong autocorrelation for both statistics types. Note that a two-sided ***p***-value wasreported, which was the probability that the observed riverine, larval habitat, unmixed, kriged coefficient lay farther away from $\lfloor Z \rfloor$ on either side of the coefficient's expected value—that is, lower than **–Z** or higher than **Z.** The sign of **Z** for both Moran's i coefficient and Geary's *c*coefficients indicated positive autocorrelation in the endmember*S. damnosum* s.l. larval habitat data values (Table 9).

An Ordinary kriged-based algorithm for predicting the shade, canopied, *S. damnosum s.l.*, larval habitats in ArcGIS was used to identify the reference, canopy, biosignature variables generated from the extraction algorithms overlaid onto the DEM. Semivariogram plot of the logit scale model residuals confirmed a short-range spatial pattern up to a distance of approximately 5 km from the predicted, productive, shade, canopied, riverine, larval, *S. damnosum* s.l. habitat sites. To carry out this process, residuals for all observed points were calculated on the logit (ln (p/1 - p)) scale of the model.

A kriged map of deviance residuals was then calculated, which was added to the predicted values on the logit scale. Spatial dependence displayed by these plots was analyzed using the semivariogram. The addition of kriged residuals allowed the map to deviate from the model and move closer to the original sampled, georeferenced, covariate, parameter estimator, coefficient, indicator measurement values of possible georeferenced, prolific, canopy, shaded habitats. These smoothed values improved the final maps of the forecasted, *S. damnosum* s.l., habitats and its associated hanging, floating and dead vegetation-related LULC components.

An exponential model was fitted to the semivariogram employing a range of 71.9 m, a nugget of 0.14 (variance), a lag size of 12.7 m with 12 lags and a partial sill of 0.21 (variance). The coordinates of the putative breeding sites were recorded and the sites visited to ground truth the model predictions. Of the 25 sites predicted to be larval habitats by the model, (72%) were found to contain *S. damnosum s.l.* larvae when visited. We geosampled an additional 50 habitats not predicted by the model. Based on the number of prolific habitats predicted by the black fly model and the randomly sampled habitats, the sensitivity of the model was 78.26 and the specificity was 1.00.In addition, surveys of the habitat located 200 m upstream and downstream of the predicted breeding sites revealed no evidence of *S. damnosum* s.l. larvae. In a second validation of the model, we generated a dataset of Voroni tessellations

Figure 19 reveals both the classical and robust empirical *S. damnosum* s.l. larval habitat semivariograms. In addition, the plot features the approximate 95% confidence limits for the classical semivariance. The figure exhibited a typical behavior of the computed semivariance uncertainty, where in general the variance increased with distance from the origin at *Distance*=0. The needle plot in the lower part of the figure provides the number of pairs that were used in the computation of the empirical semivariance for each lag class shown. We noted that the number of pairs shown in the needle plot depended on the particular criteria specified in the COMPUTE statement of PROC VARIOGRAM. Importantly the habitat distances shown for each lag on the Distance axis were not the midpoints of the lag classes as in the

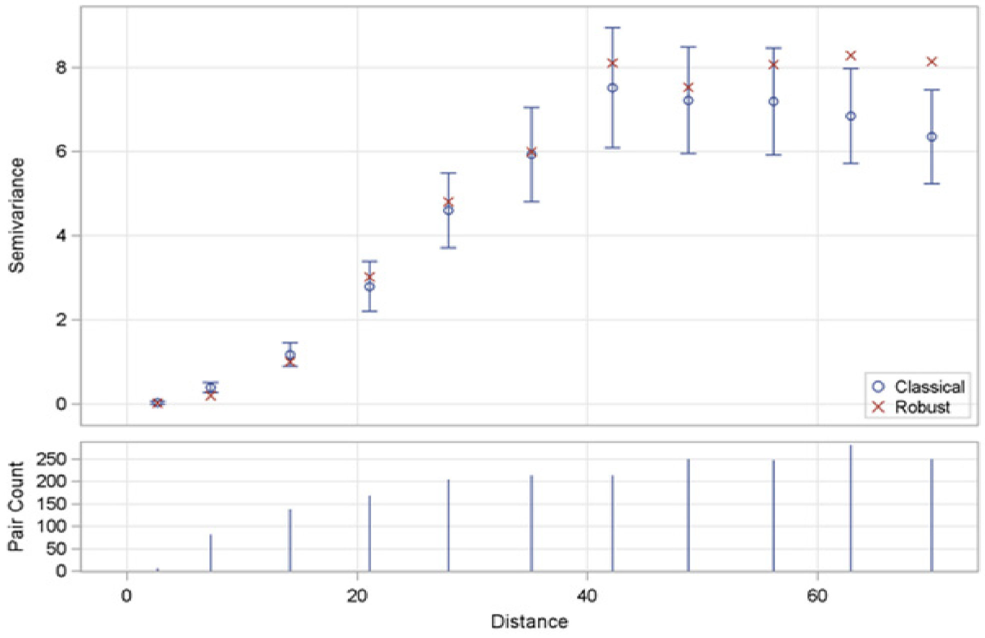

Figure 19: Empirical canopied *S. damnosum s.l* larval habitat semiovariogram with 95% Wald confidence limits.

pairwise distances plot, but rather the average distance from the origin *Distance*=0 of all predicted, prolific, shade, canopied, *S. damnosoum* s.l. larval habitats in a given lag class.

We assumed that for the spatial random field (SRF) **Z(S)** had measurements $\mathbf{Z}_i$ whose sample mean was estimatable by $\overline{Z}$. The hypothesis of ergodicity dictated that $\overline{Z} = E\left[Z(S)\right]$. In general, an SRF **Z(S)** is characterized as ergodic if the statistical moments of its realizations coincide with the corresponding ones of the SRF [12]. In spatial analysis you are often interested in the first two statistical moments, and consequently a more relaxed ergodicity assumption is made only for them. [65]

An Ordinary kriged-based algorithm for predicting the shade, canopied, *S. damnosum s.l.*, larval habitats in ArcGIS was used to identify the reference caopy biosignature variables generated from the extraction algorithms overlaid onto the DEM. Semivariogram plot of the logit scale model residuals confirmed a short-range spatial pattern up to a distance of approximately 5 km from the predicted, productive, shade, canopied, riverine, larval, canopied, *S. damnosum* s.l. habitat sites. To carry out this process, residuals for all observed points were calculated on the logit (ln (p/1 - p)) scale of the model.

A kriged map of deviance residuals was then calculated, which was added to the predicted values on the logit scale. Spatial dependence displayed by these plots was analyzed using the semivariogram. The addition of kriged residuals allowed the map to deviate from the model and move closer to the original sampled, georeferenced, covariate, paramter estimator coefficient indicator measurement values of possible georeferenced, prolific, canopy, shaded habitats. These smoothed values improved the final maps of the forecasted *S. damnosum* s.l. habitats and its associated hanging, floating and dead vegetation components.

An exponential model was fitted to the semivariogram employing a range of 71.9 m, a nugget of 0.14 (variance), a lag size of 12.7 m with 12 lags and a partial sill of 0.21 (variance). The coordinates of the putative breeding sites were recorded and the sites visited to ground truth the model predictions. Of the 25 sites predicted to be larval habitats by the model, (72%) were found to contain *S. damnosum s.l.* larvae when visited. We geosampled an additional 50 habitats not predicted by the model. Based on the number of prolific habitats predicted by the black fly model and the randomly geosampled habitats, the sensitivity of the model was 78.26 and the specificity was 1.00. In addition, surveys of the habitat located 200 m upstream and downstream of the predicted breeding sites revealed no evidence of *S. damnosum* s.l. larvae. In a second validation of the model, we generated a dataset of Voroni tessellations.

We then generated a dataset of Voroni tessellations in ArcGIS for the kriged, decomposed, Red Eye, NDVI, stochastic interpolator. The Voronoi decomposition produced a set of polygons V_i with area f_i (i=1,...,*n*). An approximation, based on the midpoints of the legs and center of the triangle were used to evaluate the area covered by each Voroni geospectral, endmember, *S. damsnosum* s.l., larval habitat, eco-epidemiological,polygon. A new canopied geosample point was calculated using the importance metric (i.e., Gamma) in all Voronoi polygons which was generated according to were the emissivity estimates of the decomposed, Red Edge, canopy, biosignature data in the polygon were geolocated. Gamma (u, v) was the importance metric of that sub-mixel, geospectrally, interpolated, canopy spectra, and C (p) was the coordinates of the new polygon center (i.e., the predicted *S. damnosum s.l.* riverine larval habitat). To do this calculation on each polygon we used a scan conversion. We ran a scan conversion and examined the frame buffer for each polygon. The unknown global mean z_D was estimated by a weighted mean of the predicted, *S. damnosum s.l.,* larval habitat, canopy spectral, geometrical values using: $m_g = \sum_{i=1}^{n} f_i Z_i / \sum_{i=1}^{n} f_i$. The extension error of each polygon was calculated by then employing a discrete version of $\sigma_E^2 = 2\overline{\gamma}(V,v) - \overline{\gamma}(V,V) - \overline{\gamma}(v,v)$. If the elementary error terms are uncorrelated, errors can be combined to an estimate of the global error: $\sigma_E^2 = \frac{\sum_{i=1}^{n} \sigma_{Ei}^2 f_i^2}{\left(\sum_{i=1}^{n} f_i^2\right)}$ where the summation is over all polygonsV_i [101].

By convention we assumed a normal probability distribution for the global error z_D - m_g and achieved a 90% confidence limits for z_D $m_R - 1.65 * \sigma_R \le Z_D \le m_R + 1.65 * \sigma_R$. The global estimation error decreased with an increasing number of predictive geosamples but some local deviation from this tendency did occur due to large polygons(i.e., the predicted productive, shade canopied, *S. damnosum s.l.* larval habitats). We noted that as the number of predictive geosamples increased the global estimation error converged to zero. The Voronoi diagram provided a spatial trend analyses of the error in the geospectral, canopy endmember, decomposed, explanatorily interpolated, Red Edge, NDVI, canopied, unmixed, biosignature reflectance model which revealed that all geo-spatiotemporally, geosampled photosynthetic and NPV explanatorial, covariate coefficients were within normal statistical limitations (Figure 20).

Discussion

Initially,a RapidEye™ Red edge, NDVI model was generated in ENIV of a prolific, canopied,georeferenced, *S. damnosum* s.l. riverine,larval habitat geosampled at the Chutes-Dienkoa,eco-epidemiological, study site. We noticed that the VI capitalized on the sensitivity of the 5m-imaged, vegetation, LULC-related data synthesized within the Red Edge band. VIs differs from other NDVIs by using bands along the RedEdge, instead of the main absorption and reflectance peaks [2,4]. Because the red and NIR regions were adjacent (red was approximately between 600 and 700 nm and NIR began at around 700

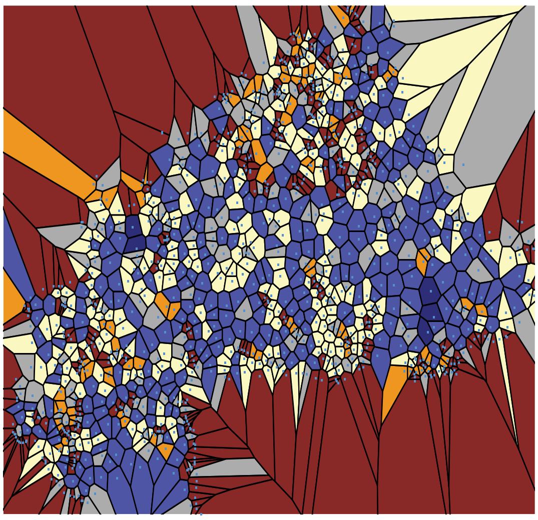

Figure 20: Voroni tessellations of the interpolated Red Edge NDVI *S. damnosum s.l.* habitats signature at the Achwa study site.

and stretched to about 1200 nm), the low vegetation reflectance in the canopy red regions was immediately followed by a sharp increase to the high reflectance in the NIR. The sharp reflectance contrast between transition zone in the RedEdge, *S. damnosum* s.l., riverine, canopied, larval habitat, mapped NDVI was probably due to the normalized difference values between the reflectance in the red visible (0.6µm) and the NIR (0.8µm) reflectance in the visible and NIR wavelength regions. The steep increase in reflectance in the 690-710 nm regions wasthe optimal peak reflective Red Edge NDVI larval habitat model region.

The red-NIR transition zone in the RapidEye™ Red edge NDVI marked the boundary between the red visible region, and scattering which may have been due to the 5 m, imaged, geosampled, larval habitat, shaded, canopy, leaf structures. Most NIR canopy radiation is scattered by leaf mesophyll resulting in high reflectance and transmittance values (approximately 40-50% each) [115]. Leaf chlorosis can cause an increase in visible reflectance and transmission [4]. The NIR plateau (700 nm - 1100 nm), is a region where biochemical absorptions are limited to the compounds typically found in dry leaves, primarily cellulose, lignin and other structural carbohydrates [27]. However, foliar reflection in this region may be also affected by multiple scattering of photons within a geosampled, georefernced, shaded, riverine, larval habitat canopy leaf, related to the internal structure, fraction of air spaces, and air-water interfaces that refract light within the leaves. Multiple scattering of radiation between air and cell wall in leaf tissue leads to high reflectance values in NIR [31].

Based on the canopied, Red Edge biosignature, the leaf reflectance was greatest in the 5 m spectral bands centered at between 1940 nm, and 2500 nm, with indirect or secondary effects at between 400 nm and 700 nm. The visible bands (400-700 nm), light absorption by leaf pigments dominates the reflectance spectrum of the leaf and lead to generally lower reflectances (15% maximum). The primary and secondary absorptions of water in the leaf reflectance were greatest was centered at 1450, nm, with important secondary absorptions at 980 nm, and 1210 nm. By assuming that the RedEdge, 5m, NDVI described the steeply sloped shade, canopied, *S. damnosum* s.l. larval habitat geosampled region of the vegetation-related, LULC reflectance curve between 690 nm and 710 nm ,the transition from chlorophyll absorption and NIR leaf scattering was then highly probable based on low/high chorophyll content geolocations in the productive flooded riverine larval habitat canopy.

The quantized chlorophyll NDVI values emitted from the shade, vegetated, georeferencable, canopied, productive, *S. damnosum* s.l. larval habitat, strongly absorbed radiation in the red and blue wavelengths an also reflected green wavelength which acted as diffuse reflector of NIR wavelengths. Reflected red irradiance (IRED) Rapid Eye™ was strongly diminished probably through chlorophyll absorption, with peak chlorophyll absorption occurring at 697 nm. Chlorophyll contained in vegetation absorbs most of the light in the visible part of the spectrum but becomes almost transparent at wavelengths greater than 700 nm [4]. Both red and NIR irradiance are strongly influenced by plant cover [2,27,115]. Red irradiance (IRED) decreased with plant cover, as NIR irradiance (INIR) increased. The chorophyll irradiance within a given Rapid Eye™ waveband was integral of the spectral irradiance with respect to the 5 m wavelengths associated to the shade canopied, *S. damnosum* s.l., riverine, larval habitat, NDVI biosignature.

Chlorophyll distribution in the canopy vegetation of the shaded, georeferenced, *S. damnosum* s.l. larval habitat NDVI bisignature was scattered with the lower cover reflecting lesser spectral internsity. In the *S. damnosum* s.l. NDVI biosignature, eco-epidemiological, risk model these changes were reflected in the green peak reflectance (~550 nm) and along the Red Edge (590 to 650 nm). Chlorophyll content may decline more rapidly than carotenoid content towards the lower part of the riverine larval habitat canopy cover [4,115]. Lower habitat canopy cover may be also where the canopy plants experience more seasonal stress due to leaf senescence.

Eco-physiologically, the variation in the tabulated leaf chlorophyll between the within,*S. damnosum* s.l., larval habitat, canopy, leaf species and how it responds to changing biotic and abiotic, seasonal factors (e.g., trailing vegetation, solar radiation etc) may be of seasonal entomological importance. Most indices sensitive to chlorophyll content were strongly affected by the differences in canopy, shaded, vegetation-related, LULC-oriented, georeferenced, eco-hydrological covariates. The main factors governing canopy, vegetated, prolific, georefernced, shade canopied, *S. damnosum* s.l. riverine, habitats geo-spatiotemporally- geosampled in African riverine ecosystems are adequate water velocity (.70-1.5 m/sec) which is linked with oxygenation and food supply and the presence of suitable supports, which may be rocks, stones, sills, sidewalks of structures, spillways and gates [5]. Whilst the riverine, habitat, canopy indices revealed strong relationships with chlorophyll content in the RedEdge, NDVI, biosignature, additional seasonal validation metrics may be required to understand how immature *Similium* productivity is associated to 5m measured proxy canopy changes at the leaf scale. When scaling up from a leaf to a branch or canopy, and in flooded field conditions, shaded, canopy, vegetation-related, LULC, explanatorial, predictor variables, (e.g., hanging canopy density) may affect a measured Rapid Eye ™reflectance signal.

Chlorophyll content is also linked to carbon cycles and its role in photosynthesis and net primary productivity is important within regional and global carbon models [8]. Plants convert the carbon in atmospheric CO_2 into carbon-containing organic compounds, such as sugars, fats, and proteins then stores it in carbohydrates like cellulose during photosynthesis [2].Carbon dioxide is converted into sugars in a process called carbon fixation. Carbon fixation is an endothermic, reaction, so photosynthesis needs to supply both a source of energy to drive this process, and the electrons needed to convert carbon dioxide into a carbohydrate. This addition of the electrons is a reduction reaction. In general outline and in effect, photosynthesis is the opposite of cellular respiration, in which glucose and other compounds are oxidized to produce carbon dioxide and water, and to release exothermic chemical energy to drive the organism's metabolism. However, the two processes take place through a different sequence of chemical reactions and in different cellular compartments.

The general equation for photosynthesis as $CO_2 + 2H_2A +$ photons → $[CH_2O] + 2A + H_2O$ (i.e, carbon dioxide + electron donor + light energy → carbohydrate + oxidized electron donor + water) [4]. Since water is used as the electron donor in oxygenic photosynthesis, the equation for remotely qualitatively quantitating a geo-spatiotemporally, geosampled, *S. damnosum* s.l., riverine, larval habitat would be then:$n\ CO_2 + 2n\ H_2O$ + photons → $(CH_2O)_n + n\ O_2 + n\ H_2O$(i.e., carbon dioxide + water + light energy → carbohydrate + oxygen + water). This equation emphasizes that water is both a reactant in the light-dependent reaction in the riverine, larval, habitat canopy and a product in light-independent reactions in the within-canopy, LULC explanatorial, geospectral covariate, parameter estimator ,coefficients but canceling *n* water molecules from each side will render the net equation: $n\ CO_2 + n\ H_2O$ + photons → $(CH_2O)_n + n\ O_2$ (i.e., carbon dioxide + water + light energy → carbohydrate + oxygen). Photosynthesis occurs in two stages. In the first stage, canopy light-dependent reactions capture the energy of light and use it to make the energy-storage molecules (e.g., ATP and NADPH). During the second stage, the light-independent reactions use these products to capture and reduce carbon dioxide [4,115]. The accurate monitoring of canopy chlorophyll in georefernced, geosampled, productive, canopied, larval habitat content across a range of temporal and spatial scales is therefore paramount for monitoring and understanding a number of riverine ecosystem responses to seasonal variation in immature productivity. Most organisms that utilize photosynthesis to produce oxygen use visible light to do so, although at least three use shortwave infrared or, more specifically, far-red radiation [2].

Analyzing the relationship between chlorophyll and nitrogen content in the 5m proxy vegetation index allowed remotely correlating relations between wavelength of the Red Edge biosignature reflectance estimates in the red region of the canopy spectrum. Indeed, chlorophyll measurement provides information on the plant ecophysiological status as leaf chlorophyll concentration is linked to nitrogen content and therefore to photosynthesis [13]. Studies have been surprisingly successful at estimating leaf and canopy from reflectance measurements despite challenges associated with radiosity modeling of leaf nitrogen [4,115]. At the leaf level, spectral reflectance is a function of the chlorophyll and nitrogen absorption rates, internal structure, leaf thickness, air-water interface, distribution of pigments and chemical constituents [27], as well as leaf surface properties, such as waxy cuticle, and pigment concentrations and distribution [115]. At the canopy level, *S. damnosum* s.l. riverine, larval habitat, spectral reflectance,however, may be a function of LAI, leaf clumping, leaf angle distribution, vegetation-related, LULC cover, and source-target illumination geometry. As a consequence, interpolation exercises for satisfactorily estimating nitrogen employing a decomposed, Rapid Eye™, VI content at the leaf level of a riverine resampled, georefernced, *S. damnosum s.l.,* larval habitat, eco-epidemiological, forecasting, risk model might perform poorly, as the factors that affect habitat reflectance vary according to seasonal scale. Later in the season, LAI values may lose sensitivity for measuring canopy nutritional content. For example, Inada [19] found a high correlation between leaf nitrogen and leaf optical properties ($r^2 = 0.90$). At the canopy level, the correlation between canopy nitrogen concentration and canopy reflectance decreased as a function of the canopied *S. damnosum s.l.,* riverine, larval, habitat LAI. Overall, regression results suggest that bare ground cover also had an influence on the ability to remotely estimate the *S. damnosum s.l.,* larval habitat canopy nitrogen concentration.

The eco-epidemiological model, residual forecasts indicated that the greener region of the larval habitat absorbed light from the blue-violet and the red regions of the visible spectrum and reflected green light. This was confirmed in the continuum removal analysis of the 5m, red, wavelength region which revealed that the increase in the wavelength in the riverine, larval, habitat canopy compared with only minor differences in the blue absorption band depths between the 5m imaged relocations. Therefore, the use of Rapid Eye™ geospectral measurements and indicators for the determination of seasonal chlorophyll, content, for example may be based on the fact that chlorophyll, as well as a number of other pigments is strong absorbers of light in certain well-defined 5m wavelengths, specifically in the blue and the red spectral region. Since the red portion of the georefernced, resampled, riverine, larval, habitat canopy was one of the areas where chlorophyll strongly absorbed light in our experiment, and since the NDVI-NIR was where the canopy leaf cell structure produced strong reflection variations in both the chlorophyll content and the leaf structure in the *S. damnosum* s.l., riverine, larval habitat, eco-epidemiological, forecasting geospectral, risk model, these geospectral zones may be linked to seasonal immature productivity to study seasonal clustering tendencies in prolific, shade, canopied, immature habitats.

The RapidEye™ RedEdge domain of the proxy graphical indicator was sensitive to chlorophyll content and nitrogen status. We analyzed the relationship between leaf nitrogen content and the eddy covariance CO_2 flux measurements obtained at a range of diverse, canopied, leaf, area sites of the prolific, shade, canopied, *S. damnosum* s.l., riverine, larval habitat geosampled at the Chutes Dienkoa study site. We concluded that leaf nitrogen content is a strong factor influencing both optimum canopy light use efficiency and thus canopy photosynthesis rate. Based on our RedEdge reflectance model output the canopy chorophyll content was a physically sound quantity that represented the optical path in the canopy where absorption by chorophyll dominated the Rapid Eye 5m radiometric signal. Thus, absorption by chorophyll may provide the necessary link between Rapid Eye™ 5m remote sensing observations and geo-spatiotemporally, geosampled, *S. damnosum* s.l., riverine, larval habitats, canopy-state, empirical, predictor variables which may be subsequently employed as indicators of nitrogen status and photosynthetic capacity.

An entomologist or experimenter may estimate the chlorophyll Rapid Eye™ RedEdge using a the green chlorophyll index, and a terrestrial chlorophyll index which may provide accurate, spectral, biophysical, explanatorial estimators of prolific shaded, *S. damnosum* s.l., riverine, larval habitat, canopy chlorophyll and nitrogen contents. Bands of Rapid Eye™ in the green and RedEdge are well positioned for deriving these indices. Results may confirm the particular importance of the 5m data for seasonal, canopy, vegetation-related LULC covariate coefficient quantification as it would provide access to green and RedEdge waveband data information. Importantly, by so doing, non-destructive nitrogen and chlorophyll content retrieval from a seasonally productive, georeferenced, Rapid Eye™ imaged, riverine, larval habitat, 5m scene may geo-spectrally geolocalize red absorption bands delineating where canopy absorption saturates at low to-moderate chorophyll values in the larval habitat canopy. Thus, geo-spatiotemporal relationships between nitrogen and chorophyll contents at the leaf and canopy levels may be remotely qualitatively regressively tabulated. Optimal spectral ranges in the green and the RedEdge regions may allow accurate estimation of nitrogen and chlorophyll contents in a georefernced, prolific, *S. damnosum s.l.* canopied, riverine, larval habitat over a wide range of leaf area index values. Performances of chlorophyll-related, vegetation –related LULC indices to retrieve nitrogen and chlorophyll contents in both leaf and canopy of a prolific, riverine geosampled *S. damnosum* s.l. larval habitat may be also tested.

It may be demonstrated that partitioning of nitrogen between protein fractions of soluble and thylakoid proteins remain unaltered with increasing seasonal nitrogen content in a geosampled, georeferenced, prolific, canopied, *S. damnosum* s.l., riverine, larval habitat. Changes in leaf nitrogen content may result in similar changes to the thylakoid pigment protein complex, that consists primarily of chloropyll, and the carbon fixing soluble protein enzyme activity of RuBP in 5m, Rapid Eye ™ imaged, riverine, larval habitat canopies. Ribulose-1,5-bisphosphate is an organic substance that is involved in photosynthesis [13]. It may be concluded that canopy chorophyll absorption content is a physically sound quantity that represents the optical path in the riverine larval habitat canopy where absorption by chlorophyll dominates the Rapid Eye^{TM} radiometric signal. The RedEdge inflection point wavelength (λi) may be used as an indicator for this shift in a canopied, riverine, *S. damnosum* s.l., larval habitat normalized differencial vegetation, eco-epidemiological, forecasting, risk-related, regression model.

Besides nitrogen and chrophyll other absorption-related, explanatorial, photosynthetic and NPV parameter estimators were confirmed in the first derivative canopied, *S. damnosum* s.l., riverine, larval habitat, reflectance curve in the RedEdge region. Since RedEdge position in our Rapid Eye^{TM} forecasting eco-epidemiological, risk model was the tabulated point of maximum slope on the reflectance spectrum of vegetation-related, LULC, regression-related, 5m, covariate, paramter estimators, coefficient, integer values between red and NIR wavelengths amongst all the reflectance geomarkers. Analyses with the RapidEye^{TM} proxy, eco-epidemiological, risk-related, remotely synthesized, explanatorial, residual, geo-spatiotemporal forecasts along with the ground truth data revealed relatively high accuracy (i.e., RMSE, < 1μg/l) between the eco-geographically predicted and observed, canopied, georeferenced, larval habitat, NDVI-related, biosignature, data feature attribute values which were obtained for riverine geolocations associated with ecohydrologically low vegatation (i.e., < 10 μg/l) content as well. By choosing the RedEdge band, instead of the red band for the NDVI calculation, a lower saturation over highly vegetated areas in the *S. damnosum* s.l. georferenced, larval habitat geosampled at the Chutes-Dienkoa, riverine, eco-epidemiological, study site was achieved.For retrieval of explanatorial, vegetation-related LULC, canopy, spectral, biophysical, time series dependent properties, the relationship between NDVI and fractional, vegetation, LULC, radiance cover based on a empirically regressed dataset of a spectrally, unmixed, risk, model, probabilistic coefficients must be examined [115]. Our results revealed strong spatial scale dependencies of the RedEdge NDVI over the riverine eco-epidemiological study site heterogeneous LULC surfaces, indicating that 5m values may be optimal for remotely robustly discerning canopied geosampled, georferenced prolific, shade canopied, *S. damnosum* s.l., riverine, larval habitats.

Our RedEdge NDVI calculated using simulated PAR and NIR albedo compared well to the vegetated-related, LULC, explanatorial, geospectral values extracted from the georeferenced, geosampled, *S. damnosum* s.l., riverine, larval, habitat canopy biosignature which coincidentally revealed similar forecasts as those reported by Asrar et al.[131] who suggested that vegetated LULC values of canopies dominated by horizontally oriented leaves were not dependent on θs. On the contrary he suggested that values of canopies were dominated by vertically oriented leaves which are dependent on θs. In horizontally oriented leaves, there are usually more stomata on the protected lower side than on the exposed upper side. Vertical leaves usually have similar numbers of stomata on both sides [46]. Although stomata occupy 1% of the leaf surface, they lose huge amounts of water in to the atmosphere [13].

Perturbing effects of the background albedo within the visible spectrum corresponded to PAR observed changes in the visible albedo which estimated FAPAR directly from the NDVI values. The linear relationship between changes in visible and NIR albedo defined a weak 'soil-line' to account for changes in background NIR albedo. Departures from the correlated variation in NIR background represented by the 5m soil-line and a lack of consistency in observation/ illumination geometries between the 5m remotely sensed, riverine, larval habitat observables (e.g. direct and/or diffuse canopy radiation emitted from the geosampled, larval habitat) and in-situ field measurements helped quantitate the FAPAR of the geosampled *S. damnosum s.l.,* canopy cover .

The nonlinearity of the riverine, larval habitat, RedEdge, NDVI variables over partially vegetated canopied, LULC surfaces became prominent with darker canopy backgrounds and with the presence of shadows. The relationship between NDVI and vegetation fraction was nonlinear as the NDVI yielded distinct curves with the vegetation-related explanatorial, LULC cover changes corresponding to different canopied type geospatial objects (e.g., hanging vegetation). Using a linear mixture reflectance model we found that the 5m NDVI *S. damnosum* s.l. larval habitat biosignature to be dependent not only on the NDVI of the mixel components and their proportions, but also on the brightness of the components. We independently obtained identical square root relationships between the scaled RedEdge, *S. damnosum* s.l., riverine, larval habitat, NDVI values and shade, fractional, radiance, vegetation cover canopied, LULC coefficients values. However, in the the *S. damnosum* s.l. habitat model, the reflectances of bare soil were fixed for all simulations. So, the variations of soil background were not taken into account between the NDVI and the canopy vegetation LULC cover. The RedEdge NDVI may be suitable to infer canopy LULC vegetation fraction of a georeferenced, seasonal, geosampled, *S. damnosum* s.l, riverine, larval habitat using within-canopy geospatial objects (e.g., immersed vegetation), because of its nonlinearity and non-soil scale effects.

The reduced 5m NIR reflectance at the georefernced, canopied riverine, larval habitat eco-epidemiological study site may have resulted from the increased surface soil moisture content. Mesic and dry sites (e.g., high, canopy, shaded layers) had nearly similar reflectance spectra at the shorter wavelengths of the NIR, but at the wet site (e.g., within canopy leaves) there was higher nadir-coverage of moss and lower contribution from taller vegetation layers (e.g shaded canopy), which reduced the 5m NIR reflectance below 900nm. For medium resolution remote sensing applications, the contribution from riverine ecosystems will have an influence on the reflectance of highly heterogenous landscapes and on the NDVI [83].The spectral behavior in the NIR region in the Rapid Eye^{TM} data may have been mainly influenced by the soil moisture and mean canopy, LULC, vegetation height. For example, the very low RedEdge NDVI-NIR reflectance at the bottom of the georeferenced, habitat, canopy layer may have been due to the high surface moisture conditions (e.g., up to 60 Vol% canopy soil moisture). Interestingly, the quantitated, contrasting, geosampled, canopy LULC, sites enabled differentiating the dry fallow LULC, sites (e.g., 32 Vol% soil moisture) and wet site (e.g., 74 Vol %) of the habitat.

The scaled difference vegetation index (SDVI), a scale-invariant index based on linear spectral mixing of red and NIR reflectances, may be a robust approach for parsimonious retrieval of Rapid Eye^{TM} 5m, vegetation-related, LULC, canopied, fractional, radiance estimates from a geosampled, prolific, *S. damnosum* s.l., riverine, shade, canopied, larval habitat particularly over highly heterogeneous riverine, in-canopy, soil surfaces. The scaled difference vegetation index may be applied to calculate the riverine, larval habitat, canopy, gap fractions. Also, LAI may be inverted from these SDVI derived gap fractions employing the Beer Lambert Law of light extinction. The Beer law is commonly applied to mathematical physics and chemical analysis measurements used in understanding attenuation in physical optics, for photons, neutrons or rarefied gases[121].

The robustness of the SDVI may be evaluated when employing ground/riverine-based LAI 5m measurments when qualitatively quantitating probabilstically regressable geo-spatiotemporally-geosampled, prolific, georeferencable, shade, canopied, *S. damnosum* s.l. seasonally prolific, geosampled, riverine larval habitat predictors. This method may be also performed by independently qualitatively quantitating simulated Rapid Eye^{TM} data within a PROPECT and SAIL coupled radiative transfer model. The effects of atmospheric corrections and scales may be then investigated for all geo-spatiotemporally, geosampled, shade, canopied, explanatorial, operationizable, riverine, *S. damnosum* s.l., larval habitat LAI retervial methods. The SDVI may be found suitable for large scale LAI inversion due to the sensitivity to scale and atmospheric effects in prolific, immature, habitat geolocations (e.g., flooded meandering African riverine tributaries). The SDVI is virtually and atmospherically invariant [13]. The proposed method may be validated with experimental, field geo-spatiotemporally, geo-spectrally interpolated, geosampled, 5m, Rapid Eye ^{TM}, count data. Interestingly, the main RedEdge NDVI reflectance spectral difference along the canopy gradient in the geosampled, riverine, larval habitat geolocations was the percentage cover of sedge and standing dead vegetation.Canopy, riverine, larval habitat, reflectance spectra within the shaded sedges were up to 30 cm long and revealed NIR reflectance plateaus with stronger slopes between the beginning and end of the Rapid Eye ^{TM} NIR reflectance plateau. The standing dead material within the larval habitat canopy led to an increase in the reflectance in the Rapid Eye^{TM,}5m, red wavelength, sensor region probably due to reduced chlorophyll absorption at these sites.

Remotely, qualitatively, regressively, quantitating homogenous, individualized, shaded, canopy cover reflectance-related, explanatorial, covariate,wavelenght, parameter estimators of standing dead material (e.g., sedges), *over a region of multiple, geosampled, georefernced, riverine, productive, *S. damnosum* s.l., geo-spatiotemporal, larval habitats with clustering tendencies may reveal an increase in the reflectance in 5m red and blue wavelength regions with no development of a green reflectance peak due to reduced seasonal, canopy, leaf, pigment absorption. The high percentage cover of standing dead material at the georeferenced, riverine, larval, habitat site increased the reflectance in the RapidEye^{TM}5m red, wavelengths bands, whereas the moist and dry sites were greener which may have been related to deeper canopy chlorophyll absorption at these sites.

Leaf orientation distributions in the geosampled, riverine, *S. damnosum* s.l., larval habitat canopy were classified by the predominant angle class, for example, as erectophile (vertical) or planophile (horizontal). Lower reflectance was noted from the erectophile portion of the canopy in the riverine, *S. damnosum* s.l., larval habitat, RedEdge NDVI which may have been attributable to scattering of radiation into the lower, canopy, leaf layers by vertical leaves. In contrast higher reflectance was recorded for the planophile portion of the larval habitat canopy which may have been due to greater reflection from horizontal leaves in the upper part of the canopy.

Interestingly, nadir-viewed values were approximately 20% higher from a planophile than from an erectophile, riverine, larval habitat canopy, although LAI and leaf optical properties were similar. The structural dependence on planophil and erectophile canopy vegetation LULC structures on the NIR reflectance allowed us to conduct a robust, geo-spatiotemporal, canopy, risk-based, geospectral analyses of the prolific, georeferenced, riverine, *S. damnosum* s.l. , larval habitat geosampled at the Chutes-Dienkoa, eco-epidemiological study site.

Leaf angle distribution [LAD] and leaf area determined the exact gap fraction of the riverine, larval, habitat canopy and penetration of radiation to the underlying reflection of the within canopied surfaces (e.g., sedge,).Leaf angle distribution is a key parameter to characterize canopy structure and plays a crucial role in controlling energy and mass balance in soil-vegetation-atmosphere-transfer systems [2]. The relative angles between the riverine, geosampled, *S. damnosum* s.l.,larval habitat,canopy leaves and light source and viewing directions may need to be calculated seasonally due to shifting patterns of reflected and transmitted LULC radiation.

Quantitating configuration complexeties in external and within canopy geometries of geosampled, georeferenced, *S. damnosum* s.l., productive, canopied, larval habitats* may help detect canopy gaps. The geometrical structure of plant canopies has many implications for plant functioning, microclimatic conditions, and plant-pathogen/herbivore interactions [115]. Plant geometry can be described at several scales [4]. At moderate resolution scale, riverine, geosampled, *S. damnosum* s.l., larval habitat, canopy structure includes the shape, size, location, and orientation of each geospatial object in the canopy. By so doing, an empirical georeferencable dataset of 5m Rapid Eye^{TM} variables can report the 3-D geometry of a set of shade, canopied, prolific, riverine, larval habitat at the leaf scale. A 3-D magnetic digitizer may be employed to measure the spatial coordinates and the orientation angles of each canopy leaf, namely, the azimuth and inclination angles. In addition, for most moderate resolution canopied NDVIs of vegetated LULCs, branching or flush order may be given as well as the ranking of leaves along branches and the leaf identity of leaflets employing compound-leaved predictors. Leaf length may be then robustly measured for the riverine habitats. Leaf width also can be measured or estimated based on allometric relationships. The prolific, georferenced, riverine, geosampled, *S. damnosum* s.l., larval habitat leaf area may be then derived from qualitatively quantized allometric relationships with leaf length and width of canopy. Most of the temporally dependent regressors may be therefater used to show how seasonal geosampled canopy geometry determines light interception and subsequently plant primary production in a productive, seasonal, georeferenced, geosampled, riverine, larval habitat. A empiricial, geosampled dataset may be employed to test the quality of innovative methods for the riverine, larval habitat, canopy, geo-spatiotemporal, structure description. Overall, a regressed georeferenced dataset of geo-spatiotemporally, empirical, geosampled, *S. damnosum* s.l., larval habitat photosynthetic and NPV covariate parameter estimators, LULC coefficients may provide explicit plant canopy architectures suitable for spatial regressive modeling plant physiological interactions. By so doing, an experimenter /ecologist may determine the mechanisms through which climate impacts ecobiological explanatorial, processes involved in the shaded, riverine habitat, canopy functions.

The probability of canopy gaps generally decreases as the off-nadir increases [12]. Directional gap probability, $P_{gap}(θ)$, is defined as the probability of a light beam of infinitesimal width at zenith angle θ to the local normal, being directly transmitted through a vegetation geoclassifed, LULC canopy [4]. $P_{gap}(θ)$, along with canopy height and LAI, are some of the most important structural parameters used to directly interpret the transfer of radiation, carbon, and related processes in canopied systems [4,115]. $P_{gap}(θ)$ is a structural parameter estimator that may be near-directly retrieved from airborne measurements [115]. The importance of $P_{gap}(θ)$ is its relationship to radiation interception within the canopy and hence other canopy structure parameters, like LAI and above-ground biomass [2]. These latter properties may be modeled for a geo-spatiotemporally, geosampled, prolific, *S. damnosum* s.l., larval habitat using different expressions, combinations or spatial variance of canopy height and $P_{gap}(θ)$, since the $P_{gap}(θ)$ represents the integrated effect of several scale-dependent canopy structural properties (in particular LAI and LAD).

In practice, $P_{gap}(\theta)$ is often calculated over a narrow range of angles e.g. close to nadir ($\theta = 0°$) and is then referred to simply as P_{gap}. Many studies have estimated P_{gap} or fractional cover (1- P_{gap}) using small footprint discrete lidar datasets. Quantifying the proportion of pulses intercepted by the canopy is the most common method to estimate the P_{gap} [7]. However, remote estimations based on discrete lidar returns, tend to rely on site-, sensor- and lidar survey-specific calibrations, which limit the application of such methods for rigoriously modeling prolific, riverine shade canopied, *S. damnosum* s.l. larval habitat areas. In particular, topography and scan angle (as well as other things such as sensor flying height and even canopy structure and crown shape) combine in practice to modify the lidar return by changing the size and shape of the footprint and the path length through the canopy and hence the returned energy[2]. These factors can introduce significant bias into estimates of properties derived from the footprint, even in 'simple' metrics such as seasonally specified, geosampled ,riverine, *S. damnsoum* s.l, habitat canopy height.

The geomorphological, and ecohydrological DEM explanatorial, predictor variables of the geo-spatiotemporally-geosampled, explanatorial, shade, canopied, prolific, explanatorial, *S. damnosum* s.l. riverine larval habitat site influenced the LAD resulting in differences in leaf area and pigment composition, vegetation biomass and height, cover of the canopy plant functional types and total, vegetation-related, LULC cover.The leaf inclination angle density function is a fundamental property of plant canopy structure and is needed for computing distributions of leaf irradiance [4]. These catchement shed computations may be important for predicting canopy photosynthesis and energy balance, and for estimating bidirectional reflectances of prolific, *S. damnosum* s.l., riverine, larval habitat, plant canopies in 5m,remote sensing applications.

Interestingly, several LAD functions found in literature have been proposed to account for the non-random distribution of leaf inclination angle with one or two parameters functions (e.g., Beta distribution function, ellipsoidal function, rotated-ellipsoidal function, Verhoef's algorithm and de Wit's functions). We employed the Beta distribution function to determine the riverine, larval habitat, leaf-oriented, inclination angles. *G*-statistics and χ^2 tests were applied to the estimates of the LAD. We employed the predictions of LAD by the function to calculate an extinction coefficient and to separate the larval habitat canopy foliage into sunlit and shaded parts. The results suggested that, ellipsoidal function may be suitable to be retrieved with the Rapid Eye™ RedEdge NDVI data as the fraction of sunlit foliage of the geosampled, riverine, larval habitat employing the beta distribution function which would require only a single parameter, namely the ratio of the horizontal semi-axis length to the vertical semi-axis length of the ellipsoid.

The ENVI approach related recognition of prolific, riverine, *S. damnosums*.l., larval habitat georefernced patterns by distinguishing noise, from the abstraction of structure in the medium resolution, remotely sensed, data attributes. In the object-based classifier all the geosampled, *S. damnsoum s.l.* habitat data points based on the 5 m-sub-mixel, data encompassing the shaded, canopy, vegetation LULC explanatorial, photosynthetic and NPV components were examined in *n*-dimensional space. Canopy endmembers present in the scene were found at the vertices of the simplex. The interior space of the simplex represented feasible mixtures. ENVI algorithms identified the fractional presence of each derivative spectra in the unmixed, Rapid Eye™ RedEdge, *S. damnosum s.l.* habitat, NDVI mixel.

The FLASSH™ model generated in ENVI generated extinction coefficient values. The extinction coefficient represented the area of shadow cast onto a horizontal surface by the riverine habitat canopy divided by the area of leaves in the canopy. We calculated the geosampled, georefernced, prolific, shade, canopied, *S. damnosum* s.l. riverine, larval habitat employing the distribution of leaf area in the canopy which we approximated by the distribution of surface on spheres, cylinders and cones. Values for K were then determined by finding the ratio of shadowed, riverine, larval habitat, canopy area to surface area for these shapes. The model provided a K value and also very crude approximations of actual foliage inclination angle densities. Only the spherical distribution provided a range of leaf angles. Measurements indicated that certain portions of the canopy (e.g., shaded sedges) were discontinuous in the larval habitat model. Fortunately, K values are not extremely sensitive to variation in leaf angle distribution functions [13], so the riverine larval habitat extinction coefficients calculated from our Rapid Eye™ model provided adequate leaf angle densities.

ENVI Endmember visualization approaches can play a vital role in geo-spatiotemporally, remotely, qualitatively, quantitating canopy light, subtle patterns within complex, shade, canopied, Rapid Eye™ ,RedEdge, NDVI-related, geospectral, *S. damnosum* s.l., riverine, larval habitat, canopied endmembers that may not be immediately apparent in strictly unmixing analysis methods. The critical step in our object-based classification, for example, was the determination of the canopied LULC, endmembers employed as the references for the unmixing ENVI decomposition analysis of the the RedEdge, NDVI, riverine, geospectral, larval habitat, Rapid Eye™ image. These included applications in target detection and unsupervised image segmentation. Segmentation is a fundamental process in digital image processing which has found extensive applications in areas such as content-based image retrieval, medical image processing, and remote sensing image processing[12,115]. The remote purpose of our model application was to extract labelled regions or boundaries for targeted objects for subsequent processing such as surface description and object recognition. Importantly, canopy endmember geo-visualization and decomposition of a RedEdge NDVI biosignature may serve to stimulate hypothesis generation.

A simple Markov Random Field model (MRF) in ArcGIS with a new implementation scheme was employed for image segmentation based on the unmixed shade, canopied, *S. damnosum* s.l., riverine, larval habitat,georeferncable, image features. The traditional two-component MRF model for segmentation requires training data to estimate necessary model parameter estimators [132]. The new implementation scheme introduced a function-based weighting parameter between components in the eco-epidemiological, forecasting, risk model. The simple MRF model was able to automatically estimate the model phostsynthetic and NPC canopy-related predictors and produce accurate unsupervised segmentation results.

Improved estimates of the canopied larval habitat extinction coefficients were obtained by stratifying a geo-spatiotemporally, geosampled, 5m, imaged canopy into several leaf angle classes employing the conical distribution. A simple formula, similar to the spherical distribution formula, but with more flexibility realistically, described the density function of individual canopied leaf areas in the geosampled, georeferenced, prolific, shaded, riverine, *S. damnosum* s.l., riverine, larval habitat, Rapid Eye™ scene which was very useful in the canopy radiation model. An existing riverine, *S. damnosum* s.l.

riverine larval habitat canopy radiation, eco-epidemiological, model may be modified, in future contributions, to incorporate ellipsoidal distributionof seasonal canopy foliage elements, which then may be found to be continuous over a wide range of leaf angles in a functional analyses. Subsequently horizontal or vertical tendencies of the canopy may be formly geo-spatiotemporally qualitatively quantitated.

In the modern view, functional analysis is seen as the study of complete normed vector spaces over a dataset of real or complex numbers [27]. Such spaces are called Banach spaces. Banach space is a vector space*X* over the field R of real numbers, or over the field C of complex numbers, which is equipped with a norm and which is complete with respect to that norm, that is to say, for every Cauchy sequence $\{x_n\}$ in *X*, there exists an element *x* in *X* such that $\lim_{n\to\infty} x_n = x$, or equivalently: $x_1, x_2, x_3, \ldots$ [65]. A sequence $x_1, x_2, x_3, \ldots$ of real numbers is called a Cauchy sequence, if for every positive real number ε, there is a positive integer *N* such that for all natural numbers *m*, *n*>*N* $|x_m - x_n| < \varepsilon$, where the vertical bars denote the absolute value [12]. To define Cauchy sequences in any metric space X in a geosampled, georeferncable, prolific, shade canopied, 5m imaged, Rapid Eye™ *S. damnosum* s.l., riverine, larval habitat, eco-epidemiological, forecasting, geospectral, time series, risk model the absolute value $|x_m - x_n|$ must be replaced by the distance $d(x_m, x_n)$ (where $d : X \times X \to$ R with some specific properties,(e.g., meteric mathematics) between x_m and x_n.Formally, given a metric space (*X*, *d*), a sequence $x_1, x_2, x_3, \ldots$ is Cauchy, if for every positive real number (geo-spatiotemporally-geosampled, prolific, georeferenced, shade canopied, *S. damnosum s.l.* larval habitat decomposed photosynthetic covariate coefficient value) ε> 0 there is a positive integer*N* such that for all positive integers *m*, *n*>*N*, the distance $d(x_m, x_n) < \varepsilon$.

More generally, an empricial geo-spatiotemporal, geosampled, riverine, larval habitat, eco-epidemiological, regression-related, geospectrally dependent, functional analysis can include the study of Fréchet spaces and other topological vector spaces not endowed with a norm. Topological vector space *X* is a Fréchet space if and only if it satisfies the following three properties:it is locally convex, its topology can be induced by a translation invariant metric, (i.e. a metric $d: X \times X \to$ R such that $d(x, y)=d(x+a, y+a)$ for all *a*, *x*, *y* in *X*) [65]. This means that a subset *U* of *X* is open in a parameter estimator, time series dependent, *S. damnosum* s.l., riverine, larval habitat, empirical, geosampled, Rapid Eye™ 5m imaged dataset if and only if for every *u* in *U* there exists an ε > 0 such that $\{v : d(v, u) < \varepsilon\}$ is a subset of *U*. An important object of study in remotely based functional analysis are the continuous linear operators defined on Banach and Hilbert spaces [115]. These lead naturally to the definition of C*-algebras and other operator algebras.

An important example of acomplete normed, vector, shade, canopied, explanatorial, *S. damnosum* s.l, larval habitat, canopy endmember, biosignature-related, decomposition spaces would be Hilbert space, where the norm arises from an inner product. These spaces are of fundamental importance in the mathematical formulation of quantum mechanics. Hilbert spaces can be completely classified: there is a unique Hilbert space up to isomorphism for every cardinality of the base [27]. Since finite-dimensional Hilbert spaces are fully understood in linear algebra, and since morphisms of Hilbert spaces can always be divided into morphisms of spaces with Aleph-null ($\aleph_0$) dimensionality [65], functional analysis of Hilbert spaces for a spectrally dependent, geosampled, geo-spatiotemporal, prolific, geosampled, *S. damnosum* s.l. Rapid Eye™ 5m, sseasonal imaged, riverine, larval habitat eco-epidemiological, forecasting, canopy, risk modelcan deal with the unique Hilbert space of dimensionality Aleph-null, and its morphisms. In future functional analysis research it may be interesting to prove that every operator on a Hilbert space in a seasonal, shade canopied, *S. damnosum* s.l. prolific, georferenced, larval habitat has a proper subspace which is invariant.

Consider a linear, geospectrally dependent, geo-spatiotemporal, geosampled, *S. damnosum* s.l. prolific, riverine, canopied, larval habitat eco-epidemiological, forecasting, Rapid Eye™, 5m, imaged, decomposed, sub-mixel, risk map *T* in ArcGIS that transforms: $T : R^n \to R^n$.An invariant subspace **W** of **T** may then have the property that all vectors $\upsilon \varepsilon W$ which may be transformed by **T** into vectors also contained in **W**. In mathematics, an invariant subspace of a linear mapping*T*: *V* → *V* from some vector space*V* to itself is a subspace*W* of *V* that is preserved by *T*; that is, $T(W) \subseteq W$ [12]. This can be alternatively stated as $\upsilon \varepsilon W \Rightarrow T(\upsilon) \varepsilon W$ in the model residual forecasts. Since Tcould map every prolific, shade, canopied, *S. damnosum* s.l. riverine, larval habitat, predictive, risk vector in R^n into R^n $\{0\}$ and since the linear map could be adjusted so$0 \to 0$, a uni-dimensional invariant subspace may be the basis of resolving the canopy model in uni-dimensional space. Consequently, any vector $x \varepsilon U$ in the canopied, time series, geospectrally dependent, larval habitat, eco-epidemiological, forecasting, risk model can be represented as $\lambda \upsilon$ where λ is a real scalar. If a ecologist or experimenter represents ***T*** by an uncertainty-orinted probabilistic matrix **A** then, for U to be an invariant subspace the model residual forecasts must satisfy: $\forall_{x \varepsilon U} \exists_{\alpha \varepsilon R} : Ax = \alpha \upsilon$.We know that $x \varepsilon U \Rightarrow x = \beta \upsilon$ with $A\upsilon = \lambda \upsilon$ [27]. Therefore, the condition for existence of a uni-dimensional invariant subspace in the forecasts may be expressed as: $A\upsilon = \lambda \upsilon$ Note that this is the typical formulation of an eigenvalue problem, which means that any eigenvector of A can also form a uni-dimensional invariant subspace in **T** in a robust, explanatorial, geo-spatiotemporal, shade, canopied, *S. damnosum* s.l., riverine, larval habitat, eco-epidemiological, forecasting, endmember, Rapid Eye™ specified, sub-mixel, risk model.

An invariant subspace of a linear mapping$T : V \to V$in ArcGIS from some vector space*V* to itself may be a subspace*W* of *V* such that *T*(*W*) is contained in *W*in a georfernced, prolific, shade canopied, *S. damnosum* s.l., riverine, larval habitat, predictive, 5 m, Rapid Eye™, canopy, imaged endmember, decomposed, eco-epidemiological, sub-mixel, forecasting, time series dependent, risk model. An invariant subspace of *T*may be also *T* invariant [132]. If *W* is *T*-invariant, an ecologist or expeimenter can restrict *T* to *W* to arrive at a new linear mapping$T \mid W$: *W* → *W*employing multiple geo-spatiotemporal, geosampled, riverine canopied, larval habitat model parameter estimators. By so doing, an ecologist or expeimenter may generate a few immediate examples of invariant subspaces. Certainly *V* itself, and the subspace {0}, would be trivially invariant subspaces for every linear operator *T*: *V* → *V* in the resdiual model output. For certain linear operators in an eco-epidemiological, canopied, *S. damnosum* s.l. riverine, larval habitat, geospectrally dependent, eco-epidemiological, risk model there may be only a non-trivial invariant subspace; thus, considering a rotation of a two-dimensional real vector space may not be far-fetched.

Let *v* be an eigenvector of *T*,(i.e. *Tv* = λ*v*) in the geospectrally dependent, georefernced, geosampled, *S. damnosum* s.l., geo-spatiotemporal, forecasting, eco-epidemiological, risk-related, Rapid Eye™,5m, imaged canopy, endmember, decomposed, model. Then *W*

= span $\{v\}$ would be$T$ invariant. As a consequence of the fundamental theorem of algebra, every linear operator on a complex finite-dimensional vector space with dimension at least 2 would have an sub-mixeleigen vector. Thereafter, every such linear operator in the riverine, larval habitat, canopied, eco-epidemiological, risk model output would have a non-trivial invariant subspace. The fact that the complex, geosampled, empirically geosampled, *S. damnosum* s.l., riverine, larval habitat, endmember, photosynthetic and NPV covariate coefficient, unmixed values may be algebraically closed. As such, the invariant subspaces of a linear transformation would be dependent upon the underlying scalar field of V in the model. An invariant vectorfixed point of T in the model, other than 0, would span an invariant subspace of dimension 1. An invariant subspace of dimension 1 would be acted on by T by a scalar therefater, and would consist of invariant vectors if and only if the scalar is 1 in the eco-epidemiological, geo-spectrally dependent, riverine larval, habitat forecasting, eco-epidemiological, risk model regression estimators.

As the above examples indicate, the invariant subspaces of a given linear transformation Tin a geosampled, georeferenced, prolific, canopied, *S. damnosum* s.l.,-related, eco-epidemiological, forecasting, diagnostic, risk model constructed in ArcGIS may shed light on the structure of T. When V is a finite dimensional vector space over an algebraically closed field, linear transformations acting on V may be characterized by the Jordan canonical form, which decomposes V into invariant subspaces of T. In linear algebra, a Jordan normal of a linear operator on a finite-dimensional vector space is an upper triangular matrix of a particular form called a Jordan matrix, representing the operator with respect to some basis [27]. Many fundamental questions regarding T may then be translated to questions about invariant subspaces of T in an eco-epidemiolovical, prolific, georfernced, geosampled, canopied, riverine, larval habitat, risk model. More generally, invariant subspaces may bedefined for sets of operators as subspaces invariant for each operator in the set in the model residual forecasts.

Let L (V) denote the algebra of linear transformations on V, and let (T) be the family of subspaces invariant under $T \in L$ (V). The "Lat" notation refers to the fact that Lat (T) forms a lattice [27]. Given a nonempty set $\Sigma \subset L(V)$, an ecologist or expeimenter may consider the invariant subspaces invariant in an explanatorial, shade canopied, Rapid Eye™ 5m, imaged,, seasonally productive, *S. damnosum* s.l., georeferenced, riverine, larval habitat, forecasting, eco-epidemiological, geospectrally dependent, eco-epidemiological risk model under each $T \in \Sigma$ using symbols, $Lat(\Sigma) = \bigcap_{T\varepsilon} Lat(T)$. For example, it is clear that if $\Sigma = L$ (V), then Lat $(\Sigma) = \{\{0\}, V\}$[65]. Given a representation of a group G on a vector space V, an ecologist or expeimenter may also achieve a linear transformation $T(g) : V \to V$ for every element g of G in the canopied, riverine, larval habitat model. If a subspace W of V is invariant with respect to all these transformations, then it would be a sub-representation and the group G would act on W in a natural way. As another example, let $T \in L(V)$ and Σ be the algebra generated by $\{1, T\}$ in the eco-epidemiological, geo-spatiotemporally, geosampled, eco-epidemiological risk model where 1 is the identity operator. Then Lat (T) = Lat (Σ). Because T lies in Σ trivially, Lat (Σ) $\subset$ Lat (T) would occur in the resdiual forecasts. On the other hand, Σ may consist of polynomials in 1 and T, therefore the reverse inclusion would hold as well in the forecasts.

Over a finite dimensional vector space every linear transformation $T : V \to V$ can be represented by a matrix once a basis of V has been chosen in ArcGIS. Suppose now W is a T invariant subspace in a geospectrally dependent, robust, *S. damnosum* s.l. georeferenced, shade, canopied, prolific, riverine, larval habitat, forecasting, eco-epidemiological, risk model. A basis $C=\{\boldsymbol{v}_1,.., \boldsymbol{v}_k\}$ of W may be selected and completed to a basis B of V. Thereafter, with respect to this basis, the matrix representation of Tin the model would take the form: $T = \begin{bmatrix} T_{11} & \mathrm{T}_{12} \\ 0 & \mathrm{T}_{22} \end{bmatrix}$ where the upper-left block T_{11} would be the restriction of T to W. In other words, given an invariant subspace W of T, V in aRapid Eye™, imaged, eco-epidemiological, decomposed, endmember,, shade canopied, productive, *S. damnosum* s.l. riverine larval habitat, geo-spatial, risk model, the sub-mixel, forecasts can be decomposed into the direct sum$V = W \oplus W'$. Viewing T as an operator matrix $T = \begin{bmatrix} T_{11} & T_{12} \\ T_{21} & T_{22} \end{bmatrix} : \underset{W'}{\overset{W}{\oplus}} \to \underset{W'}{\overset{W}{\oplus}}$, would then validate that T_{21}: $W \to W'$ must be zero. Determining whether a given subspace W is invariant under T would be ostensibly a problem of geometric nature. Matrix representation allows one to phrase this problem algebraically to be resolved [12]. The projection operator P onto W may be then optimally be defined by $P\ (w + w') = w$, where $w \in W$ and $w' \in W'$ in the riverine, canopied, larval habitat, eco-epidemiological model. The projection P would then have a matrix representation of $P = \begin{bmatrix} 1 & 0 \\ 0 & 0 \end{bmatrix} : \underset{W'}{\overset{W}{\oplus}} \to \underset{W'}{\overset{W}{\oplus}}$.

A straightforward calculation may show that W = R and P where the range of P, is invariant under T if and only of $PTP = TP$ in a eco-epidemiological, georeferenced, shade canopied, prolific, *S. damnosum* s.l. forecasting, endmember, Rapid Eye™ imaged sub-mixel, decomposed, 5m, eco-epidemiological risk model In other words, a subspace W being an element of Lat(T) would be equivalent to the corresponding projection satisfying the relation $PTP = TP$. If P is a projection (i.e. $P^2 = P$), so would be $1 - P$, where 1 is the identity operator. It follows from the above logic that $TP = PT$ in the *S. damnosum s.l.* related, canopy, endmember forecasting, eco-epidemioloigical risk model, if and only if both Ran P and Ran $(1 - P)$ are invariant under Tin the model resdiual output. In that case, T would have a matrix representation

$$T = \begin{bmatrix} T_{11} & 0 \\ 0 & T_{22} \end{bmatrix} : \underset{\mathrm{Ran}(1-P)}{\overset{\mathrm{Ran}P}{\oplus}} \to \underset{\mathrm{Ran}(1-P)}{\overset{\mathrm{Ran}P}{\oplus}} \cdot$$

Colloquially, a projection that commutes with T "diagonalizes" T [65].

Interestingly, a Rapid Eye™ 5m, imaged, riverine, larval, habitat canopy may be divided into thin layers, and the foliage elements within each layer which may be then classified into leaf inclination and azimuth angle classes. Simplications of the model can include options for varying the thickness of the canopy layers and the number of angle classes, for accurate, forecast, eco-epidemiological, sub-mixel, risk modeling, georeferenced, riverine, larval habitat, higher canopy geolocations as a single layer, and for partitioning the foliage elements in each layer into sunlit and shaded fractions, with disregard of leaf angle classes. This canopy radiation model and its simplications may be implemented in a computer simulation module thereafter for estimating canopy photosynthesis and transpiration in the georeferenced larval habitat canopy. Simulation runs may be performed for seasonal conditions with low and high LAI and irradiance. It may be found that canopy photosynthesis and transpiration estimates, may be optimally regressively seasonally qualitatively quantitated in a riverine, *S. damnosum* s.l., larval habitat, geo-spectrally dependent, decomposed endmember, sub-mixel, eco-epidemiological, Rapid Eye™, risk model employing canopy layer thickness of 0.5 LAI, for example,with three inclination and azimuth angle classes which may, in turn,be found to render only negligible error in the eco-epidemiological explanatorial, residual forecasts.These spectral uncertainties may be determined to be small if only average irradiance over sunlit and shaded leaf fractions by layer are constantly quantized by calculating fluctuations from 0% to 10% for the entire empirical dataset of decomposed photosynthesis covariate coefficient estimators, for example, and/or from 0% to 5% for transpiration estimates.

Simplified canopy radiation models result in a dramatic decrease of computation time, up to 1/60of that required by the standard [116]. The distribution of the predicted, prolific, geo-spatiotemporally-geosampled, Rapid Eye™ 5m, imaged,riverine, larval habitats can thus be generalized by considering the distribution of area on prolate or oblate spheroids, rather than just spheres in decomposed,canopied, endmember, ArcGIS datasets. By adjusting the ratio of horizontal to vertical axis of the spheroid, LAD of any geosampled, georeferenced, 5m imaged *S. damnosum* s.l. canopy from erectophile to planophile may be be simulated.

Geovisually detectable Rapid Eye™, 5m, imaged, georeferenced, *S. damnosum* s.l. larval habitat, explanatorial, leaf optical properties geosampled in African riverine environments may be controlled by internal leaf structure and attenuated by seasonal leaf water content. Mild water stress decreases relative water content (RWC) 10 to 20% and decreases turgor slightly [91]. Relative water content is probably the most appropriate measure of canopy plant water status in terms of the ecophysiological consequence of cellular water deficit [13]. Water potential as an estimate of the energy status of canopy plant water is useful in dealing with water transport in the soil-plant-atmosphere continuum [26].

Mild water stress decreases relative water content (RWC) 10 to 20% and decreases turgor slightly [91]. Relative water content is probably the most appropriate measure of canopy plant water status in terms of the ecophysiological consequence of cellular water deficit [13]. Water potential as an estimate of the energy status of canopy plant water is useful in dealing with water transport in the soil-plant-atmosphere continuum [26].

However, in georeferenced, geospectrally decomposed, Rapid Eye™ specified, *S. damnosum* s.l., larval habitat, canopied, vegetation materials geosampled in a African riverine environment, RWC may not not account for seasonal osmotic adjustment (OA). The OA is a powerful mechanism of conserving cellular hydration under drought stress [13]. Regardless, the same geosampled, riverine, larval habitat, canopy, leaf water potential can have two different cultivars which in turn can have different leaf RWCs, indicating a corresponding difference in leaf hydration, leaf water deficit and physiological water status. Hence, RWC may be an appropriate 5m, remotely-sensed, heuristically optimizable, regressive estimate of a geosampled, Rapid Eye™ 5m imaged, georefernced, *S. damnosum* s.l., riverine, larval habitat, canopy plant, water status which may be quantitated in terms of cellular hydration under the possible effect of both leaf water potential and OA. Normal values of RWC range between 98% in fully turgid transpiring leaves to about 30-40% in severely desiccated and dying leaves, depending on canopy plant species [13,33]. In most crop species the typical leaf RWC wilting is about 60% to 70% [26]. Seasonal decreases in RWC in *S. damnosum* s.l., habitat, riverine canopies may be accompanied by cell wall relaxation, decreases in cell dimension, cell surface, cell volume, and lengthening of intercellular space of photosynthetic materials which also may be geospectrally qualitatively regressively quantized by analyzing decomposed,Rapid Eye™,5m, geospectrally dependent, vegetation indices.

Rapid Eye™ 5m, derived Leaf Water Content Index (LWCI) in ArcGIS may also determine RWC of a geosampled, geoTefernced, *S. damnosum* s.l., prolific, shade, canopied, riverine, larval habitats with different seasonal leaf morphologies. Thereafter, the Moisture Stress Index (MSI) may be regressively quantitated along with the Equivalent Water Thickness (EWT). Reflectance factors at 0.82 μm and 1.6 μm were measured on leaves of *Quercus agrifolia* (sclerophyllous leaves), *Liquidambar styraciflua* (hardwood deciduous tree leaves), *Picea rubens* and *Picea pungens* (conifer needles), and *Glycine max* (herbaceous dicot leaves) employing RWC and EWT which were then measured concurrently with moderate resolution reflectance measurements [126]. The results showed that LWCI was equal to RWC for the species tested.Thus, the results of a sensitivity analysis for an explanatorial, georefernced, geosampled, seasonally productive, decomposed empirical, geosampled, riverine, *S. damsnoum* s.l., larval habitat, endmember analyses may indicate canopy reflectances at 1.5 μm, for example, for two different geo-spatiotemporally extracted RWCs. By so doing, MSI and LWCI may be found to be seasonally correlated to the quantized, georferenced, riverine, larval habitat, Rapid Eye™ 5m specified, canopy RWCs with each having a different regression equation and $\log_{10}$ EWT values on the same regression line.

Because EWT is correlated with LAI [127-130,133] MSI may also be correlated with Rapid Eye™ 5m specified, geospectrally decomposed, *S. damsnoum* s.l., georeferencable, riverine, larval habitat, endmember, empirical phostosynthetic and NPV explanatorial, time series dependent, geosampled, parameter estimators. Assuming that the regression equation of MSI to EWT can be applied to the decomposed, larval habitat, endmember canopy values, then the minimum significant change of RWC may also be detected. Even though for most canopy plants, the natural variation in RWC from water stress is only about 20%[2],Rapid Eye™proxy indices derived from decomposed NIR reflectances may be employed to remotely-sensed water stress in the shaded canopy cover in a georeferenced, *S. damnosum* s.l., larval habitat, 5m scene, geosampled in an African riverine environment.

In future it may be advisable when decomposing Rapid Eye™, endmember, shade, canopied, *S. damnosum* s.l., riverine, larval habitat geosampled biosignature to remotely extrapolate more geo-spatiotemporal, water-related, LULC classes from the RedEdge NDVI data in ArcGIS. Many band ratios have been proposed to estimate water content, including the normalized difference water index [134] and the plant water index [135]. Gao and Goetz [136] calculated an equivalent water thickness (i.e., the depth of water across a SPOT mixel) by fitting a water spectrum across the feature centered at 980 nm. Zhang et al. [137] and Sanderson et al. [138] used endmember medium resolution data (+ETM) to map canopy water absorption and content in salt marshes. Thus, robustness of an explanatorily, qualitatively, regressed endmember, Rapid Eye™ , 5m forecast may be improved when geospectrally, explanatorily interpolating a decomposed, 5m, RedEdge, NDWI biosignature reterived from a georeferenced shade vegetated, canopied, *S. damnosum* s.l, riverine, larval habitat by including more flooded, riverine, LULC classes, for example, for remotely targeting unknown, unsampled, seasonally geospectrally, productive habitats based on field geosampled immature count data.

Light in a canopy is attenuated exponentially with increasing leaf area and biomass [4,13].We simulated spectral reflectances which were analyzed by the Rapid Eye^{TM},5m data in the geosampled, *S. damnosum* s.l. larval habitat geo-spatiotemporal, endmember model to regressively quantify reflectance differences between different and equivalent, canopy-related, riverine water thicknesses level. Simulated results coupled with consideration of atmospheric transmission properties and the incident solar quantized the 5m spectral irradiance which subsequently resulted in identifying plant canopy water status between the 0.7–2.5 µm region of the spectrum. Since,in the RedEdge visible spectrum, underlying substrate is generally more reflective than the vegetative component (www.satellite imaging corporation), so regressively quantitating BDRF values derived, from unmixed, RapidEye^{TM}, *S. damnosum* s.l., larval habitat, endmember data may decrease with increasing LAI.

As LAI increases seasonally, leaf optical properties may dominate in georeferenced, geosampled, *S. damnosum* s.l., riverine, larval habitat canopies owing to multiple scattering, resulting in an increase in NIR, RedEdge, NDVI decomposable, qualitatively regressively quantizable values. An ArcGIS, stochastic, leaf radiation model constructed using decomposed Rapid Eye^{TM} 5m data may predict leaf spectral reflectance as a function of leaf water content for mapping unknown, unsampled, geospectrally/geospatially explanatorily interpolated prolific, shade, canopied, geosampled, georeferencable, *S. damnosum* s.l., riverine, larval habitats. A stochastic leaf radiation model based upon physical and eco-geophysiological explanatorial properties of an empirically geosampled, eco-epidemiological, time series dependent, geospectral dataset of river larval habitat, canopied dicot leaves may be then developed. The model may accurately predict the absorbed, reflected, and transmitted radiation of normal incidence as a function of Rapid Eye ^{TM} wavelengths resulting from the leaf–irradiance interaction over the spectral interval of 0.40-2.50 *µ*m, for example.

In our ArcGIS *S. damnosum s.l.* related remote model, the leaf optical system was represented as Markov process with a unique transition matrix at each 0.01-*µ*m increment between 0.40 *µ*m and 2.50 *µ*m, therefater. Probabilities were calculated at every Rapid Eye™ wavelength interval from leaf thickness, structure, pigment composition, and water content. Simulation results indicated that the stochastic, canopied, georeferenced, geosampled, *S. damnosum* s.l., riverine, larval habitat, time series dependent, explanatorial, radiation, model approach rendered accurate regressive estimators of actual measured values for dicot leaf absorption which was subsequently tested to determine if a 5 m RapidEye™ derived wavelength reflection function could robustly remotely target prolific unknown, unsampled, canopy, shaded, habitats in an African riverine environment.

Although the radiative transfer equation was developed for a 3-D media, the propagation of light one direction must considered [2]. Let $I(x, \mu)$ be the intensity of monochromatic radiation at a position x in the interior of the leaf, traveling in a small volume element $dx.dy$, in the direction θ [120]. We defined $\mu=\cos\theta$ and $\mu'=\cos\theta'$in the geosampled, *S. damnosum* s.l,-related, forecasting, eco-epidemiological, risk model as the axial cosines of the angle of light propagation before and after scattering, respectively. We used the probabilistic etsimates where $\sigma e(x)$ was the extinction coefficient of the medium defined as $\sigma e(x)= \sigma k(x) + \sigma s(x)$. In the Rapid Eye™ model $I(x)$ was intensified by coherent single scattering emerging from multiple canopy directions and thermal emission of the medium, at the local thermodynamic equilibrium. The medium includes inhomogeneities in the form of small particles that scatter the radiation beam in all direction [13]. The scattering is called coherent because the scattered radiation has the same wavelength as the incident radiation [4].

The distribution of scattered radiation over all the directions in the Rapid Eye™, 5 m, riverine, larval habitat, sub-mixel, eco-epidemiological, time series, risk model was characterized by a phase function $P(\mu, \mu')$ that was normalized to 1: $\frac{1}{4\pi}\int_{4\pi} p\left(u,u'\right)d\Omega'=1$ where $P(\mu, \mu')$ wasthe probability that the endmember, radiation falling in the direction μ was based on incidence scattered in the direction μ' of the geosampled, canopied, larval habitat, explanatorial observations. As a consequence, the multiple scattering source function that corresponded to the canopy habitat radiation falling on a volume element of the medium from all directions wasequal to: $\frac{1}{4\pi}\sigma_S(x)\int_{4\pi} p\left(u,u'\right)I(x,u)\,d\Omega'$ Moderate resolution emissions of this small volume element may be expressed in terms of the Planck function for the intensity of radiation of an ideal blackbody$M(T(x))$: $\sigma_e(x)M\left(T(x)\right)$ in future research. Then the source function $J(x, \mu)$ would be sum of these twoprocesses:. $J(x,u)=\frac{1}{4\pi}\sigma_S(x)\int_{4\pi} p\left(u,u'\right)I(x,u)\,d\Omega'+\sigma_e(x)M\left(T(x)\right)$ Further, the Rapid Eye™, 5 m-related, radiative transfer equation may express the infinitesimal variation of flux dI in the slab at position x is an integro-differential geo-spatiotemrporal, *S. damnosum* s.l. forecasting equation [e.g., $u\frac{dI(x,u)}{dx}=-\sigma_e(x)I(x,u)+\frac{1}{4\pi}\sigma_S\int_{4\pi} p\left(u,u'\right)I(x,u)\,d\Omega'+\sigma_e(x)M\left(T(x)\right)$]. In the solar domain from 400 nm to 2500 nm in the RedEdge signal there be no thermal emission but intense scattering may occur which may be then subsequently simplified by $u\frac{dI(x,u)}{dx}=-\sigma_e(x)I(x,u)+\frac{1}{4\pi}\sigma_S\int_{4\pi} p\left(u,u'\right)I(x,u)\,d\Omega'$

A SPA algorithm in ArcGIS was then employed to further unmix the RedEdge NDVI biosignature. By employing the average of multiple, shade, canopied, Rapid Eye^{TM} 5m imaged *S. damnosum* s.l., riverine, larval habitat,geospectrally decomposed, georeferenced, canopy endmembers from the extracted RedEdge, NDVI mixel as one canopy endmember, we noticed that the SPA-derived spectra appeared noise-less (e.g. smooth). Given that geospatially adjacent, explanatorial, canopied, *S. damnosum* s.l., riverine, larval habitat data extracted from a 5m mixel was not likely to be simultaneously spurious, the use of adjacency–related endmember tabulations may have made the SPA more sensitive to isolated, noisy, Rapid Eye^{TM} mixels,thus avoiding inherent problems such as uncertainty probability estimation and propagation of autocovariate decomposition erroneous variabes commonly seen in other convex–based, endmember-search, unmixing algorithms.

Metropolis-within-Gibbs sampler for piecewise convex hyperspectral unmixing and canopy endmember extraction may be presented for unmixing a seasonally prolific, shade canopied, *S .damnosum* s.l., riverine, larval habitat The standard linear mixing model used for hyperspectral unmixing assumes that hyperspectral data reside in a single convex region[4]. However, hyperspectral data are often nonconvex. Further, in standard, canopy, endmember extraction and unmixing methods, the endmembers are generally represented as a single pointin the high-dimensional geospace. However, the geospectral, canopied, bioisignature for an explanatorialy decomposed, Rapid Eye^{TM},5m, imaged, geosampled, georefernced *S. damnosum* s.l., riverine, larval habitat, unmixed sub-mixel material may vary as a function of the inherent variability of the unmixed material and riverine ecosystem conditions. Therefore, it is would be appropriate to represent each decomposed, riverine, larval habitat, canopyend member with a full distribution of the variable radiance capability and use this information during LULC classification. The proposed method would search for several sets of canopy endmember distributions. By employing several sets of endmember distributions, a piecewise convex mixing model may be applied. By so doing, each *S. damnosum* s.l., riverine, larval habitat, unmixed canopied endmember, in a decomposed empirical dataset would then represent a random simplex. The vertices of the random simplex could thereafter be modeled by the endmember distributions. Optimally, the data would be partitioned into sets associated with each of the extracted endmember distributions using a Dirichlet process prior.

In probability theory, Dirichlet processes are a family of stochastic processes whose realizations are probability distributions[12]. In other words, a Dirichlet process in a geo-spatiotemporally, geosampled, productive, georeferenced, *S. damnosum* s.l. riverine, eco-epidemiological, forecasting, risk-related, larval habitat model would be a probability distribution whose domain is itself a set of probability distributions. The Dirichlet process prior would estimate the number of sets in the Rapid Eye™ 5m, imaged, riverine, larval habitat, ,risk-related eco-epidemiological, decomposition exercise. Thereafter, the Metropolis-within-Gibbs sampler could partition the data into convex regions, estimate the required number of convex regions, and estimate the canopy endmember abundance values for all convex regions, if so desired. Results may be presented on real hyperspectral and/ or simulated riverine, larval habitat, geosampled data that indicate the ability of the method to effectively explanatorily geo-spatiotemporally tabulate distributions and the number of sets of canopy endmember distributions.

One of the major extracting tools for generating the the georeferencable, SPA-based, spectral explanatorial, forecasted residuals from the Rapid Eye™, RedEdge, *S. damnosum s.l.* habitat, explanatorial, NDVI, decomposed biosignature was the sensitivity of two parameters namely, the k (the number of so-called skewer [i.e., random initial canopied endmembers]) and t (cut-off threshold value) which became evident during the final selection of the canopy, shaded, endmembers from the unmixed reference biosignature-related predictor variables. These parameters were implemented using a Minimum Noise Fraction(MNF) transform, which performed dimensionality reduction on the geospectrally decomposed, RedEdge, canopied, *S. damnosum s.l.* riverine, larval habitat, 5m, Rapid Eye™ biosignature-related sub-mixel covariate coefficients. Due to the fact the MNF was associated to second order statistics, it may be possible to capture additional higher order statistical information when decomposing a Rapid Eye™, Red Edge, NDVI canopied biosignature. Endmembers are traditionally characterized by higher order statistics (127,131,139-141).

The SPA-based algorithms utilized the high order statistical-based transformation to perform dimensionality reduction of the Rapid Eye™5m imaged, *S. damnosum* s.l., larval habitat individualized RedEdge, NDVI, decomposed biosignature, radiance estimates. The canopy endmember determination quantified the unmixed dataset of distinct visible and NIR decomposed spectra that comprised the 5m mixel. The inversion stage produced abundance planes that provided estimates of the fractional abundances of the endmember spectrum.

An additional 5m byproduct measurement rendered by the SPA was generated while unmixing the RedEge NDVI, shade-related, explanatorial, *S. damnosum* s.l. riverine, larval habitat, Rapid Eye™canopy, endmember biosignature which was quantaited as the change of the simplex volume ratio between successive iterations during the endmember extraction process.For example, we noted that the SPA illustrated the influence of a new riverine larval habitat canopied endmembers on the decomposed RedEdge, NDVI image data structure, and provided information on the convergence of the algorithm. Though the rate of convergence speed varied with the complexity of the decomposed, 5m,biosignature, eco-geographiocally representing the seasonally prolific, shaded, *S. damnosum* s.l., riverine, larval habitat, canopied endmember, explanatorial, geospatial covariates, the merging revealed large changes in volume ratio, followed by progressively smaller changes and convergence towards a plateau. The spectral, decomposed, canopy, endmember biosignature search terminated before the convergence point (i.e., when the volume ratio was close to 1.0).

Although, in Jacob et al.[1] the SPA was specific for sub-meter resolution,field, operationizable, decomposition-related, canopy endmember, sub-mixel georeferencable applications (e.g. spatial continuity of a, riverine, georeferenced, geospectrally explanatorily interpolatble, productive, *S. damnosum* s.l. geospatiotemporally geosampled, riverine, larval habitat) ArcGIS,SPA offers potential for a variety of Rapid Eye™ 5m applications especially where the premise of spatial adjacency applies to canopy plant communities associated to riverine-related, unknown, unsampled, prolific, larval habitat endmembers. There may be some specifications required to accomodate the SPA decomposition process for future research for remotely qualitatively regressively quantitating mitigating georeferenced, decomposable, RedEdge, NDVI, riverine, larval habitat, canopy endmember variability as opposed to a sub-meter resolution biosignature, which may include: (i) the use of multiple, shaded, sub-mixel covariates for each interpolated decomposed component in the iterative mixture analysis cycle, (ii) the selection and quantitation of a subset of explanatorial stable, geospectral, within-canopy, (e.g., hanging immersed vegetation), LULC data, feature, endmember attributes, (iii) the spectral weighting of the RedEdge bands; and, (iv) quantization of logarithmic, 5m, geospectral, signal transformations.

We noted that variations in LAI, chlorophyll, dry matter, and water content interacted to cause nonlinear changes in the geosampled, georeferenced, 5m, *S. damnosum* s.l., larval habitat, SPA decomposed, canopy endmembers. Because changes in LAI had the greatest effect in the 5m visible and NIR regions between 400 and 1300 nm, and dry plant residues in the riverine habitat canopy has the greatest effect in the IR region between 2000 and 2400 nm, remotely regressively quantized endmember observations of the full 400- to 2500-nm spectrum for a decomposed, Rapid Eye™ 5mRed Edge ,NDVI,*S. damnosum* s.l., larval habitat, sub-mixel biosignature may provide the best basis for analyzing and geospectrally interpolating fractional quantitative photosynthetic and NPV estimates.

The explanatorily, geo-spatiotemporally decomposed, Red Edge,Rapid Eye™, 5m imaged ,NDVI, georeferenced, shaded, *S. damnosum s.l.* riverine, larval habitat, canopied,endmember emissitives rendered from the SPA were then imput into a 3-D radiative transfer model in ArcGIS. The medium resolution, NDVI, canopy invariants expressed canopy spectral transmittance and reflectance by independent 5m wavelengths. The model forecasts determined a small, explanatorial, unmixed dataset of canopy structural, radiatively transferable, geospectrally operationizable, predictor variables. This dataset included the canopy interceptance based on the recollision and the escape probabilities. These variables specified an accurate relationship between the spectral response of the georeferenced, riverine, larval habitat, vegetation canopy to the incident solar radiation at the leaf and the canopy scale which was robustly remotely tabulated employing the decomposed, georeferenced, *S. damnosum s.l.,* riverine, larval habitat, RedEdge, NDVI time series regressors. The estimates rendered from the model allowed for a simple and accurate parameterization for partioning the incoming radiation canopy transmission, reflection and absorption at any 5m Rapid Eye^{TM} wavelength spectrum.

We then conducted a retrieval of the canopy endmember-related, sub-mixel, riverine, larval habitat, photosynthetic and NPV feature data attributes employing a geometric-optical model. The scene reflectance of each decomposed, explanatorial, operational, shade canopied, geospectral component was classified. We retrieved the larval habitat, structural parameter estimators employing the canopy endmember data using a linear spectrum decomposition embedded in the geometeric optical algorithm in ArcGIS to determine the 5m reflectances of the RedEdge NDVI, endmember, geospectral scene components, which were regarded as prior knowledge in the retrieval of the riverine, larval habitat, canopy cover.

The geometric optics scene included four components: sunlit canopy, shadowed canopy, sunlit background, and shadowed background. The radiance or reflectance of the Rapid Eye^{TM} scene as a whole was modeled based on the canopied reflectances of the individual endmember components as weighted by their areal proportions. The areal proportions of the components were determined by principles of geometric optics as applied to the shapes of the habitat canopy envelopes. These partions yielded the expected proportions of the components as a function of angles of irradiance and exitance.

The empirical geospatiotemporal, geosampled, BRDF model was derived using the apparent trends quantitated between TOA reflectance versus solar zenith angle and viewing zenith angle of the decomposed canopied habitat. While the obvious disadvantage of using the empirical model is the need for the large number of data samples to build the statistical model, it may be shown that the model works reasonably well for Rapid Eye^{TM} sensors if the sensor viewing angles are restricted to within ±20 degrees of nadir.

Various models from the literature have classified BRDF as physical semi-empirical or empirical models [2]. A physics-based BRDF model—taking, for instance, sand—is based on the complete characterization of physical characteristics of the sand such as its composition, irregular particle shape, refractive index, surface roughness, spectral reflectance, etc [27]. Widely used semi-empirical models such as the Ross-Li model, Roujean model, and Snyder model are kernel driven, whereas BRDF is modeled as a weighted sum of volume scattering, geometric scattering and isotropic terms A geometric-optic radiative transfer (GORT) model may model BRDF in ArcGIS which may be able to explore the impact of topography, crown shape and scan angle on large seasonal footprint 5m *S. damnosum s.l.,* larval habitat Rapid Eye^{TM} data. It may be shown that the impact of riverine LULC topography and scan angle on waveform properties quantitated from a geo-spatiotemporally, geosampled, shade, canopied, productive *S. damnosum* s.l., larval habitat are similar and the returned waveform shape thus reducing the energy returned with height through the canopy, potentially resulting in trailing vegetation, habitat, height quantification. A Rapid Eye^{TM}ArcGIS model also may show that the impact of within-crown distribution of leaf and woody LULC material on simulated, shade canopied, geosampled, georeferencable, *S. damnosum* s.l. larval habitat where returns may vary with footprint and scan angles. All of these effects can impact estimates of P_{gap} on the riverine habitat typically by acting to reduce it if the path length through the canopy which may be increased by scan angle or topography (and vice versa).

For future contributions, at the leaf level, the canopy envelope of a eco-epidemiological,geosampled, georefernced, Rapid Eye^{TM},5m, imaged,*S. damnosum* s.l., riverine, larval habitat, forecasting, canopied, endmember, unmixing, eco-epidemiological, forecasting, wavelenght, risk model can be treated as containing an assemblage of leaves in ArcGIS. By so doing, the radiance or larval habitat canopied reflectance would beconsidered a function of the areal proportions of sunlit leaf, shadowed leaf, sunlit background, and shadowed background. Because the proportions of unmixed, LULC, scene components would be dependent upon the directions of irradiance and exitance, the larval habitat endmember model may account for the "hotspot"in a Rapid Eye^{TM} 5m *S. damnosum* s.l., riverine, larval habitat scene.

The directional radiance of the georeferenced, geo-spatiotemorally, geosampled, shade, canopied, decomposed *S. damnosum* s.l. riverine larval habitat at the Chutes Dienkoa eco-epidemioloigcal riverine study site was dependent on the mixture of four components-sunlit and shaded canopy crown, and sunlit and shaded background-that was seen from a given viewing illumination angle. The areal proportions of these four components, for given illumination and viewing directions was a function of the sizes, shapes, orientations, and placements of the canopied objects (i. e., individual tree crowns)within the scene. Moreover, the size, shape, and orientation of the shade canopied, Rapid Eye^{TM}, riverine, larval habitat was characterized by distributions with known parameters, and object centers which were distributed randomly. This model accounted for the changes in proportions that occurred with random overlapping of objects as the density of objects increased.

The principles of Boolean models was easily extended for qualitatively, remotely qualitatively, regressively quantizing the larval habitat canopy leaves in ArcGIS as objects in successive layers above the background canopy trailing vegetation. By so doing, the bidirectional reflectance or radiance of leaf canopies of the geo-spatiotemporally, geosampled, Rapid Eye^{TM} 5m-imaged georefernced, shade canopied, prolific, *S. damnosum* s.l., riverine, larval habitat was efficiently cartographically, ecogeographically delineated. The 5m scene was modeled as consisting of four components: sunlit leaf, shaded leaf, sunlit background, and shaded background. As in the case of canopy envelopes, the objects, shape, size, orientation and spacing of the canopy leaves was the covariate, parameter estimators that drove the estimation of bidirectional radiance or reflectance in the, *S. damnosum* s.l. shade, canopied, georefernced, larval habitat, forecasting, eco-epidemiological, Rapid Eye 5m^{TM} risk model. This extension lead to the formulation of two-stage models, in which leaves were geospatial endmember objects inside the canopy envelopes of the Booleanized, *S. damnosum* s.l., larval habitat, risk-related, eco-epidemiological, wavelenght model. A 3-D geospatial resdiualized output thereafter provided the mathematical basis for parsimoniously regressively quantitating the bidirectional radiance which were dependent upon the directions of irradiance and exitance, for accounting and validating the georeferencable "hotspot" .Because both whole-canopy and individual canopied, forecasting, geo-spectral, eco-epidemiological, probabilistically regressable, risk models may be driven by the same principles of geometric optics and Booleanization, they may easily be combined together in a single or a two-staged, geosampled, georefernced, *S. damnosum* s.l. riverine, larval habitat, forecasting, canopy, risk model. Moreover, through further application of the mathematics of random sets, the averaging and variance quantification that occurs when a 5m scene may be optimally imaged by the Rapid Eye™ sensor with a finite field of view. In addition Boolean and geometeric-optical, explanatorily geosampled, *S. damnosum* s.l., riverine, larval habitat, geo-spatiotemporally-dependent, eco-epidemiological, time series dependent, canopied, risk models may be capable of inversion, yielding estimates of size, shape, and spacing of crowns and/or leaves from directional and spatial statistical, sequential, probabilistic,explanatorily interpolatable, algorithmic residuals representing 5m remotely sensed radiances.

Employing the unmixing algorithm, two main absorption bands, in blue (450 nm) and in red (670 nm), where found due to the absorption of the two main leaf pigments: the chlorophyll a and b which accounted for 75% of the total leaf pigments of the habitat canopy plants.We also found that, the yellow to orange-red pigment, the carotene, had a strong absorption in the 350-500 nm range and was responsible for the color of some habitat leaves without chlorophyll. The red and blue pigment, the xantophyll, had a strong absorption in the 350-500nm range and may have been responsible for the leaf color also. In the Rapid Eye™ NIR geospectral domain (700-1300 nm), geosampled, leaf structure explained the canopy optical properties. Leaf pigments and cellulose are transparent to NIR wavelengths and therfore leaf absorptance was very small (5% maximum), but not the leaf reflectance and transmittance, which can reach 50% [2] In this region, there was a reflectance plateau in the *S. damnosum* s.l., riverine, larval habitat, canopied, leaf spectrum. The level of this plateau was dependant on the internal leaf structure as well as on the space amount in probably the mesophyll which probably could herewith employed to remotely quantitate interfaces with different refraction indices (air or watercells). Leaf reflectance increases for more heteregeneous cell shapes and contents as well as with increasing number of cell layers, number of intercell spaces and cell size [2]. This reflectance is therefore dependent on the relative thickness of the mesophyll in the riverine habitat canopy. Near-infrared spectral region has two main spectral regions: (1) between 700 and 1100 nm, where the reflectance is high, except in two minor water-related absorption bands (960 and 1100 nm) and (2) between 1100 and 1300 nm, which corresponds to the transition between the high NIR reflectances and the water-related absorption bands of the shortwave IR [4,120]. The last optical domain is the shortwave IR (1300 -2500 nm) characterized by the light absorption by the canopy leaf water. Because water strongly absorbs radiation in 1450, 1950 and 2500 nm, these wavelengths may not be used for reflectance measurements [27]. For all the three mainspectral domains, factors affecting canopy leaf optical properties are: internal or external structure, age, water status, mineral stresses and, healthness

Extracting the individual, fractionalized, canopy leaf,radiance values from Rapid Eye™ 5m,RedEdge, NDVI, spectrometer endmember, sub-mixel data employing explanatorial, geo-spectral,linear, spectral unmixing and convex, geometrical, optical algorithms can generate powerful, robust, eco-epidemiological, risk forecasts from geospectrally decomposable, georeferencable, *S. damnosum s.l.,* riverine, larval habitat, endmember, canopy maps. For example, in our Rapid Eye™ RedEdge, NDVI, geo-spectrometric, eco-epidemiological, dataset, levels of major plant pigment classes, including chlorophylls, carotenoids and anthocyanins were detected. The spectral characteristics of the vegetation spectrum we assumed were related with the leaf pigments, leaves internal structure and water content within the riverine, larval habitat, canopy leaves. A close analysis of the canopy vegetation, geospectral LULC-related, sub-mixel, unmixed, biosignature reflectance provided information on the phase of vegetation life cycle, health, and even the identification of individual, vegetation-related, types. Pigment levels can indicate conditions of canopy stress and assess photosynthetic activity [2]. Spectral bands sensitive to the pigment concentration have been identified, and linear models for non-destructive assessment of anthocyanins, and carotenoids, via chlorophyll fluorescence measurements have been put forward [115,127].

The riverine, larval habitat, canopy pigments primarily absorbed carotenoids in the Rapid Eye ™ 5m blue wavelengths while remotely allowing longer wavelengths to be scattered producing a yellow color. The geosampled carotenoids absorbed wavelengths ranging from 400-550 nm (violet to green light). Cartenoids serve two key roles in plants and algae: they absorb light energy for use in photosynthesis, and they protect chlorophyll from photodamage [2]. Carotenoids are very long-chain water-repelling pigments that are synthesized in the plastids of plant cells.(http://harvardforest.fas.harvard.edu/leaves/pigment). Anthocyanins in the riverine, larval habitat, unmixed canopy were absorbed in the blue-green wavelengths, allowing the red wavelengths to be scattered by the canopy plant tissue. Anthocyanins in the larval habitat canopy were absorbed around 540-550 nm.

Since anthocyanin and chlorophyll contents in georeferened, geo-spatiotemporally-geosampled, *S. damnosum* s.l. riverine, larval habitat shaded, canopied, decomposed leaves can provide valuable information about the ecophysiological status of the habitat canopy there is a need for more accurate, endmember, unmixing decomposition algorithms to estimate optimizable, biochemical parameter estimators of seasonal geosampled, canopy vegetation, LULC-related, covariate, parameter estimator cofficients. For example, the performance and accuracy of several non-destructive, reflectance-based techniques employing RapidEye™ data may be employed for estimating anthocyanin and chlorophyll contents in geosampled, *S. damnosum* s.l., riverine, larval habitat, canopy leaves to remotely probabilistically, regressively quantitate varying pigment content and compositions which seasonally occur which may then be subsequently linked to immature seasonal productivity.

Conversely, an anthocyanin reflectance index, reflectances in the green and RedEdge spectral bands, and a modified anthocyanin reflectance index, may be employed, in addition, to the NIR band to accurately estimate leaf anthocyanin with no reparameterization of the unmixing algorithms. By so doing, total chlorophyll content may be accurately estimated by a RedEdge chlorophyll index, for example, that employs 5m spectral bands in the NIR. These approaches may be also employed to estimate anthocyanin and chlorophyll non-destructively and allow the development of simple handheld field instrumentation with built-in gridded Rapid Eye™ data. For the non-linear model, a supervised procedure based on the training of a multi-layer perceptron neural network using intelligently selected prolific, geo-spatiotemporally, geosampled, *S. damnosum* s.l. riverine, larval habitat, shade, canopied, training samples may also be parsimoniously derived in a parallel fashion.

Subtle changes in pigment ratios-anthocyanin and chlorophyll-carotenoid ratios in particular —from the decomposed dataset of georeferenced, Rapid Eye™,5m, RedEdge, explanatorial, shade, vegetated, geosampled, *S. damnosum* s.l., riverine, larval habitat, canopied endmembers revealed altered photosynthetic activity in the time series dependent, geospectrally decomposed, sub-mixel, biosignature-related, forecasting, risk model derivatives. eco-epidemiological, riskmodel. For example, the photochemical reflectance index was formulated in ArcGIS to indicate diurnal interconversion of xanthophyll cycle pigments that were closely tied to photosynthetic activities of the unmixed, seasonal, georeferenced, riverine, larval habitat, shade, canopied, categorical, explanatorial, predictor variables. Over seasonal periods, photochemical reflectance index measures have demonstrated relative levels of chlorophylls and carotenoids which have revealed geo-spatiotemporal, explanatorial LULC patterns of photosynthetic activity for entire canopied ecosystems [130]. Newer approaches that involve the inversion of unmixed, shade, canopied, riverine-based, vegetated, larval habitat spectra in 3-D radiative transfer models and other associated unmixing algorithms may yield improvements over traditional index approaches for correlating canopy photosynthetic pigments with seasonal, immature, *Similium* productivity. By so doing, an ecologist or experimenter may carefully consider the ecophysiological and hydrostructural, explanatorial, time series unmixed, geospectral component contributions of each extracted, stochastically/deterministically interpolatable, riverine, larval habitat, sub-mixel, geoerferenced, data, feature attribute with with a field geosampled black-fly larval count.

The presence of other canopy pigments did significantly affect estimation of chlorophyll from the 5m, Rapid Eye^{TM} decomposed spectral reflectance. The carotenoid and anthocyanin indices performed well across the whole canopy endmemeber dataset. We found that the estimation of xanthophyll pigment changes was related to carotenoid/chlorophyll ratios in the riverine, larval habitat, shade, canopied, green leaves. Our results demonstrate that geospectrally interpolating Red Edge, NDVI, decomposed vegetation LULC, wavelengh transmittance can seasonally capture varying, canopied, shaded and non-shaded, geosampled, georeferenced, prolific, *S. damnosum* s.l., riverine, larval habitat, leaf structures without the necessity for extensive calibration.

Rapid Eye^{TM} RedEye estimates of above seasonall ground carbon storage, including woody stems and plant litter could improve predictions of prolific, geosampled, shade, vegetated, *S. damnosum* s.l., canopied, larval habitat, Rapid Eye^{TM} imaged, riverine, ecosystem processes. For example, increases in the dry litter fraction have been used in tropical forests and grasslands to estimate environmental stresses [131]. The nutrient limitations of NPP and carbon storage in humid tropical riverine ecosystems may be exploited by combining dry residue indices [139]. Carbon absorption features such as NPV in an explanatorial, shade, vegetated, georeferenced *S. damnosum* s.l, prolific, canopied, geosampled, riverine, larval habitat may be remotely interpretable between 2000 and 2200 nm, for example, which may be algorithmically further remotely validated in a spectroscopic, decomposed, 5m resolution, canopied endmember, dataset. In sparse, semiarid, riverine environments, the low canopy cover permits direct detection of plant litter, making it easier to estimate stand characteristics, canopy disturbance conditions, eco-physiological state and biogeochemical processes [14]. The spatial patterns of dry plant residues in shriver shrub and grassland LULC specified may be employed to provide 5m, Rapid Eye^{TM}, geo-spectrally interpolatable, explanatorial, robust, graphical indicators of desertification of a shade, canopied, seasonally prolific, *S. damnosum s.l* larval habitat, canopy vegetated, larval habitats, geosampled in an African riverine environment.

Measures of structural carbon (cellulose, lignin, and other carbon compounds) provide a chlorophyll-independent estimate canopy of biomass [4,115,127]. Mapping concentrations of canopy lignin may be vital for parsimonious 5m, Red Edge, NDVI, sub-mixel, decomposition and subsequent geo-spectral explanatory interpolation of a Rapid Eye^{TM} reference endmember, biosignature for identifying unknown, unsampled, prolific, *S. damnosum* s.l., shade, canopied, riverine, larval habitats. However, the ability to obtain an independent measure of canopy lignin in spectroscopic5m data may be limited because of lignin's spectral similarity to cellulose and other cell wall materials [13]. Using samples of ground dry leaves, Kokaly and Clark [140] found smaller errors in time series, explanatorily, regressed reflectance, emissivity transmittance estimates of lignin than in regressed estimates of cellulose, although cellulose comprised a substantially larger fraction of dry weight. Ecologists or experimenters have had difficulty studying fresh and dry leaves specifically retrieving separate lignin and cellulose concentrations [141], but better results have been claimed for lumped estimates of dry plant canopy matter. Retrievals of dry plant canopy residues in the Rapid Eye^{TM}5m spectrum may be measurable from high-fidelity, full-range imaging spectrometric VIs.

The quantity of dry plant material is a direct indicator of carbon production, turnover, and decomposition (heterotrophic respiration) [142]. Asner et al. [131] found that aboveground stocks of dry and live biomass were tightly coupled to soil, organic, carbon pools across a wide range of heterogenous riverine ecosystems. Because sub-mixel decomposition of surface litter is at least partially geospatially and temporally correlated with soil decomposition and respiration, measures of non-green (i.e.,NPV) plant material, soil carbon efflux in a canopied, endmember georeferencable, shade, vegetated, *S. damnosum* s.l. riverine-based, 5m, Rapid Eye^{TM} geosampled, larval habitat, RedEdge NDVI eco-epidemiological, forecasting, risk model may be easily constrained.

We then generated a kriged smoothed map which displayed the geospatial patterns of all productive *S. damnosum s.l.* larval habitats at the eco-epidemiological riverine study site in northern Uganda based on the explanatorily interpolated, decomposed, canopy endmember, reference, 5m, Rapid Eye^{TM}, explanatorily interpolatable, biosignature-related, explanatorial predictor variables generated from the inverted model and the unmixing algorithms. We found that the interpolated, sub-mixel index reflectance in the RedEdge region was sensitive to LULC variation at the study site.Specifically, the interpolation of the unmixed endmember,interpolated leaf pigment content was relatively sensitive to the riverine, larval, habitat canopied, leaf structure LULC variations (e.g twigs in hanging immersed vegetation). We also quantified the degree of geospectral interference between the larval habitat canopy pigments which occured within the leaf tissue. Leaf surface reflectance appeared to be the most important factor in the interpolated decomposed, endmembers. By developing a new spectral index the effect of differences in leaf surface reflectance and the correlations with chlorophyll content may be significantly improved for identifying unsampled, unknown, prolific, georeferencable, *S. damnosum* s.l., riverine, larval habitats at 5m resolution. The residualized, canopy endmember, explanatorily, geospectrally interpolated, eco-epidemiological, risk forecasts from a stochastic interpolator could be applied in larger scale remote-sensing studies without extensive calibration.

The semivariogram georeferencable, *S. damnosum* s.l., riverine, larval habitat, eco-epidemiological, time series, risk analysis made implicit use of the ergodicity hypothesis. The ergodicity hypothesis is one of the foundations of current stochastic theories of groundwater flow and contaminant transport [4]. The ergodic hypothesis is often assumed in the statistical analysis of computational physics [2]. The ecologist or expeimenter could thus assume that the average of a process photosynthetic and NPV covariate, parameter estimator, coefficient, reflectance, emissivity transmittance parameter estimator over time and the average over the statistical ensemble are similar. Unfortunately ,this assumption that the ergodicity hypotheses is as good to simulate a system over a long time as it is to make many independent realizations of the same system may not always be correct in a seasoanlly, decomposed, medium resolution, interpolated, NDVI, endmember, biosignature-related, *S. damnosum* s.l., riverine, larval habitat due to intense seasonal canopy changes.

An updated discussion on physical and mathematical aspects of the ergodic hypothesis in classical equilibrium statistical mechanics may be alternatively presented in a seasonal, *S. damnosum* s.l. larval habitat regression-related paridym. Then a practical attitude for the justification of the microcanonical ensemble may be indicated in the foreasted residuals representing, explanatorily interpolated, unknown, unsampled prolific habitats. It may be remarked however that the diffculty in proving the ergodic hypothesis should be expected, since in the foreacasts the central concern of ergodic theory would the behavior of a dynamical system when it is allowed to run for a long time. The first result in this direction is the Poincaré recurrence theorem, which claims that almost all points in any subset of the phase space eventually revisit the set. As mentioned this may not be true for robustly interpolating, decomposed, Red Edge, NDVI, unmixed, endmember georeferencable, shade, vegetated, *S. damnosum s.l.* riverine-based, 5m, Rapid Eye™ geosampled, larval habitat, biosignature components due to geo-spatiotemporal canopy radiance variations.

More precise information is provided by various ergodic theorems which assert that, under certain conditions, the time average of a function along the trajectories exists almost everywhere and is related to the space average. One of the most important theorems is that of Birkhoff (1931) who assert the existence of a time average along each trajectory (exiting canopy radiance from a geo-spatiotemporally, geosampled productive, riverine, *S. damnosum* s.l. georefernced, larval habitat). For the special class of ergodic systems, this time average is the same for almost all initial points: statistically speaking, the system that evolves for a long time "forgets" its initial state [27]. Stronger properties, such as mixing and equidistribution, have also been extensively studied. The problem of metric classification of systems is another important part of the abstract ergodic theory which may be applicable for robustly parsimonioulsy, explanatorily interpolating, decomposed Rapid Eye ™ 5m, canopied, seasonally productive, riverine, larval habitats. An outstanding role in ergodic theory and its applications to stochastic processes such an an explanatorily interpolated, *S. damnosum* s.l. riverine larval habitat , eco-epidemiological, forecasting, canopy biosignature, endmember risk analyses modes may be played by the various notions of entropy for dynamical African riverine eosystems.

The concepts of ergodicity and the ergodic hypothesis are central to applications of ergodic theory. The underlying idea is that for certain systems (prolific, geosampled, *S. damnosum* s.l., shade, canopied, georeferencable, larval habitat) the time average of their geospectral decomposition properties may be equal to the average over the entire eco-epidemiological, interventional study site in ecogeographic, probabilistic, regression space. Thus geometry, methods of ergodic theory may be used to study the geodesic flow on Riemannian manifolds, starting with the results of Eberhard Hopf for Riemann surfaces of negative curvature in an empirical datset of geospectral, geo-spatial, explanatorial, *S. damnosum* s.l.-related seasonally prolific larval habitat Markov chains. Ergodic theory has fruitful connections with harmonic analysis, Lie theory (representation theory, lattices in algebraic groups), and number theory (the theory of diophantine approximations, L-functions) [115,130] may be applicable to geo-spatiotemporally, cartographically delineating regression estimates rendered from a wavelenght transmittance, eco-epidemiological, emissivity vulnerbility-oriented,unmixed, risk model.

In addition to the constant $E\left[Z(S)\right]$ and the assumption of intrinsic stationarity, ergodicity is a necessary third hypothesis to estimate the empirical semivariance [27]. We generated a spatial random field (SRF) *Z(S)* so as to have have an emprical dataset of time series, geosampled, robust, *S. damnosum* s.l. larval habitat geospatial forecasted measurements Z_i whose sample mean was estimated by $\overline{Z}$. The hypothesis of ergodicity then dictated that $\overline{Z} = E\left[Z(S)\right]$. In general, an SRF *Z(S)* is characterized as ergodic if the statistical moments of its realizations coincide with the corresponding ones of the SRF [27]. In geospatial eco-epidemiological risk analysis you are often interested in the first two statistical moments, and consequently a more relaxed ergodicity assumption is made only for them [130]. See Christakos (1992, section 2.12) for the use of the ergodicity hypothesis in SRF, and Cressie (1993, p. 57) for a more detailed discussion of ergodicity.

The semivariogram analysis made implicit use of the ergodicity hypothesis in the riverine larval habitat model. The VARIOGRAM procedure worked with the residual centered values $V(S_i) = v_i = z_i - \overline{Z}$, $i = 1,\ldots,n,$ where it is assumed that the sample mean $\overline{Z}$ was the constant expected value $E\left[Z(S)\right]$ of $Z(S)$. This was equivalent to using the original values, since $V(S_i) - V(S_j) = Z(S_i) - Z(S_j)$, which revealed that the optimal property of the semivariance could be parsimonioulsy tabulated by filtering out the mean. PROC VARIOGRAM uses to compute the empirical classical $\hat{\gamma} = (h)$ and robust $\hat{\gamma} = (h)$ semivariances (www.sas.edu).

The VARIOGRAM procedure worked with the residually centered, shade canopied, geospectral, interpolated, productive, *S. damnosum* s.l. riverine larval habitat geosampled values (i.e., $V(S_i) = v_i = z_i - Z, i = 1,\ldots,n$) where it was assumed that the sample mean $\overline{Z}$ was the constant expected value $E\left[Z(S)\right]$ of $Z(S)$. This was equivalent to employing the original geo-spatiotemporally, geosampled, values, since $V(S_i) - V(S_j) = Z(S_i) - Z(S_j)$ showed the property of the semivariance to filter out the mean. Additionally, since the random field was ergodic, the time series regressors corresponded to the variance in the canopy reflectance model.

We defined a practical range and defined the distance at which 95% of the sill was reached for a asymptotic variogram. A Voroni decomposition error matrix then assessed the accuracy of the unmixing systematics as well as the proper selection of the explanatorial, shade, canopied, endmember, eco-epidemiological,covariate parameter estimator,reflectance, emissivity, transmittance coefficients of the decomposed,*S. damnosum* s.l.,autoregressive, riverine, larval habitat, explanatorial, operationial eco-epidemiological, biosignature-related, risk model. The model output revealed that the kriged sub-mixel, riverine, larval habitat, biosignature, derivative spectra revealed the estimates were within normal statistical thresholds. A field verification exercise revealed an accuracy of 72%.

Spectral models and indices are being developed to improve vegetation canopied LULC, sensitivity by accounting for atmosphere and soil effects. Soil properties have spectral features that can be detected using spectroscopy [143]. Baumgardner et al. [144] identified five basic spectral shapes related to organic matter content, iron oxide content, and soil texture. Using factor analysis, Price [145] and Huete and Escadafal [146] found four basic combinations of soil properties. In general, soils, like plants, have only a few recognizable narrow absorption features. Soils typically have broad, shallow absorption features related to iron oxides and organic matter at wavelengths between 400 and 2500nm [2,115].Reflectance decreases as organic matter increases [17].

In soils with low levels of organic matter, the curve between 400 and 1000nm is convex; in soils with high levels of organic matter, it is concave [144]. Ferric or ferrous iron causes absorptions in the visible and NIR spectra, particularly around 860nm in moderate resolution data [4,143]. In contrast to organic matter and iron oxides, various clay minerals like those found around prolific, canopy, shaded, *S. damnosum* s.l., larval habitats, geosampled in African riverine landscapes (e.g., montmorillonite, kaolinite, illite, smectite) and carbonates may have distinctive, narrow-band, absorption levels. Nonetheless, it may be not simple to quantitatively remotely qualitatively regress these interpolated, canopied, soil properties. Understanding alteration mineral assemblages may reveal specific geomorphological, geo-spatiotemporal, terrain-related, patterns at 5m associated with low canopied, shade, vegetated productive geosampled, riverine larval habitats.

Typically, a first step to detecting soil properties is to mask vegetated mixels. Palacios-Orueta and Ustin [147], Palacios-Orueta and colleagues [148], Hill and Schutt [149], and Leone and Sommer [150] have used vegetation masks, landform classes, and other hierarchical segregation methods to distinguish soil from vegetation. Palacios-Orueta et al. [148] employed a hierarchical analysis to seasonally quantify soil organic matter and iron oxide concentrations from two valleys, performing a two-step singular value decomposition that classified the soils, first by their valley of origin and second by their concentrations of organic matter and iron oxides. The combined data may be employed to produce a robust, endmember, prolific, shade, canopied, *S. damnosum* s.l. riverine, larval habitat, RedEdge, 5m, resolution, canopy, endmember maps. Despite complex topography and riverine landscape heterogeneity, the results of a RapidEye^{TM} soil survey map reveal a range of distinct measurements for robust, geospectral interpolation of explanatorily decomposed 5m, Rapid Eye^{TM} imaged, prolific, *S. damnosum* s.l. larval habitat endmembers for targeting, prolific, unknown, unsampled, shade, canopied habitats in African riverine environments.

When vegetative LULC cover is sparse, soil is prominent and canopy visible reflectances will contain a strong backscatter component. This component may be nonexistent toward maturity as the canopy cover may mask the bare soil of an 5m,Rapid Eye^{TM} imaged, georeferenced, geosampled, prolific, shade, canopied, *S. damnosum* s.l., riverine, larval habitats. The soil effect also may disappear whenthe canopy is viewed at an oblique angle, since the sides of the canopy dominate the observed spot and obscure the underlying surface. As well, the soil backscatter effect may be less pronounced in georeferenced, productive, explanatorial, riverine, larval habitat's, NIR, canopy reflectance. Variations in the distribution of visible and NIR BRF values decrease as canopy biomass increases [115].

RapidEye^{TM} nadir reflectance values of non-shaded and shaded, georeferncable, geosampled, riverine *S. damnosum* s.l., riverine, larval habitat vegetative LULC canopies in ArcGIS may be a function of solar zenith angle (0s) and may vary with wavelength and soil substrate. Both factors must be considered when qualitatively, remotely, regressively quantitating, geosampled, prolific, riverine, larval habitat geo-spatiotemporal, canopy trends as shown by the results reported by Jacob [1]. We determined that the surface reflectance in the decomposed, georeferenced, geosampled, riverine, larval habitat, shaded, vegetated LULC canopy was classified as non-Lambertian. Functions of wavelength, illumination and viewing directions, soil moisture content, particle size, organic matter content, soil mineralogy, and surface roughness determine if Lambertian assumptions are violated [115].

Solutions for general non-Lambertian scenes have only been pursued recently. For example, the rank constraint of radiance tensor as a discrepancy indicator may measure canopied correspondences in georeferenced, prolific, shade canopied, immature, *Similum,* larval habitats geosampled in African riverine environments. This reflectance sensitive method may handle highly seasonally heterogeneous canopy leaf specularity radiance reflected from a prolific, georeferenced, riverine, larval habitat. Shapes from shading and photometric stereo methods make use of such information to recover 3D shapes. These methods usually assume that surface reflectance properties are known. Much work on shape from shading is based on the non-lambertian and Lambertain model which both use a single view, or assumes simple lighting conditions [150-153].

The solutions to specular, ArcGIS, reflection models object solution relies on strong regularization. However, remote endmember, explanatorial, geospectral quantization exercises performed on an empirical dataset of geosampled, *S. damnosum* s.l., georeferenced, productive canopied, riverine, larval habitat, topographic, reflectance, emissivity, transmittance regressors may be perturbed by atmospheric scattering of sun light which tends to smooth the angular dependence of non-Lambertian surface reflectances, an effect that is not present in the case of Lambertain surfaces. Regardless, this illuminary effect may be tabulated to evaluate the validity of a Lambertain assumption for robustly explanatorily regressing, reflectance unmixed, covariate , parameter estimator coefficient values as rendered from an geospectral unmixing algorithm for optimally decomposing an eco-epidemiological, geo-spatiotemporal, geosampled, prolific, shade canopied, *S. damnosum* s.l., riverine, larval habitat, capture point, ArcGIS polygon.

Within the backscattering region, however, the use of the non-Lambertian assumption can result in a considerable error in geo-spatiotemporally derived surface reflectance of a geosampled, *S. damnosum* s.l., riverine, larval habitat. Accuracy of satellite data deteriorates with increasing solar zenith angle [2]. The angular distribution of the canopy surface reflectance derived from 5m Rapid Eye^{TM} remote measurements may be smoother than that at the surface. The effect of surface non-Lambertianity on RedEdge, NDVI, decomposed, biosignature-oriented, photosynthetic, covariate, parameter estimator, reflectance, emissivity transmittance, coefficient values is presently unknown. Since the effect would be similar in the geosampled, *S. damnosum* s.l., riverine, larval habitat, visible and NIR part of the solar spectrum for remotely, robustly, regressively, qualitatively, quantitating canopy, vegetation-related, LULC reflux treated in the decomposition algorithms, the procedure may be canceled in deriving the vegetation index. The effect of the diffuse skylight on canopy surface reflectance measurements at ground level for the riverine geosampled riverine larval habitat may be then discussed.

In general, single view shape from shading problem is ill-conditioned, more so for non-Lambertian objects with unknown reflectance. Lambertian reflectance is the property that defines an ideal "matter" or diffusely reflecting surface [4]. In computer graphics, Lambertian reflection is often used as a model for diffuse reflection. This technique causes all closed polygons (such as a triangle within a 3D mesh) to reflect light equally in all directions when rendered. In effect, a point rotated around its normal vector will not change the way it reflects light. However, the point will change the way it reflects light if it is tilted away from its initial normal vector since the area is illuminated by a smaller fraction of the incident canopy radiation. The reflection is calculated by taking the dot product of the surface's normal vector, **N**, and a normalized light-direction vector, **L** pointing from the surface to the light source.

The dot product can be defined for two vectors **X** and **Y** by $X.Y = |X||Y|Cos\theta$ where θ is the angle between the vectors and $|X|$ is the norm [27]. It follows immediately that X.Y = 0 if X is perpendicular to Y. The dot product therefore has the geometric interpretation as the length of the projection of X onto the unit vector $\widehat{Y}$ when the two vectors are placed so that their tails coincide.

By writing $A_x = ACos\theta_A\ B_x = B\cos\theta_B \quad A_y = ASin\theta_A\ B_y = BSin\theta_B$ it follows that a geo-spatitemporally, geosampled, canopy endmember decomposed *S. damnosum* s.l. larval habitat yields

$$A.B = AB\cos(\theta_A - \theta_B) = AB(Cos\theta_A\ Cos\theta_{\mathrm{B}} + Sin\theta_A\ Sin\theta_{\mathrm{B}})$$

$$= ACos\theta_A\ BCos\theta_{\mathrm{B}} + ASin\theta_A\ BSin\theta_{\mathrm{B}} = A_xB_x + A_yB_y$$

So, in general, $X.Y = \sum_{i=1}^{n} x_i y_i = x_1y_1 + \ldots + x_ny_n$ This may be written very succinctly using Einstein summation notation as $X.Y = x_iy_i$ The dot product is implemented in the Wolfram Language as Dot [*a*, *b*], or simply by using a period, *a*. *b*.(http://www.wolfram.com/programming-cloud). The dot product is commutative $X.Y = Y.X$, and distributive $X.(Y+Z) = Y.X + X.Z$ [130]. The associative property is meaningless for the dot product in a riverine habitat eco-epidemiological, forecasting, risk model because *(a.b).c* is may not be defined since *a.b* is a scalar and therefore cannot itself be dotted. However, the forecasts would not satisfy the property $(rX).Y = r(X.Y)$ for **r** a scalar. The derivative of a dot product of vectors is $\frac{d}{dt}[r_1(t)\cdot r_2(t)] = r_1(t).\frac{dr_2}{dt} + \frac{dr_1}{dt}r_2(t)$ [13]. The dot product may be found to be spectrally invariant under rotations $A'.B' = A'_i\,B_i' = a_{ij}A_ja_{ik}B_K = (a_{ij}a_{ik})A_jB_K = \delta_{jk}A_jB_K = A_jB_j = A.B$, in a riverine habitat model where Einstein summation has been used [1]. The dot product is also called the scalar product and inner product. In the latter context, it is usually written $\langle a,b\rangle$. The dot product is also defined for tensors *A* and *B* by $A.B \equiv A^{\alpha}B_{\alpha}$ So for four riverine larval habitat vectors $\underset{\mu}{a}$ and $\underset{\mu}{b}$, it is defined by $a_\mu.b_\mu = a_\mu b^\mu = a^\circ b^\circ - a^1b^1 - a^2b^2 - a^3b^3 = a^\circ b^\circ - a.b$ where *a.b* is the usual 3-D dot product.

A normalized light-direction vector number may then be multiplied by the color of the surface and the intensity of the light hitting the canopied riverine *S. damnosum* s.l. larval habitat shaded surface: $I_D = L.NCI_L$, where I_D would be the intensity of the diffusely reflected light (surface brightness), *C* is the color and I_L $L.N = |N||L|$ is the intensity of the incoming light. Because $L.N = |N||L|Cos\alpha = Cos\alpha$, where α is the angle between the direction of the two vectors, the intensity in the riverine habitat, eco-epidemiological, reflectance, emissivity transmittance, risk model maybe the highest if the normal vector points in the same direction as the light vector ($Cos(0) = 1$), where the habitat canopied surface would be perpendicular to the direction of the light, and the lowest if the normal vector is perpendicular to the light vector [i.e., $Cos\left(\frac{\pi}{2}\right) = 0$]. Lambertian reflection from polished surfaces are typically accompanied by specular reflection (gloss), where the surface luminance is highest when the observer is situated at the perfect reflection direction (i.e. where the direction of the reflected light is a reflection of the direction of the incident light in the surface), and falls off sharply [27]. This may be simulated in computer graphics with various specular reflection, geosampled, *S. damnsoum* s.l., larval habitat, canopy, endmember models.

The Phong reflection model may be also constructed, to remotely qualitativley regressively quantitate the intensity of the specular highlight in a geo-spatiotemporally, geosampled, riverine, *S. damnosum* s.l., georefernced, larval habitat which may be calculated as: $k_{Spec} = \|R\|\|V\|Cos^n\beta = (\hat{R}.\hat{V})^n$ where *R* is the mirror reflection of ethe light vector larval habitat canopy surface and V is the viewpoint vector. In the Blinn-Phong model the intensity of a specular, riverine, larval, habitat canopy highlight may be calculated as: $k_{Spec} = \|N\|\|H\|Cos^n\beta = (\hat{N}.\hat{H})^n$ where *N* is the smooth surface normal and *H* is the half-angle direction (i.e., the direction vector midway between *L*, the vector to the light, and *V*, the viewpoint vector). The number *n* is called the Phong exponent, and is a user-chosen value that controls the apparent smoothness of the surface [4]. These equations may regressively quantiate the distribution of microfacet normals which may find that a Rapid Eye ™ geospectrally decomposed, RedEdge, NDVI, interpolated biosignature of a riverine larval habitat is approximately Gaussian distribution (for large η), or approximately Pearson type II distribution, for qualiatively quantizing corresponding illumination angles in a geosampled, *S. damnsoum* s.l., larval habitat, canopy geolocation.

Another similar formula, but calculated differently for remotely explanatorily qualitatively quantiating geo-spectrally decomposable, *S. damnsoum* s.l., larval habitat, stochastic/deterministic, explanatorily interpolatable, (i.e., $k = (\vec{L}\cdot\vec{R})^n = [\vec{L}\cdot(\vec{E} - 2\vec{N}(\vec{N}\cdot\vec{E}))]^n,$) biosignatures is where R is an eye reflection vector, E is an eye vector (view vector), N is surface normal vector and L is a light vector. All vectors may then be normalized $(\|\vec{E}\| = \|\vec{N}\| = 1)$. For example, suppose a georeferencable, seasonal prolific canopied, *S. damnosum* s.l., riverine, larval habitat, reflectance, model, regressive equation is $\vec{N} = \{0;1;0\};\ \vec{E} = \{\frac{\sqrt{3}}{2};\frac{1}{2};0\};\ \vec{L} = \{-06;0.8;0\};\ n = 3$ then: $k = [\vec{L}\cdot(\vec{E} - 2\vec{N}(\vec{N}\cdot\vec{E}))]^n = [\vec{L}\cdot(\vec{E} - 2\vec{N}(0\cdot\frac{\sqrt{3}}{2} + 1\cdot 0.5 + 0\cdot 0))]^3 =$ This model forecasts may determine geolocations of interpolated unsampled, unknown, prolific, habitats by employing

$$= \left[\vec{L}.\left(\vec{E} - \vec{N}\right)\right]^3 = \left[\vec{L}.\left(\left\{\frac{\sqrt{3}}{2} - 0; \frac{1}{2} - 1; 0 - 0\right\}\right)\right]^3 = \left[-0.6.\frac{\sqrt{3}}{2} + 0.8.(-0.5) + 0.0\right]^3 =$$

$$(-0.5196 - 0.4)^3 = 0.9196^3 = 0.777$$

The approximate formula in the quantization decomposition procedure then would then be

$$k = (\vec{N}\cdot\vec{H})^n = (\vec{N}\cdot((\vec{L} + \vec{E})/2))^n = (\vec{N}\cdot((\{-06 + \frac{\sqrt{3}}{2}; 08 + 05; 0 + 0\})/2))^3$$

$$= (\vec{N}\cdot((\{0266;1.3;0\})/2))^3 = (\vec{N}\cdot(\{0.133;0.65;0\}))^3 = (0\cdot 0.133 + 1\cdot 065 + 0)^3 = 065^3 = 0274625.$$

If vector **H** is then normalized in the *S. damnosums*.l., larval habitat, eco-epidemiological, geospectral, risk model

then $\frac{\vec{H}\{0133; 0.65; 0\}}{\backslash\vec{H}\backslash} = \frac{\vec{H}\{0133; 0.65; 0\}}{\sqrt{0133^2 + 065^2}} =$ and then $\frac{\vec{H}\{0133; 0.65; 0\}}{0.668} = \{020048; 0.979701; 0\}$,

$k = (\vec{N} \cdot \vec{H})^n = (0 \cdot 0.2 + 1 \cdot 0.9797 + 0 \cdot 0)^3 = 0979701^3 = 0940332.$

Soils composed of low-absorption particles, such as quartz sand, can scatter light strongly in the forward scatter direction (direction away from light source in the principal plane) with a maximum BRDF value occurring at a view zenith angle (0v) greater than the illumination zenith angle [154]. Therefore, geosampled, riverine, *S. damnosum* s.l., larval habitat, Rapid Eye™, 5 m, vegetative, canopy reflectance may be more pronounced in ArcGIS, in the backscatter direction (e.g., direction back toward the light source in the principal plane) than in the forward scatter direction from soils of highly absorbing particles, such as clay soils, since shadows will dominate in the forward scatter direction. The proportion of shadows increases as the sensor moves away from nadir to oblique views in the forward scatter position [4]. In contrast, few shadows would be present in low-absorption sand particles of a geosampled, prolific, shaded, georeferenced, riverine, *S. damnosum* s.l., larval habitat, since 5m canopy radiation would be multiply scattered or transmitted.

Spectral properties of the soil, depends on soil constituents such as soil organic matter, iron oxides and soil water, and soil roughness such as particle and aggregate size [155]. High soil water and high organic matter contents show lower reflectance while soils with low water content and smooth surface tend to be brighter [156]. In the presence of iron oxides soil reflectance is higher in the red portion of medium resolution endmember spectrum [152]. Crop residues on soil surface also causes variation in reflectance compared to bare soil and partial canopy cover [157-159]. Spectral reflectance emittance properties of georefernced, geosampled, *S. damnosum* s.l., riverive, habitat canopy covered soils may be thus employed to extensively predict, time series dependent, ecohydrological explanatory variables, such as percent vegetation cover, plant biomass, green leaf area index and other LULC, biophysical characteristics.

The soil-adjusted vegetation index (SAVI) was developed to minimize soil influences on canopy spectra by incorporating a soil adjustment factor L into the denominator of the NDVI equation. L varies with the reflectance characteristics of soil (i.e. color and brightness) [151]. The L factor chosen depends on the density of the vegetation. For very low vegetation L factor can be taken as 1.0 while for intermediate; it can be taken as 0.5 and for high density 0.25 [2]. The best L value is to select where the difference between SAVI values for dark and light soil is minimal. For L=0, SAVI equals NDVI [4]. Mathematically SAVI is defined as, SAVI = {(NIR - RED) / (NIR+RED+ L)} * (1+L) [152]. For optimal adjustment of the soil effect, the L factor should vary inversely with the amount of the shaded, canopy vegetation-related LULC and soil moisture present at a georeferenced, geosampled, riverine, *S. damnosum* s.l., shade canopied, geo-spatiotemporal, larval habitat, eco-epidemiological study site. Further, a modified SAVI (MSAVI) that replaces the constant L in the SAVI equation with a variable L function may also be constructed for predicting, seasonally prolific, vegetated, shade, canopied, unknown, unsampled, *S. damnosum* s.l., riverine larval habitats. The L function may be derived by induction or by employing the product of the NDVI and weighted difference vegetation index (WDVI).The WDVI is ascertained as a weighted difference between the measured NIR and red reflectance's assuming that the ratio of NIR and red reflectance's is constant (i.e., the weighting factor) [153].

Results based on canopy, SAVI, endmember, shade, vegetated, canopied, *S. damnosum* s.l., larval habitat may thus be explanatorily decomposed and geospectrally robustly interpolated. The VI endmember biosignature may be shown to increase the dynamic range of the 5m resolution Rapid Eye^{TM}vegetation signal while minimizing the soil background LULC influences, resulting in greater canopy vegetation sensitivity for robustly, remotely, regressively targeting prolific, *S. damnosum* s.l., seasonal, georeferenced, shade, canopied, larval habitats. To understand how VIs are designed, it is essential to know some concepts related to influence of soil use of the soil line and vegetation isoline [40,160, 161]. Since soil-line vegetation indices, use the information of soil line in NIR-Red reflectance to reduce the effect of the soil on canopy habitat LULC, wavelenght of other indices such as reflectance other Optimized Soil Adjusted Vegetative Index (OSAVI) and Transformed Soil Adjusted Vegetative Index (TSAVI)) generated from RapidEye^{TM} data may be useful also for quantitatively, remotely, regressively, targeting, geospectrally interpolatable, seasonal, vegetated, shade, canopied, *S. damnsoum* s.l., larval habitats, geo-spatiotemporally-geosampled, in African riverine environments.

Soil vegetation indexes are relatively insensitive to ecosystems with the low biomass characteristic of semi-arid systems (between 0 and 60 megagrams carbon per hectare [ha]), because of systems' low leaf biomass and discontinuous canopies [162]. Estimates of dry plant residues using the RedEdge Rapid Eye^{TM} 5m spectrum may help surmount these difficulties. Although arid and semi-arid African riverine ecosystems do not sequester large masses of carbon, and have low fluxes on a per-area basis, these ecosystems are the most abundant terrestrial landscapes, which are also highly sensitive to climate perturbations [163].Thus, an explanatorily interpolatable, decomposed, RedEdge, NDVI Rapid Eye^{TM} canopied biosignature focusing on carbon fluctuations may regressively target seasonally productive, shade, vegetated, *S. damnosum* s.l. riverine larval habitats and their photosynthetic and NPV seasonal, georeferencable covariate parameter estimator, reflectance, emissivity transmittance coefficients with higher efficiency than a non-carbon oriented biosignature.

Intrinsic covariance matrix estimation may provide a sample of *n* independent explanatorial, *S. damnosums*.l. riverine, larval habitat endmember covariance observations $x_1,.., x_n$ of a *p*-dimensional, zero-mean, Gaussian, explanatorial, random variable X with covariance R, where the MLE of R may be given by $\hat{R} = \frac{1}{n}\sum_{i=1}^{n} x_i x_i^{\mathrm{T}}$. The parameter R belongs to the set of positive-definite matrices, which is a Riemannian manifold, not a vector space, hence, the usual vector-space notions of expectation, (i.e. "E[R^]"), where the estimator bias must be generalized to manifolds to make sense of the problem of covariance matrix estimation [130]. This can be robustly conducted by defining the expectation of an manifold-valued, *S. damnosums*.l., riverine, larval habitat, georeferenced, canopied, endmember, covariance estimator R^ with respect to the manifold-valued point R

as $\mathrm{E}_{\mathbf{R}}[\hat{R}] \overset{\text{def}}{=} \exp_{\mathbf{R}} \mathrm{E}\left[\exp_{\mathbf{R}}^{-1} \hat{R}\right]$ where

$\exp_{\mathbf{R}}(\hat{R}) = \mathbf{R}^{\frac{1}{2}} \exp\left(\mathbf{R}^{-\frac{1}{2}} \hat{R} \mathbf{R}^{-\frac{1}{2}}\right) \mathbf{R}^{\frac{1}{2}}$ and

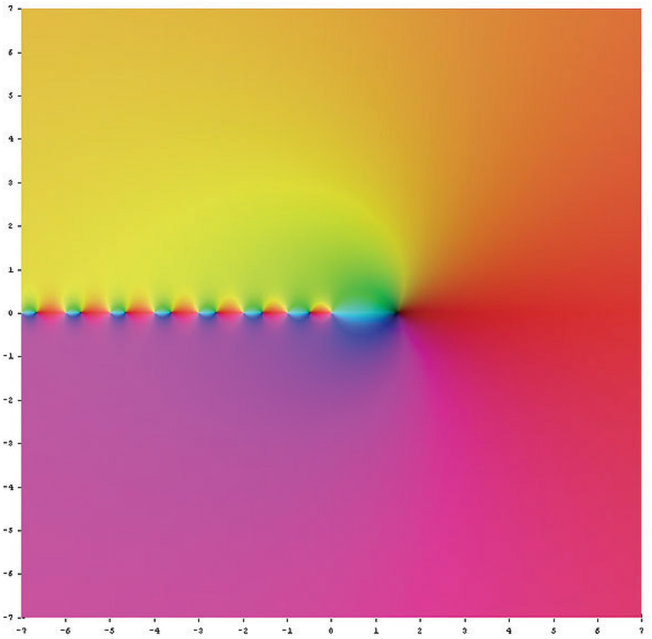

Figure 21: Digamma function *ψ*(*s*) in the complex plane where color of a sub-mixel decomposed prolific, georferenced *S. damnosum* s.l. riverine larval habitat point *s* encodes the value of *ψ*(*s*).

$\exp_{\mathbf{R}}^{-1}(\hat{R}) = \mathbf{R}^{\frac{1}{2}}\left(\log \mathbf{R}^{-\frac{1}{2}}\hat{R}\mathbf{R}^{-\frac{1}{2}}\right)\mathbf{R}^{\frac{1}{2}}$ are the exponential, explanatorial, riverine, larval habitat, canopy endmember map and inverse exponential map, respectively. The "exp" and "log" in these maps may denote the ordinary matrix exponential and matrix logarithm, thereby allowing E[·] to be the ordinary expectation operator defined on a vector space (i.e., the tangent space of the manifold).

Bias of the sample explanatorial, *S. damnosums*.l. riverine, larval habitat, canopy endmember, covariance matrix can thereafter be based on the intrinsic bias vector field of the endmember time series estimator R^ which could be defined to be $\mathbf{B}(\hat{R}) = \exp_{\mathbf{R}}^{-1} \mathrm{E}_{\mathbf{R}}\left[\hat{R}\right] = \mathrm{E}\left[\exp_{\mathbf{R}}^{-1}\hat{R}\right]$. The intrinsic estimator bias may then be given by $\exp_{\mathbf{R}} \mathbf{B}(\hat{R})$ in the estimation model. For complex Gaussian endmember, sub-mixel, explanatorial, random variables this bias vector field can be shown to equal $\mathbf{B}(\hat{R}) = -\beta(p,n)\mathbf{R}$ where $\beta(p,n) = \frac{1}{p}\left(p\log n + p - \psi(n-p+1) + (n-p+1)\psi(n-p+2) + \psi(n+1) - (n+1)\psi(n+2)\right)$ and ψ(·) are the digamma function. In mathematics, the digamma function is defined as the logarithmic derivative of the gamma function (Figure 21). In mathematics, the digamma function is defined as the logarithmic derivative of the gamma function.

The digamma function, often denoted also as $\psi_0(x)$, $\psi^0(x)$ or Ϝ (after the shape of the archaic Greek letter F digamma), is related to the harmonic numbers in that $\psi(n) = H_{n-1} - \gamma$ where H_n is the n-th harmonic number, and γ is the Euler-Mascheroni constant [130]. For half-integer values, it may be expressed as $\psi\left(n+\frac{1}{2}\right) = -\gamma - 2\ln 2 + \sum_{k=1}^{n}\frac{2}{2k-1}$. The Euler–Mascheroni constant (also called Euler's constant) is a mathematical constant recurring in analysis and number theory, usually denoted by the lowercase Greek letter gamma(γ) [25]. It is defined as the limiting difference between the harmonic series and the natural logarithm: $\gamma = \lim_{n\to\infty}\left(\sum_{k=1}^{n}\frac{1}{k} - \ln(n)\right) = \int_1^{\infty}\left(\frac{1}{x} - \frac{1}{x}\right)dx$. By so doing, the intrinsic bias of the sample covariance matrix may be equatable to $\exp_{\mathbf{R}} \mathbf{B}(\hat{R}) = e^{-\beta(p,n)}\mathbf{R}$ and the SCM would be asymptotically unbiased as $n \to \infty$. Similarly, the intrinsic inefficiency of the sample covariance matrix depends upon the Riemannian curvature of the space of positive-define matrices [164].

The curvature of a Riemannian prolific, georefernced, shade canopied, *S. damsnoum* s.l., larval habitat manifold can be described in various ways; the most standard one is the curvature tensor, given in terms of a Levi-Civita connection (or covariant differentiation) ∇ and Lie bracket $[\cdot,\cdot]$ by the following formula: $R(u,v)w = \nabla_u\nabla_v w - \nabla_v\nabla_u w - \nabla_{[u,v]}w$. Here $R(u,v)$ would be a linear transformation of the tangent space of the manifold in the larval habitat model; it would be linear in each argument. In Riemannian geometry, the Levi-Civita connection is a specific connection on the tangent bundle of a manifold. More specifically, it is the torsion-free metric connection, (i.e., the torsion-free connection on the tangent bundle) is an affine connection preserving a given pseudo-Riemannian metric. If $u = \partial/\partial x_i$ and $v = \partial/\partial x_j$ are coordinate vector, shaded, prolific, *S. damnosum*s.l., larval habitat, vegetated, riverine canopied fields then $[u,v] = 0$ could be simplified to $R(u,v)w = \nabla_u\nabla_v w - \nabla_v\nabla_u w$. The linear transformation $w \mapsto R(u,v)w$ is also called the curvature transformation or endomorp. The the curvature tensor measures noncommutativity of the covariant derivative [131].

The ability to remotely predict the geolocations of seasonally productive, shade, canopied, *S. damnosum s.l.* georeferenced, breeding sitesemploying an empirical dataset of geospectrally interpolatable, 5 m, Rapid Eye™, proxy, explanatorial, geo-spatiotemporal, biophysical variables such as those of a decomposed, dataset of NDVI, biosignature, sub-mixel, reflectance, emissivity transmittance predictor variables is extremely useful in mapping onchocerciasis transmission foci as the current African onchocerciasis control programs move into the era of cost effective elimination. For example, some of the countries endemic for onchocerciasis currently suffer from various levels of political and economic instability, making ground-based geolocation and verification of prolific aquatic sites difficult or impossible due to the high cost of the sub-meter resolution data. As such, employing cost effective RapidEye™ 5 m data (e.g., explanatorily interpolatable, eco-epidemiological, empirically decomposed dataset of RedEdge, NDVI, biosignature endmembers) can provide robust mapping of prolific *S. damnosum s.l.* habitat sites in eastern Democratic Republic of Congo and Southern Sudan, for example, both of which currently suffer from political instability and a lack of infrastructure. As such, the ability to predict and precisely, geolocate, prolific, riverine sites employing 5 m, RapidEye™, remote sensing, satellite data will provide specific geolocation-based data for explanatorial, forecast, eco-epidemiological, risk mapping the extent of transmission zones (e.g., hyperendemic, meosendemic) especially in areas around international borders where it may be difficult to establish cross border collaborations to conduct ground based studies and coordinated control initiatives.

Better discrimination of vegetation explanatorial, time series dependent, Rapid Eye^{TM} LULC classes may help further identify and predict shade canopied, geo-spatiotemporally, geosampled, prolific, *S. damnosum* s.l., riverine, larval habitats. By remotely measuring the many absorption features of the decomposed, Red Edge, NDVI, biosignature, geo-spectrometric, time series , empirical information may be associated to leaf pigments (e.g., canopy chorophyll) which then may be subsequently associated with seasonal, immature productivity. Because of its greater spectral dimensionality, decomposed and geospectrally interpolated, 5m, RapidEye^{TM},spectroscopic data can discriminate among shaded,prolific, geospectrally explanatorily interpolatable, *S. damnosum* s.l., larval habitat, canopy plant species more effectively than standard indices of vegetation and therefore has the potential to provide superior seasonal mapping capability in riverine –related, African ecosystems.

In conclusion, RedEdge, NDVI, decomposition, endmember, spectral analysis in ENVI revealed the resampling induced periodicity in a shaded, canopied, *S. damnosum* s.l., riverine, larval habitat in aRapidEye^{TM} scene. Remotely quantizable, probabilistically regressable changes in geo-spatiotemporally dependent, explanatorial, ecobiological data feature attributes of a geosampled, vegetative, riverine, *S. damnosum* s.l., larval habitat, surface canopy altered radiative interactions and therefore the amount of radiation reflected from the habitat surface received by the 5m remote sensing detector. For example, the reflectance spectra of the main plant functional types (i.e., hanging, and immersed vegetation), in our geosampled, riverine, larval habitat, RedEdge, NDVI endmember, reflectance model, revealed extensive, discontinous, reflectance and absorption features along the canopy gradient. Based on the canopy, 5m, Red Edge, biosignature, the leaf reflectance was greatest in the 5m spectral bands centered at between 1940nm, and 2500 nm, with indirect or secondary effects at between 400 nm and 700 nm. Unmixed, LULC topographic effects on bidirectional and hemispherical reflectance rendered from the riverine, larval, canopy, habitat surface were calculated with a SPA algorithm, 3-D radiative transfer equation and a geometric-optical model in ArcGIS. The final model employed a hemispherical integration of a BRDF which also provided an albedo estimate of the geosampled, riverine, larval habitat and its geospectrally associated, canopied, reflectance values. We were able to encompass the effects of the shaded habitat, LULC topography employing the BRDF and the surface albedo generated from the larval habitat canopy cover and its decomposed endmember, sub-mixel, reflectance, emissivity transmittance data feature attributes. The model output identified the fractional presence of each decomposed endmember of the *S. damnosum s.l.* habitat and its associated emissivity attributes based on proportions of sunlit canopy, sunlit background and shadow fraction. This data was then interpolated. The residuals revealed that 72% of the forecasted prolific habitat were found to contain *S. damnosum s.l.* larvae when field verified. The sensitivity of the test was 78.26 while the specifity was 100.

Acknowledgements

We would like to thank Oyet William Sam, District Vector Control officer/ NTDFP-Pader District Local Government, Alinda Peter, Vector Control Officer National Onchocerciasis Control Programme Ministry of Health Uganda and Munu Denis at The Carter Center Uganda Office. We would also like to thank Rockford K. Jalil at the College of Public Health, University of South Florida who helped describe the remote variables. This research was funded by the National Institute of Health Grant (Unnasch Thomas) University of South Florida.

References

1. Jacob B, Novak RJ, Toe L, Sanfo MS, Caliskan S, et al. (2013) Unbiasing a Stochastic End member Interpolator Using ENVI Object-Based Classifiers and Boolean Statistics for Forecasting Canopied Simuliumdamnosums. I. Larval Habitats in Burkina Faso. J Geophys Remote Sensing 2: 109.
2. Jensen JR (2005) Introductory digital image processing a remote sensing perspective. (3rdedn) Jacob BG, et al. (ed.), Prentice Hall series in geographic information science, Upper Saddle River, NJ Prentice Hall, 526.
3. Suplick-Ploense MR, Alshammary SF, Qian YL (2011). Spectral Reflectance Response of Three Turf grasses to Leaf Dehydration. Asian Journal of Plant Sciences, 10: 67-73.
4. Gamon JA, Surfus JS (1999) Assessing leaf pigment content and activity with a reflectometer. New Phytologist 143: 105-117.
5. Gallagher AC (2005) Detection of linear and cubic interpolation in JPEG compressed images. Proc 2nd Canadian Conf. Computer and Robot Vision, WashingtonDC 65-72.
6. Popescu AC, Farid H (2005) Exposing digital forgeries by detecting traces of resampling IEEE Trans. Inf. Forensics Security 53: 758-767.
7. Mahidan B, Saic S (2008) Blind authentication using periodic properties of interpolation, IEEE Trans. Inf. Forensics Security 3: 529-538.
8. Mahdian B, Saic S (2007) Detection of copy-move forgery using a method based on blur moment invariants. Forensic SciInt 171: 180-189.
9. Kitchner M (2008) Fast and reliable resampling detection by spectral analysis of fixed linear residu in Proc. 10th ACM Workshop Multimedia and Security, Pp.11-20.
10. Prasad, Ramakrishman (2006) On resampling detetction and its application to detect image tampering in P Proc IEEE Int. Conf. Multimedia and EXPO, pp.1325-1328.
11. Crosskey RW (1960) A taxonomic study of the larvae of West African Simuliidae (Diptera: Nematocera) with comments on the morphology of the larval blackfly head. J Bull British Museum (Natural History) Entomology, 10: 1-74.
12. Hazewinkel M (2001) Isomorphism. Encyclopedia of Mathematics, The European Mathematical Society: Springer.
13. KnyazikhinY, Martonchik JV, Myneni RB, Diner DJ, Running SW (1998) Synergistic algorithm for estimating vegetation canopy leaf area index and fraction of absorbed photosynthetically active radiation from MODIS and MISR data. Journal of Geophysical Research, 103: 257-276.
14. AmanA, Randriamanantena HP, Podaire A, Frouin R (1992) Upscale integration of normalized difference vegetation index: The problem of spatial heterogeneityIEEE Transactions on Geoscience and Remote Sensing, 30: 326-338.
15. Haboudane D, Miller JR, Tremblay N, Zarco-Tejada PJ, Dextraze L (2002) Integrated narrow-band vegetation indices for prediction of crop chlorophyll content for application to precision agriculture. Remote Sensing of the Environment 81: 416-426.
16. Hannan NP, Prince SU, Begue A (1997) Modelling vegetation primary production during HAPEX-Sahel using production efficiency and canopy conductance model formulations, 3: 651-675.
17. Bievre PD, Peiser HS (1992) Atomic Weight: The Name, Its History, Definition and Units. Pure and Applied Chemistry 64: 1535-1543.
18. McCree KJ (1972) The action spectrum, absorptance and quantum yield of photosynthesis in crop plants. Agriculture and For Meteo, 9: 191-216.
19. Chen P, Nicolas T, Wang JH, Philippe V, Huang WJ, et al. (2010) New index for crop canopy fresh biomass estimation. GuangPuXueYu GuangPu Fen Xi 30: 512-517.
20. Inada K (1977) Effects of leaf color and the light quality applied to leaf-developing period on the photosynthesis response spectra in crop plants. Proc. Crop Sci. Soc. Jpn 46: 37-44.
21. McCree KJ (1981) Photosynthetically active radiation. Encyclopedia of Plant Physiology 12: 41-55.
22. Clark JB, Lister G (1975) Photosynthetic action spectra of trees: Comparative photosynthetic action spectra of one deciduous and four coniferous tree species as related to photo respiration and pigment complements. Plant Physiology 55: 401-406.
23. Inada K (1976) Action spectra for photosynthesis in higher plants. Plant Cell Physiology 17: 355-365.

24. Mathews S (2006) Phytochrome-mediated development in land plants: red light sensing evolves to meet the challenges of changing light environments. Mol Ecol 15: 3483-3503.

25. Ballaré CL, Scopel AL, Sánchez RA (1989) Photomodulation of axis extension in sparse canopies : role of the stem in the perception of light-quality signals of stand density. Plant Physiol 89: 1324-1330.

26. Morgan DC, O'Brien T, Smith H (1980) Rapid photomodulation of stem extension in light-grownSinapis alba L. : Studies on kinetics, site of perception and photoreceptor. Planta 150: 95-101.

27. Gates DM (1980) Biophysical Ecology. New York, NY: Springer Advanced Texts in Life Sciences.

28. Hogewoning SW, Wientjes E, Douwstra P, Trouwborst G, van Ieperen W, et al. (2012) Photosynthetic quantum yield dynamics: from photosystems to leaves. Plant Cell 24: 1921-1935.

29. Jensen JR (1983) Biophysical remote sensing. Review article. Annals of the Associations of American Geographers 73: 111-132.

30. Rolfson D (2007) Collection of end members and their separability for spectral unmixing in rangeland applications. Masters thesis, University of Lethbridge.

31. Hobbs RJ (1990) Remote sensing of spatial and temporal dynamics of vegetation. Remote Sensing of Biosphere Functioning 79: 203-219.

32. Lambin EF (1996) Change detection at multiple temporal scales: seasonal and annual variations in landscape variables. American Society for Photogrammetry and Remote Sensing 62: 931-938.

33. DeFries RS, Hansen M, Townshend J (1995) Global discrimination of land cover types from metrics derived from AVHRR Pathfinder data. Remote Sensing of Environment 54: 209-222.

34. DeFries RS, Townshend JRG (1994) NDVI-derived land cover classifications at a global scale. International Journal of Remote Sensing 15: 3567-3586.

35. Loveland TR, Reed BC, Brown JF, Ohlen DO, Zhu Z, et al. (2000) Development of a global land cover characteristics database and IGBP Discover from 1 km AVHRR data. International Journal of Remote Sensing 21: 1303-1330.

36. Elvidge CD, Portigal FP (1990) Change detection in vegetation using 1989 AVIRIS data. SPIE Imaging Spectroscopy of the Terrestrial Environment 1298: 178-189.

37. Garcia M, Ustin SL (2001) Detection of inter-annual vegetation responses to climatic variability using AVIRIS data in a coastal savanna in California. IEEE Transactions on Geoscience and Remote Sensing 39: 1480-1490.

38. Merton R (1998) Monitoring community hysteresis using spectral shift analysis and the red-edge vegetation stress index. Proceedings of the Seventh JPL Airborne Earth Science Workshop: 275-284.

39. Roberts DA, Green RO, Adams JB (1997) Temporal and spatial patterns in vegetation and atmospheric properties from AVIRIS. Remote Sensing of Environment 62: 223-240.

40. Tyler AN, Sanderson DCW, Scott EM, Allyson JD (1996) Accounting for spatial variability and fields of view in environmental gamma ray spectrometry. Journal of Environmental Radioactivity 33: 213-235.

41. Huete AR, Jackson RD (1988) Soil and atmosphere influences on the spectra of partial canopies. Remote Sensing of the Environment 25: 89-105.

42. Oppelt N (2012) Remote Sensing of Photosynthetic Parameters. Applied Photosynthesis, Dr Mohammad Najafpour (Ed.).

43. Jiang Z, Huete A, Chen J, Chen Y, Li J, et al. (2006) Analysis of NDVI and scaled difference vegetation index retrievals of vegetation fraction. Remote Sensing of the Environment 101: 366-378.

44. Rundquist BC (2002) The influence of canopy green vegetation fraction on spectral measurements over native tallgrass prairie. Remote Sensing of the Environment 81: 129-135.

45. Huete AR, Didan K, van Leeuwen WJD, Vermote EF (1999) Global-scale analysis of vegetation indices for moderate resolution monitoring of terrestrial vegetation. Proceedings of SPIE 1: 141-151.

46. Gates DM (1970) Physical and physiological properties of plants, in Remote Sensing with spectral reference to agriculture and forestry. National Academy of Sciences: 224-252.

47. Tucker CJ (1979) Red and photographic infrared linear combinations for monitoring vegetation. Remote Sensing of the Environment 8: 127-150.

48. Monteith JL, Unsworth MH (1990) Principles of Environmental Physics, London. Butterworth-Heinemann.

49. Blackburn GA (1998) Spectral indices for estimating photosynthetic pigment concentrations: A test using senescent tree leaves. Intl. J. Remote Sensing 19: 657-675.

50. Haboudane D, Miller JR, Pattey E, Zarco-Tejada PJ, Strachan IB (2004) Hyperspectral vegetation indices and novel algorithms for predicting green LAI of crop canopies: modeling and validation in the context of precision agriculture. Remote Sensing of Environment 90: 337-352.

51. Sato N (2004) Roles of the acidic lipids sulfoquinovosyldiacylglycerol and phosphatidylglycerol in photosynthesis: their specificity and evolution. J Plant Res 117: 495-505.

52. Sprague SG (1987) Structural and functional consequences of galactolipids on thylakoid membrane organization. J BioenergBiomembr 19: 691-703.

53. Blackburn GA, Steele CM (1999) Towards the remote sensing of matorral vegetation physiology: relationships between spectral reflectance, pigment, and biophysical characteristics of semiarid bushland canopies. Remote Sensing of the Environment, 70: 278-292.

54. Monteith JL (1977) Climate and efficiency of crop production in Britain. Philos. Trans. R. Soc. London Ser. B 281: 277-294.

55. Jarvis PG, Leverenz JW (1983) Productivity of temperate deciduous and evergreen forests. Encyclopedia of Plant Physiology 12: 233-280.

56. Webb WL, Lauenroth WK, Szarek SR, Kinerson RS (1983) Primary production and abiotic controls in forests, grasslands, and desert ecosystems in the United States. Ecology 64: 134-151.

57. Givnish TJ (1988) Adaptation to sun and shade: a whole-plant perspective. Aust. J. Plant Physiol. 15: 63-92.

58. Bateson CA, Curtiss B (1996) A method for manual end member selection and spectral unmixing. Remote Sensing of the Environment 55: 229-243.

59. Van der Meer F (1999) Iterative spectral unmixing (ISU). International Journal of Remote Sensing 20: 3431-3436.

60. Bassham JA, Benson AA, Calvin M (1950) The path of carbon in photosynthesis. J BiolChem 185: 781-787.

61. Van der Meer F, De Jong SM (2000) Improving the results of spectral unmixing of Landsat Thematic Mapper imagery by enhancing the orthogonality of end-members. International Journal of Remote Sensing 21: 2781-2797.

62. Danks SM, Evans EH, Whittaker PA (1983) Structure function and assembly in Photosynthetic Systems. Wiley, New York, NY, pp.15-17.

63. Young A, Britton G (1990) Carotenoids and Stress Reponses in Plants: Adaptation and Acclimation Mechanisms. R.G. Alscher and JR Cummings, eds. Wiley-Liss, New York, NY: 87-112.

64. Rogge DM, Rivard B, Zhang J, Feng J (2006) Iterative spectral unmixing for optimizing per-pixel end member sets. IEEE Transactions on Geoscience and Remote Sensing 44: 3725-3736.

65. Hosmer DW, Lemeshow S(2000) Applied logistic regression. John Wiley and Sons, New York.

66. Griffith DA (2003) Spatial autocorrelation on spatial filtering. Springer-Verlag Berlin Heidelberg.

67. Sommerville DMY (1958) An Introduction to the Geometry of N Dimensions. New York, NY: Dover Publications.

68. Glitzmann P, Klee V (1994) Polytopes: On some complexity of some basic problems in computational convexity. NATO ASI Series 440: 373-466.

69. Uspensky JV (1948) Theory of Equations. McGraw-Hill, 256.

70. Jacob BG, Griffith DA, Mwangangi JM, Gathings DA, Mbogo CB, et al. (2011) A cartographic analyses using spatial filter logistic model specifications for implementing mosquito control in Kenya Urban Geography 32: 363-377.

71. Jacob BG, Griffith DA, Gunter JT, Muturi EJ, Caamano EX, et al. (2008) A spatial filtering specification for an auto-negative binomial model of Anopheles arabiensis aquatic habitats. Transactions in GISc.12: 515-539.

72. Jackson RD, Slater PN, Pinter Jr. PJ(1983) Discrimination of growth and water stress in wheat by various vegetation indices through clear and turbid atmospheres: Remote Sens. Environ. 13: 187-208.

73. Tucker CJ, Vanpraet CL, Sharman MJ, Ittersum GV (1985) Satellite remote sensing of total herbaceous biomass production in the Senegalese Sahel: 1980-1984: Remote Sens. Environ., 17: 233-249.

74. Moran PAP (1950) Recent Developments in Ranking Theory. Journal of the Royal Statistical Society. Series B (Methodological) 12: 153-162.

75. Cressie NAC (1993) Statistics for spatial data, revised edition. New York, NY: Wiley, 990.

76. Jacob BG, Griffith DA, Novak RJ (2008) Decomposing Malaria mosquito aquatic habitat data into spatial autocorrelation eigenvectors in a SAS/GIS Module. Transactions in GIS.12: 341-364.

77. Greiner W (2001) Quantum mechanics. New York, NY: Springer-Verlag, 79: 51-63.

78. Jacob BG, Chadee DD, Novak RJ (2011) Adjusting second moment bias in eigenspace using Bayesian empirical estimators, Dirichlet tessellations and Worldview 1 data for predicting Culexquinquefasciatus in Trinidad. Journal of Geographic Information Systems 3: 18-49.

79. Ramoelo A, Cho MA, Mathieu R, Skidmore AK, SchlerfM, et al. (2012) Estimating grass nutrients and biomass as an indicator of rangeland (forage) quality and quantity using remote sensing in savanna ecosystems. International Conference of the African Association of Remote Sensing and the Environment (AARSE).

80. Ramoelo A, Skidmore AK, Cho MA, Schlerf M, Mathieu R, et al. (2012) Regional estimation of savanna grass nitrogen using the red-edge band of the spaceborneRapidEye sensor. Int. J. Appl. Earth Obs. Geoinf 19: 151-162.

81. Vuolo F, Atzberger C, Richter K, Urso GD, Dash J (2010) Retrieval of biophysical vegetation products from RapidEye imagery. ISPRS 38: 281-286.

82. Beckschafer P, Fehrmann L, Harrison RD, Xu J, Kleinn C (2014) Mapping leaf area index in subtropical upland ecosystems using rapideye imagery and the randomforest algorithm. iForest 7: 1-11.

83. Jiali S, McNaim H, Fernandes R, Schulthess U, Storie J (2012) Estimation of crop ground cover and lead area index (LAI) of wheat using Rapid Eye satellite data: prelimary study. International Conference on Agro-Geoinformatics: 1-5.

84. Baret F, Jacquemoud S, Guyot G, Leprieur C (1992) Modeled analysis of the biophysical nature of spectral shifts and comparison with information-content of broad bands. Remote Sensing of Environment 41: 133-142.

85. Aparicio N, Villegas D, Araus J, Casadesus J, Royo C (2002) Relationship between growth traits and spectral vegetation indices in durum wheat. Crop Science 42: 1547-1555.

86. Delegido J, Fernandez G, Gandia S, Moreno J (2008) Retrieval of chlorophyll content and LAI of crops using hyperspectral techniques: application to PROBA/CHRIS data. International Journal of Remote Sensing 29: 7107-7127.

87. McCoy RM (2005) Field methods in remote sensing. New York, NY: The Guilford Press.

88. Moran MS, Maas SJ, Vanderbilt VC, Barnes M, Miller SN, et al. (2004) Application of image-based remote sensing to irrigate agriculture. Remote sensing for natural resource management and environmental monitoring. Hoboken: John Wiley & Sons, 617-676.

89. Pimstein A, Eitel JUH, Long DS, Mufradi I, Karnieli A, Bonfil DJ (2009) A spectral index to monitor the head-emergence of wheat in semi-arid conditions. Field Crops Research 111: 218-225.

90. Darvishzadeh R, Skidmore A, Schlerf M, Atzberger C, Corsi F, et al. (2008) LAI and chlorophyll estimation for a heterogeneous grassland using hyperspectral measurements. Isprs Journal of Photogrammetry and Remote Sensing 63: 409-426.

91. Liu J, Pattey E, Jego G (2012) Assessment of vegetation indices for regional crop green LAI estimation from Landsat images over multiple growing seasons. Remote Sensing of Environment 123: 347-358.

92. Nguy-Robertson A, Gitelson A, Peng Y, ViÃ±a A, Arkebauer T, Rundquist D (2012) Green leaf area index estimation in maize and soybean: combining vegetation indices to achieve maximal sensitivity. Agron. J. 104: 1336-1347.

93. Bala SK, Islam AS (2009) Correlation between potato yield and MODIS-derived vegetation indices. International Journal of Remote Sensing 30: 2491-2507.

94. Liu J, Pattey E, Shang J, Admira S, Jego G, et al. (2009) Quantifying crop biomass accumulation using multi-temporal optical remote sensing observations. Canadian Symposium on Remote Sensing: 22-25.

95. Schuster G, Forster M, Kleinschmit B (2012) Testing the red edge channel for improving land-use classifications based on high-resolution multi-spectral satellite data. International Journal of Remote Sensing 33: 5583-5599.

96. Recio JA, Helmholz P, Muller S (2011) Potential evaluation of different types of images and their combination for the classification of GIS objects cropland and grassland. The Internat. Archives of the Photogramm., Remote Sens. And Spatial Info. Sc. 38: 19-25.

97. Conrad C, Fritsch S, Lex S, Law F, Racker G, et al. (2012) Potential of the Red Edge channel of Rapid Eye to distinguish and monitor farmer schaftlicer cultivation Frachte the example of the Uzbek Bewasserungs system Khorezm. Borg, Daedelow, Johnson. Rapid Eye Science Archive: 203-214.

98. Eitel JUH, Long DS, Gessler PE, Smith AMS (2007) Using in-situ measurements to evaluate the new RapidEye satellite series for prediction of wheat nitrogen status. International Journal of Remote Sensing 28: 4183-4190.

99. Pinar A, Curran PJ (1996) Grass chlorophyll and the reflectance red edge. International Journal of Remote Sensing 17: 351-357.

100. Filella I, PeÃuelas J (1994) The red edge position and shape as indicators of plant chlorophyll content, biomass and hydric status. International Journal of Remote Sensing 15: 1459-1470.

101. Rodriguez D, Fitzgerald GJ, Belford R, Christensen LK (2006) Detection of nitrogen deficiency in wheat from spectral reflectance indices and basic crop eco-physiological concepts. Australian Journal of Agricultural Research 57: 781-789.

102. Schelling K (2010) Approaches to characterize chlorophyll/nitrogen status of crop canopies. Analysis of Remote Sensing Data workshop, Hannover.

103. Lewis P, Hillier J, Watt J, Andrieu B, Fournier C, et al. (2005) 3D dynamic vegetation modeling of wheat for remote sensing and inversion. Proc. the 9th International Symposium on Physical Measurements and Signatures in Remote Sensing (ISPMSRS), 17-19 October 2005, Beijing, China, Part 1, 144-146.

104. Grant RH (1985) The influence of the sky radiance distribution on the flux density in the shadow of a tree crown. Agricultural and Forest Meteorology 35: 59-70.

105. Glantz SA, Slinker BK (1990) Primer of Applied Regression and Analysis of Variance. McGraw-Hill Professional Publishing.

106. Huang D, Knyazikhin Y, Dickinson RE, Rautianen M, Stenberg P, et al. (2007) Canopy spectral invariants for remote sensing and model applications. Remote Sensing of Environment 106: 106-122.

107. Knyazikhin Y, Martonchik JV, Myneni RB, Diner DJ, Running SW (1998) Synergistic algorithm for estimating vegetation canopy leaf area index and fraction of absorbed photosynthetically active radiation from MODIS and MISR data. Journal of Geophysical Research 103: 32257-32275.

108. Lewis P, Disney M (2007) Spectral invariants and scattering across multiple scales from within-leaf to canopy. Remote Sensing of Environment 109: 196-206.

109. Panferov O, Knyazikhin Y, Myneni RB, Szarzynski J, Engwald S, et al. (2001)The role of canopy structure in the spectral variation of transmission and absorption of solar radiation in vegetation canopies. IEEE Trans Geosci Remote Sens 39: 241-253.

110. Shabanov NV, Wang Y, Buermann W, Dong J, Hoffman S, et al. (2003) The effect of spatial heterogeneity in validation of the MODIS LAI and FPAR algorithm over broadleaf forests. Remote Sens Environ 85: 410-423.

111. Disney M, Lewis P, Quaife T, Nichol C (2005) A spectral invariant approach to modeling canopy and leaf scattering. Proc. the 9th ISPMSRS, 17-19 October 2005, Beijing, China, Part 1: 318-320.

112. Wang YP, Jarvis PG (1990) Influence of crown structural properties on PAR absorption, photosynthesis, and transpiration in Sitka spruce: application of a model (MAESTRO). Tree Physiol 7: 297-316.

113. Li X, Strahler AH (1988) Gap frequency in discontinuous canopies. IEEE Trans. Geosci. Remote Sensing 26: 161-170.

114. Li X, Strahler AH (1985) Geometric-optical modeling of a conifer forest. IEEE Trans Geosci. Remote Sensing 23: 705-721.

115. Nilson T (1992) Radiative transfer in nonhomogeneous plant canopies. Advances in Bioclimatology 1: 59-88.

116. Schowengerdt RA (1997) Remote Sensing, Models and Methods for Image Processing, (2ndedn) San Diego, United States: Academic Press.

117. Baker JR, Briggs SA, Gordon V, Jones AR, Settle JJ, et al. (1991) Advances in classification for land cover mapping using SPOT HRV imagery. International Journal for Remote Sensing 12: 1071-1085.

118. Colby JD (1991) Topographic normalization in rugged terrain. Photogrammetric Eng. and Remote Sensing 57: 531-537.

119. Costa-Posada CR, Devereux BJ (1995) Reduction of the topographic effects in SPOT imagery: an examination of the Minnaert model. SPIE Image and Signal Processing for Remote Sensing II 2579: 137-149.

120. Suits GH (1972) The calculation of the directional reflectance of a vegetative canopy. Remote Sensing of Environment 2: 117-125.

121. Addink EA, de Jong SM, Pebesma EJ (2007) The importance of scale in object-based mapping of vegetation parameters with hyperspectral imagery. Photogrammetric Engineering and Remote Sensing 73: 905-912.

122. Myneni RB, Hall FG, Seller PJ, Marshak AL (1995) The interpretation of spectral vegetation indexes. IEEE Transactions on Geoscience and Remote Sensing 33: 481.

123. Penndorf R (1957) Tables of the refractive index for standard air and the Rayleigh scattering coefficient for the spectral region between 0.2 and 20.0 μ and their application to atmospheric optics. J. Opt. Soc. Amer. 47: 176-182.

124. Recio JA, Hermosilla T, Ruiz LA, Palomar J (2013) Automated extraction of tree and plot-basedparameters in citrus orchards from aerial images, 90: 24-34.

125. Jackson RD, Huete AR (1991) Interpreting vegetation indices. Prev. Vet. Med. 11: 185-200.

126. Green RO, Eastwood MZ, Sarture CM, Chrien TG, Aronsson M, et al. (1998) Imaging spectroscopy and the airborne visible infrared imaging spectrometer (AVIRIS). Remote Sensing of Environment, 65: 227-248.

127. Roberts DA, Gardner M, Church R, Ustin S, Scheer G, et al. (1998) Mapping chaparral in the Santa Monica Mountains using multiple endmember spectral mixture models. Remote Sensing of Environment, 65: 267-279.

128. Li X, Strahler AH (1992) Geometric-optical bidirectional reflectance modeling of the discrete crown vegetation canopy: effect of crown shape and mutual shadowing. IEEE Transactions on Geoscience and Remote Sensing 30: 276-292.

129. Edward A (2003) Interactive Computer Graphics: A Top-Down Approach Using OpenGL. Addison-Wesley.

130. Strahler AH, Jupp DL (1990) Bidirectional reflectance modeling of forest canopies using boolean models and geometric optics. Proceedings, International Geosciences and Remote Sensing Symposium: IGARSS9O, Washington DC.

131. Sanderson EW, Zhang M, Ustin SL, Rejmankova E (1998) Geostatistical scaling of canopy water content in a California salt marsh. Landscape Ecology 13: 79-92.

132. Nicodemus FE, Richmond JC, Hsia JJ (1977) Geometrical Considerations and Nomenclature for Reflectance. US Department of Commerce.

133. Schowengerdt RA (2007) Optical radiation models in Remote Sensing: models and methods for image processing, 45-88. Amsterdam. Academic Press.

134. Rahman AF, Gamon JA, Fuentes DA, Roberts DA, Prentiss D (2001) Modeling spatially distributed ecosystem flux of boreal forests using hyperspectral indices from AVIRIS imagery. Journal of Geophysical Research 106: 33579-33591.

135. Gao BC (1996) NDWI-A normalized difference water index for remote sensing of vegetation liquid water from space. Remote Sensing of Environment 58: 257-266.

136. Penuelas J, Pinol J, Ogaya R, Filella I (1997) Estimation of plant water concentration by the reflectance water index WI (R900/R970). International Journal of Remote Sensing 18: 2869-2875.

137. Gao BC, Goetz AFH (1995) Retrieval of equivalent water thickness and information related to biochemical components of vegetation canopies from AVIRIS data. Remote Sensing of Environment 52: 155-162.

138. Zhang M, Ustin SL, Rejmankova E, Sanderson EW (1997) Remote sensing of salt marshes: potential for monitoring. Ecological Applications 7: 1039-1053.

139. Asner GP, Borghi C, Ojeda R (2003) Desertification in Central Argentina: Regional changes in ecosystem carbon-nitrogen from imaging spectroscopy. Ecological Applications 13: 629-648.

140. Asner GP, Townsend AR, Bustamante MMC (1999) Spectrometry of pasture condition and biogeochemistry in the Central Amazon. Geophysical Research Letters 26: 2769-2772.

141. Kokaly RF, Clark RN (1999) Spectroscopic determination of leaf biochemistry using band-depth analysis of absorption features and stepwise multiple linear regression. Remote Sensing of Environment 67: 267-287.

142. Asner GP (1998) Biophysical and biochemical sources of variability in canopy reflectance. Remote Sensing of Environment 64: 234-253.

143. Valentini R, MatteucciG, Dolman AJ, Schulze ED, Rebmann C, et al. (2000) Respiration as the main determinant of carbon balance in European forests. Nature 404: 861-865.

144. Ben-Dor E, Irons JR, Epema G (1999) Soil reflectance in Remote Sensing for the Earth Sciences, Rencz An, ed, John Wiley and Sons, New York, NY, USA 3: 111-188.

145. Baumgardner MF, Silva LF, Biehl LL, Stoner ER (1985) Reflectance properties of soils. Advances in Agronomy 38: 1-44.

146. Price JC (1990) On the information content of soil reflectance spectra. Remote Sensing of Environment 33: 113-121.

147. Huete AR, Escadafal R (1991) Assessment of biophysical soil properties through spectral decomposition techniques. Remote Sensing of Environment 35: 149-159.

148. Palacios-Orueta A, Ustin SL (1998) Remote sensing of soils in the Santa Monica Mountains, pt. I: Spectral analysis: Remote Sensing of Environment 65: 170-183.

149. Palacios-Orueta A, PinzÃ³n, Ustin SL, Roberts DA (1999) Remote sensing of soils in the Santa Monica Mountains, pt. II: Hierarchical foreground and background analysis. Remote Sensing of Environment 68: 138-151.

150. Hill J, Schutt B (2000) Mapping complex patterns of erosion and stability in dry Mediterranean ecosystems. Remote Sensing of Environment 74: 557-569.

151. Leone AP, Sommer S (2000) Multivariate analysis of laboratory spectra for the assessment of soil development and soil degradation in the southern Apennines (Italy). Remote Sensing of Environment 72: 346-359.

152. Qi J, Chehbouni A, Huete AR, Kerr YH, Sorooshian S (1994) A modified soil adjusted vegetation index. Remote Sensing of Environment 48: 119-126.

153. Huete AR (1988) A soil-adjusted vegetation index (SAVI) Remote Sensing of Environment 29: 295-309.

154. Liu J, Pattey E, Miller JR, McNaim H, Smith A, et al. (2010) Estimating crop stresses, above ground dry biomass and yield of corn using multi-temporal optical data combined with a radiation use efficiency model. Remote Sensing of Environment 114: 1167-1177.

155. Clevers JGPW (1989) The application of a weighted infrared-red vegetation index for estimating Leaf Area Index by correcting for soil moisture. Rem. Sens. Envir.29: 25-37.

156. Rondeaux G, Steven M, Baret F (1996) Optimization of soil-adjusted vegetation indices. Rem. Sens. Env.55: 95-107.

157. Daughtry CST (2001) Discriminating crop residues from soil by shortwave infrared reflectance. Agron. J. 93: 125-131.

158. Daughtry CST, McMurtrey III JE, Chappelle EW, Hunger WJ, Steiner JL (1996) Measuring crop residue cover using remote sensing techniques. Theoretical and Applied Climatology 54: 17-26.

159. Nagler PL, Daughtry CST, Goward SN (2000) Plant litter and soil reflectance. Remote Sensing of Environment 71: 207-215.

160. Barnes EM, Sudduth KA, Hummel JW, Lesch SM, Corwin DL, et al. (2003) Remote and ground-based sensor techniques to map soil properties. Photogrammetric Engineering & Remote Sensing, 69: 619-630.

161. Huete AR (1989) Soil influences in remotely sensed vegetation-canopy spectra in Theory and Applications of Optical Remote Sensing. John Wiley and Sons, New York, NY.

162. Baret F, Guyot G (1991) Potentials and limits of vegetation indices for LAI and APAR assessment. Remote Sensing of Environment 35: 161-173.

163. Treuhaft RN, Law BE, Asner GP (2004) Forest attributes from radar interferometric structure and its fusion with optical remote sensing. BioScience 54: 561-571.

164. BakamaNume BBA (2011) A Contemporary Geography of Uganda. African Books Collective.